

CRANFIELD UNIVERSITY

J A ETCHES

INTERFACIAL AND DURABILITY ASPECTS OF
EXTRINSIC FABRY-PEROT INTERFEROMETRIC
SENSORS IN CARBON FIBRE COMPOSITES

ENGINEERING SYSTEMS DEPARTMENT

PhD THESIS

CRANFIELD UNIVERSITY

ENGINEERING SYSTEMS DEPARTMENT

PhD THESIS

Academic Year 2003/04

J A ETCHES

Interfacial and durability aspects of extrinsic Fabry-Perot
interferometric sensors in carbon fibre composites

Supervisor: GF Fernando

September 2003

© Cranfield University 2003. All rights reserved. No part of this
publication may be reproduced without the written permission of the
copyright owner.

ABSTRACT

This thesis is concerned with the interfacial and durability aspects of Extrinsic Fabry-Perot Interferometric (EFPI) sensors embedded in carbon fibre reinforced composites. Fibre optic sensors are being used in many long term applications and, as is the case for all sensor types, the ability of the EFPI sensors to monitor accurately the measurands of interest over the lifetime of the structure must be proved. Therefore, the aim of this work was to examine the interface between the EFPI sensors and the structures, and then to evaluate the durability of that interface and the sensors.

The first stage was an examination of the EFPI sensors including the method of manufacture, interrogation option and inherent strength of the sensors. It was found that the sensors have a very low tensile load to failure (~ 0.5 N). This was improved by using a resin reinforcement, which was applied to the capillary ends. However, this had implications for the overall sensor size and that influenced their embedment suitability. The second stage was interfacial characterisation; this was achieved through the examination of the surface energy of the sensors, carried out by contact angle measurements; and the interfacial shear strength of the sensors to matrix, using a new variation on the single fibre pull-out technique that involved the use of optical fibres and composite prepreg. Overall, it was found that the silane treatment of the fibres increased the surface energy but for the interfacial shear results the data was less conclusive due to the scatter present within the results.

The durability of the sensors was examined through their embedment into carbon fibre composite samples and exposure to tension/compression fatigue loading. From initial quasi-static work it was found that the embedment of the sensors had no significant effect on the composite samples. However, the sensors failed at a strain levels of 0.4% in tension and at 1.1% in compression; the compression strain level was at the point of composite failure. Under fatigue loading the sensors could survive a million cycles at $R=-1$ at a max stress level of 156 MPa and maintain their reliability. If the tensile loading was increased then the sensors would fail within a few thousand cycles. However, if the compressive stress was increased the sensors survived but the reliability was affected. Overall, it was felt that with some improvements to the sensor design they should be able to survive and provided useful data when exposed to axial tension/compression fatigue regimes.

Acknowledgements

First I would like to thank Dr G. Fernando for providing the opportunity for me to pursue this research, as well as his supervision and support during this period. I would also like to thank Professor B Ralph for his encouragement and support.

I am grateful for the financial support provided by the Engineering and Physical Sciences Research Council and the Engineering Systems Department at Cranfield University, RMCS.

I would like to thank all the member of the Sensors and Composites Research Group for their help and advice during my research, in particular Mr J Tetlow for his work on the manufacture of the EFPI sensors.

Finally I am very grateful to my family for their endless support and encouragement, with a particular thanks to Tony for his confidence in my research ability and his patience.

TABLE OF CONTENTS

1	INTRODUCTION.....	1
1.1	Structure of the thesis.....	4
2	LITERATURE REVIEW.....	5
2.1	Fibre Optic Sensors.....	5
2.2	EFPI Sensors.....	7
2.2.1	Fatigue of EFPI sensors.....	11
2.2.2	Effect of embedded fibres and sensors on the mechanical properties of composites.....	20
2.2.3	T/C fatigue of CFRP.....	27
2.3	Interfacial Aspects of Fibre Optic Sensors.....	30
2.3.1	Strain transfer to fibre optic sensors.....	30
2.3.2	Methods of investigating of interfacial shear strength.....	32
2.3.3	Silane coupling agents.....	38
2.3.4	Effect of silanes on interfacial properties.....	40
2.3.5	Summary of EFPI interfaces.....	43
2.4	Surface Energy of Silica.....	44
2.4.1	Background theory of surface energy.....	44
2.4.2	Measurement of contact angles.....	46
2.4.3	Surface energy values for silica and effect of silanes.....	47
2.4.4	Summary of surface energy of silica.....	49
2.5	Summary of the Literature Review.....	49
3	EXPERIMENTAL.....	51
3.1	Introduction.....	51
3.2	Materials.....	52
3.2.1	Optical fibre and sensor components.....	52
3.2.2	Chemicals.....	53
3.2.3	Resins.....	53
3.2.4	Composite prepreg.....	54
3.3	Sample Preparation.....	54
3.3.1	EFPI manufacture.....	55
3.3.2	Surface energy test specimens.....	56
3.3.3	Autoclave processing of prepregs.....	57
3.3.4	Preparation of interfacial shear strength samples.....	58
3.3.5	Preparation of composite samples for mechanical testing.....	59
3.3.6	Preparation of composite samples with embedded EFPI sensors for mechanical testing.....	61
3.4	Test Methods.....	62
3.4.1	EFPI sensor interrogation.....	62
3.4.2	Gauge length determination for the EFPI sensors.....	65
3.4.3	Tensile testing of EFPI sensors.....	67
3.4.4	Surface energy.....	68
3.4.5	Interfacial shear strength.....	71

3.4.6	Quality control check of the composite samples	73
3.4.7	Quasi-static testing of composite samples without and with embedded EFPI sensors.....	74
3.4.8	Loading rate effects on composite samples without and with embedded EFPI sensors	75
3.4.9	Dynamic testing of composite samples without and with embedded EFPI sensors.....	76
4	EFPI EVALUATION.....	79
4.1	Spectral Response of EFPI sensors.....	79
4.1.1	Raw spectra.....	79
4.1.2	Normalised spectra.....	80
4.1.3	FFT analysed spectra	80
4.1.4	Variations in the calculated cavity lengths	81
4.2	Variation in EFPI Manufacturing Method.....	83
4.3	Determination of the Gauge length.....	85
4.3.1	Optical measurements.....	85
4.3.2	Comparison of strain gauge and EFPI sensor data	87
4.3.3	Effect of gauge length on calculated strain values.....	90
4.4	Tensile strength of EFPI	91
4.4.1	Coated optical fibres	91
4.4.2	EFPI sensors.....	92
4.4.3	Reinforced EFPI sensors.....	94
4.5	Conclusions.....	98
5	INTERFACIAL CHARACTERISATION	99
5.1	Surface Energy	99
5.1.1	Cleaning methods.....	100
5.1.2	Surface energy comparison between capillary and fibre	102
5.1.3	Silane treatments.....	106
5.2	Interfacial Shear Strength	112
5.2.1	Sample manufacture.....	112
5.2.2	Measurement of the embedment depth.....	115
5.2.3	2-ply versus 16-ply glass fibre composite samples.....	119
5.2.4	Glass fibre versus carbon fibre composite samples	123
5.2.5	Silane treated fibres.....	126
5.2.6	IFSS results summary	128
5.2.7	Possible improvements to the pull-out method.....	129
5.3	Conclusions.....	133
6	SENSOR AND COMPOSITE DURABILITY	135
6.1	Quality of Composite Samples	135
6.1.1	Fibre volume fraction of CFRP samples.....	138
6.2	Quasi-static Tensile Testing.....	138
6.2.1	Tensile properties of reference CFRP samples.....	139
6.2.2	Tensile properties of CFRP samples with embedded EFPI sensors	140
6.3	Quasi-static Compressive Testing.....	144

6.3.1	Compressive properties of reference CFRP samples.....	144
6.3.2	Compressive properties of CFRP samples with embedded EFPI sensors.....	146
6.4	Influence of Loading Rate	148
6.4.1	Rate sensitivity of CFRP samples.....	148
6.4.2	Rate sensitivity of CFRP samples with embedded EFPI sensors	150
6.5	Dynamic Evaluation of Composite Samples	153
6.5.1	Stress ratio of -1	153
6.5.2	Varying fatigue stress ratios.....	163
6.5.3	Modification of gauge length values using UV glued sensors	169
6.5.4	Heat generation during fatigue.....	172
6.6	Summary	175
7	CONCLUSIONS AND RECOMMENDATIONS FOR FURTHER WORK.	177
7.1	EFPI Evaluation	177
7.2	Interfacial Aspects	178
7.2.1	Surface energy	178
7.2.2	Interfacial shear strengths	179
7.3	Durability Aspects	181
7.3.1	Quasi-static results	181
7.3.2	Strain rate results.....	181
7.3.3	Dynamic results	181
7.4	Recommend Further Work	182
7.4.1	EFPI sensors.....	182
7.4.2	Interface	183
7.4.3	Durability	184
8	REFERENCES	185
	APPENDIX 1.....	192

Glossary (symbols and acronyms)

γ	Surface energy
λ	Wavelength
$\mu\epsilon$	Microstrain
AFRC	Advanced fibre reinforced composite
APMS	Aminopropyltrimethoxy silane
APS	Aminopropyltriethoxy silane
C/C	Compression/compression
CCD	Charged coupler detector
CDCA	Camtel dynamic contact angle
CFRP	Carbon fibre reinforced plastic
CV	Coefficient of variation
DAQ	Data acquisition
DCM	Dichloromethane
DMSO	Dimethylsulfoxide
EFPI	Extrinsic Fabry-Perot interferometer
ERSG	Electrical resistance strain gauge
FBG	Fibre Bragg grating
FFT	Fast Fourier transform
FOS	Fibre optic sensor
GFRP	Glass fibre reinforced plastic
GPMS	Glycidoxypropyltrimethoxy silane
IFSS	Interfacial shear strength
OF	Optical fibre
R	Fatigue stress ratio
RT	Room temperature
SHM	Structural health monitoring
SLD	Super luminescence diode
SM	Single mode
Std dev	Standard deviation
T/C	Tension/compression
T/T	Tension/tension
UCS	Ultimate compressive strength
UD	Unidirectional
UTS	Ultimate tensile strength

1 Introduction

In recent years there has been a move to use advanced fibre reinforced composites (AFRC) in a wide variety of industries from aeronautical to civil engineering (Askeland, 1994). AFRC involve the use of two or more different materials to achieve properties that would not be obtainable from a single material. These composites are typically made from a fibrous reinforcing component and a matrix phase. The fibres can be short or continuous with materials such as carbon and glass. The matrix phase can be thermoplastic, thermoset, ceramic or metal in nature. The most commonly used composites in industrial applications are, at present, those based on polymeric matrices with glass, carbon or Kevlar fibres. The specific mechanical properties of these composites can exceed those of traditional materials, for example steel and aluminium, and have therefore been useful in applications where weight saving is a priority, such as aerospace. Also the properties of the composite can be tailored to actual applications by the use of a particular matrix system or the orientation of the fibres.

Structural health monitoring (SHM) is a powerful tool within the field of AFRC as it enables performance monitoring of the composite structure during manufacture and application. SHM involves the interrogation of sensors located throughout the structure of interest, which can be embedded within the structure or mounted on its surface. Many types of sensors can be used, however, in many cases the parameter of interest is the strain the structure is subjected to in-service. From the sensor data obtained, it may be possible to detect defects and failures, allowing repairs and replacement of components to be carried out as necessary.

One of the reasons for the interest in SHM for AFRC structures is the difficulty in using traditional non destructive testing techniques in the assessment of the structures. For example, the ultrasonic C-scanning technique requires a coupling medium usually water and X-ray radiography uses a dye-penetrant, therefore these techniques are limited in the usefulness particularly in the cases of on-site and continuous monitoring applications (Liu and Fernando, 1998).

Traditional strain sensors, such as electrical resistance strain gauges (ERSG) and more novel optical fibre based sensors can be employed in SHM. Fibre optic sensors (FOS) are being increasingly used for fibre reinforced composite SHM monitoring as they have several advantages over the traditional sensors. FOS can be embedded within structures or surface mounted on the structure as well as an immunity to electromagnetic interference and the opportunity for interrogation of the sensors from several kilometres away with no loss in signal. However, as with all new technologies, the ability of the FOS to monitor accurately the measurand of interest over the lifetime of the structure must be proved, which in turn builds the confidence for the technology.

There is a large range of types of FOS that can be employed to monitor various parameters such as temperature, pressure, strain and chemical state (Grattan and Meggitt, 1999). All the sensor types work on the basic principle that the measurand of interest alters a property of the light being transmitted through the sensor, which can be determined and related back to the measurand. For example, chemical sensors are typically based on spectroscopic techniques, whereas crack detection sensors usually rely on the intensity of the transmitted light (Srinivasan and McFarland, 2001).

FOS are available in many forms in the pursuit of strain measurements, these included Fibre Bragg Grating (FBG) sensors, intensity based sensors such as microbend, and sensors based on interferometric techniques (Grattan and Meggitt, 1999). For all types of strain sensors, the main requirement for successful use is efficient strain transfer from the structure to the sensor. This is usually achieved through intimate contact between the structure and the sensor and this interface must be maintained for the lifetime of the structure and the sensor. There has been some published work on the interface between some types of FOS and components; this has mainly concentrated on standard coated optical fibre (Méndez *et al.*, 1993, Ansari and Libo, 1998, Barton *et al.*, 2002.).

Another class of FOS sensors can be used to measure strain, but there is much less published work on their interface with structures. This type of sensor is an Extrinsic Fabry-Perot Interferometer (EFPI) sensor. There are two main differences between standard optical fibre and EFPI sensors, these are geometry and surface. In the case of

optical fibres, including FBG sensors, they are single pieces of fibres with a uniform cross-sectional area and typically have a polymeric coating. EFPI sensors, on the other hand, have a structure which changes in cross-section along the length of the sensor and it does not normally have any coating. This means that the surface for strain transfer is silica. Although some of the published work on FBG and optical fibres interfaces will be transferable to EFPI sensors there is a need to investigate the interface between EFPI sensors and components. In the current work it was decided that the main areas that required investigation were the characterisation and the durability of this interface.

The aims of this project were:

- Evaluation of the EFPI sensors.
This was carried out through the use of visual inspections, tensile strength measurements and performance comparison against electrical resistance strain gauges.
- Characterisation of the sensor/composite interface.
This involved the investigation of two parameters; surface energy and interfacial shear strength (IFSS). The surface energy of the EFPI sensors was determined from contact angle measurements, with the IFSS being determined from a modified single fibre pull-out technique. The influence of silane coupling surface treatments on these properties was also examined.
- Durability of the sensor/composite interface.
This aspect of the work involved the survivability of the sensors during the manufacture of the specimens, under quasi-static tensile and compressive loading, as well as the performance of the sensors under tension/compression (T/C) dynamic loading conditions.

Overall the aim of this work was to expand the understanding of the interface of FOS when embedded within a fibre reinforced composites structure. Although the work only involved the investigation of EFPI sensors the majority of the knowledge gained should be applicable to other types of optical fibre sensors.

1.1 Structure of the thesis

This thesis contains seven chapters, starting with this introduction. The second chapter concentrates on the current literature covering three main areas. The first of these areas is EFPI sensors including the current work on their response to fatigue loading and the affect of embedding these sensors on the mechanical properties of the composite samples. The second area discusses various interfacial aspects of EFPI sensors, from strain transfer to methods of determining IFSS to the effects of silane coupling agents. The final part of chapter two reviews the theory of surface energy, contact angle measurements and the surface energy response of silica surfaces. Chapter three describes the experimental philosophy and methodology for the work carried out, including the materials used, sample preparation and tests methods. Chapters four to six present the results obtained from this work with the relevant discussions. Chapter four concentrates on the evaluation of the EFPI sensors, including manufacturing issues and the tensile strength of the sensors. In chapter five the results from the contact angle and single fibre pull-out experiments are presented and discussed including the effect of the surface treatment of the sensors with silane coupling agents. The results from the various static and dynamic tests carried out on the carbon fibre reinforced samples with and without embedded EFPI sensors are reported in chapter six. The conclusions and suggestions for further work are presented in the seventh and final chapter.

2 Literature Review

This review concentrates on the use of fibre optic Extrinsic Fabry-Perot Interferometric (EFPI) sensors embedded within advanced fibre-reinforced composites (AFRC). This includes the effect of static and cyclic loading on the sensors, as well as the effects of embedding fibre optic sensors (FOS) on the mechanical properties of the composite. The review then examines the issue of strain transfer and the influence of the interface on this transfer, which includes improvements to this interface through the use of chemical surface treatments. The final section consists of a brief summary of methods used to evaluate the surface energy of silica and methods of determining interfacial shear strengths (IFSS).

2.1 Fibre Optic Sensors

Optical fibres guide light through the fibre core by total internal reflection (Hecht, 1998). This can be done over several kilometres without any significant loss of signal strength or integrity. A fibre optic sensor (FOS) allows the light being guided through the fibre to be altered in response to an external influence, which can be detected and related back to the external influence. The properties of the light that can be used in sensing applications are intensity, wavelength, polarisation and frequency. This allows parameters such as pressure, temperature, strain or chemical composition to be monitored.

One of the more popular types of FOS is a Fibre Bragg Grating (FBG). This is an intrinsic sensor mainly used to monitor temperature or strain. This type of sensor consists of a grating with a specific spacing being written onto a small section of an optical fibre using UV light and typically a mask. The UV light causes a change in the refractive index of the grating compared to the remainder of the fibre core. When a broadband light source is entered into the fibre, the Bragg grating reflects the portion of the light with a wavelength proportional to the grating spacing. This generates either a gap in the transmission spectra or a peak in the reflected spectrum; this is shown in Figure 2-1.

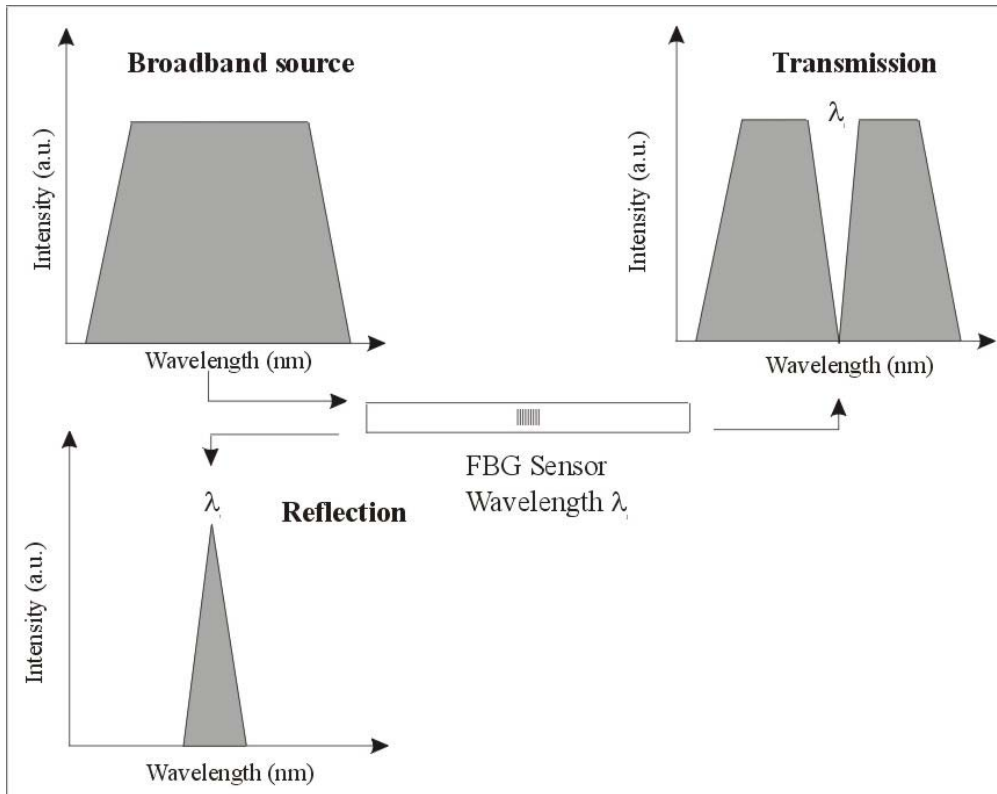


Figure 2-1 Spectral response from a fibre Bragg grating when illuminated with a broadband light source.

As the sensor is exposed to temperature or strain, the period of the grating expands or contracts thereby altering the wavelength that is reflected. These types of sensors can have an accuracy of up to $1 \mu\epsilon$, with a 1°C shift equivalent to $10 \mu\epsilon$ (Grattan and Meggit, 1999). However, one of the major disadvantages of the FBG sensor is its cross-sensitivity between strain and temperature. Therefore, a method of separating the two effects is required; one of the simplest is the use of a reference sensor. In practise this means two FBGs are placed into the component of interest with one being isolated in a strain free region, usually by inserting in a PTFE or metal tube. In this way, the reference fibre is exposed only to the temperature change while the other fibre is subjected to the temperature change and the applied strain. The wavelength shift from the isolated temperature sensor can be subtracted from the other to give the wavelength shift due to the strain only. Another method also uses two Bragg gratings but at different wavelengths, so different responses are obtained from the same measurands (Lee, 2003). As an alternative Lui *et al.* (1997) described the use of a FBG within an EFPI sensor design to enable simultaneous strain and temperature measurements of a

composite sample. The EFPI was temperature insensitive so it monitored the strain with the samples and the FBG was positioned within the EFPI sensor, thereby in a strain free region enabling it use as a temperature sensor.

Another popular fibre optic sensor design is the extrinsic Fabry-Perot interferometer sensor, which is discussed in the next section.

2.2 EFPI Sensors

The main interest of this project is the use of EFPI sensors for monitoring strain changes within a carbon fibre reinforced plastic (CFRP). The EFPI sensor design used in this study consisted of the cleaved ends of two optical fibres, with diameters of 125 μm being placed inside a silica capillary that has an internal diameter of 128 μm . The cavity length was set and two fusion welds were made on the capillary to hold the fibres in place. A schematic illustration of the EFPI sensor is shown in Figure 2-2. As the sensor is subjected to mechanical loading, the capillary is elongated thus bringing about a change in the cavity length. This change in gap was monitored and related to the applied strain.

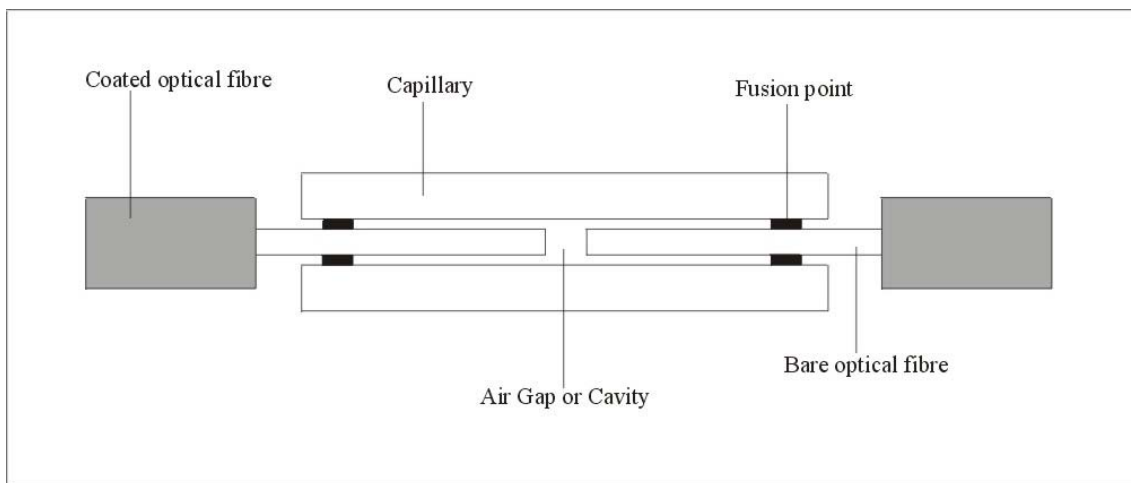


Figure 2-2 Diagram of a typical EFPI sensor design.

There are different ways to interrogate an EFPI sensor but they are all based on the Fresnel reflections that occur at the fibre/air interface when light enters into one of the fibres. Figure 2-3 shows the nature of the reflections.

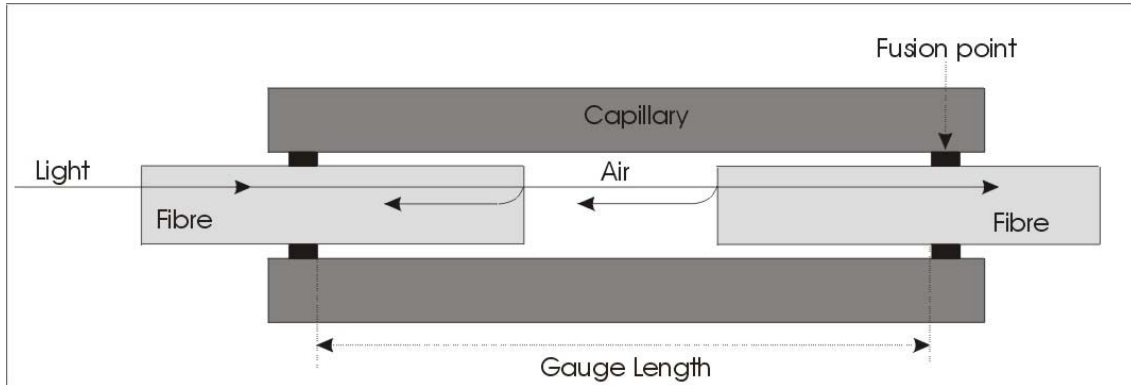


Figure 2-3 Schematic showing the main reflections and the gauge length within an EFPI sensor.

The reflection off the cleaved fibre surfaces is determined by the refractive indices of the medium in the cavity, air in this instance (n_{air}) and the cleaved silica fibre (n_{silica}). This reflectance (R) can be calculated using Equation 2-1 (Hecht, 1998):

$$R = \frac{(n_{silica} - n_{air})^2}{(n_{silica} + n_{air})^2} \quad \text{Equation 2-1}$$

This yields a reflectance of 3.9% for typical values of refractive indices (1.49 for silica and 1 for air). These two reflections then interfere to cause a spectrum from which the length of the cavity can be determined. The strain from this type of sensor is taken as the change in cavity length over a specified gauge length. The gauge length is defined as the length over which the fibres are free to move within the capillary. This is the distance between the contact points of the fibre to capillary as shown for the fused EFPI case in Figure 2-3:

Therefore the strain can be determined from the Equation 2-2:

$$\text{Strain}(\varepsilon) = \frac{\text{Change in cavity length}}{\text{Gauge length}} \quad \text{Equation 2-2}$$

One of the first reports of Fabry-Perot interferometric sensors was published by Lee and Taylor (1988). In that case, two single mode fibres were fusion spliced together with one of the ends being coated with TiO₂ corresponding to a thickness of 140 nm. The TiO₂ film caused an interference spectrum due to the refractive index difference as per Equation 2-1. This sensor was shown to be sensitive to temperature changes. However, as the authors state this type of sensors could be used for temperature or strain monitoring, but if it was to be used as a temperature sensor it would require isolation from the strain and vice versa for use as a strain sensor. Also the introduction of another material within the fibre could have an effect on the strength of the sensor.

Murphy *et al.* (1992) extended the idea of reflective mirrors to generate an air cavity based sensor, or extrinsic Fabry-Perot interferometer. This sensor was along the lines of that shown in Figure 2-2, except that the optical fibres were held inside the capillary through the use of an epoxy adhesive. In the case reported, these sensors were used in the full scale testing of an F-15 aircraft and compared to electrical resistance strain gauges. A 1300 nm light source was used and the response was monitored through intensity measurements. A good agreement was obtained between the EFPI sensors and electric strain gauges.

The research on EFPI sensors then moved on to the measurement of absolute strain opposed to the previous work on relative strain. The advantage of an absolute strain measurement means the system can be switched off without losing the strain information, unlike relative measurements. This was initially reported by Claus *et al.* (1994); the sensors were constructed as previously described but with the difference that instead of fusion welds the fibres were held in the capillary using an epoxy resin. The gauge length of these sensors was defined as the distance between the epoxy fixation points. By using a broad-spectrum light source the absolute gap between the fibre-ends could be determined. However, due to the scan speed of the spectrometer used for that research, only a single measurement could be obtained every 3 seconds. These authors did not mention how the gauge length is controlled or measured; this is an important issue as this relates the gap changes to strain values and any uncertainty with the gauge length would lead to ambiguity in the reported strain measurements.

Bhatia *et al.* (1996) furthered the work on absolute strain measurements from EFPI sensors. The authors improved the reflectivity of the cavity by the addition of a thin layer of metal on the fibre ends that formed the cavity, as this increased the refractive index difference. It was stated that by the use of a broadband source the sensor could measure cavities within the range of 40 μm to 300 μm , with a reported minimum detectable wavelength shift of 0.1 nm. It was stated that the gap was determined through the analysis of the spectrum using phase differences. An example of an EFPI sensor responding to an applied strain was shown but no correlation was made to the actual strain expected or measured strain within the sample.

Fernando *et al.* (1997) demonstrated that EFPI sensors could respond to tensile and compressive stresses. The sensors were embedded in fibre reinforced composite samples. The data obtained from the sensors were compared to surface-mounted extensometers and a good correlation was found, with the discrepancy in measured stiffness being less than 2%.

There are many other published works on the use of EFPI sensors for monitoring strain. These include work done on concrete structures (Quirion and Ballivy, 2000, Vries *et al.*, 1997) and fibre reinforced composites samples (Kalamkarov *et al.*, 1998, Liu *et al.*, 1998).

The EFPI sensor design can be used to monitor other measurands than strain for several other applications (Fernando *et al.*, 1997). These included cure monitoring and vibration. In the case of cure monitoring, a section of the capillary is removed to enable the ingress of the resin. The spectra obtained during cure can show the consumption of the raw materials and the production of the cured material. Temperature can also be monitored using the EFPI sensor design (Degamber and Fernando, 2003). The EFPI sensor is usually insensitive to temperature as it is made completely of silica. However, in that case, soda glass was introduced into the sensor design as the reflector. Due to the differences in thermal expansion between silica and soda glass, the cavity length changed with temperature.

Summary

The EFPI sensor can be a useful strain-monitoring device as it is insensitive to transverse strain, it can also be designed to be insensitive to temperature by ensuring all the components have the same coefficient of thermal expansion. However, its main disadvantages lies in the geometry of the sensor compared to a plain optical fibre (Zhou and Sim, 2002). Further information regarding the use and suitability of EFPI sensors in composite materials is presented in the following sections.

2.2.1 Fatigue of EFPI sensors

Fatigue response of the sensor to dynamic loading is a very important factor for the sensor as most components undergo some form of load cycling during their use. For this reason it is essential that the fatigue performance of the EFPI sensors be known, to ensure that the sensor will survive mechanically for the duration of the component's life and the response of the sensor will be reliable.

There are three main types of axial fatigue loading: tension/tension (T/T), tension/compression (T/C) and compression/compression (C/C). T/T fatigue of EFPI sensors has been reasonably well researched as will be discussed in this section. However, there is very limited published work on fatigue testing that involves a compressive loading. This is mainly due to the complication that when a compressive regime is included in axial testing the samples must be supported to prevent buckling and premature failure. There is currently no accepted standard to achieve this, however, an ISO standard is in the process of being approved (ISO/PRF 13003). A review of the T/C fatigue of carbon fibre composite materials will be dealt with in Section 2.1.3.

The most recent study on the tensile strength and fatigue performance of EFPI sensors is by Lee *et al.* (2002) who considered the sensors individually as well as embedded in a neat epoxy resin sample, and a carbon fibre epoxy composite. The EFPI in this case was made using polyimide coated fibres and hollow fibre, which were held together by an epoxy adhesive. The gauge length was defined as the distance between the two

adhesive points and was between 3 mm and 5 mm for the sensors used in the testing. From the diagram of the sensor it appears that the adhesive enters the hollow fibre to some extent and the gauge length is then the distance between the ends of the adhesive, but there is no mention of how the gauge length was determined or controlled.

Lee *et al.* (2002) started by examining four sensors to determine their mechanical failure properties. The average failure load was 20 N and an average failure strain of 4800 $\mu\epsilon$. A failure stress was not calculated due the variation of the sensor cross-section. Another set of sensors were then subjected to a T/T fatigue regime with $R=0.1$ at a frequency of 1 Hz. The maximum load was set at 55%, 65% and 75% of the failure load. 3 sensors were tested at 55%, one at 65% and two at 75%, all sensors failed prior to a million cycles. All sensors failed by the debonding of the epoxy from the hollow fibre. From the S-N curves provided, it was seen that at the 55% load level one sensor failed at approximately 5000 cycles, while the other two reached a few hundred thousand cycles. This is a large difference between EFPI sensors and more testing should have been done to confirm the results. Also there can only be limited confidence in the remaining results due to this discrepancy, such as the extrapolation to determine the level of loading at which an EFPI could survive a million cycles. This was quoted as being 45% of the failure load, equivalent to approximately 2200 $\mu\epsilon$.

The next stage of the work by Lee *et al.* (2002) was the embedment of the sensors into a neat epoxy resin sample. In static testing the resin had a failure strain approaching 15800 $\mu\epsilon$ with the EFPI sensors responding until failure of the sample and showing good agreement with an electrical resistance strain gauge. However, it was noted that the failure initiated at the sensor, but it was unclear if the sensor failure caused the sample to fail or if the sensor generated a local stress concentration causing premature failure of the resin. Again samples were subjected to T/T fatigue with initial strain levels of 3000 $\mu\epsilon$, 4000 $\mu\epsilon$ and 5000 $\mu\epsilon$ at a ratio of 0.1 and a frequency of 10 Hz. The failure also initiated from the sensor region in the sample and only the sample with an initial strain of 3000 $\mu\epsilon$ survived a million cycles. Again repeatability of the results could be questioned as only one sample was tested at each stress level. The authors do not mention the fatigue properties of this resin without an embedded sensor, but they

concluded that the inclusion of an EFPI in the case of a neat resin samples is detrimental to the resin's properties. It is suggested that this is due to the difference in stiffness, 3 GPa for the resin and 50 GPa for the sensor and the effect of the sensor geometry causing local stress concentrations.

The final stage of the work by Lee *et al.* (2002) was the embedment of the EFPI sensors into a carbon fibre epoxy composite. For the static tensile properties four samples were tested, three had a sensor embedded. The failure strain of the composite was about 14000 $\mu\epsilon$ and the sensors survived up until failure of the composite. There was no noticeable influence on the composite's properties by the inclusion of a sensor. For the fatigue studies five samples were tested each at a different load level varying from 20% to 60% of the ultimate tensile strength with $R=0.1$ and a frequency of 5 Hz. For the 20% loading level, approximate strain level of 2800 $\mu\epsilon$, the composite survived a million cycles with the EFPI also surviving and maintaining good correlation with the foil strain gauge. At 40% load the composite and sensor survived a million cycles, but the authors report that the EFPI sensor showed an unrealistic response at cycles over 10^5 . However, as the strain gauge had failed at 10,000 cycles, and there was no extensometer in use, it was unclear how the response was deemed unrealistic. The investigation into this response was continued; the sample was sectioned, polished and examined under a microscope. It was claimed that debonding had occurred between the sensor and the composite due to fatigue at the hollow fibre/composite interface and a manufacturing void at the end of the sensor. It is also possible that the act of sectioning and polishing the sample could have altered the evidence. However, the authors go on to report that these two effects could lead to a change in the gauge length of the sensor and therefore drastically alter the strain response.

It can be seen from the work by Lee *et al.* (2002) that although the EFPI sensor in this case is capable of measuring large strains in static testing, ($\approx 15000 \mu\epsilon$), during fatigue loading, whether it be embedded in a neat resin sample or a fibre reinforce composite the maximum strain the sensor can tolerate to enable survival to a million cycles is about 3000 $\mu\epsilon$.

Fatigue testing of the EFPI sensor design has been carried out under various conditions. In some cases the design of the sensor used had been altered, to show this a few of the different designs are shown in Table 2-1. It was seen that the different sensor designs could impact on the comparison of results from the different published works. The main difference between the designs is the method of attaching the optical fibres to the capillary, which is typically either an adhesive or a fusion weld. The fatigue studies carried out on these sensors follow after Table 2-1.



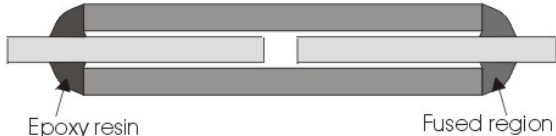
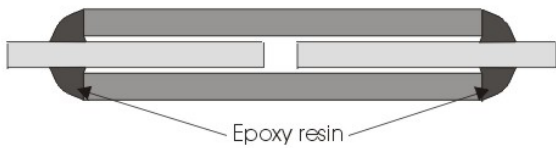
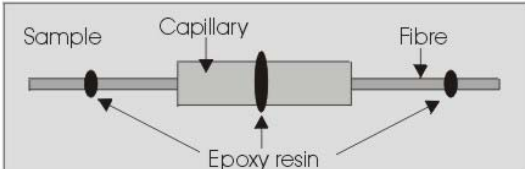
Sensor design type	Schematic of EFPI design	Reference
Fused		Badcock & Fernando (1995)
Tapered and fused		Levin & Nilsson (1996)
Fused and glued		Shyprykevick <i>et al.</i> (1993)
Glued		Lee <i>et al.</i> (2002) Lee, <i>et al.</i> (2001) Carman <i>et al.</i> (1993)
No fibre/capillary attachment		Mitrovic & Carman (1994) Carman <i>et al.</i> (1993)

Table 2-1 A selection of different EFPI sensor designs investigated for fatigue performance.

Fatigue testing was performed on intensity-based optical fibre sensors embedded in glass fibre reinforced epoxy composites (Lee *et al.*, 2001). The sensors were based on

an EFPI sensor construction. The T/T fatigue testing was done at a stress ratio (R) of 0.1 and at a frequency of 5 Hz. Three stress levels were tested, which equated to strain levels of 0.23%, 0.4% and 0.46%. In each case the sensor survived well past a million cycles, which compared to electrical resistance strain gauges, with a fatigue life of a million cycles at $\pm 0.15\%$ strain, show that these sensors should be suitable for use in fatigue applications. At the lowest stress level, the composite and sensors survived until the test was stopped at 3.35×10^6 cycles. In the cases of higher applied stress, the sensors failed prior to the failure of the sample. For many of the samples, it was concluded that the sensor failed where the optical fibre entered the capillary tube. This was determined by the presence of light bleed out from the sensor. In the results reported the EFPI sensors matched closely the strain measurements from the extensometer, though only one specimen seemed to have been tested for each experimental set-up.

Kalamkarov *et al.* (2000) worked on embedded EFPI sensors in pultruded glass and carbon fibre composite tendons, that were subjected to fatigue loading at a stress ratio of $R=0.6$ at a frequency of 1 Hz. The fatigue loading regime related to approximate strain values of $900 \mu\epsilon$ to $1400 \mu\epsilon$ for the carbon fibres samples and $2000 \mu\epsilon$ to $3250 \mu\epsilon$ for the glass fibre samples. EFPI sensors in both glass and carbon fibre composite samples were subjected to 10^5 cycles, after which agreement was found between the sensor and a surface-mounted extensometer. There is no indication of the number of samples used to investigate this effect and no reference tendons appeared to have been tested, so no conclusions could be drawn on the effect of embedded sensors on the fatigue performance of the composite tendons.

Levin and Nilsson (1996) investigated EFPI sensors in tensile and compressive static testing and dynamic tensile testing. The sensors were embedded into carbon fibre epoxy composites. From the static tests the EFPI sensor had a function limit of 0.20% strain in tension and 0.79% strain in compression. The fatigue testing was carried out to only 100,000 cycles at four tensile strain levels, and with a stress ratio of 0.02 at a frequency of 1 Hz. To determine the reliability of the EFPI sensors during fatigue loading, the strain response was compared to the response from the first cycle. There

was no strain gauge or extensometer used to compare the strain response from the EFPI sensors, so the work was carried out on the assumption that the properties of the composite did not change over the test period. Three samples were tested at a strain level below 0.2%, two of these showed no more than 1% strain discrepancy over the 100,000 cycles compared to the first cycle. The third sample showed some discrepancy after 10,000 cycles. For the samples above 0.2% strain the discrepancy was visible from the beginning of testing. Therefore, this work concluded that the EFPI sensors still respond after 100,000 cycles provided the strain does not exceed 0.2%. As no other means of assessing the strain levels within the samples was used, it was not clear whether the strain data from the EFPI sensors was accurate. Samples were only tested to 100,000 cycles which is only a portion of a typically service life of a composite component.

An EFPI sensor was used to investigate the fatigue performance of carbon fibre reinforced epoxy composites (Badcock and Fernando, 1995). Fatigue testing was carried out at stress ratios of $R=0.1$ (T/T) and $R=-1$ (T/C) which generated a maximum strain of 0.4%. The testing was carried out at a constant load rate of $250 \text{ kN}\cdot\text{s}^{-1}$ as the rate sensitivity of the composite was unknown. It was reported that the inclusion of an optical fibre sensor in the composite sample made no significant difference in the fatigue performance of the composite in both T/T and T/C loading regimes. The performance of the sensor though was more complicated. In the case of the testing at $R=0.1$ when the sensor was compared to the extensometer response, it was found that scatter had developed after 50,000 cycles. The authors suggested that the reason for this was debonding of the sensors from the matrix. In the cases where a compressive element was introduced to the loading regime ($R=-0.25$), the sensor response deviated from the predicated values. This was attributed to the endfaces of the sensors coming into contact during the compressive loading. This prevented the effect of compressive fatigue loading on the response of the EFPI sensors to be investigated fully.

Mitrovic and Carman (1994) report the use of EFPI sensors in the investigation of T/T fatigue performance of metal matrix, ceramic matrix and polymer matrix composite systems. However, in the case of the polymer matrix composite samples, no sensor data

was provided. For the metal matrix and ceramic matrix composites the EFPI sensors were surface mounted. The fibres were not attached to the hollow tube, instead each component of the sensor was attached to the sample individually using an adhesive, with the hollow tube purely used for the alignment of the optical fibres. This meant that the gauge length of the sensors was the distance between these adhesive fixings. However, no mention is made of how the gauge length was determined or its accuracy. The performance of this type of sensor is dependant on the adhesive used to attach the components to the sample. For the metal matrix composites, the gauge length was approximated to be 12 mm, and for comparison an electric resistance strain gauge was also attached although this only survived for 10,000 cycles. Therefore, for the majority of the testing there was no reference strain data to compare to the performance of the EFPI sensor. Of the 5 metallic samples tested, only 1 survived to a million cycles, therefore, only 1 sensor was subjected to a million cycles, which it survived. For the ceramic matrix composite samples, the EFPI sensors were mounted alongside an extensometer. During static testing the EFPI and extensometer maintained agreement, but during fatigue the results were inconsistent, but both did survive until a million cycles. Overall from this published work it can be stated that the EFPI sensors design used can survive up to a million cycles on metal and ceramic matrix composites, but it is not clear as to accuracy of the strain data produced. The authors also note that the choice of resin used to adhere the EFPI was critical for this work, particularly on the ceramic matrix composites. To deal with the surface cracks that developed during fatigue testing of the ceramic composite the adhesive had to be changed from a cyanoacrylate to an epoxy resin, but it was not clear as to why this change succeeded.

Shyprykevich *et al.* (1993) attached EFPI sensors to metallic (aluminium) and carbon fibre composite samples that were then subjected to T/T fatigue loading. All samples had an EFPI sensor and electrical resistance strain gauge surface mounted; the composite samples also had an EFPI sensor embedded. For the composite sample the EFPI sensors showed negligible hysteresis up to 100,000 cycles at a maximum cycling load equivalent to 4,000 $\mu\epsilon$. There was, however, no correlation of the EFPI sensors to the strain gauges shown or a correlation between the surface-mounted and embedded EFPI sensors. During testing of the metallic sample, the crack tip passed the EFPI

sensor at 10,000 cycles but did not break it. After this point the sensor was responding to crack opening displacements not strain within the material, so this generated limited information on the long-term fatigue performance of the EFPI sensors.

Carman *et al.* (1993) tested two samples to investigate the survivability of EFPI sensors to fatigue loading. Both CFRP samples had EFPI sensors embedded and the first sample also had a surface mounted EFPI sensor alongside an extensometer. There was a difference between the designs of the surface mounted and embedded EFPI sensors. The surface mounted sample did not have the optical fibres adhered to the hollow tube; instead the individual components were directly attached to the sample using an epoxy adhesive. The embedded sensors had the optical fibre adhered to the hollow tube also by the use of an epoxy resin. For the first specimen, which was cycled to a maximum strain of 3600 $\mu\epsilon$, the surface mounted EFPI sensors were within 4% of the extensometer readings up to 90,000 cycles. At this point, delamination began and it is concluded by the authors that the deviation of the surface mounted EFPI is due to its location nearer the edge of the composite compared to the extensometer which was positioned in the centre of the sample. The embedded EFPI showed a difference in strain of 17% when compared to the external sensors, which was attributed to the epoxy used to adhere the fibres to the hollow tube being unsuitable for the temperature experienced during the processing of the composite. The EFPI sensors still provided data up to the point where the test was stopped at 7 million cycles. However, on examining the graph presented for the strain measured by the EFPI sensors the usefulness of the obtained data is questionable and this author opinion's is that a life time of approximately 100,000 cycles would be more realistic for the sensors. The second sample was subjected to a higher loading level, equivalent to 6200 $\mu\epsilon$. Again with this sample the measured strain by the EFPI-embedded sensor was significantly larger than expected and was explained by the degradation of the epoxy resin used in the sensor manufacture affecting the gauge length of the sensor. The sample failed around 100,000 cycles, with the EFPI sensor still responding prior to failure. This work shows that the EFPI sensors can survive tension/tension fatigue; however, getting the response to be reliable during the fatigue loading is a more difficult problem.

Summary

The examination of EFPI sensors under cyclic loading has been mainly constrained to T/T loading. Within that work it has been shown that it is possible for the EFPI sensors to survive a fatigue-loading regime but the extent of that survival is variable as is the reliability of the response of the sensors. From Table 2-2 it can be seen that in the case of the results report from testing carried out at a maximum of 4000 $\mu\epsilon$, the sensor response varies from survival until 2,724,000, survival to 100,000 cycles or the development of scatter after 50,000 cycles.

Reference	Material	Fatigue Conditions	Maximum Strain	Results
Lee <i>et al.</i> (2002)	CFRP 24 ply (90, ± 45 , 0) _{s3}	R=0.1 Frequency=5Hz	2800 $\mu\epsilon$	Testing stopped at 10 ⁶ cycles, sensor survived
			5500 $\mu\epsilon$	Testing stopped at 10 ⁵ cycles as scatter developed in response
Lee <i>et al.</i> (2001)	GFRP 16 ply (0 ₂ , 90 ₂ , 0 ₂) _s	R=0.1 Frequency=5Hz	2300 $\mu\epsilon$	Test stopped 3,350,000 cycles, sensor survived
			4000 $\mu\epsilon$	Sensor failed at 2,724,000 cycles
			4600 $\mu\epsilon$	Sensor failed at 1,160,000 cycles.
Kalamkarov <i>et al.</i> (2000)	CFRP Pultruded 62% volume fraction	R=0.6 Frequency=1Hz	1400 $\mu\epsilon$	After 10 ⁵ cycles the sensors were still in agreement with extensometer
	GFRP Pultruded 64% volume fraction		3250 $\mu\epsilon$	
Levin & Nilsson (1996)	CFRP 20 ply (0 ₂ , 90 ₂ , 0 ₂ , 90 ₂ , 0 ₂) _s	R=0.02 Frequency=1Hz	2000 $\mu\epsilon$	Testing stopped at 10 ⁵ cycles, sensor survived
Badcock & Fernando (1995)	CFRP 16 ply (0, 90 ₂ , 0 ₂ , 90, 0, 90) _s	R=0.1 Loading Rate = 250 kN·s ⁻¹	4000 $\mu\epsilon$	Scatter apparent after 50,000 cycles
Shyprykevich <i>et al.</i> (1993)	CFRP 16 ply (± 45 , 90, 0 ₂ , ± 45 , 0) _s	R=0.1	4000 $\mu\epsilon$	Testing stopped at 10 ⁵ cycles, sensor survived

Table 2-2 Summary of EFPI survival during fatigue testing.

There could be several reasons for the differences in the published work, such as different sensors designs were employed, which were then applied to different composites, glass or carbon, polymer or ceramic. This leads to difficulties in the application of EFPI sensors to fatigue conditions, as without doing an investigation into a particular design's fatigue response, little confidence can be achieved in the performance of the sensor.

However, most authors seem to agree that the static response range of the sensors is greater than that in fatigue, with a fatigue strain limit of approximately 0.3% being typical compared to over 1% in static applications.

Overall the extent of the investigations into the fatigue responses of EFPI sensors is limited. The published works do not agree and there is very limited work on the response when compression is included in the loading cycle.

2.2.2 Effect of embedded fibres and sensors on the mechanical properties of composites

The work in Section 2.2.1 mainly dealt with the effect of fatigue loading on the response of the EFPI sensors. There is, however, another aspect that needs to be considered when embedding any sensor type into a structure, that is the effect of the inclusion of a sensor on the mechanical properties of that sample. Most of the work on this topic deals with optical fibres embedded in composites rather than EFPI sensors. This is still relevant as an optical fibre is a best-case scenario in comparison to an EFPI sensor.

2.2.2.1 Effect of embedded optical fibres on the static mechanical properties of AFRC

This section deals with the effect of embedding an optical fibre or optical fibre sensor into fibre reinforced composite samples on the static mechanical properties of the composite.

Roberts and Davidson (1991) investigated the effect of embedded optical fibres on various mechanical properties of a carbon fibre/epoxy composite. The properties examined were transverse and longitudinal tension, longitudinal compression, inter-laminar and in-plane shear. Initial transverse tensile testing was carried out on a range of fibres with cladding diameters varying from 80 μm to 300 μm and coating diameters of 93 μm and 500 μm , with all fibres placed parallel to the reinforcing fibres. It was found that the fibres had little effect on the reported Young's modulus for the samples but the failure stress was reduced. This was most noticeable for the larger diameter fibres with strengths reduced by 44% due to the inclusion of a bare fibre with a diameter of 300 μm .

The authors then moved on to the remaining tests of longitudinal tension and compression, and inter-laminar and in-plane shear. For this work only two of the fibres were used, the 103 μm acrylate coated fibre and the 93 μm polyimide coated fibre, with samples having the optical fibres orientated parallel and perpendicular to the reinforcing fibres. There appeared to be no effect on the longitudinal tensile, inter-laminar shear and in-plane shear results due to the inclusion of either optical fibre type or either orientation. A reduction of approximately 26% for the longitudinal compression strength was seen when the optical fibres were placed perpendicular to the reinforcing fibres, but not when the optical fibre was parallel to the reinforcing fibres. However, when the same tests were repeated but on a different carbon fibre-epoxy composite system, no reduction was seen in the compressive strength for either orientation of optical fibre. The authors do not suggest any reasons for this discrepancy. From this it can be concluded that the effect of embedding an optical fibre within a composite can be minimised by the selection of fibre size and orientation within the matrix. Also particularly for compressive properties the choice of composite appears to be important.

The static axial tensile properties of a glass fibre reinforced transparent composite with either 1 or 3 embedded optical fibres was investigated (Lee *et al.*, 1995). Also reference samples with no optical fibres were made. Unidirectional and cross-ply samples were evaluated with optical fibres placed centrally in the 0° direction. The optical fibres used had their acrylate coating stripped off prior to embedment, leaving the cladding exposed

with a diameter of 125 μm . Axial test specimens were manufactured and on testing no significant effects were found on stiffness, strength or Poisson's ratio of the samples, although slightly more scatter was apparent for the samples with 3 optical fibres.

Surgeon and Weavers (1999) reported on the testing of a quasi-isotropic carbon fibre composite with embedded polyimide optical fibres. The laminate lay-up was $[0^\circ, \pm 45^\circ, 90^\circ]_s$ with an optical fibre placed in each sample along the 90° direction at one of the following interfaces: $0/+45$, $+45/-45$, $-45/90$ or $90/90$. The mechanical testing carried out included tensile, 3-point bend and 4-point bend. For all test methods, a reduction was only noticed for those samples with an optical fibre at the $0/+45$ interface. In the tensile testing the reduction was about 7%, rising to 25% for the 4-point bend and 51% for the 3-point bend testing. It was mentioned that 5 samples were tested for each case, but there was no indication of the scatter on any of the results presented. The explanation given by the authors was that the main loading bearing ply, 0° , was significantly distorted by the inclusion of the optical fibre in the 90° direction, and this was the cause of the premature failure. This explanation was reinforced by the fracture mechanism, only the samples with the optical fibre near the 0° ply failed through the initiation of a crack at the same location as the optical fibre.

Several other published works also show that when the optical fibres are embedded in the same direction to the nearby reinforcing fibres there is little detrimental effect of that inclusion. Fox *et al.* (1991) found that it was unlikely the inclusion of an optical fibre aligned with the reinforcing fibres would cause any major problems. But, if they were placed perpendicular, the generation of voids or resin rich regions could significantly affect the properties of the composite. Similar results were found when mechanical testing of CFRP samples with embedded optical fibres was carried out by Skontorp (2000) and Leka and Bayo (1989).

Carman and Sendekyj (1995) reviewed the effects of embedding optical fibres within composite materials. Overall it was reported that the inclusion of an optical fibre at any orientation did not have a significant effect on tensile strength. However, for

compressive strengths an overall degradation was noticed, particularly when the fibre was positioned perpendicular to the reinforcing fibres and loading direction.

Case and Carman (1994) further examined the effect of optical fibres embedded perpendicularly to the reinforcing fibre in the composite structure under compressive loading. An analytical model of the geometry of the plies around the optical fibres was implemented in a compression strength analysis. The results from the model showed the trends associated with the compression strength degradation reported from experimental work. Also the model showed that optical fibres at an angle of 30° to the reinforcing fibres can have as significant effect on the strength as those at 90° .

Summary

There are many factors that can contribute to the magnitude of the effect caused by the embedment of optical fibres; these include the mechanical property of interest, the laminate stacking sequence and the orientation and position of the optical fibre within the composite sample. The effect is typically minimised by positioning the fibre between two plies with the same orientation as the desired direction of the sensor. Also it has been reported that compressive properties are more affected than tensile properties.

2.2.2.2 Effect of embedded optical fibres on the fatigue properties of AFRC.

This section deals with the effect on fatigue properties of fibre reinforced composite samples when an optical fibre or optical fibre sensor is embedded.

Roberts and Davidson (1992) examined the short term T/T fatigue behaviour of a carbon/epoxide composite system with embedded NiTiNOL wire actuators and a $125\ \mu\text{m}$ optical fibre with a $15\ \mu\text{m}$ thick coating of polyimide. The actuators were embedded parallel to the reinforcement in a unidirectional lay-up. The optical fibres were placed in a cross-ply laminate parallel to the 90° reinforcement at a $0^\circ/90^\circ$ interface. Transverse tensile specimens were manufactured. Static results obtained showed that neither the actuator nor the optical fibres had any significant effect on the transverse

strength of the composites. The fatigue results from the unidirectional composite showed a large range of scatter but with no obvious effect from the inclusion of the actuators. The embedment of the optical fibres within the cross-ply did not appear to initiate premature fatigue degradation of the composite. However, for the optical fibre samples each sample was tested at a different load level and no reference samples were tested.

The effect of including optical fibres sensors on the T/T fatigue performance of a glass fibre reinforced composite was examined by Lee *et al.* (1995). The work from this paper involving the effect on static mechanical properties was presented in Section 2.2.2.1. In the fatigue investigation, reference unidirectional and cross-ply laminates were investigated, followed by the inclusion of 3 optical fibres in the unidirectional laminates and 1, 3, 5 or 7 optical fibres embedded in the cross-ply laminate. The number of cycles required to fail the samples decreased significantly as the number of optical fibres was increased. This is in contrast to the static results where there was no significant effect of including optical fibres into these composite laminates. Although this work is on glass fibre composites, it shows that even if static properties are not affected by the inclusion of optical fibres the fatigue properties can still be reduced significantly. The authors also noted that under fatigue loading the optical fibres failed at a few cycles, thereby making simultaneous studies into the fatigue properties of optical fibres and the composite very difficult.

Benshekchou and Ferguson (1998) used flexural fatigue testing to examine the effect of stripped optical fibres on the performance of carbon fibre composite samples. The lay-up sequence used was $[(\pm 45^\circ, 90^\circ, 0^\circ)_2]_s$, with a total of four samples manufactured. One sample had no embedded optical fibre, the others had an optical fibre positioned at one of the following interfaces, $90^\circ/0^\circ$, $0^\circ/0^\circ$ or $\pm 45^\circ$. The testing was stopped at specified intervals to allow ultrasonic examination of the samples. The results show that the inclusion of an optical fibre reduced the fatigue performance of this composite, the effect being more pronounced when the optical fibre is not parallel to nearby reinforcing fibres. To enable more confidence in these results, the experiments should have been repeated, as one test per set-up is insufficient to draw meaningful conclusions.

In 1999 Surgeon and Wevers also reported on the fatigue testing of quasi-isotropic carbon fibre composite with embedded polyimide optical fibres. The laminate lay-up was $[0^\circ, \pm 45^\circ, 90^\circ]_s$ with the an optical fibre (OF) placed in each sample along the 90° direction at one of the following interfaces: $0/+45$, $+45/-45$, $-45/90$ or $90/90$. The fatigue regime followed was T/T at $R=0.1$ with maximum stress levels of 50%, 65% and 80% of the ultimate tensile strength (UTS). Four samples were tested for each interface/stress level combination. At 50% all samples survived up to 10^6 cycles, so no difference could be detected. At the 80% stress level the scatter was too severe for meaningful discussions, with the reference samples failing on average at 81189 cycles, but with a standard deviation of 96570 cycles. The cycles to failure results obtained from the testing at 65% stress are presented in Table 2-3.

Sample	Number of cycles to failure				
	Reference	OF at $0/+45$ interface	OF at $+45/-45$ interface	OF at $-45/90$ interface	OF at $90/90$ interface
1	1,000,000	487,455	1,000,000	47,275	1,000,000
2	1,000,000	30,000	18,288	123,175	1,000,000
3	1,000,000	200,000	1,000,000	47,090	1,000,000
4	1,000,000	300,000	776,035	1,000,000	1,000,000

Table 2-3 Summary of fatigue results carried out at 65% stress level on composites with embedded optical fibres by Surgeon and Wevers (1999).

It was seen from the data that only the reference samples and those with the optical fibre embedded between two aligned plies consistently survived to a million cycles. The other results show significant scatter, but overall the samples with the optical fibre embedded near the 0° ply appear to on average perform worst. It was concluded that the inclusion of an optical fibre does affect fatigue performance, with the worst case being the optical fibre embedded near to and perpendicular to the 0° .

Surgeon and Wevers investigated further this fatigue behaviour by interrupting the tests to allow the damage accumulation to be studied by radiography (2001). The samples were made as in the previous paper (Surgeon and Wevers, 1999), with the testing limited to one stress level (65% of UTS). This was the stress level at which the previous study had shown significant differences between the samples. Testing was

stopped at 100, 1000, 10000, 25000, 50000 and 100000 cycles to study the damage. The steps involved in the damage accumulation in this type of laminate is as follows:

- i) matrix cracking in 90° ply;
- ii) matrix cracking in $\pm 45^\circ$ plies;
- iii) cracks then interact at the $-45^\circ/90^\circ$ interface to form delaminations; and
- iv) these lead to an increased load on the 0° plies and thereby fracture.

Three parameters were used to quantify the damage in this study, the number of 90° matrix crack, total length of 90° matrix cracks and delamination area. In all cases but the samples with the fibre at the $-45^\circ/90^\circ$ interface, the results were very similar. The inclusion of the optical fibre at the $-45^\circ/90^\circ$ interface showed an increase in the number and length of matrix cracks present and the delamination area. These results agree with the previous data in that the presence of an optical fibre at the $-45^\circ/90^\circ$ interface reduces the fatigue performance of the composite. However, these results do not explain the reduction in the performance of the sample with the optical fibre at the $0^\circ/45^\circ$ interface, as no difference is noted between that sample and the reference sample. This is due to the optical fibre affecting the strength of the 0° ply not the build up of matrix damage.

Summary

From the work presented on the influence of embedded optical fibres on the fatigue performance of fibre-reinforced composites, most authors agree that the optical fibre can degrade the fatigue life. This is most noticeable when the fibre is not aligned with the surrounding reinforcing fibres, or when placed at an interface where fatigue damage is typically initiated. However, when the optical fibre is aligned with the reinforcing fibre and the loading direction the effect appears to be minimised and in some cases no effect is noticed. For example, Lee *et al.* (2002) and Badcock and Fernando (1995) found that the inclusion of EFPI sensors aligned with the reinforcing fibres appeared to have no significant effect on the fatigue performance of carbon fibre reinforced composite samples.

2.2.3 T/C fatigue of CFRP

Curtis (1987) presented a detailed review on the fatigue of fibre-reinforced composites. The T/C fatigue loading was described as the worst regime for fibre reinforced composite samples as it combines damage from both tension and compression loading. For carbon fibre composite samples under tensile loading the failure is dominated by the properties of the fibres. However, in compressive loading the fibres are still the principal load bearing elements, but the matrix and fibre/matrix interface must stop the fibres from becoming unstable and undergoing microbuckling. The integrity of the matrix and the interface are, therefore, much more critical in compressive loading as compared to tensile. Also, because layers without fibres in the test direction can develop damage that in tensile loading is not an issue, the fibres aligned with the loading direction continue to take the load. Whereas in compression this damage can lead to local layer instability and layer buckling, this can occur before resin and interface damage leads to fibre micro-buckling. Because of this reason the fatigue life in T/C loading is usually shorter than that for tension only or compression only loading regimes. This was shown by Curtis (1989) through an S-N plot for a CFRP material. On this plot were curves showing the response of samples to a T/T loading regime and a T/C loading regime. There was a significant drop in the number of cycles before failure from the T/T regime to the T/C loading.

The reduction in fatigue life due to T/C loading has been demonstrated by Nyman (1996) and Gamstedt and Sjögren (1999). Nyman investigated CFRP laminates under a range of stress ratios, including $R=-1$ (T/C). For the data obtained on quasi-isotropic laminates it was shown that the T/C fatigue loading caused a reduction in the fatigue resistance of the samples compared to T/T. In the case of T/C loading the samples failed at 10^5 cycles at a strain of 0.55%, whereas under T/T loading the strain required to reach failure at 10^5 cycles was around 1%. Gamstedt and Sjögren also described how T/C fatigue was worse than T/T for fibre reinforced composite samples, with a note that the reasons for this behaviour are not fully understood. However, it was suggested that for multidirectional laminates a transverse crack could cause delamination and buckling

of the composite under compression, leading to fibre breakage in the tensile phase of the loading cycle.

Rotem and Nelson (1989) examined the T/C fatigue performance of carbon fibre composite samples. The laminates investigated were unidirectional (UD), cross-ply ($0^\circ/90^\circ$) and angled ply ($\pm 45^\circ$). Short samples were used for this work, rather than guides to prevent buckling of the samples. It was found that the type of fatigue failure, tensile or compressive, was mainly determined by the static properties. The unidirectional and cross-ply samples had a lower compressive strength than tensile and most of the fatigue failure occurred in compression. Whereas for the angled ply samples the tensile strength was lower and the fatigue samples failed in tension. It was also shown that the introduction of cross plies reduced the lifetime of the component significantly. For the UD samples Rotem and Nelson found that they would survive to 10^5 cycles at an amplitude stress of 1200 MPa, whereas the $0^\circ/90^\circ$ cross-ply samples could only reach that number of cycles at an amplitude stress of 600 MPa.

Other works on T/C fatigue of CFRP laminates include stiffness change (Rotem, 1989), life predication (Lamela *et al.*, 1997 and Gathercole *et al.*, 1994), the effect of notches (Soutis *et al.*, 1991) and even the effect of cryogenic temperatures (Hartwig *et al.*, 1998).

2.2.3.1 Effect of frequency on the fatigue behaviour of fibre reinforced composites

Another aspect of fatigue testing of fibre reinforced composites is the choice of test frequency; this is due to the viscoelasticity and low thermal conductivity of the polymeric matrix (Hull and Clyne, 1996). At higher frequencies the strain is applied at a higher rate that can cause greater damage as there can be insufficient time for creep and stress relaxation generating hysteresis heating. The low thermal conductivity can prevent the sample from dissipating this heat and if the resin was to reach its glass transition temperature significant changes will occur to its mechanical properties, which could lead to premature failure of the composite.

Rotem (1993) also investigated the effect of test frequency on the fatigue performance of an isotropic carbon fibre/epoxy laminates. The frequencies studied were 0.1, 1, 2.8, 10 and 28 Hz. In this case there was a reduction in fatigue life of the samples tested between 2.8 and 10 Hz, but the failure process was not dependant on frequency as all samples failed in a similar manner. The reason given for the detrimental effect of frequency on the fatigue life was hysteresis heating, but no temperature measurements were carried out to examine this possibility.

Barron *et al.* (2001) examined the frequency effect on the fatigue behaviour of unidirectional, $0^\circ/90^\circ$ cross-ply and $\pm 45^\circ$ angled ply laminates. Testing was carried out at 5, 10 and 20 Hz at a stress ratio of 0.1. For the unidirectional laminates no effect of the frequency changes was noticed, possible due to the large scatter within the results. The cross-ply samples also showed significant scatter, with no differences noticed in the S-N curves. The main difference was shown in the maximum strain monitored during testing. At 10 and 20 Hz larger strains were observed compared to the samples tested at 5 Hz, which due to the load controlled nature of the testing indicated a change in the modulus of the material as the frequency increased. The angled ply samples showed a much greater dependence on the testing frequency. The samples tested at 20 Hz showed much shorter fatigue lives with a significant increase in maximum strain experience compared to those at 5 and 10 Hz. In agreement with Rotem (1993), hysteresis heating was given as the reason for the reduction in fatigue performance due to the increasing frequency. In this case temperature measurements were reported for the cross-ply samples. Unfortunately, the description of the results and the results presented in the graph do not match up, so it was difficult to assess the results. The results appear to indicate that at 5 Hz the samples increase in temperature by approximately 10°C , whereas at 10 and 20 Hz the increase is up to 25°C , with the 10 Hz samples taking almost an order of magnitude more cycles to achieve this than those at 20 Hz.

Curtis (1989) suggests that to reduce the influence of hysteresis heating, the fatigue testing should be carried out at a constant rate of stressing. Also, the laminates that are most susceptible to hysteresis heating are those with few or no fibres in the loading direction and where the resin has viscoelastic behaviour. It was summarised that for

laminates that have the majority of fibres in the loading direction and testing involving small strains, test frequencies of 10 Hz are suitable, whereas for resin dominated laminates, the tests should be carried out at frequencies below 5 Hz.

Summary

The performance of CFRP under fatigue conditions has shown that the resistance to T/C regimes is less than that for either T/T or C/C. This is due to T/C fatigue generating tensile and compressive damage, whereas the other regimes only have one of these types. Also, the inclusion of transverse and angled plies reduces the fatigue life of the composite.

As for the effect of frequency on CFRP composite samples, it appears that care needs to be taken as the properties can be dependant on the frequency chosen, mainly due to hysteresis heating of the samples.

2.3 Interfacial Aspects of Fibre Optic Sensors

It is important for any type of sensor to be in good contact with the sample being monitored. In the case of a strain sensor, the sensors must be in a position to be subjected to the strain experienced by the sample. This typically means in intimate contact with the sample, therefore generating an interface between the sample and the sensor. The durability of this interface is also important, as if it were to degrade with time or loading conditions the sensors would no longer be subjected to the strain experienced by the sample.

2.3.1 Strain transfer to fibre optic sensors

The requirement for the sensor/sample interface, in the case of strain sensors, is successful strain transfer from the sample to the sensor. Most of the work associated with the modelling and investigation of strain transfer to FOS examines the use of

coated optical fibres. In the case of EFPI sensors the surface generating the interface is silica, not polymeric as in the case of coated optical fibres.

Méndez *et al.* (1993) attempted to use optical fibre cables as intensity-based stress sensors within cement samples. Initial testing involved pull-out of the cable from cement to determine the interfacial bond strength. It was found that all the cables pulled out from the cement with little resistance (approximately 3 N). On examination of the cable it was found that the outmost plastic jacket was not developing any bond with the cement. To evaluate the cable as a strain or damage sensors, 4-point bend tests were carried out on cement cylinders with embedded cables. During testing, the throughput intensity from the cable showed very little change, with the cable surviving the failure of the samples. These results showed that without a bond between the sensor and the sample, the sensor could not sense any of the stress changes within that sample.

Discussions by Urruti and Wahl (1990) on the affect of coating on fibre performance lead to the conclusion that optical fibre sensors must have sufficient bond to the surrounding materials to enable thermal or mechanical changes in the matrix to affect the light transmission in the fibre. It was also said that thinner coatings were likely to be best for sensing applications but with these coatings the strength of the fibres was likely to be reduced. However, there was no evidence presented to support the reduction in strength of the fibre due to different coatings. Urruti and Wahl suggested that a compromise is required between the strength of the sensors and their sensitivity. However, the more likely compromise, in the opinion of this author, is one between sensitivity and size of fibre, as it is the size of the fibre which must be chosen to minimise any effect on the sample it is embedded in.

A stage further in the optimisation of the coating for FOS was described by Barton *et al.* (2002). From the finite element modelling carried out it was determined that there was a optimum combination of coating thickness and Young's modulus, typically as coating thickness increased the Young's modulus also needed to increase.

Ansari and Libo (1998) carried out an investigation of the strain transfer to coated optical fibres. The coatings of optical fibres are typically polymeric and due to their differences in mechanical properties compared to the fibre and specimen can cause incomplete strain transfer. This is because a portion of the strain is lost through the interface shear transfer within the polymeric coating. Also, all interfaces were assumed to have perfect bonding. It is suggested by the authors that in the case of bare fibres, i.e. silica surfaces, there should be no strain loss, still assuming a perfect bond was present.

Yuan and Zhou carried out similar investigation for the embedment of fibre optic strain sensors (1998). A sensitivity coefficient was used to evaluate the percentage of strain applied to the composite that was actually transferred to the optical fibre. It was found that this coefficient was dependent on the length of optical fibre and the material properties of the fibre coating.

There is little work on the strain transfer to EFPI sensors and how efficiently the strain is transferred from the capillary into cavity changes.

2.3.2 Methods of investigating of interfacial shear strength

In the field of fibre reinforced composites there is a large body of work devoted to the investigation of the interface. The silica/resin interface could be considered similar to that of E-glass fibres in composites, this should allow some of the techniques and theories used to evaluate the E-glass fibre/resin interface to be useful in this current work. There are significant differences in the composition of E-glass and optical fibres, these are shown in Table 2-4.

E-glass reinforcing fibres		Optical fibres	
SiO ₂	52%	SiO ₂	99.95%
Al ₂ O ₃ + Fe ₂ O ₃	14%		
CaO	17%		
MgO	5%		
BaO	11%		

Table 2-4 Typical compositions for E-glass reinforcing fibres and optical fibres. (Hull and Clyne, 1996 and Grattan and Meggit, 1999)

Although the compositions are different the factors that affect the glass surface chemistry of the reinforcing fibres can be used to understand that of the optical fibres. However, care needs to be taken in as differences can exist as demonstrated by Eske and Galipeau (1999). In that work quartz surfaces were compared to glass microscope slide surfaces using atomic force microscopy and contact angle measurements. Various treatments were carried out on the surface including acid and base treatments, exposure to etchants and Argon sputtering. Contact angle measurements were performed against distilled water and although the measured values of contact angle were different between the glass and the quartz, similar trends could be observed for the different surface treatments, as seen by the examples given in Table 2-5. Other properties that could be of interest for the E-glass and silica are presented in Table 2-6.

<i>Material</i>	<i>Treatment</i>	<i>Advancing contact angle</i>
Glass	Baseline	50
	Phosphoric acid	28
	Chromic acid	19
	Hydrochloric acid	33
Quartz	Baseline	71
	Phosphoric acid	41
	Chromic acid	27
	Hydrochloric acid	47

Table 2-5 Selection of contact angle results from glass and quartz surfaces. (Eske and Galipeau, 1999)

Property	E-glass reinforcing fibres	Silica optical fibres
Typical diameter	12 μm	125 μm
Density	2600 $\text{kg}\cdot\text{m}^{-3}$	2200 $\text{kg}\cdot\text{m}^{-3}$
Coefficient of thermal expansion	$5.0 \times 10^{-6} \text{ K}^{-1}$	$5.4 \times 10^{-7} \text{ K}^{-1}$
Tensile strength	3.45 GPa	3.6 GPa
Young's modulus	76.0 GPa	73.1 GPa
Refractive index	1.55	1.46

Table 2-6 Selected physical properties of E-glass and optical fibres. (Grattan and Meggit, 1999)

Two main areas that fall within this category of reinforcing fibres information that can be used to understand optical fibres interfaces are the methods used to determine interfacial shear strength (IFSS) and improvements to the interface using silane coupling agents.

2.3.2.1 Main techniques for interfacial shear strength determination

There are currently several methods for assessing the interface between a fibre and a resin system. These vary from the more traditional methods such as pull-out (DiFrancia *et al.*, 1996), fragmentation (Tripathi and Jones, 1998) and micro-indentation (Kalinka *et al.*, 1997) to more novel techniques which include single particle composites (Harding and Berg, 1997), single fibre Broutman test (Ageorges *et al.*, 1999) and non-destructive techniques (Wu *et al.*, 1997a; Mai *et al.*, 1998).

This section deals with the commonly used techniques for determining interfacial shear strength, namely single fibre pull-out or microbond, single fibre fragmentation and micro-indentation. Schematic illustrations of these selected test methods are shown in Figure 2-4 with the main advantages and disadvantages for each technique summarised in Table 2-7.

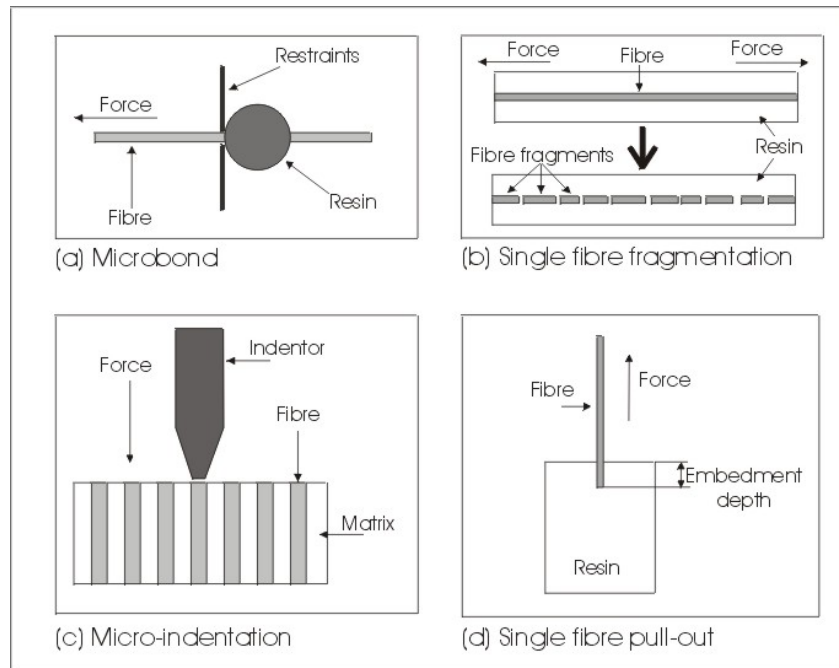


Figure 2-4 Schematics for the common methods of interfacial shear stress determination. (a) Microbond. (b) Single fibre fragmentation. (c) Micro-indentation or push-out. (d) Single fibre pull-out (Etches and Fernando, 2002).

Technique	Advantages	Disadvantages
Pull-out/ Microbond	<ul style="list-style-type: none"> • Direct measurement • Any fibre/matrix combination 	<ul style="list-style-type: none"> • Can have very small embedment depths • Meniscus formation • Difficult sample preparation
Single fibre fragmentation	<ul style="list-style-type: none"> • Large amount of information for statistical analysis • Failure process can be observed 	<ul style="list-style-type: none"> • Limits fibre/matrix combinations • Calculations can be over simplified
Micro-indentation	<ul style="list-style-type: none"> • Real samples • Multiple data points 	<ul style="list-style-type: none"> • Surface preparation could effect results • Failure modes cannot be observed • Fibres can be crushed rather than pushed

Table 2-7 Brief summary of advantages and disadvantages of main interfacial shear stress methods (Herrera-Franco and Drzal, 1992).

Herrera-Franco and Drzal (1992) reviewed these techniques, concentrating on the assessment of the fibre/matrix interactions and the theoretical analyses. It was concluded that none of the techniques provided a complete and definitive method for determining interfacial shear strengths, as although trends could be compared between techniques the actual values were not comparable. It was also recommended that the reliance on these types of results to predict composite properties should be avoided until further research is complete on the understanding of these test methods.

A round-robin programme was undertaken to evaluate the different methods of determining interfacial shear strength (Pitkethly *et al.*, 1993). The methods chosen for investigation were single fibre pull-out, microdebond, fragmentation and micro-indentation. All the laboratories involved in this project were supplied with the same fibre type and resin system, all from the same batch and all followed the same cure schedule. However, each of the laboratories followed their own procedures for the testing of the samples. The authors reported the scatter within each laboratory was acceptable; however, the pull-out/microdebond results have coefficients of variations (CV) between 3% and 33%, the fragmentation tests between 7% and 36%, with the indentation performing best with CV from 9% to 17%. Also, the actual values reported

from each laboratory were significantly different as shown in Table 2-8, but these calculations do not include the scatter from individual laboratories.

	Pull-out	Microbond	Fragmentation	Indentation
No. of laboratories	3	4	6	2
Overall average IFSS (MPa)	64.6	48.3	23.8	47.8
Standard deviation	8.2	14.1	6.6	0.5
Coefficient of variation	13%	29%	28%	1%

Table 2-8 Summary of results from round-robin on IFSS methods (Pitkethly *et al.*, 1993).

The two laboratories that performed micro-indentation testing followed an identical test method and therefore their results were very similar. It was also noted that when the results from the different methods were compared, the values of IFSS were significantly different. The overall average of IFSS determined by fragmentation was 23.8 MPa, whereas for pull-out it was 64.6 MPa. From this it can be seen that it is difficult to compare IFSS results obtained through different methods, and even within the same type of testing due to the variations between individual procedures.

These IFSS test methods may not necessarily reflect the situation where optical fibre-based sensor systems are embedded in the composite. For example, the presence of the reinforcing fibres does not generally feature in the preparation of the test specimen. Furthermore, some of the conventional test methods require specific resin systems to be used. In this current work, an ideal test method would enable a silica/CFRP interface to be investigated. There is some previously reported work on interfaces of optical fibres and resins; however, the work is typically carried out on coated optical fibres.

One example of work done on coated optical fibres is reported by Tsai and Kim (1991). In this case the optical fibres either had a coating of gold or acrylate polymer. The pull-out samples were manufactured from epoxy resin. The aim of the work was to study interface friction, not adhesion or strength. In the case of the acrylate coated fibre the

failure occurred at the silica/acrylate interface. This would be expected, as the acrylate coating is not designed to bond well to the silica, as sections of it are needed to be removed during the application of optical fibres.

Zolfaghar and Folkes (1999) performed single fibre pull-out testing of coated and stripped optical fibres from epoxy resin samples. A reverse casting method was used that eliminated the meniscus from the samples. This was a two stage method involving the manufacture of silicone rubber moulds, followed by the manufacture of the actual samples. There was no mention of control or measurement of the embedment depth. The average interfacial shear strength of the stripped optical fibre with an epoxy resin was reported as 8.1 MPa, with a maximum value of 10.1 MPa. This allows optical fibres to be investigated but only involves a resin not a fibre-reinforced composite.

In the case of the EFPI sensors used in this work, no coating is applied so it is a silica surface that needs to be investigated. To enable the investigation of the silica/CFRP interface to be carried out a variation on the single fibre pull-out technique was developed. This method used stripped optical fibres to provide the silica surface, and carbon fibre prepreg for the manufacture of the sample. The details of this method are presented in Section 3.3.4.

Peters *et al.* (2002) investigated the possibility of measuring the strain within the fibre during a single fibre pull-out test. Samples had 11 or 15 optical fibres embedded with a spacing of 2 mm. The central fibre was a FBG sensor, with a total grating length of 13 mm, half of which was embedded in the epoxy sample. Samples were not taken to failure as the aim of this work was to access this method of measuring strain within a fibre pull-out sample. From the images shown in the paper, it can be seen that significant menisci have built up around the fibres. Although the FBG response alters with applied load it is not clear how this relates to the strain within the specimens. This is an innovative technique that requires further validation to enable better understanding of the fibre pull-out test.

2.3.3 Silane coupling agents

This section presents a brief overview of the chemistry of silane coupling agents. Silane coupling agents are used widely in glass fibre reinforced composites to promote strong bonding between the resin and fibre and improve the interface durability particularly against moisture ingress (Plueddemann, 1991). There are other classes of coupling agents available and some of these are summarised in Table 2-9.

Coupling Agent	General Structure	Typical application	Reference
Silane	$R^1-Si(OR^2)_3$	Glass reinforcing fibres	Plueddemann (1991)
Titanate	$R^2-Ti(OR^1)_3$	Filler particles for polymers	Comyn (1997)
Zirconates	Similar to titanates	Primers for polyolefin films	Kinloch (1987)
Chrome complexes	Inorganic polymers	Aluminium/polyethylene interfaces	Kinloch (1987)

Table 2-9 Summary of selected coupling agents reported in the literature.
 R^1 represents a group to react with the resin, R^2 is typically methyl or ethyl groups

Coupling agents are usually applied as part of the *size*, this is a coating applied to the fibres during processing. A size normally consists of an aqueous solution with a film forming polymer, a lubricant and the coupling agent and is sprayed on to the fibres immediately after manufacture. The aim of the size is to protect the fibres from damage, to aid subsequent processing and to enable a chemical bond between the glass and matrix (Hull and Clyne, 1996).

2.3.3.1 Theory of interaction of silanes with silica

To start with the silica fibres are hydrolysed by the moisture in the air to form the structure as shown in Figure 2-5 (Comyn, 1997; Suzuki and Ishida, 1996).

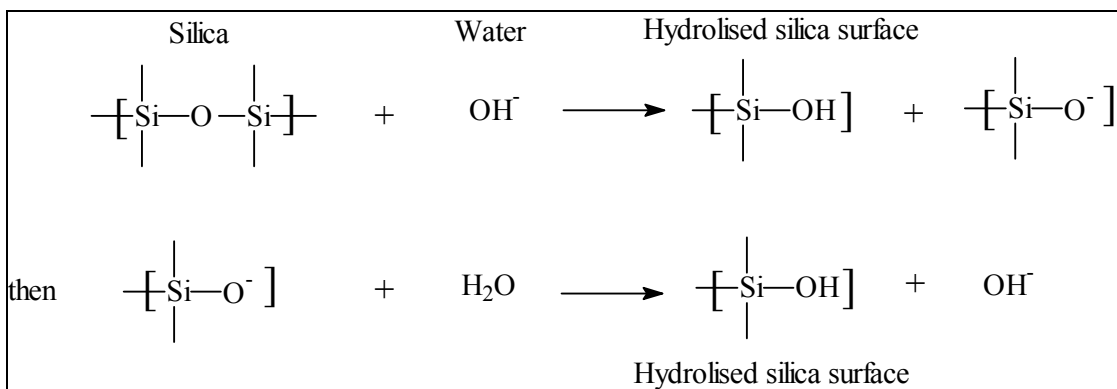


Figure 2-5 Reaction scheme for the hydrolysis of silica.

Silanes are also hydrolysed to the corresponding silanol in an aqueous solution. The silane shown in Figure 2-6 has an R group that represents a group that is likely to interact with the matrix resin.

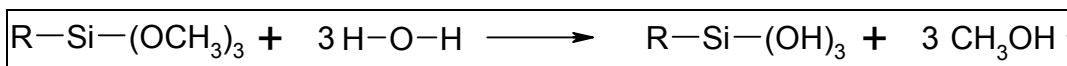


Figure 2-6 Reaction scheme for the hydrolysis of silane (Comyn, 1997).

For example, in the case of an epoxy/amine resin the R group could be an amine molecule designed to interact with the epoxy from the matrix resin, as demonstrated in Figure 2-7.

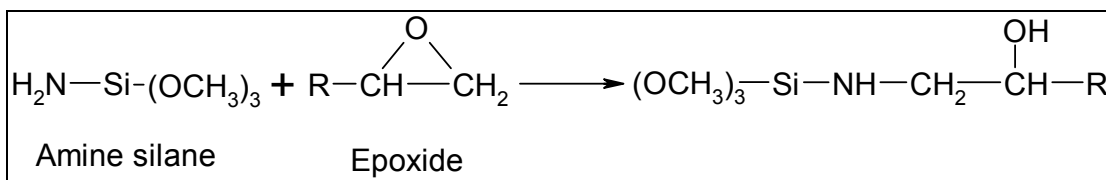


Figure 2-7 Reaction between an amine based silane and an epoxy group. (Comyn, 1997).

When the silica fibres are exposed to this hydrolysed silanol solution from Figure 2-6, the silanol molecules compete with the water molecules to form hydrogen bonds with the hydroxyl groups on the fibre surface. The fibres are then dried which drives the water off and then condensation reactions occur between the silanol and fibre surface and between nearby silanol molecules. This produces a polysiloxane layer bonded to the glass surface presenting a layer of matrix reacting groups to the surface as shown in Figure 2-8.

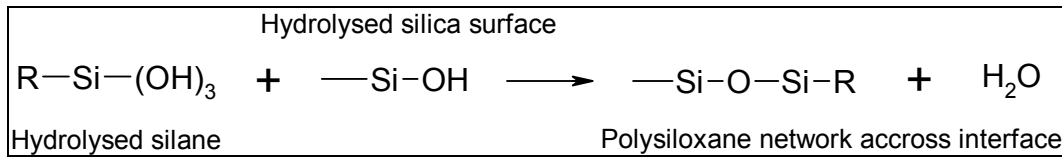


Figure 2-8 Reaction scheme for the formation of a polysiloxane network.
(Comyn, 1997).

2.3.4 Effect of silanes on interfacial properties

As silane coupling agents are designed to interact with both the fibres and the matrix within a composite, it is expected that they would alter the interface between the fibre and the matrix. In line with this a significant amount of work has been published on the affect of silane coupling agents on the interface and the mechanical properties of the composite.

2.3.4.1 Use of silanes on optical fibres

Waite *et al.* (1988) used silane-treated optical fibres as damage and strain sensors in woven glass fibre composite. The optical fibre was used in three states; buffered (not specified), stripped fibre treated with silane and stripped fibre treated with release agent. It was found that the buffered and silane-treated fibres responded well to the strain changes, with the release agent significantly reducing the strain transfer to the fibre. However, no stripped untreated fibres were used, so it is unclear whether the silane treatment enhances the interface between the optical fibre and the resin.

Zolfaghar and Folkes (1999) performed single fibre pull-out testing of optical fibres from epoxy resin samples. Several optical fibres were examined, which were:

- i) acrylate and polyimide coated;
- ii) uncoated optical fibres;
- iii) uncoated fibres treated with an amino-silane in ether solution.

The results showed that the treatment of the optical fibres with silane solutions improved the interfacial shear strength. The untreated optical fibres had an average IFSS of 8.1 MPa while the silane treatment increased the IFSS to 25.8 MPa.

2.3.4.2 Use of silanes on reinforcing fibres

This section deals with the use of silane coupling agents to modify the interface between E-glass reinforcing fibres and resin systems. There is a large volume of work on the effects of silane coupling agents treated E-glass fibres on various physical properties of composites. A selection of published work is presented in Table 2-10.

Property and Test Method		Silane Used	Results		Reference
			Without silane	With silane	
IFSS Microindentation		Aminosilane within P139 commercial epoxy size	72 ±9 MPa	87 ±9 MPa	Bezarti <i>et al.</i> (2001)
IFSS	Fragmentation	3-amino propyl triethoxy silane (γ -APS)	43 ±15 MPa	73 ±18 MPa	Zhou <i>et al.</i> (2001)
	Pushout		30 ±7 MPa	43 ±11 MPa	
Flexural Strength		epoxysilane	394 MPa	605 MPa	Pape (1997)
Transverse tensile strength		γ -APS	27.3 MPa	72.9 MPa	Pisanova <i>et al.</i> (2001)
Adhesion energy Single particle composite		3-amino propyl methyldiethoxy silane	51 mJ·m ⁻²	140 mJ·m ⁻²	Miller and Berg (2003)
Surface energy Capillary rise technique	Dispersive component	Cationic amino silane	16 mJ·m ⁻²	37 mJ·m ⁻²	Bledzki <i>et al.</i> (1997)
	Non-dispersive component		27 mJ·m ⁻²	7 mJ·m ⁻²	

Table 2-10 Selection published data on the effect of silane treatments on various physical properties.

As seen from the results in Table 2-10, silane treatments typically improves the properties of interest, which in most cases is what is required. There are a few exceptions to this typical improvement one of which is reported by Berg and Jones (1998). In that case, the effects of silane treatment on glass fibres were investigated through the use of the single fibre fragmentation technique. The silane used was γ -aminopropyltriethoxy (γ -APS) at 0.1% and 1% concentrations in aqueous solutions. A summary of the IFSS measured by single fibre fragmentation is presented in Table 2-11.

Treatment	IFSS (MPa)
Untreated	49 ±6
0.1% γ -APS	41 ±7
1.0% γ -APS	38 ±10

Table 2-11 Summary of IFSS as reported by Berg and Jones (1998).

The IFSS appeared to decrease with the inclusion of a silane treatment and continued to reduce as the silane treatment level is increased. The authors' explanation of this is that the silane generated an interphase that had reduced shear yield strength. That would explain these results, but does not explain why other work in this field has found a general increase in IFSS due to silane treatment of fibres.

Mäder *et al.* (1994) examined the surface treatment of carbon and glass fibres in an investigation of the relationships between surface, interphase and composite properties. The surface treatment involved the application of an aminosilane or a complete size. Contact angle measurements were performed using a capillary rise technique, which involves the time dependence of the liquid rising within a fibre bundle. The advancing contact angle is calculated through the use of a modified Washburn equation (Jaycock and Parfitt, 1981), which is given in Equation 2-3:

$$\frac{W^2}{t} = \frac{K \cdot \rho^2 \gamma_e \cos \theta}{2\eta} \quad \text{Equation 2-3}$$

Where:

W	weight gain
η	viscosity of test liquid
γ_e	surface tension of test liquid
θ	Contact angle
t	time
ρ	density
K	geometric factor determined by the use of completely wetting liquids

The dispersive and polar components of the surface energy were then calculated from the contact angle, using the Owens and Wendt approach, which is discussed in Section 2.4.1. From the surface energy and pull-out experiments performed, a plot of debonding shear stress against thermodynamic work of adhesion was produced. From this it could be seen that the silane treatment resulted in a reduction in the work of adhesion, from 82 $\text{mJ}\cdot\text{m}^{-2}$ to 73 $\text{mJ}\cdot\text{m}^{-2}$, but a slight rise in the debonding shear strength,

from 39 MPa up to 43 MPa. The lowering of the work of adhesion value was attributed to the aminosilane being hydrophobic and the contact angle testing was carried out against water. The authors reported that at least 10 contact angle measurements were performed for each combination of treatments, but there was no mention of the number of pull-out samples tested and on the results presented there was no indication of the scatter recorded for the samples. It was also reported that a correlation between debonding shear stress, interlaminar shear strength and bending strength existed. However, the correlation is not clear from the results presented.

Wu *et al.* (1997b) examined the effects of silane coupling agents on the performance of glass fibre reinforced composites. Two different types of coupling agents were used, methacryloxysilane (A174) and aminosilane (A1100) as well as mixtures of these two coupling agents. From the experimental work and molecular modelling, the authors concluded that for dry strength, the reaction between the coupling agent and the resin is more important than the reaction with the glass surface. But the chemisorption of the silane agent to the glass surface is essential for hot-wet durability as it is the water absorption to the silane which causes the degradation of the interface and the reduction in mechanical properties.

Bezarti *et al.* (2001) examined the influence of fibre surface treatments on the transverse properties of unidirectional glass/epoxy composites. The surface treatments involved the application of sizes that included an aminosilane coupling agent but had different modifiers. The effect of these sizes was to increase the transverse failure stress and strain of the composite samples. An increase in the interfacial shear strength, measured by micro-indentation, was also an effect of the sizes.

2.3.5 Summary of EFPI interfaces

The interface is regarded as being very important for the implementation of FOS in general. Work has shown that without sufficient interfacial bonding the sensors cannot respond to any strain within the sample.

The type of materials under investigation and the disadvantages of all the methods dominate the current work on IFSS measurement. This leads to the conclusion that for comparison testing the recommended method appears to be whichever method suits the materials of interest.

Silane coupling agents have been shown, in general, to improve the strength of the interface between glass fibres and polymeric matrices. Due to the similarities in the composition of glass fibres and optical fibres, silanes should also improve the adhesion between optical fibres and polymeric matrices.

2.4 Surface Energy of Silica

As discussed in the previous section the interface between the sensors and composite is very important. One parameter that can have significant effect on the interface between two components is the surface energies of those components.

2.4.1 Background theory of surface energy

One method of determining the surface energy of a solid is to measure the contact angle response when tested against a few liquids of known surface energy. This section aims to explain how this is achieved (Comyn, 1997).

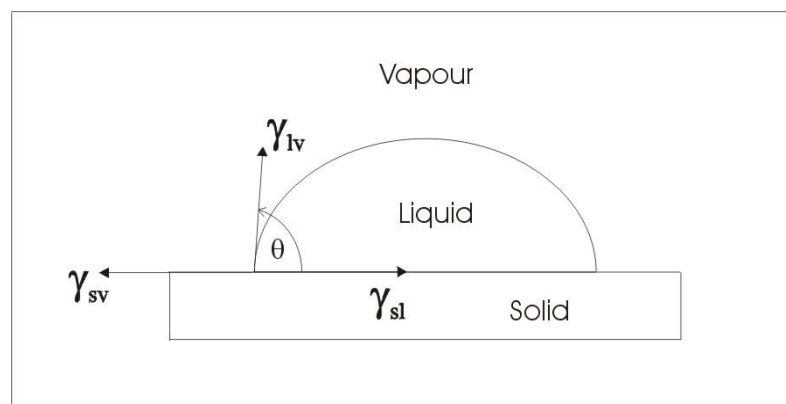


Figure 2-9 Interaction between a solid, liquid and vapour in defining the contact angle.

In Figure 2-9 is shown the contact angle between a liquid and solid. In this figure, γ is the surface energy with the subscripts v , l and s representing vapour, liquid and solid respectively. From this Young's equation (Equation 2-4) can be determined by balancing the forces in the horizontal plane:

$$\gamma_{SV} = \gamma_{SL} + \gamma_{LV} \cos \theta \quad \text{Equation 2-4}$$

This alone is not particularly useful in determining the surface energy of a solid from only knowing information regarding the liquid, as there are two unknowns, the surface energy of the solid and the surface energy of the solid-liquid interface. Therefore, another route needs to be considered.

Surface energies can be split into dispersive and polar components that are related to the dispersive and polar forces at the sample surface, as shown in Equation 2-5, where d represents the dispersive and p the polar components.

$$\gamma_a = \gamma_a^d + \gamma_a^p \quad \text{Equation 2-5}$$

These are both van der Waals forces that are attributed to different effects. The polar component of the energy arises from the orientation of permanent electric dipoles, and their induction effect on polarisable molecules. The dispersive component energy is generated by the internal electron movements that are independent of dipole moments (Kinloch, 1987).

Using the concept of dispersive and polar components, the surface/interface energy between a solid and liquid can be described using Equation 2-6 through the Fowkes and Owen/Wendt geometric mean approaches (Kinlock, 1987).

$$\gamma_{LS} = \gamma_{LV} + \gamma_{SV} - 2(\gamma_L^d \gamma_S^d)^{\frac{1}{2}} - 2(\gamma_L^p \gamma_S^p)^{\frac{1}{2}} \quad \text{Equation 2-6}$$

By substituting Equation 2-6 into the Young's equation (Equation 2-4), the resulting equation (Equation 2-7) allows the surface energy of a solid to be determined by knowing the contact angle between a specific liquid and the solid, as well as the polar and dispersive surface energy components of that liquid.

$$\frac{\gamma_{LV}(1 + \cos \theta)}{2(\gamma_L^d)^{\frac{1}{2}}} = (\gamma_S^d)^{\frac{1}{2}} + (\gamma_S^p)^{\frac{1}{2}} \left(\frac{\gamma_L^p}{\gamma_L^d} \right)^{\frac{1}{2}} \quad \text{Equation 2-7}$$

As Equation 2-7 is in the form of a straight-line graph, it is usual for contact angle measurements to be taken between the solid of interest and several liquids. These results can be plotted on a graph, which should give a straight line with the gradient of $(\gamma_S^p)^{\frac{1}{2}}$ and intercept of $(\gamma_S^d)^{\frac{1}{2}}$. Thereby allowing the surface energy of the solid to be calculated.

2.4.2 Measurement of contact angles

If the solid of interest is a horizontal flat plate, there are three main ways of determining the contact angle between that solid and a liquid. The first two are variations on the sessile drop technique, both involve a drop of a known liquid being placed onto the plate and then either:

- i) directly measuring the angle using a goniometer; or
- ii) measuring the radius and height of the drop and using Equation 2-8:

$$\tan\left(\frac{\theta}{2}\right) = \frac{h}{r} \quad \text{Equation 2-8}$$

Both these techniques require the use of a microscope or projector system. Alternatively, if the sample can be held vertically and attached to a microbalance, the Wilhelmy technique can be used. This involves measuring the force as the solid is partially immersed into the liquid, from which the contact angle can be determined.

However, for this current project, the main concern is the measurement of the surface energy of optical fibres, or very small cylinders. In this case there are two main methods, either a Wilhelmy technique or drop profile method.

Wilhelmy Method

In this case a fibre is suspended from a microbalance and lowered into the test liquid (Comyn, 1997). As the fibre is immersed into the liquid the microbalance records the force experienced by the fibre. This force can be related to the contact angle between the fibre and liquid by Equation 2-9, which is the balancing of the forces in the vertical direction.

$$\text{Force} = \text{weight of fibre} + X \cdot \gamma_l \cdot \cos\theta - \text{bouyancy in liquid} \quad \text{Equation 2-9}$$

Where X is the perimeter, or circumference, of the fibre in contact with the liquid.

Drop profile method

This involves the placement of a liquid droplet directly on to the fibre, and measuring various parameters, such as drop size and fibre diameter (Kinloch, 1987). An example of this technique was demonstrated by Wolff *et al.* (1999). The length and the height of the droplet were measured as well as the fibre diameter. These values were then analysed by a computer program using pressure difference between the liquid and gas and the fibre and drop curvature radii to obtain the contact angle.

2.4.3 Surface energy values for silica and effect of silanes

Silica

A large part of surface energy investigations involving silica is concerned with silica powder rather than fibre and typically contact angle measurements are not used. Silica is classed as having a high-energy surface and has reported surface energy properties shown in Table 2-12:

Component	γ_s	γ_s^p	γ_s^d
Source	(mN·m ⁻¹)	(mN·m ⁻¹)	(mN·m ⁻¹)
Comyn (1997)	287	209	78
Legrand (1998)	259	-	-
Park <i>et al.</i> (2001)	99	51	48

Table 2-12 Surface energy values of silica.

Comyn (1997) and Legrand (1998) do not specify how these results were obtained and Park *et al.* (2001) used a sessile drop method. Legrand (1998) also stated that surface

energy determinations are highly dependent on the type of silica, the condition of the silica surface and test method used. For example, the surface energy of dry amorphous silica was reported as $259 \text{ mN}\cdot\text{m}^{-1}$, whereas the value for a hydrated surface was $129 \text{ mN}\cdot\text{m}^{-1}$, also the surface energy of quartz (crystalline silica) was shown as $180 \text{ mN}\cdot\text{m}^{-1}$. Jańczuk and Zdziennicka (1994) also found that the surface energy of quartz was dependent on environment and the amount of physically adsorbed water on the surface.

Until the advent of FOS there had been only a limited requirement for information on the surface properties of silica fibres, with the majority of the work on silica involving the use of silica particles (Legrand, 1998). Some work has been carried out on coated optical fibres, but this is not relevant to the current research into EFPI sensors as they do not have a polymeric coating.

E-glass fibres

As with the IFSS investigation, work has been carried out on the effect of silane treatments on the surface properties of E-glass reinforcing fibres for use within composites.

Weinberg (1997) performed contact angle measurements on carbon and glass reinforcing fibres using the Wilhelmy plate technique. Three liquids were used, water, ethylene glycol and glycerol. Two sets of glass fibre samples were tested, bare and γ -aminopropyl silane (A-1100) treated. The bare glass gave a surface energy of $45 \text{ mN}\cdot\text{m}^{-1}$, with 33% dispersive component and the silane treated had a surface energy of $31 \text{ mN}\cdot\text{m}^{-1}$ with a 43% dispersive component. These values were calculated from the advancing contact angle data. This shows that the treatment of E-glass fibres with a silane solution leads to a reduction in surface energy but with a change of balance between the dispersive and polar components.

Mäder (1997) investigated the effect of silane and size treatments of reinforcing fibres on surface energy as well as interfacial shear strength. From this work it was also found that treating E-glass fibres with γ -APS caused a reduction in surface energy, from $58.3 \text{ mN}\cdot\text{m}^{-1}$ for untreated fibres to $31.6 \text{ mN}\cdot\text{m}^{-1}$ for the treated fibres.

Bledzki *et al.* (1997) also investigated the effect of silane treatment on E-glass fibres through a capillary rise technique. However, in this case the total surface energy rose slightly from 43 to 50 $\text{mJ}\cdot\text{m}^{-2}$, with the dispersive component increasing from 16 to 37 $\text{mJ}\cdot\text{m}^{-2}$ and the non-dispersive reducing from 27 to 7 $\text{mJ}\cdot\text{m}^{-2}$.

2.4.4 Summary of surface energy of silica

Surface energy values of silica are reported as being dependant on the type and condition of the material under examination, with very little work concentrating on the silica surface of optical fibres.

Also with the silanes treatments the majority of the work has been carried out on E-glass reinforcing fibres, opposed to silica optical fibres. Even within the work published on E-glass/silane interactions there are inconsistencies, possibly due to test methods, sample preparation or the types of silanes used in the work.

2.5 Summary of the Literature Review

There is a wide variety of FOS available for use in many different applications, with two common sensors for strain measurement being FBG and EFPI sensors. This work has concentrated on EFPI sensors as there is less published work on their interfaces with structures. EFPI sensors have been used in a wide range of applications from F-15 aircraft, concrete structures and embedded into fibre reinforced composite structures.

The EFPI sensors have not been fully characterised for use in T/C fatigue of fibre reinforced composites. Although testing within a compressive regime needs to be carried out as a large majority of structures, which FOS are likely to be used in, will see compressive loads. Work has been done on T/T fatigue with most authors agreeing that the static limit of an EFPI is around 0.4% strain, whereas the fatigue limit is still open to

debate with the main factor in the different results reported being the variations in the sensor design used by the various research groups.

Another issue with the embedment of any FOS into a composite structure is the effect of the FOS on the mechanical properties of that structure. There are many factors which influence the extent of the effect of the inclusion of FOS on the structure; these include the number of fibres, geometry of the sensors, orientation of the sensors in relation to nearby reinforcing fibres and the mechanical property of interest. The effect is usually minimised by positioning the FOS between two plies with the same orientation as the FOS.

The interface between a strain sensor and structure is very important to ensure adequate strain transfer. The area of interfaces of FOS has begun to be explored although there is still a large amount to do before the area is understood. This is exacerbated by the number of different types of sensors, their different applications and the different host materials used. A large portion of the work associated with modelling of the interface deals with standard polymeric coated optical fibres, not EFPI sensors.

To investigate the interface of the EFPI sensors, it was decided to follow the example of glass fibres within composite materials. The outer surface of the EFPI sensor is the silica capillary and it was felt that this was similar enough to the E-glass of the reinforcing fibres to enable the use of the techniques and procedures for assessing and improving the interface in GFRP in the case of the EFPI interface in fibre. Therefore, parameters of interfacial shear stress and surface energy were chosen. None of the traditional IFSS methods suited the current project so a new technique was developed based on the single fibre pull-out method. For the other parameter, surface energy determination, contact angle measurements by the Wilhelmy plate technique were chosen as it was a suitable method for single fibres. For the improvement of the interface it was decided to investigate silane coupling agents as they had been well used within E-glass/thermoset composites.

3 Experimental

3.1 Introduction

Within this chapter, the various techniques and equipment used to investigate the interfacial and durability aspects of EFPI sensors are described. This begins with an examination of the manufacture of these sensors, including an assessment of the strength of the sensor. This section is important to ensure the operation of the EFPI sensors is understood. The remainder of the investigation can be split into two main areas, interfacial and durability aspects.

Interface

The interface between the sensor and the sample is important as this allows the transfer of strain from the samples to the sensor. This work began with an assessment of the interface and then the effect of modifying this interface. To this end two parameters were investigated, surface energy and interfacial shear strength.

Surface energy is the driving force behind interface interactions. Therefore for a solid/liquid interface the solid should have a higher surface energy compared to the liquid to encourage the liquid to wet out the surface. There are other influences that affect the ability of a liquid to wet out a solid, such as surface roughness, chemical composition, impurities and temperature. The surface energy was determined from contact angle measurements using the Wilhelmy plate technique.

The interfacial shear strength (IFSS) is a measure of the shear strength of an interface; it will be used as a means to quantify the interface. As shown in Section 2.2.2, there are different methods of obtaining IFSS data, each with their own advantages and disadvantages depending on the interface under investigation. In this case none of the traditional methods were suitable so a modified single fibre pull-out technique was used. The modification of the sensor surfaces through the use of silane treatments was also examined using surface energy and IFSS methods.

Durability

The durability aspects of the EFPI sensor while embedded in carbon fibre reinforced plastic (CFRP) began with the static mechanical properties of the composite. Testing was carried out to determine the axial tensile and compressive properties of the cross-ply CFRP. The same laminate containing EFPI sensors was used to examine the effect of embedding a sensor on the static properties of the CFRP. A series of loading rate tests were also performed on the reference CFRP samples and CFRP samples with embedded EFPI sensors. These were to ensure that the static and dynamic data would be comparable, and that there were no detrimental effects caused by the inclusion of EFPI sensors. The final stage of investigation was the examination of the fatigue properties of the CFRP. The fatigue cycling chosen involved a tensile and compressive region in each cycle. This cycle pattern was chosen as it is the regime that causes most problems for advanced fibre reinforced composites (AFRC), as it involves the damage mechanisms from both tensile and compressive loadings (Curtis, 1987). Reference samples and those with embedded EFPI sensors were subjected to various fatigue regimes to examine the effect of the fatigue loading on the performance of the EFPI sensors and the effect of the presence of an embedded sensor on the fatigue performance of the CFRP.

3.2 Materials

This section lists all the materials used to carry out the experiments as part of this project.

3.2.1 Optical fibre and sensor components

The optical fibre used in the manufacture of the sensors and the interfacial studies was single mode based at 800 nm (SM800). This fibre was supplied by FibreCore, UK with an acrylate coating. The core diameter was 5 μm with a cladding thickness of 60 μm and a coating thickness of approximately 63 μm .

The capillary used as part of the EFPI sensor was silica with an internal diameter of 128 μm $\pm 3/-0$ μm and an external diameter of 300 μm ± 5 μm . This capillary was precision drawn and supplied by Composite Metal Services, UK.

3.2.2 Chemicals

Table 3-1 presents a list of the chemicals used in various aspects of the testing. All were obtained from Aldrich, UK.

<i>Chemical</i>	<i>Purity</i>	<i>Structure</i>
Dichloromethane (DCM)	99%	CH_2Cl_2
Acetone	99%	$\begin{array}{c} \text{O} \\ \\ \text{H}_3\text{C}-\text{C}-\text{CH}_3 \end{array}$
Propan-2-ol	99%	$\begin{array}{c} \text{OH} \\ \\ \text{H}_3\text{C}-\text{C}-\text{CH}_3 \\ \\ \text{H} \end{array}$
Ethylene Glycol	99+%	$\text{HOCH}_2\text{CH}_2\text{OH}$
Formamide	98.5%	$\begin{array}{c} \text{H}-\text{C}-\text{NH}_2 \\ \\ \text{O} \end{array}$
Dimethylsulphoxide (DMSO)	99+%	$\begin{array}{c} \text{H}_3\text{C}-\text{S}-\text{CH}_3 \\ \\ \text{O} \end{array}$
Aminopropyltrimethoxy silane (APMS)	97%	$\text{H}_2\text{N}-(\text{CH}_2)_3-\text{Si}-(\text{OCH}_3)_3$
Glycidoxypropyltrimethoxy silane (GPMS)	98%	$\begin{array}{c} \text{H}_2\text{C}-\text{CH}-\text{CH}_2-\text{O}-(\text{CH}_2)_3-\text{Si}-(\text{OCH}_3)_3 \\ \diagup \quad \diagdown \\ \quad \quad \quad \text{O} \end{array}$

Table 3-1 List of chemicals used as supplied by Aldrich, UK.

3.2.3 Resins

The first set of resins used was in the reinforcement of EFPI sensors. These resins are shown in Table 3-2 with their recommend cure schedule and approximate pot-life. The resin used in the end-tapping of the composite samples was 3M Adhesive Scotch-weld 9323. For attaching electrical resistance strain gauges to samples the Vishay MBond 200 cyanoacrylate was used.

Supplier	Name	Type	Recommended cure schedule	Approx pot-life (RT)	Typical Use
Permabond	C2	Cyanoacrylate	RT	1 min	General purpose
Vishay	MBond 200	Cyanoacrylate	RT	2 min	Strain gauge bonding
RS	Quickset	Epoxy	RT for 24 hours	5 mins	General purpose
Epotek	OG-142	Epoxy	UV exposure for 30 mins	N/A	Optical components
Araldite	2011	Epoxy	RT for 10 hours	100 minutes	General purpose
Araldite	2020	Epoxy	RT for 24 hours	45 minutes	Glass bonding
Araldite	2026	Polyurethane	RT for 4 hours	5 minutes	Glass bonding

Table 3-2 Resins used within the reinforcement of EFPI sensors.

3.2.4 Composite prepreg

The prepregs used in the composite sample preparation were either glass or carbon fibre reinforced epoxy resins systems. The prepregs were supplied by Hexcel with the 913 resin system. The glass fibre prepreg was 913G-E-5-30% and the carbon fibre was 913C-HTA(12K)-5-34%, both had a ply thickness of 0.125 mm. The prepregs were supplied on a reel with a 300 mm width. These reels were stored at -18°C within containers to maximise the shelf life of the resin. On removal of the prepreg from the storage conditions, it was allowed to equilibrate to ambient room temperature prior to the container being opened. This was to minimise water absorption by the prepreg, as an additional precaution silica gel was placed within the container to absorb any condensation that might form.

3.3 Sample Preparation

This sections deals with the manufacture of the various samples that were required to investigate the interfacial and durability aspects of the EFPI sensors.

3.3.1 EFPI manufacture

As described previously, the EFPI sensors consist of optical fibres fixed in place in a precision bore capillary. The sensors used in this study were manufactured in-house by Mr J. Tetlow (Group technician). The fibres were stripped of the acrylate coating using mechanical methods and then cleaved. Using a BIT Communications Model BFS-60 fusion splicer, each fibre was positioned into the capillary. A schematic illustration of this is presented in Figure 3-1. Once the fibre and the capillary were in place, an electric arc was initiated between the electrodes on the fusion splicer that caused the fibre and capillary to soften and fuse. The sensor was normally interrogated during manufacture so that the second fibre could be positioned inside the capillary to give the required cavity. The interrogation method will be dealt with in Section 3.4.1. The size of the cavity is important as it is one of the main parameters for controlling the strain range of the sensor.

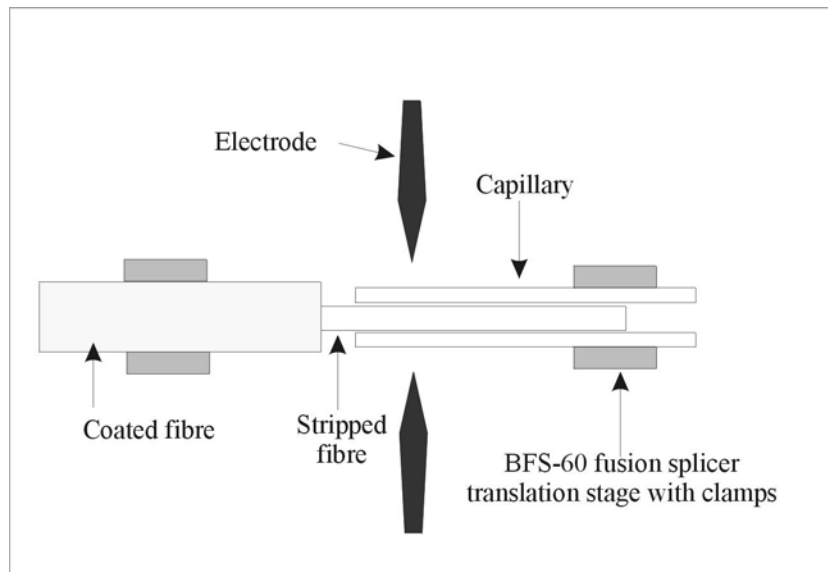


Figure 3-1 Schematic of the set-up used to position the optical fibres within the capillary in the custom-modified fusion splicer.

An electric arc was then struck to fuse the fibres to the capillary. During manufacture the fusion points were set at a distance of approximately 2 mm from the end of the capillary. Therefore a typical 18 mm capillary would have a nominal gauge length of 14 mm. This distance needed to be confirmed due to variations in the striking of the

electric arc. The gauge length is also an important parameter as this controls the strain resolution of the sensor. The manufacture of the sensor is complete at this stage. In some cases a reinforcement resin is required, in which case a small drop of resin is placed at each end of the capillary and allowed to cure. Ideally this drop should be just enough to seal the fibre into the capillary.

3.3.2 Surface energy test specimens

3.3.2.1 Cleaning methods

The first stage in the preparation of the fibres was the selection of an appropriate cleaning method. The acrylate coating of the optical fibres had to be removed which achieved in one of two ways, either chemically which involves soaking the fibre in dichloromethane (DCM), or mechanically using a fibre stripping tool (Auriga Europe, plc.). A fibre-stripping tool typically contains a set of blades which when pressed together leave a gap the size of the diameter of fibre to be stripped. These blades cut through the polymeric coating of the optical fibre and allow the coating to be pulled off. The stripped fibres were then cleaved so a flat edge was obtained to ensure that all samples had a similar geometry. For the contact angle work, a section of approximately 20 mm of bare fibre was left exposed out of a total length of around 50 mm. This allowed sufficient depth for the testing to minimise the effect of any variation along the fibre length. The preparation methods investigated were:

- i) DCM stripped, cleaved then acetone wiped using lint-free cloth;
- ii) DCM stripped, acetone wiped using lint-free cloth then cleaved;
- iii) DCM stripped, cleaved then propan-2-ol wiped using lint-free cloth;
- iv) mechanically stripped, cleaved then acetone wiped using lint-free cloth;
- v) mechanically stripped, cleaved then propan-2-ol wiped using lint-free cloth; and
- vi) mechanically stripped, cleaved then cleaned using HellmanexTM silica cleaner.

Hellmanex IITM is an alkaline cleaner designed for silica and was used in a solution of 1.5% with distilled, deionised water. The fibres were placed in the solution for 2-3 hours at room temperature, following by a rinse of distilled, deionised water and allowed to air dry as recommended by the supplier (Hellma Ltd, UK). For each preparation method at least 10 individual samples were prepared.

3.3.2.2 Silane treatments

The experimental details for the silane treatment of bare optical fibres are presented. The silanes used were APMS and GPMS as summarised in Table 3-1.

Silane solutions were made using distilled, deionised water at levels of 1% and 5%. The silane solutions were allowed to hydrolyse for 40 minutes at room temperature (Naviroj *et al.*, 1984). The cleaned fibres were then dipped into the silane solutions for 2 minutes. The treated fibres were dried at ambient, 60°C and 100°C to drive off the water.

3.3.3 Autoclave processing of prepreps

All the composite samples prepared as part of this work were subjected to autoclave processing, to ensure that the composite samples were of a good quality.

The autoclave was manufactured by Aeroform and the chamber has approximate dimensions of 0.8 m diameter and 1 m length. The composite samples were all processed with a vacuum applied through the use of a vacuum bag. A schematic of a vacuum bag assembly is shown in Figure 3-2. The suppliers recommended cure schedule for the 913 resins system is 1 hour at 120°C, reached at a rate of 3°C·minute⁻¹, with a pressure of 690 kPa (100 psi).

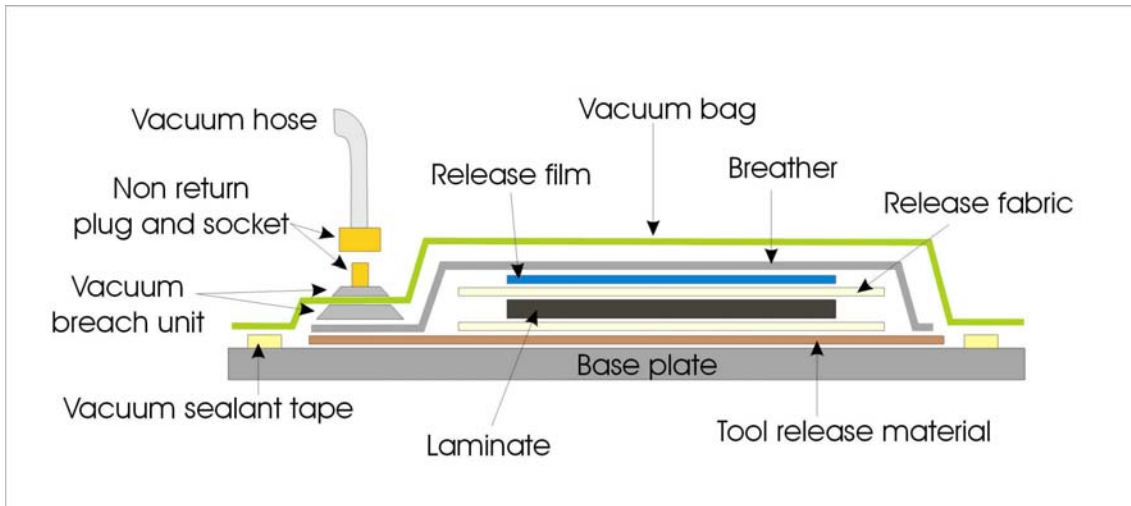


Figure 3-2 Schematic of vacuum bag set-up.

3.3.4 Preparation of interfacial shear strength samples

This section describes a new technique for the manufacture of the samples for determining interfacial shear strength based on the single fibre pull-out method.

The optical fibres were prepared in a similar fashion to those for the surface energy measurements as described in section 3.3.2. The cleaning method chosen was the one deemed the optimal from the surface energy measurements. Silane treated fibres were also used for interfacial shear strength samples and these were prepared as section 3.3.2.2, except the drying of all the samples was done at 100°C. The other difference in the preparation was the length of exposed bare fibre, in this case it was kept to about 2 mm.

Both the glass fibre and the carbon fibre prepreg as described in section 3.2.4 were used in the manufacture of these samples. The prepreg was cut into strips with approximate dimensions of 20 mm by 70 mm by the use of a guillotine. Unidirectional lay-ups were used, however some sets of samples had 2 plies while other had 16 plies. Due to the difference in thickness of the samples, two slightly different set-ups were required.

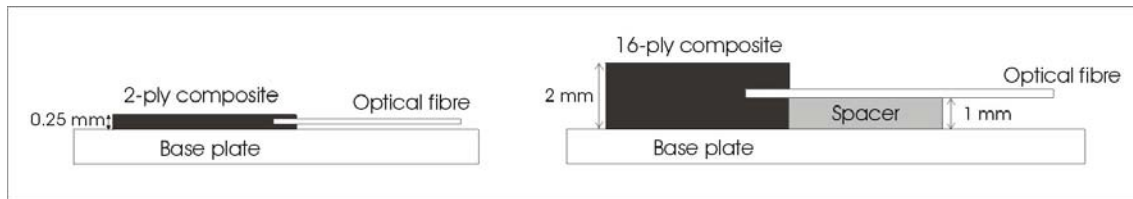


Figure 3-3 Schematic of the setup for the manufacture of IFSS specimens.

For the 2-ply samples this involved the placement of the bottom ply onto a porous release fabric. The optical fibre was then carefully placed onto this ply, and then the top ply was pressed into position. Once the batch of samples was completed, the final backing sheet of the prepreg was removed and a second layer of porous release fabric was put on the top, the vacuum bag was then finished.

Due to the difference in thickness between the 2 and 16-ply samples, extra stages were required in the 16-ply sample preparation process. The optical fibres were positioned in the centre of the sample, with 8 plies below and 8 plies above. Spacers had to be used in order to maintain this position when the vacuum and pressure was applied. A PFTE spacer was manufactured with slots in it that held the fibre approximately 1 mm from the bottom of the composite sample (a 16-ply sample produces a thickness of approximately 2 mm after cure). Pre-crosslinked silicone sealant was placed in the fibre slots to hold the fibres in position and to prevent resin flow up the slots. These samples were also prepared onto a porous release fabric and covered with another layer of the release fabric, prior to the completion of the vacuum bag.

All samples were subjected to the recommended cure schedule for 913 resin prepregs as described in section 3.3.3.

3.3.5 Preparation of composite samples for mechanical testing

All the samples used for the mechanical testing were made from the carbon fibre prepreg. Flat plates were produced of dimension 300 mm by 300 mm. The lay-up sequence used was $[0,90,90,0,0,90,0,90]_s$, to give a total of 16 plies and an approximate

thickness of 2 mm. These samples were processed by the procedure described in section 3.3.3.

The samples for the static and dynamic mechanical testing were produced in accordance with CRAG Methods 301 and 401 (Curtis, 1988). The samples were cut to dimensions of 20 mm by 200 mm using a diamond tipped cutting wheel, guides were used to aid in the reproducibility of the width.

In-line with the CRAG methods the samples were end-tabbled to ensure good contact with the grips of the test machines and for the dynamic work to aid in heat dissipation. A sheet of 1.6 mm aluminium, grade 7075, was used as the end-tab material. This was grit blasted and cut into tabs 20 mm wide by 50 mm long. The grit blast process promotes adhesion to the sample due to an increase in the surface area. The tabs were subjected to acetone cleaning in an ultrasonic bath for about 15 minutes prior to bonding to the composite samples to ensure no grease was present. The composite samples also had the areas to which the end-tabs were to be bonded lightly sanded and degreased with acetone prior to bonding. The adhesive used was 3M Scotch-Weld 9323, and to achieve a good bond the end-tabs were cured to the composite using a hydraulic press with heated platens. The temperature was set to 40°C with a pressure of approximately 700 kPa and the samples were cured for at an hour at these conditions. A schematic of a completed specimen is shown in Figure 3-4.

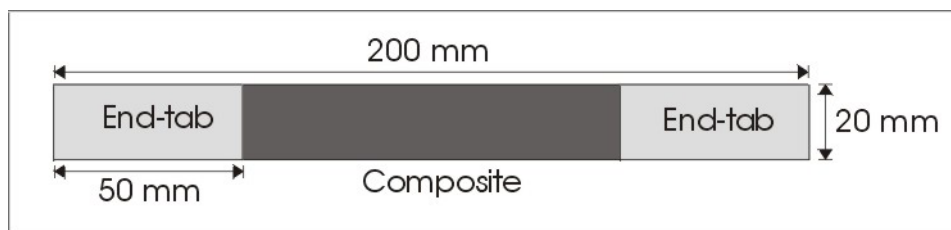


Figure 3-4 Schematic of a completed composite specimen for mechanical testing.

Once the samples were end-tabbled, the edges were polished using a silicon carbide 1200 grit paper. This was to ensure that there was no damage to act as crack initiating points. Samples for the static mechanical testing had biaxial electrical resistance strain gauges attached. These were 120Ω gauges with gauge lengths of 2 mm, supplied by Micromeritics Group, UK. The surface of the composite was gently sanded and

then degreased using acetone prior to the bonding of the strain gauge using MBond 200 cyanoacrylate adhesive. The axes of the strain gauges were aligned with the 0° and 90° directions of the reinforcing fibres. The samples for the loading rate and fatigue testing had a clip-on extensometer (50 mm gauge length) used to monitor strain, which was attached just prior to testing using the cyanoacrylate resin. To allow the samples to acclimatise to the test conditions, all samples were stored at ambient conditions in the room where the testing would be carried out.

3.3.6 Preparation of composite samples with embedded EFPI sensors for mechanical testing

These were prepared in similar manner to that as described in the previous section; due care and attention had to be taken with the EFPI sensors due to their fragile nature. This involved some slight changes to the procedure. To protect the lead in and out optical fibres, PTFE protective tubing was used at the entry and exit points. During lay up of these only limited force can be applied to the stacked plies once the sensors are in place. Therefore the prepreg layers were assembled in two parts, below and above the sensor location, with the sensors then being sandwiched between these two parts. To minimise disruption to the composite structure the sensors were placed in the 0° direction in between two 0° plies.

Normally, 8 EFPI sensors were used per composite panel, the sensors were even spaced out across the panel. This left a gap of around 30 mm between each sensor. In an attempt to maintain alignment of the sensors with the reinforcing fibres, a template was used. This template consists of a series of parallel lines, which were orientated in the direction of the reinforcing fibres. The sensors were positioned in line with the template and fixed in position using tape. This held the sensors while the top part of the lay-up sequence was positioned. Once this top part was in place the tape was removed and the composite panel was transferred to the base plate of the vacuum bag. Care was needed when assembling the vacuum bag for these panels containing sensors, as the lead in/out fibres had to be protected. Therefore the breach units had to be located in areas where there was no optical fibre, otherwise during the application of the vacuum and pressure the fibres would have been fractured, as shown in Figure 3-5.

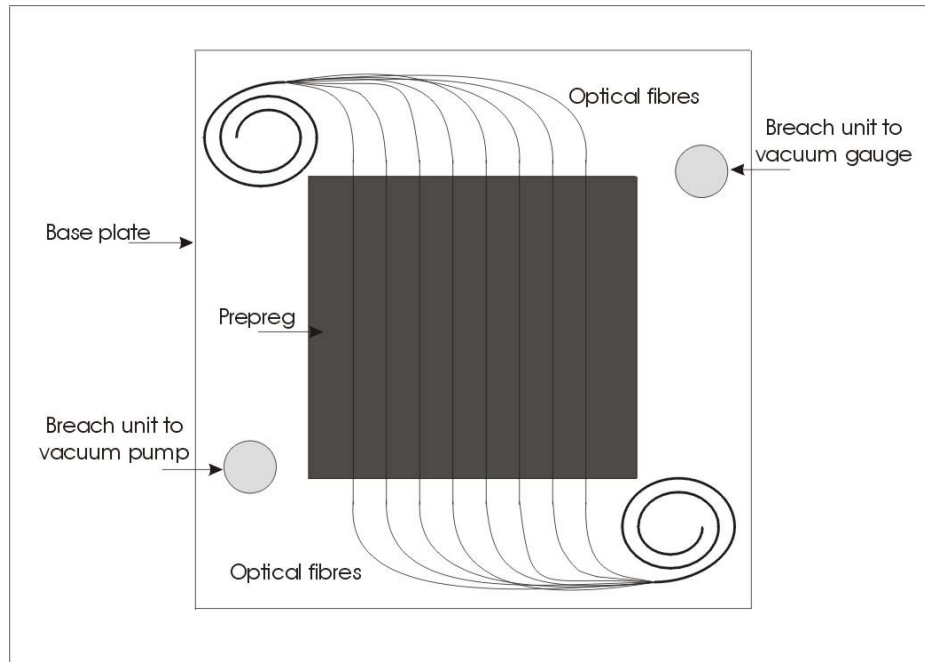


Figure 3-5 Schematic showing arrangement of components when sensors were involved in autoclave process.

3.4 Test Methods

This section deals with the descriptions of the test method used in this project. It begins with the description of the interrogation method employed for the EFPI sensors, and then going onto the determination of gauge length and tensile strength of the sensors. The techniques used to investigate the interfacial aspects are then dealt with, including the surface energy and interfacial shear strength measurements. The final part of this section deals with those methods used on the composite samples, including the quality check method, static and dynamic testing.

3.4.1 EFPI sensor interrogation

Interrogation of the EFPI sensors was carried out through the use of an Ocean Optics S2000 Charged Coupled Detector (CCD) Spectrometer with a wavelength range of 700 nm – 900 nm and a resolution of 0.12 nm. In conjunction with this, a super luminescence diode (SLD) was used centred at 850 nm and a 2×2 optical fibre coupler suited for use with SM800 fibre. The experimental set-up is shown in Figure 3-6 :

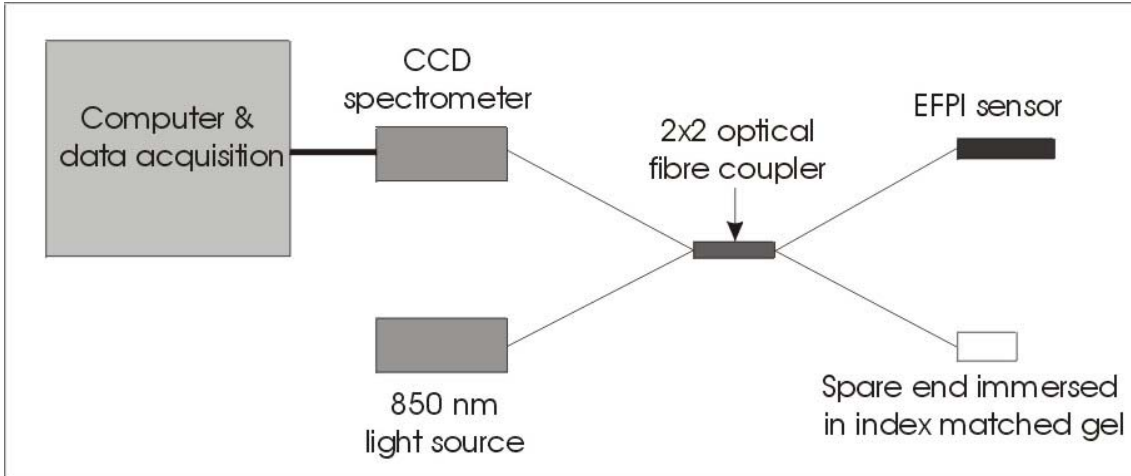


Figure 3-6 Schematic of the experimental set-up used for interrogating of the EFPI sensors.

This interrogation system was chosen, as it was a good compromise between cost, resolution and portability. The system needed to be portable so it could be moved between the various testing equipment locations. The coupler is employed so the sensor can be interrogated through reflection. The spare end is immersed in index matching gel to prevent reflections from this end interfering with the spectrum from the sensor.

To enable interpretation of the interference spectra generated by this set-up a program was written in Labview based on the Labview drivers supplied by Ocean Optics. This program is presented as DAQ Method 1 in Appendix 1. The program can use two different methods to obtain the information regarding the cavity length. The first is “peak counting” and the second is fast Fourier transformation.

3.4.1.1 Peak counting method

This method uses the formula shown in Equation 3-1 to calculate the cavity length:

$$Cavity\ length\ (\mu m) = \frac{n\lambda_1\lambda_2}{2000(\lambda_2 - \lambda_1)} \quad \text{Equation 3-1}$$

In this equation λ_1 and λ_2 are the wavelengths in nm of two peaks, n is the number of cycles between those peaks. This equation is generated from the phase differences at two wavelengths (Hecht, 1998).

At the first wavelength, λ_1 , the phase difference is given as shown in Equation 3-2, where d the cavity gap. Equation 3-3 show the phase difference at a second wavelength, λ_2 .

$$\phi_1 = \frac{2\pi \cdot 2d}{\lambda_1} \quad \text{Equation 3-2}$$

$$\phi_2 = \frac{2\pi \cdot 2d}{\lambda_2} \quad \text{Equation 3-3}$$

The optical path of the light is twice the cavity length, as the light travels along the gap and is then reflected back along the gap to the original point. For constructive interference the difference between the phases ($\Delta\phi$) must be equal to a multiple of 2π (a complete cycle). The multiple is the number of peaks (n) between the two wavelengths chosen. The derivation is shown in Equation 3-4 to Equation 3-7.

$$\Delta\phi = n2\pi = \frac{2\pi \cdot 2d}{\lambda_1} - \frac{2\pi \cdot 2d}{\lambda_2} \quad \text{Equation 3-4}$$

$$n2\pi = 4\pi \cdot d \left(\frac{1}{\lambda_1} - \frac{1}{\lambda_2} \right) \quad \text{Equation 3-5}$$

$$d = \frac{n \cdot \lambda_1 \cdot \lambda_2}{2(\lambda_2 - \lambda_1)} \quad \text{Equation 3-6}$$

$$d = \frac{n \cdot \lambda_1 \cdot \lambda_2}{2000(\lambda_2 - \lambda_1)} \mu m \quad \text{Equation 3-7}$$

3.4.1.2 Fast Fourier transform method

Another method to obtain the gap measurements is to perform a fast Fourier transform (FFT) on the spectrum. The frequency of the interference pattern is controlled by the cavity length and the FFT analysis enables this frequency to be determined. From this value the cavity length can be calculated through knowledge of the amount of data analysed and the resolution and range of the spectrometer. The average pixel spacing of the spectrometer (0.1238 nm) gives the theoretical minimum peak width that can be

observed and from this the maximum gap that the spectrometer could resolve can be calculated (2918.438 μm). The last piece of information required was related to the number of data points that are subjected to the FFT analysis. The conversion from FFT data points to cavity gap is shown in Equation 3-8:

$$\text{Cavity Length } (\mu\text{m}) = \text{FFT peak position} \times \frac{\text{Maximum Gap}}{\left(\frac{\text{Number of data points}}{2} \right)} \quad \text{Equation 3-8}$$

The reason the number of data points is divided by two is because the FFT results in symmetrical data so only half of it can be considered at any one time. The result from these calculations is as follows in Equation 3-9 for the equipment setup used in this work:

$$\text{Cavity Length } (\mu\text{m}) = \text{FFT peak position} \times 1.43 \quad \text{Equation 3-9}$$

This technique can be used to monitor more than one sensor at a time, as in this case a peak on the FFT analysis is generated for each sensor attached to the system. The limitations on this technique are that the sensor peaks must be distinct enough to avoid interference and also to prevent overlap of the peaks during strain application. Another consideration is to ensure sufficient signal is received from each of the sensors so that the associated FFT peak can be clearly observed.

3.4.2 Gauge length determination for the EFPI sensors

The gauge length is an important parameter as it controls the response of the sensors to the applied strain. Initially this was achieved by optical microscopic examination of the sensor. The equipment used was a Leica DMLM optical microscope set with a camera and Leica “QWin” image acquisition software. The distance between the fusion points was measured using the vernier scale on the microscope translation stage. The vernier scale had a resolution of ± 0.1 mm.

To check this optically observed gauge length, 6 EFPI sensors were attached to a steel sample. These samples were instrumented with a surface-mounted electrical resistance strain gauge (ERSG) attached using MBond 200 adhesive. The EFPI sensors were placed alongside the strain gauges and attached using the same resin system, as shown in Figure 3-7.

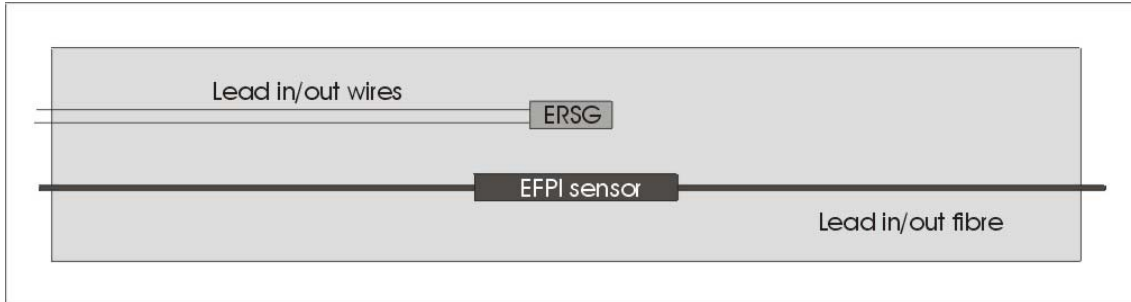


Figure 3-7 Schematic of ERSG and EFPI on steel specimen.

The samples were then subjected to tensile loading on a Zwick 1484 at a cross-head displacement of $0.5 \text{ mm}\cdot\text{minute}^{-1}$ at ambient conditions. The response of the EFPI sensors was compared to that of the strain gauges. The strain gauges were attached to a Vishay Measurements Group Strain Gauge Conditioner 2120A and then onto a National Instruments TBX-86T block and a NI435 data acquisition (DAQ) board. The data from the EFPI sensors and the strain gauges was recorded using a Labview program. This program was based on that used to interrogate the EFPI sensors but had an additional section to monitor and record the output from the strain gauges. This program is presented as DAQ Method 2 in Appendix 1.

From the data obtained regarding the strain and the change in cavity during the test, the gauge length of the EFPI sensors could then be determined. This method was not suitable for checking every sensor used in this project, as it required the EFPI to be adhered to the metal specimen, the main purpose of this testing was to ensure that the measurements obtained using the microscope were consistent.

3.4.3 Tensile testing of EFPI sensors

It was felt that the inherent strength of the sensors was important to enable an understanding of any weak points, typical failure locations and to gain an appreciation of the fragility of the EFPI sensors. This set of tests were carried out using an Instron 1026 with a 500 N load cell which could be set to have a full-scale load of 50 N, 100 N, 250 N and 500 N. To enable the data from this machine to be recorded on a PC, it was connected to the data acquisition system as described in section 3.4.2. The Labview program required a small change to enable load to be recorded instead of strain.

All testing was carried out at ambient laboratory conditions. To ensure that the pneumatic grips of the Instron 1026 were suitable for gripping optical fibres, a set of tensile tests were carried out on the acrylate-coated optical fibres. 10 samples were tested at a crosshead speed of 5 mm·minute⁻¹. Graph paper was used to assist with the alignment of the samples within the grips. This involved attaching the sample parallel to the vertical lines on the graph paper. The paper and sample were then placed into the grips using the vertical and horizontal lines on the graph paper to ensure the sample was in the centre of the grips. Once the sample was in position, the paper was cut and removed to allow the testing of the sample, a schematic of this is shown in Figure 3-8.

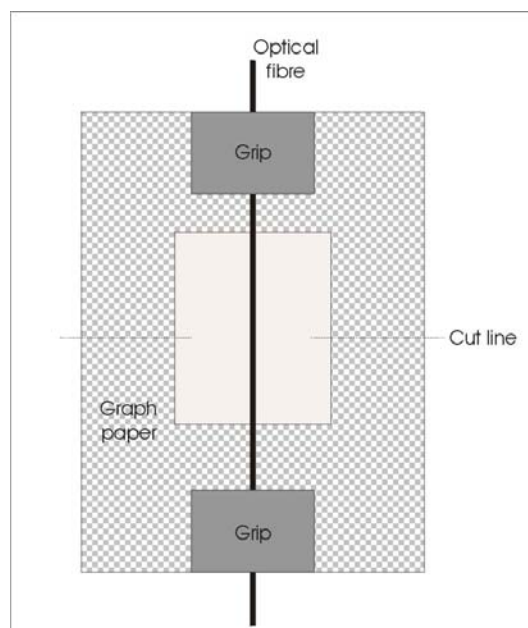


Figure 3-8 Schematic of the setup for the tensile testing of optical fibres.

The testing then moved onto the EFPI sensors. 10 unreinforced sensors and at least 6 of each type of resin-reinforced sensors were tested. The resins used to reinforce the sensors are described in Table 3-2. Testing was carried out at $0.5 \text{ mm}\cdot\text{minute}^{-1}$ while recording the changes in the cavity length and the load from the Instron through the DAQ system.

3.4.4 Surface energy

This is one of the parameters used to assess the interface of the EFPI sensors. Surface energy can be determined by the measurements of the contact angle between the solid of interest and different liquids with known surface energy values.

The equipment used in this current research was the Camtel Dynamic Contact Angle Tensiometer (CDCA-100F). The rate of movement of the stage was selectable in the range 0.001 to $4 \text{ mm}\cdot\text{s}^{-1}$ and the balance had an accuracy of $\pm 1 \mu\text{g}$. A schematic of the CDCA is shown in Figure 3-9.

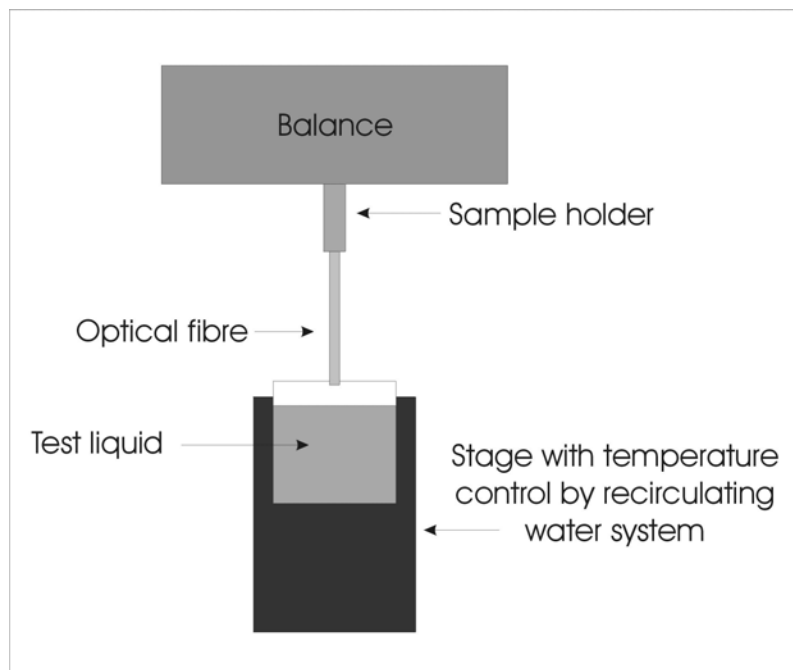


Figure 3-9 Schematic of the Camtel Dynamic Contact Angle Tensiometer.

The experiments were based on the Wilhelmy plate technique where a force versus immersion depth plot is produced from which the advancing and receding contact angle between the fibre and the test liquid can be calculated. The stage speed was set at $0.2 \text{ mm}\cdot\text{s}^{-1}$, with a final immersion depth of 15 mm. The main advantage of this method is that it allows cylindrical objects to be investigated that are difficult to achieve using the sessile drop methods.

Due to the temperature-sensitive nature of contact angle measurements, the machine was temperature controlled this was achieved using a re-circulating water bath that had a resolution of $\pm 0.1^\circ\text{C}$, as cited by the manufacturer. The water bath was set at 25.0°C for all the testing. However, the temperature of the CDCA had a variation of $\pm 0.3^\circ\text{C}$ as monitored by the CDCA software. The difference between the resolution of the water bath and the variation recorded by the CDCA was likely to be caused by heat lost through the water pipes and heat generated by the equipment during operation.

The manufacturer supplied the control and data acquisition software for the CDCA. The data acquired during a test was the immersion depth, load on the balance and the temperature of the stage. A graph of force against immersion depth was produced, from which both the advancing and receding contact angles were obtained using linear regression analysis within the software. The regression analysis calculated the force at a zero immersion depth that is in turn used in Equation 3-10 to obtain the contact angle.

$$\cos\theta = \frac{F - W_f - B}{\gamma\pi d} \quad \text{Equation 3-10}$$

where F is the force recorded by the CDCA, W_f is the weight of the fibre, B is the buoyancy of the fibre in the selected liquid, γ is the surface tension of the liquid, d is the diameter of the fibre and θ is the contact angle.

The weight of the fibre is tared from the balance at the beginning of the test, and the buoyancy was taken into account by the software having knowledge of the density of the test liquid and the geometry of the fibre. This information along with the diameter

of the fibre and the surface energy of the test liquid allows the contact angle to be determined.

3.4.4.1 Cleaning methods

To examine the effect of different cleaning methods on the optical fibres as described in Section 3.3.2.1 at least 10 samples of each type were tested for their contact angle response against formamide. The tests were to look for repeatability of the different cleaning methods. Once the optimum cleaning method was chosen the work moved on to examining the surface energy of the optical fibres.

3.4.4.2 Capillary/optical fibre comparison

From the EFPI sensor construction, the interface of the sensor is the surface of the silica capillary. A set of experiments were designed to examine if the bare fibre could be used as a more convenient replacement for the capillary for the surface energy and the interfacial shear strength measurements. To enable the capillaries to be compared with the bare fibres using the CDCA, one end needed to be sealed for the Wilhelmy technique to be applicable. The capillaries were placed into the fusion splicer, with the end to be sealed placed between the electrodes. When an arc was struck this melted the end of the capillary, thereby sealing it. This setup is shown schematically in Figure 3-10.

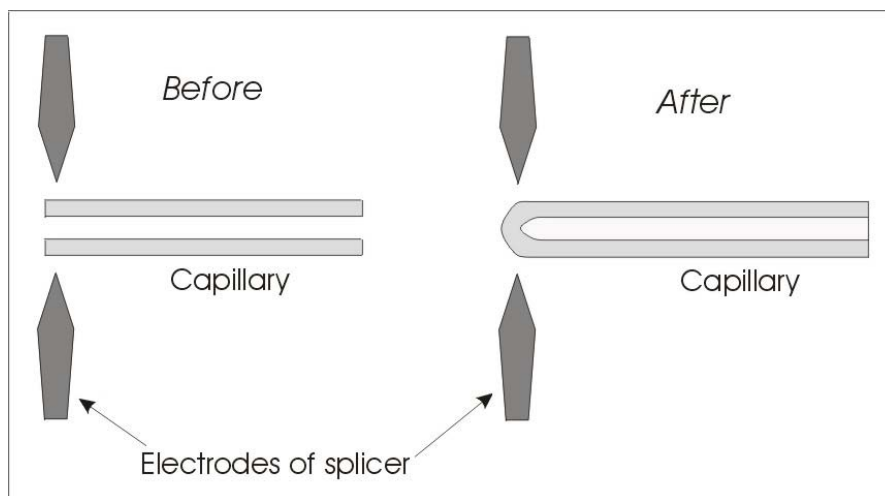


Figure 3-10 Sealing the capillary to enable use in the contact angle measurements.

The sets of samples were then tested against three liquids with different surface energies, where a set of samples consisted of either 10 fibres or 6 capillary lengths.

The test liquids chosen are shown in Table 3-3 with their corresponding surface energy values, including the dispersive and polar components:

Liquid	Surface Energy (γ_l) mN·m ⁻¹	Dispersive Component (γ_l^d) mN·m ⁻¹	Polar Component (γ_l^p) mN·m ⁻¹
Formamide	58.2	39.5	18.7
Ethylene Glycol	48.3	29.3	19.0
DMSO	43.54	34.86	8.68

Table 3-3 Summary of surface energy values for specified liquids (J Comyn, 1997).

3.4.4.3 Silane treated optical fibres

The fibres were treated as described in Section 3.3.2.2 with at least 10 individual samples being tested against each chosen liquid, shown in Table 3-3. This resulted in 12 sets of samples being tested to examine the effect of different silane surface treatments on the surface energy of silica fibres.

3.4.5 Interfacial shear strength

This section deals with the testing of the interfacial shear strength samples manufactured as in Section 3.3.4. To enable the measurement of the embedment depth, each sample was examined under the microscope prior to testing; this allowed an image to be stored. After testing the optical fibre was re-examined under the microscope and compared to the corresponding stored image. This comparison allowed the embedment depth to be measured and is shown schematically in Figure 3-11. The examination of the fibre after testing also allowed the optical fibre to be checked to ensure pull-out rather than fibre fracture had occurred.

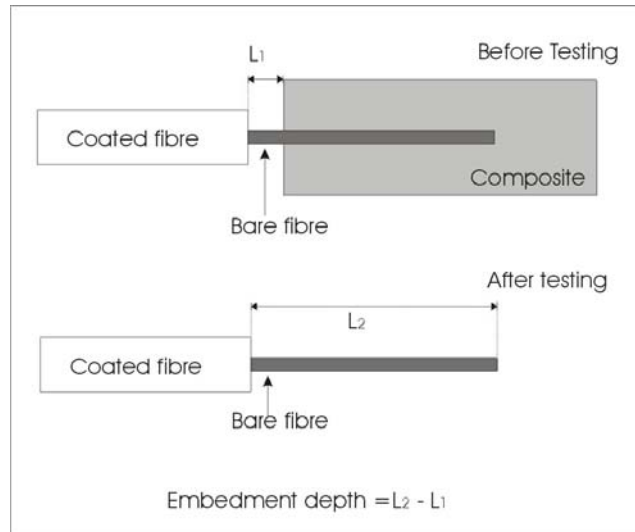


Figure 3-11 Schematic showing calculation of embedment depth for pull-out samples.

The samples were tested on a Zwick 1445 tensometer with a 200 N load cell controlled by TestXpert™ software. The optical fibre was held using a compressed air fibre grip with ceramic face inserts and the composite by a mechanical grip. The cross-head speed was set to 0.5 mm·minute⁻¹ during testing with the load and cross-head position monitored during testing until failure of the sample. The testing was carried out under ambient conditions.

Through the knowledge of the fibre diameter (D), the embedment depth (l) and the failure load (F), the IFSS (τ) can be calculated using the Equation 3-11:

$$IFSS (\tau) = \frac{F}{\pi \cdot D \cdot l} \quad \text{Equation 3-11}$$

This is a simple method of obtaining a value for the IFSS; which does not take into account issues such as end-face adhesion and the variation of the IFSS along the embedded length.

3.4.6 Quality control check of the composite samples

To check the quality of the flat plates produced, two techniques were employed. The first method was an ultrasonic technique called C-scan and the second was optical microscopy.

C-scan is a method by which the extent of damage or voids within a composite can be evaluated (Hull and Clyne, 1996). The samples to be examined are placed in a tank of water and an ultrasonic transducer of 5 Hz is transversed over the samples. Reflected echoes were received from the front and back face of the specimens. The back face reflections were monitored as the transmission of the signal is affected by the quality of the materials the signal has to pass through to reach the back face. If the signal reaches a delamination or void, the signal is attenuated and the back face reflected echo is reduced. This generates an image of the sample that shows regions where voids might have occurred. The transducers, software and computer hardware used in the C-scan set up were supplied by Physical Acoustics Ltd, UK.

For the optical microscopy, small samples were sectioned from the plate and mounted in a polyester resin (Struers Ltd.). The resulting component was then suitable for polishing. The polishing equipment used was a Labopol 21 with a LaboForce 3 specimen mover and a multidoser attachment as supplied by Struers Ltd., UK. Once the samples were ground and initially polished with silicon carbide, a final polishing stage was completed using diamond suspensions. The silicon carbide papers used started at a grit level of 240, moving down in stages to a final level of 2400 grit. The water-based diamond suspensions used started at 6 μm , going through 3 and 1 μm with a final stage using 0.25 μm suspension. The component was then ready for examination under the microscope, enabling the structure of the composite to be observed along with any defects in that section. The microscope used was a Leica DMLM as described in section 3.4.2.

3.4.7 Quasi-static testing of composite samples without and with embedded EFPI sensors

As part of the durability investigation the static axial mechanical properties of the carbon fibre composite was evaluated. This included reference samples and those with embedded EFPI sensors. All this work was conducted in ambient laboratory conditions on an Instron 8501 hydraulic machine with hydraulic grips. The actuator speed was set to $2 \text{ mm}\cdot\text{minute}^{-1}$ for the testing.

All the samples had $0^\circ/90^\circ$ electrical resistance strain gauges connected to a Vishay Measurements Group Strain Gauge Conditioner 2120A and then onto a National Instruments TBX-68T connector block and a NI435 data acquisition (DAQ) board. A Labview program was used that recorded the response from the strain gauges and the load data from the Instron. This program is shown as DAQ Method 3 in Appendix 1. For the samples with embedded EFPI sensors DAQ Method 1 (Interrogation of sensors) was incorporated into Method 3.

Tensile testing was carried out on 6 reference samples and 5 samples with embedded sensors. Compressive testing requires the composite to be restricted from buckling. To prevent buckling an anti-buckling jig was used in line with CRAG Method 401. A schematic diagram of the jig is shown in Figure 3-12.

Compressive testing was carried out on 6 reference samples and 5 samples with embedded EFPI sensors.

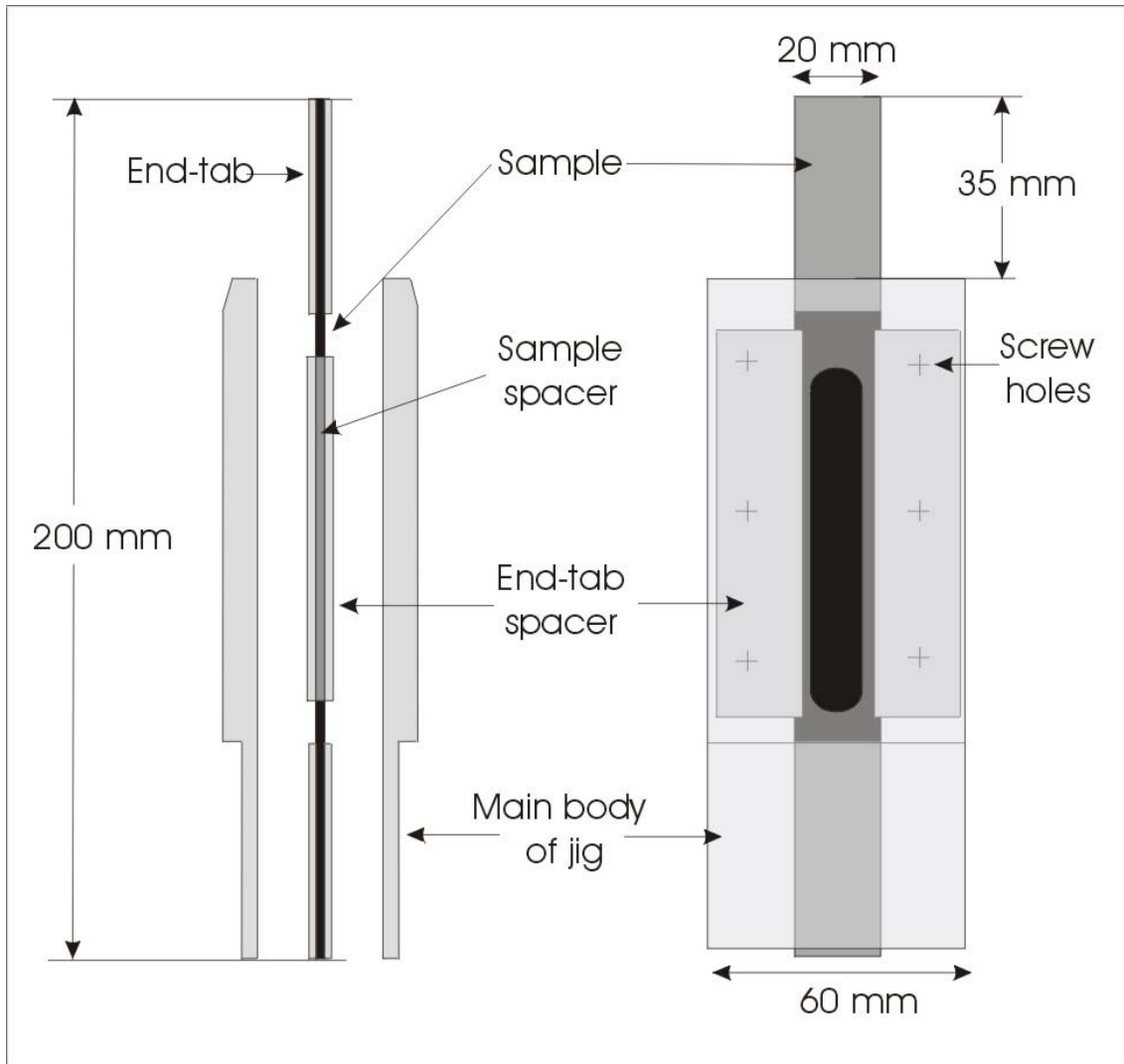


Figure 3-12 Schematic of the anti-buckling jig.

3.4.8 Loading rate effects on composite samples without and with embedded EFPI sensors

Some materials can have mechanical properties that are dependent on the speed of testing (Askeland, 1994). Therefore, to ensure that data obtained from static and dynamic results were comparable, a series of tensile tests were carried out to investigate the effect of loading rate on the properties of the CFRP composite samples. The static testing was carried out at $0.16 \text{ kN}\cdot\text{s}^{-1}$ (equivalent to $2 \text{ mm}\cdot\text{minute}^{-1}$) whereas the fatigue testing was performed at $250 \text{ kN}\cdot\text{s}^{-1}$. A range of loading rates was chosen that covered 5 orders of magnitude. The rates were 0.025 , 0.25 , 2.5 , 25 and $250 \text{ kN}\cdot\text{s}^{-1}$. Data from

these experiments were gathered using a Labview based data acquisition system monitoring load, cross-head position, clip-on extensometer and an electrical resistance strain gauge (ERSG) and where appropriate the EFPI sensor responses. The extensometer had a gauge length of 50 mm and was attached using knife-edge blades held on with cyanoacrylate and a set of springs. The ERSG had a resistance of 120 Ω and a 2 mm gauge length.

Two different Labview programs were used for this work, the first was DAQ Method 3 used in the quasi-static work, modified to include the extensometer data. At the higher loading rates the acquisition speed of this program was insufficient. Therefore, it was modified to enable sufficient data to be recorded, it presented as DAQ Method 4 in Appendix 1. Each sample was subjected to the whole range of loading rates and in total 6 samples were tested, 3 reference CFRP samples and 3 with embedded sensors.

At the higher rates of loading it was not possible to interrogate the EFPI sensors during the test due to the scanning speed of the CCD spectrometer. At the fastest setting, the time taken by the spectrometer to acquire a complete spectrum was 3 ms. At a test speed of 25 the cavity length change within that 3 ms was of sufficient magnitude that the spectra consisted of several cavity lengths which could not be separated. Therefore, the effect of loading rate on the EFPI sensors could only be examined at the following speeds, 0.025, 0.25 and 2.5 $\text{kN}\cdot\text{s}^{-1}$. The samples with embedded sensors were still tested at the higher speed to investigate the effect of including sensors on the loading rate response of the carbon fibre composite.

3.4.9 Dynamic testing of composite samples without and with embedded EFPI sensors

This section of the experimental work deals with the fatigue testing of the CFRP samples. This testing was also carried out using an Instron 8501 servo-hydraulic machine. All fatigue loading was performed under load-controlled cycling with a constant loading rate of 250 $\text{kN}\cdot\text{s}^{-1}$. The strain in the samples was monitored using an

extensometer with a gauge length of 50 mm. All the data were recorded using a Labview program in accordance with DAQ Method 5 in Appendix 1.

The loading condition considered was T/C fatigue as this combines behaviour from both tension/tension and compression/compression fatigue conditions (Rotem and Nelson, 1989).

As this cycling involves a compressive load, the anti-buckling jig was used as described for the static loading in Section 3.4.7. To ensure that the jig did not inhibit the sample movement the parts of the jig in contact with the sample had a thin layer of molybdenum disulphide grease applied. Also to ensure the jig did not loosen during testing a thread-locking adhesive was used on the bolt threads. Once the sample was loaded into the hydraulic grips, the bolts were tightened to a torque of 2 Nm. The thread-lock adhesive was then allowed to cure prior to the start of testing, typically overnight.

Due to the restrictions of the CCD spectrometer acquisition speed the sensors could not be monitored during the cycling of the samples. Therefore, to enable the durability of the sensors to be monitored, the fatigue cycling of all samples was stopped at regular intervals to allow a ramp loading of the sample to take place. These intervals were typically after 10^3 , 10^4 , 10^5 , 3×10^5 , 5×10^5 , 7×10^5 and 10^6 cycles. Prior to the start of fatigue testing and at the intervals stated, a ramp loading, which included tensile and compressive components, was carried out at a rate of $10 \text{ kN} \cdot \text{s}^{-1}$.

Stress ratios (R) of -1 , -2.5 and -3 were used during this investigation. The stress levels varied from 20% to 85% of the ultimate compressive strength of the composite.

Heat generation can be a problem in the fatigue testing of AFRC so an investigation was carried out to examine if there was any significant heating of the composite due to the testing or due to the embedment of a sensor. The temperature of two samples was monitored during fatigue cycling using a thermal imaging camera. Out of the two samples only one had an EFPI sensor embedded.

The thermal imager used was an Agema Thermovision 880 series camera (loaned from the EPSRC Instrument Pool). The images were acquired with a Thermal Image computer running CATSE software and analysed using IrWin Image control software. This is a cryogenically-cooled system with a temperature range of -20°C to 1500°C and a sensitivity of up to 0.07°C at 30°C . Both samples were run at a stress level of 40% UCS and a ratio of $R=-1$. Thermal images were recorded for the first 100,000 cycles of testing only, due to time and equipment limitations. Images were acquired at a rate of 1 image per minute for the first 10,000 cycles and then at a rate of 1 image every 5 minutes for the remainder of the testing.

4 EFPI Evaluation

This chapter presents the results from the evaluation of the EFPI sensors. The first aspect of the research was to examine the various ways of assessing the sensors' responses to the interrogation methodology. The next stage was the investigation of the manufacturing process of the sensors. This included the variations associated with the manufacture and the determination of the gauge length of the sensors. The final aspect of this section of the work was an assessment of the tensile strength of the sensors.

4.1 Spectral Response of EFPI sensors

The optical response from the sensor was dealt with in different ways to obtain the cavity length during the project. There were 3 analysis methods employed; raw spectra, normalised spectra and FFT analysed spectra.

4.1.1 Raw spectra

This was the spectra as received from the sensors by the CCD spectrometer, an example is shown in Figure 4-1. The sensor was interrogated with a light source centred at 850 nm, and this spectrum was the result of the interference pattern from the sensor superimposed onto the light source spectrum.

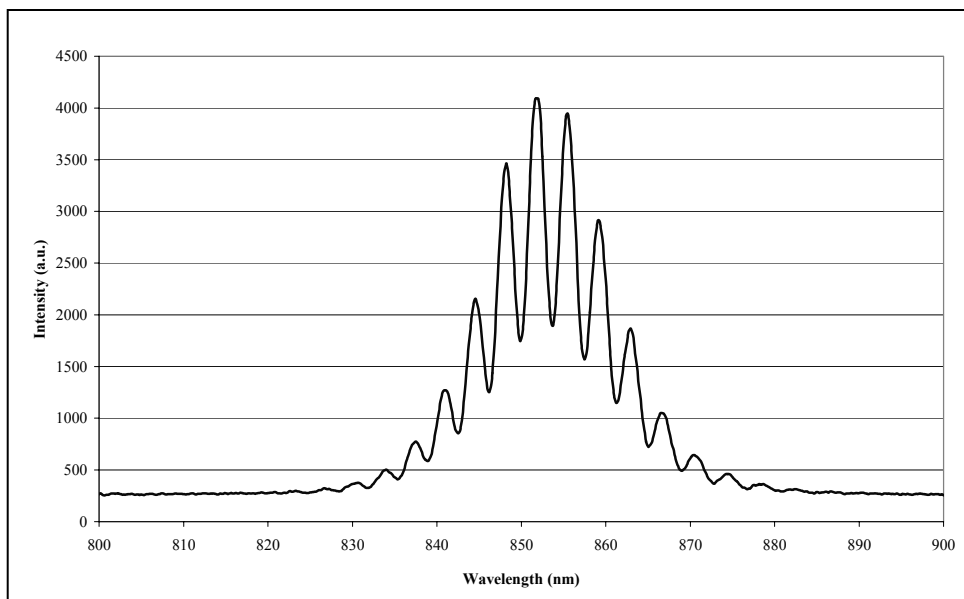


Figure 4-1 Spectrum from an EFPI sensor as received by spectrometer.

4.1.2 Normalised spectra

For this case, a reference spectrum was recorded of the light source prior to the interrogation of the sensor. This was then subtracted from the raw spectrum, to allow just the interference pattern to remain. An example of this is shown in Figure 4-2. At large cavity lengths, greater than 100 μm , this method became more usable compared to the analysis of the raw spectrum as the interference pattern can become masked by the light source.

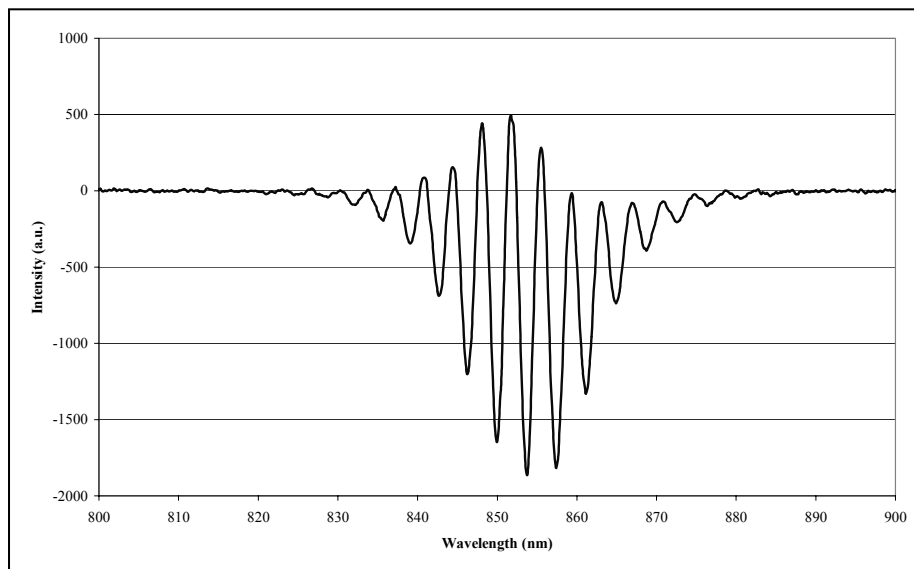


Figure 4-2 Normalised EFPI spectrum.

For the raw and normalised spectra the peak counting method as described in Section 3.4.1 can be used.

4.1.3 FFT analysed spectra

For this case, the spectra obtained from the sensors was subjected to an FFT analysis as described in Section 3.4.1. An example of the outcome of the analysis is presented in Figure 4-3. The result was symmetrical due to the nature of the FFT analysis. The lower peaks were used to obtain the cavity lengths through the method resulting in Equation 3-9. The FFT analysis was performed on either the raw or normalised spectra.

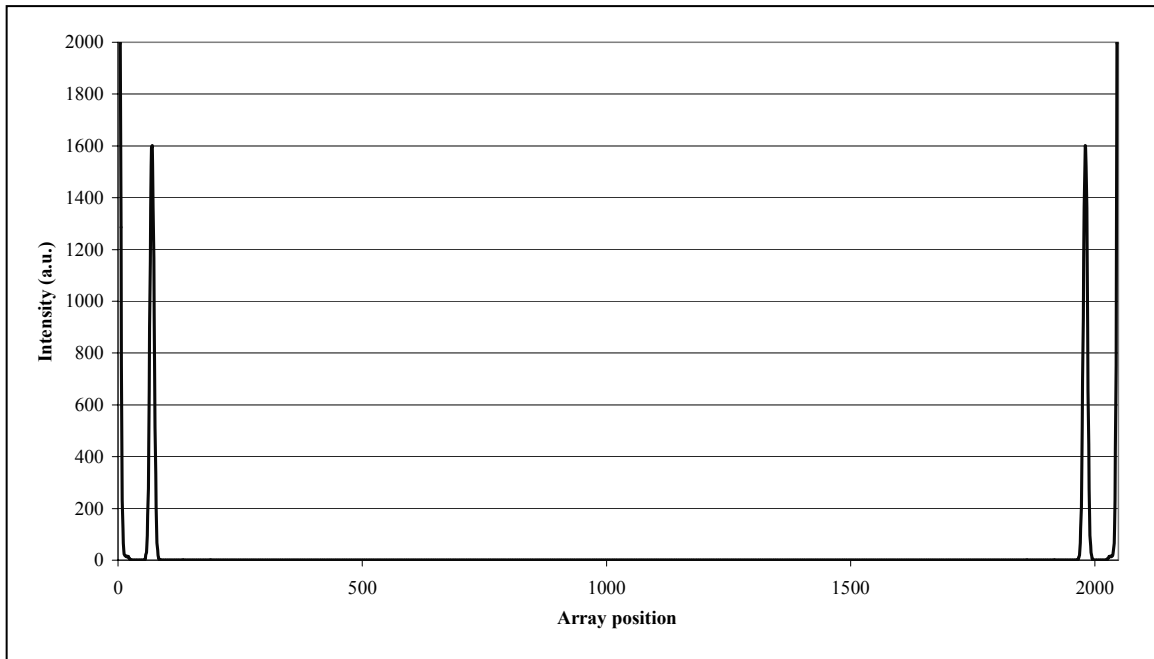


Figure 4-3 FFT analysis of the EFPI spectrum.

4.1.4 Variations in the calculated cavity lengths

It was noticed that the slight variations in the calculated cavity length were obtained during the testing, when using the different analyses methods on the same sample, these variations are described below.

The first observation was made when the peak counting method was employed. It was found that the calculated cavity length depended on which peaks were chosen for use in the equation. To demonstrate this, for the spectrum given in Figure 4-1, the centre two peaks and 2 peaks which were several cycles apart were chosen to for use in the calculation of the cavity length. The results of these calculations are shown in Table 4-1.

Spectrum	Peaks	λ_1 (nm)	λ_2 (nm)	No. of cycles	Cavity (μm)
Raw	Centre 2 peaks	851.83	855.47	1	100.1
Raw	1 st and last peak	841.03	866.66	7	99.5

Table 4-1 Effect on peak choice on the calculated cavity length.

This discrepancy occurs as the calculation to obtain the cavity length relies on the actual wavelengths chosen. For this method to be used successfully in testing the number of

complete cycles between the chosen wavelengths used in the calculation should ideally be kept the same. However, this was very difficult to implement as the number of cycles in the spectrum varies with the cavity length.

The second difference noticed was between the cavity lengths calculated from the raw and normalised spectra, as presented in Table 4-2.

Spectrum	Peaks	λ_1 (nm)	λ_2 (nm)	No. of cycles	Cavity (μm)
Scope	1 st and last peak	841.03	866.66	7	99.5
Normalised	1 st and last peaks	840.69	867.07	7	96.7

Table 4-2 Cavity length calculated from the raw and normalised spectra.

In this case, the presence of the light source spectrum distorts the interference spectrum in the raw data. This alters the position of the peaks, and due to the sensitivity of the calculation to absolute peak position, the cavity length value. Therefore, when the light source spectrum was removed, the observed peaks were purely from the interference pattern generated by the sensor.

The third difference was found between the peak counting and FFT analysis of the spectra, this effect is shown in Table 4-3.

Method	Cavity length (μm)	Method	Cavity length (μm)
Raw peak count	99.5	Raw, FFT	98.5
Normalised peak count	96.7	Normalised, FFT	98.8

Table 4-3 Showing the variation in cavity length calculations due to the analysis method chosen.

The FFT analysis was less dependant on the type of spectrum, raw or normalised, used as it was based on the frequency of the interference pattern as opposed to the wavelength of the peaks. Therefore the FFT analysis was predominately used for the interrogation of the EFPI sensors used in this project.

However, there are also other sources of discrepancies of the data. The FFT analysis assumes that the data points are equally spaced and this is not the case for the CCD spectrometers used in this project. The pixel spacing varies from 0.130 nm to 0.127 nm over the wavelength range used within this project, 800 nm to 900 nm. This can cause a

broadening of the FFT peak generated, but the change is relatively small and the same range was used for all the samples which should minimise this discrepancy. Another possible source for discrepancy was the SLD light source used, the spectrum of this drift with temperature. This was minimised through the use of a piezoelectric thermal controller and ensuring that the light source was switched on

4.2 Variation in EFPI Manufacturing Method

During the manufacture of the EFPI sensors, it was found that some variations occurred during the formation of the fusion points when the electric arc was used to attach the capillary to the optical fibres, as shown in Figure 3-1. The location of this join was important as it determined the gauge length of the sensor.

Figure 4-4 shows an example of a good fusion point. There is no visual distortion of the capillary or fibre.

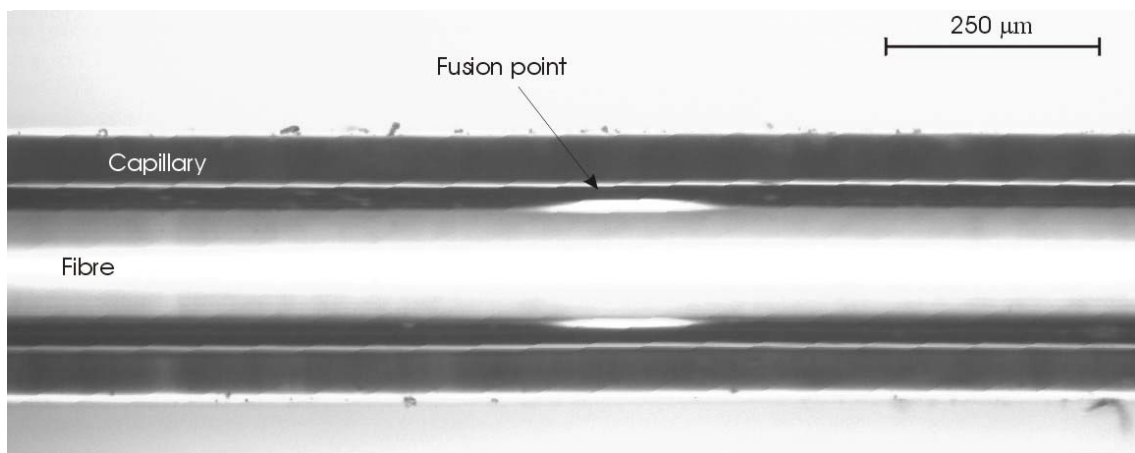


Figure 4-4 Image of a sensor with a good fusion point.

Figure 4-5 shows what can happen when the manufacture setup was incorrect. In this case the electric current for the arc was set too high and this caused the severe bending of the capillary and fibre. Mr Tetlow noted that on a daily basis the setup for the electric arc needed minor alterations to the current and time settings. This was achieved through performing test joins until a suitable setup was achieved to enable good fusion points. It was felt that this was at least due in part to the different day-to-day

environmental affects, such as the external temperature and humidity (J Tetlow, personal communication). It has been noted by Berg and Johanse (1995) that environmental conditions can have serious implications in the production of high quality splices, including dust particles in the atmosphere and the humidity of the environment.

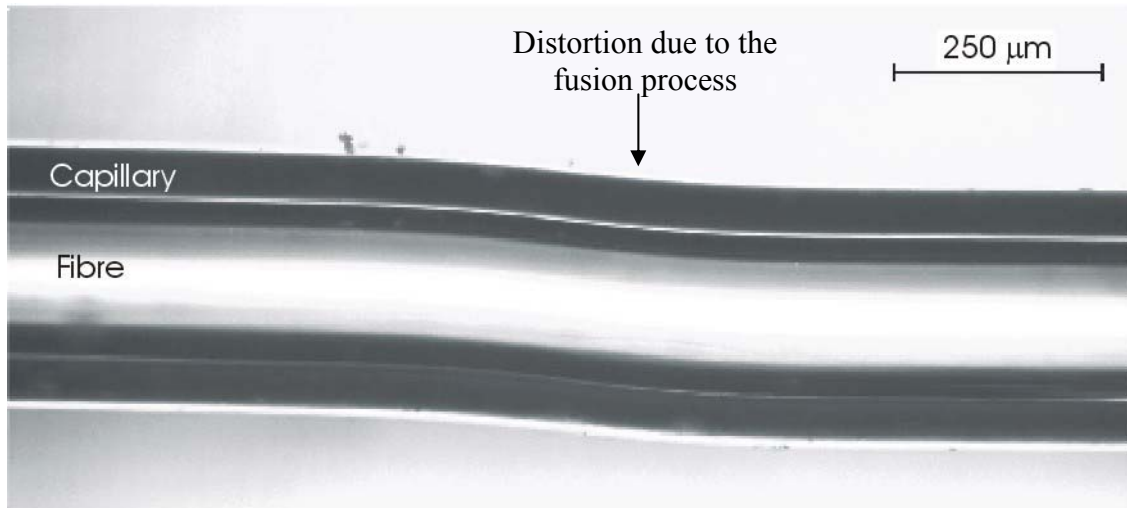


Figure 4-5 Severe bending of an EFPI sensor due to the fusion-based manufacturing process.

Distortions generated within the sensors during manufacture could cause problems during application of the sensors. The first issue is the formation of the fusion point, if this is missing the sensor will not respond as expected to the applied strains as the gauge length will be undefined. Secondly, if severe bending occurred as in Figure 4-5, this could lead to problems during embedment of the sensor, it would not lie alongside the reinforcing fibres and it could generate a large resin rich or void area. The deformation could also affect the strength of the sensors preventing them from operating over the designed strain range. Another issue associated with any bending occurring during manufacture could be the affect on the response of the sensor to loading, possibly generating a non-linear response. Therefore, great care was taken to ensure that the sensors used in this project were free of distortion by a visual inspection of the fused regions during and after manufacture.

4.3 Determination of the Gauge length

The gauge length is an important parameter for the use of EFPI sensors to monitor strain, as it is this value that is required to derive the strain from the change in cavity length. At this stage, due to the variations in the manufacturing process, this value was likely to be different for each sensor and would therefore need individual determination.

4.3.1 Optical measurements

This method involved examining the sensors under a microscope, observing both fusion points and measuring the distance between them. A problem encountered with this method was that it was not always clear as to the exact location of the fusion point. Figure 4-6 shows a sensor where a fusion point has been made, the optical fibre cannot be removed from the capillary so the fibre and capillary are joined; however, the fusion point is not clearly visible. It is likely to be the small light area as shown by the arrow, but this could also be a reflection due to the lighting under the microscope.

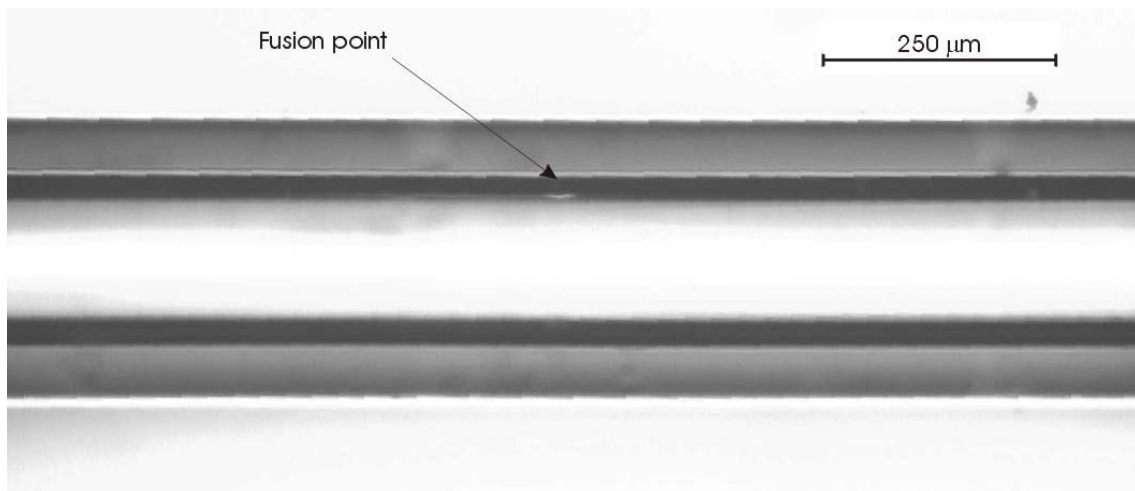


Figure 4-6 An image showing the difficulty in locating fusion points.

One explanation for this was that the fusion point was only on one side of the sensor, as the arc can only go one side or the other of the capillary. The sensors can be rotated to enable examination of the other side in an attempt to locate the fusion point, but due to

the fragile nature of the sensors this can be difficult to achieve without causing fracture of the sensors.

A separate study on the observation on these fusion points was carried out by Mr D Winter, Group Technician. Several sensors were examined under the microscope and images were taken at the start position and after rotations of 90°, 180° and 270°. The images for one of the sensors are presented in Figure 4-7, from this it can be seen that the fusion point was only visible on one side of the sensor. However, during this observational work at least two sensors fractured, but it showed that if sufficient care was adopted that the fusion points for a EFPI sensor could be located, thereby allowing the gauge length to be measured.

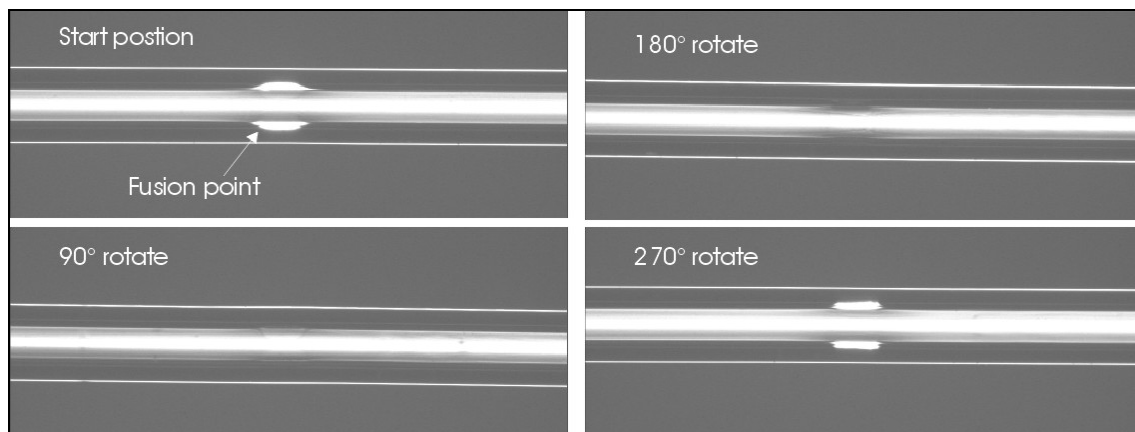


Figure 4-7 Images of an EFPI sensor rotated to enable all sides of the fusion point to be seen.

The use of the electric arc is the limiting factor in any attempt to improve this situation. Multiple arc points or electrodes could be employed to generate a more complete fusion point, but great care would be required in the setup and application stages to ensure that no deformation of the sensors could occur. Ideally, the sensors required fusion points that would be completely circumferential; this would require a completely different method of generating the fusion points. Possible other methods for achieving a fusion point could be either the use of a glass solder (Daniel *et al.*, 1994) or CO₂ laser heating (Khoe and Lyndtin, 1986). These also have their disadvantages as well as advantages over the electric arc fusion point. A current application of glass solder is to attach optical fibres to a silica substrate in fibre optic couplers. This involves similar materials

to those found in the EFPI sensors so this could be an option. The glass solder's main disadvantage is that it is usually applied as a slurry and then heated. This could lead to difficulties in the control of the position of the capillary/fibre contact point due to the placement of the slurry. CO₂ laser heating is used as a method for fusion splicing of optical fibres. Again this is similar to what is required in the manufacture of EFPI sensors and could be an option. In the case of the CO₂ laser, it does not have a problem with the control of heating location, but on repeatability of the energy pulses that controls the heating of the fibres.

Overall, there seems to be no definitive answer on the best method of achieving a good join between the capillary and fibre further work into this area is definitely required. However, it was outside the timescale of this project.

4.3.2 Comparison of strain gauge and EFPI sensor data

This method to determine the gauge length involved the EFPI sensor being surface mounted onto a steel specimen with electrical resistance strain gauges alongside. The major disadvantage with this method was that it required very great care to remove the EFPI sensors from the samples after testing; the majority of sensors fractured during this process. Therefore, it was only used to ensure the optical measurements were suitable for determining the gauge length. During the loading of the steel specimens the responses of the EFPI sensors and electrical resistance strain gauges were recorded.

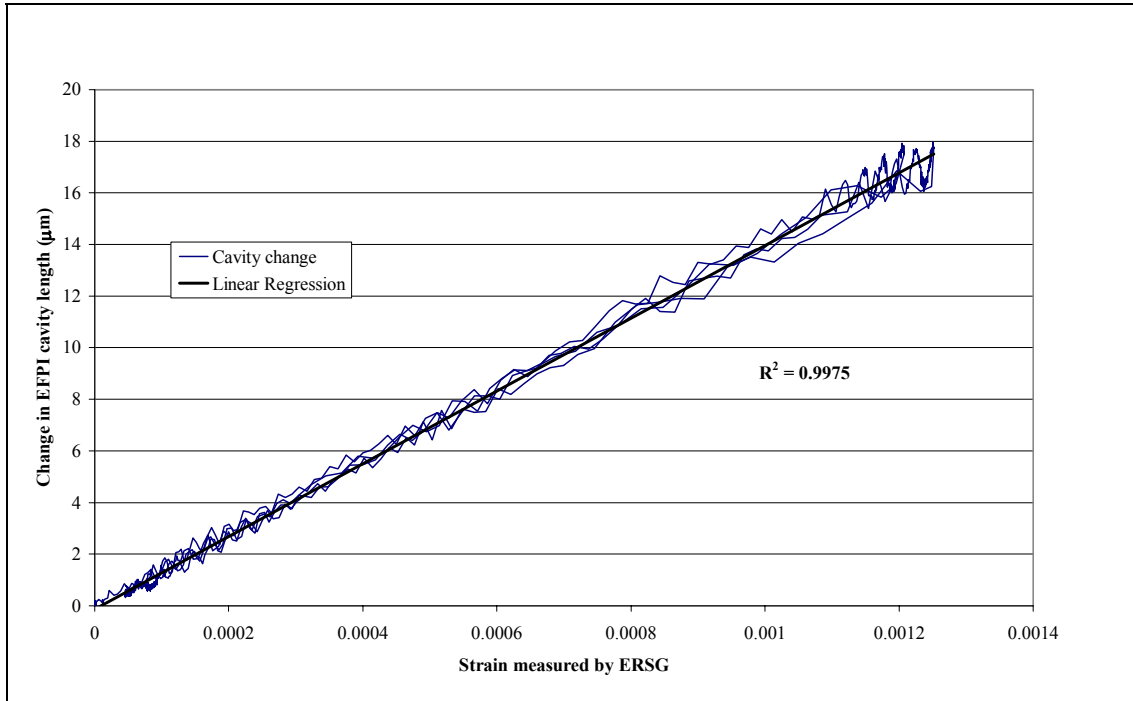


Figure 4-8 A graph comparing the ERSG and EFPI responses to an applied load.

Figure 4-8 shows the change in cavity length of an EFPI sensor compared to the strain data obtained from an electrical resistance strain gauge. The gauge length was determined from the gradient of the line of best fit of Equation 2-2, and described in Section 2.2. It can be seen from Table 4-4 that the values obtained from the strain gauge comparison are lower than those measured optically.

EFPI sample	Optical measured gauge length (mm)	Gauge length determined from steel samples (mm)
1	13.7	10.0
2	14.1	12.2
3	14.2	10.4
4	14.1	11.3
5	14.2	11.4

Table 4-4 Comparison of gauge length determination from optical and resistance techniques.

A possible explanation for this was that the adhesive used to attach the sensors to the steel sample was entering the capillary and flowing past the fusion points, thereby reducing the gauge length of the sensor. To further investigate the possibility of the adhesive flowing into the capillary, a sensor was taken and a drop of adhesive, that was

used to bond the sensors to the steel, was placed at the capillary ends. The results can be seen in Figure 4-9.

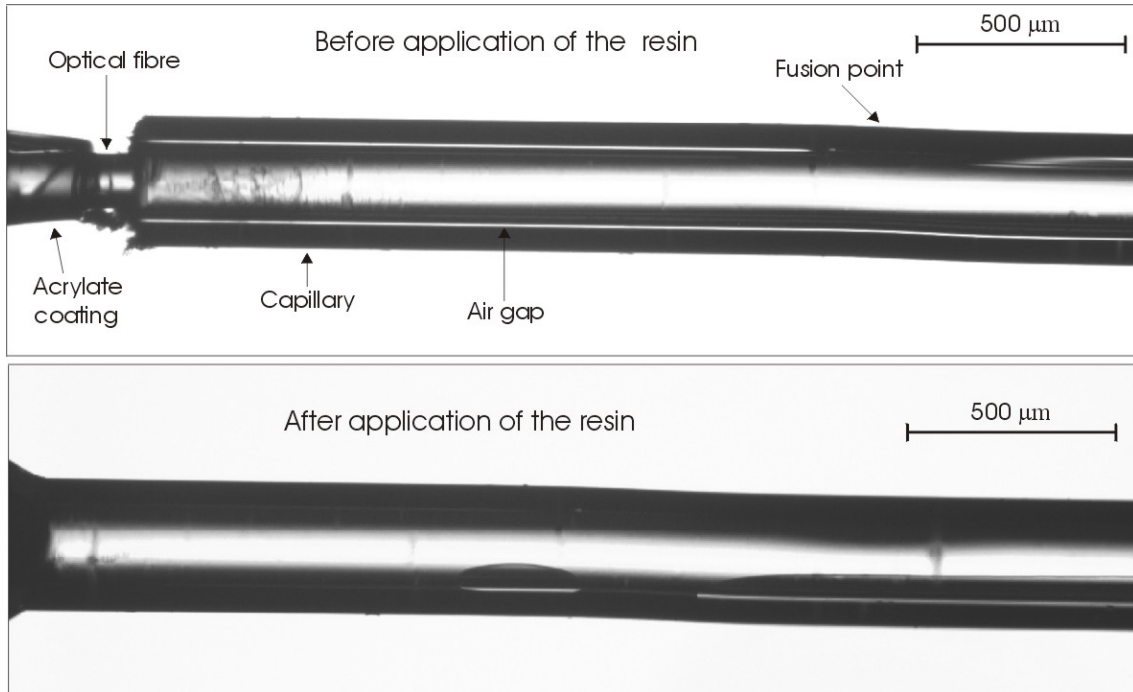


Figure 4-9 Effect of the application of an adhesive on an EFPI sensor.

From Figure 4-9 it can be seen that the fusion point was no longer visible after the application of the resin, and the air gap is less distinct. As the resin has flowed up to and possibly past the fusion point the gauge length would no longer be between the fusion points, in this case the gauge length would have to be defined as the distance between the edges of the resin flow. An attempt to confirm that the resin flowing into the capillary altered the gauge length was made by attaching the sensors by the capillary surface, not the ends so as to minimise resin flow resin up the capillary. These results are shown in Table 4-5.

EFPI sample	Optical measured gauge length (mm)	Gauge length determined from steel samples (mm)
6	13.4	14.5
7	14.2	14.1
8	14.7	10.2
9	13.6	14.0

Table 4-5 Results from the EFPI sensors attached to the steel specimen only by the capillary.

This attempt was partially successful with three of the four sensors showing gauge lengths comparable with the optical measurements. Therefore, by ensuring care was taken to minimise the availability of the resin to flow into the capillary, the optically measured gauge lengths were comparable with those surface mounted on the steel samples.

4.3.3 Effect of gauge length on calculated strain values

Although the gauge length is important, how accurately it must be measured is a different issue. Shown in the Figure 4-10 is a stress-strain graph for a composite sample with an embedded EFPI sensor.

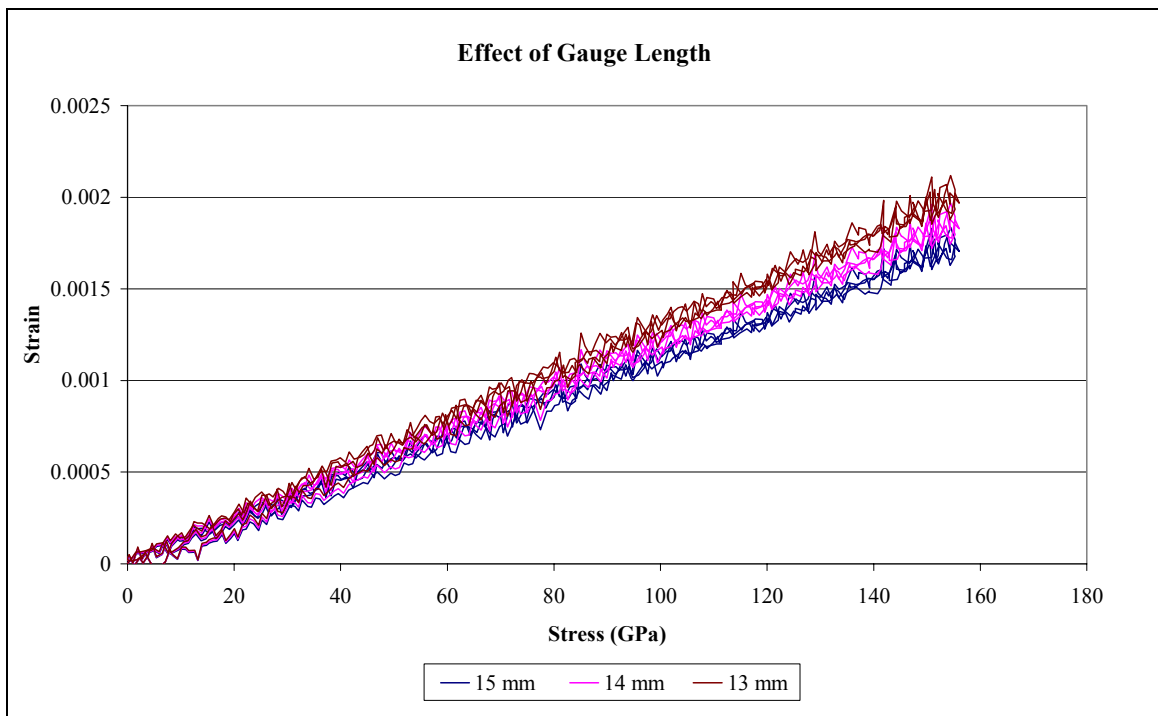


Figure 4-10 Effect of change in gauge length on the strain value obtained.

The strain was calculated from the EFPI sensor using three different gauge length values 13, 14 and 15 mm. Even though the lines were noticeably different the noise in the sensor's response was more significant at that stage. Therefore, if the optical method allows the gauge length to be known within ± 0.5 mm this should be sufficient until the sensor variation can be reduced. The variation in the response of the sensor

could be due to the resolution of the spectrometer and the light source variations. As shown in Section 4.1, small changes in the absolute wavelength can have a significant effect on the measured cavity length.

Overall it was felt that the measurement of the gauge lengths of the sensors by visual examination through an optical microscope provided sufficient information to allow the EFPI sensors to be constructively used.

4.4 Tensile strength of EFPI

This section deals with the investigation of the tensile properties of the EFPI sensors. This part of the work was designed to develop an understanding of the failure mechanisms of the sensors and to obtain an appreciation of issues relating to their fragility.

4.4.1 Coated optical fibres

To ensure the equipment chosen was suitable for use with optical fibres; several acrylate coated optical fibres were tested to failure. The average failure load was 53.6 N with a standard deviation of 0.6. A selection of the load/displacement curves are presented in Figure 4-11.

All the samples failed at the grips, therefore providing the loads when testing the sensors do not reach more than 50 N the grips should have no significant influence on the measured strength of the EFPI sensors.

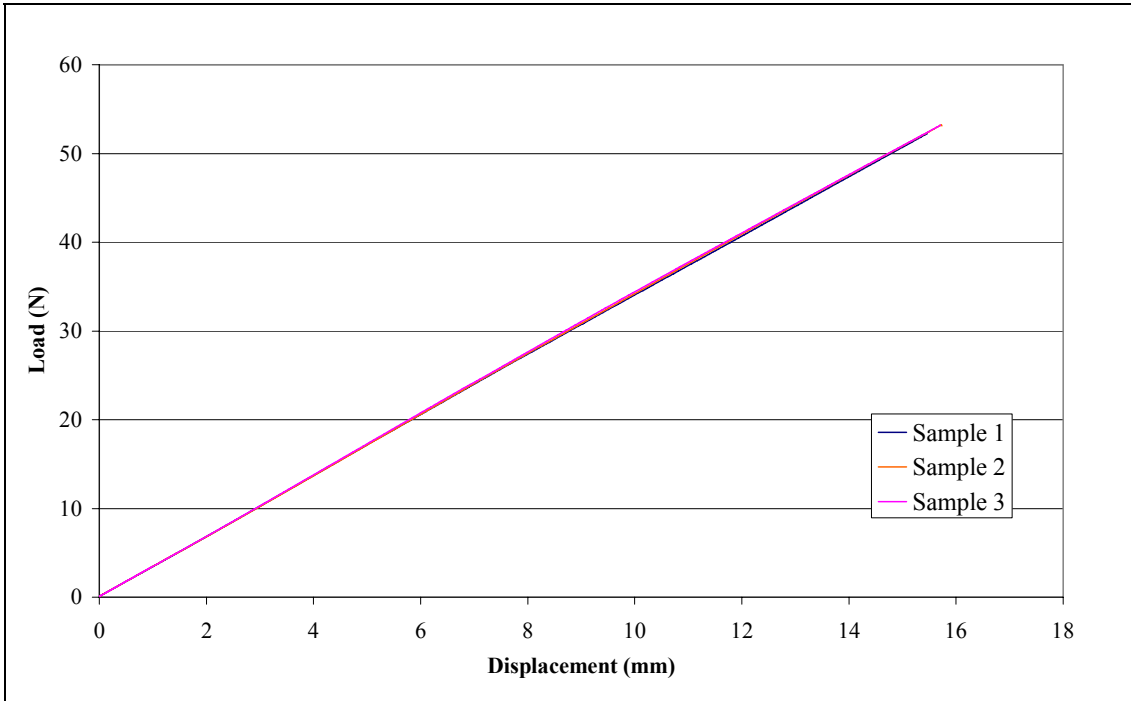


Figure 4-11 Load/displacements plots for three acrylate-coated fibres.

4.4.2 EFPI sensors

10 EFPI sensors were tensile tested to failure, with the results reported in Figure 4-12.

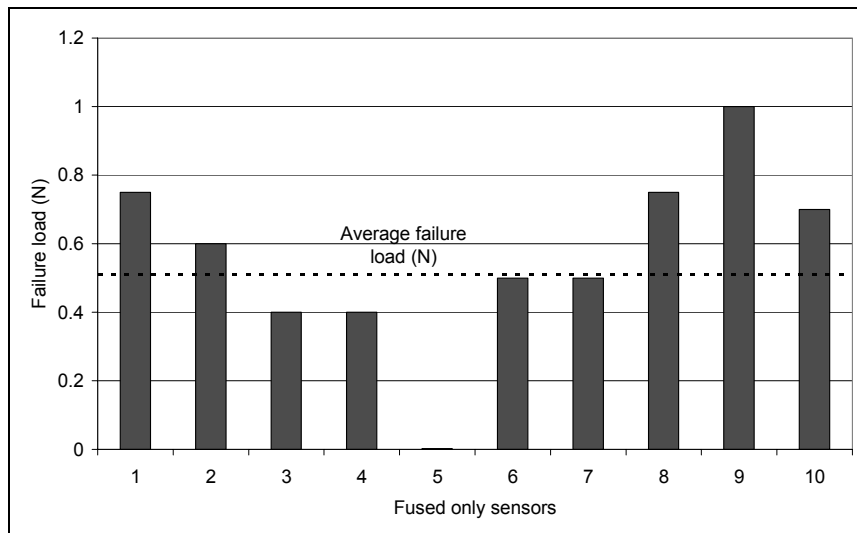


Figure 4-12 Tensile failure of unreinforced EFPI sensors.

From these results it was seen that the EFPI sensors were very fragile, with some of the sensors failing during placement into the grips. The sensors failed by the optical fibre being pulled out of the capillary, indicating that the failure was occurring at the fusion points.

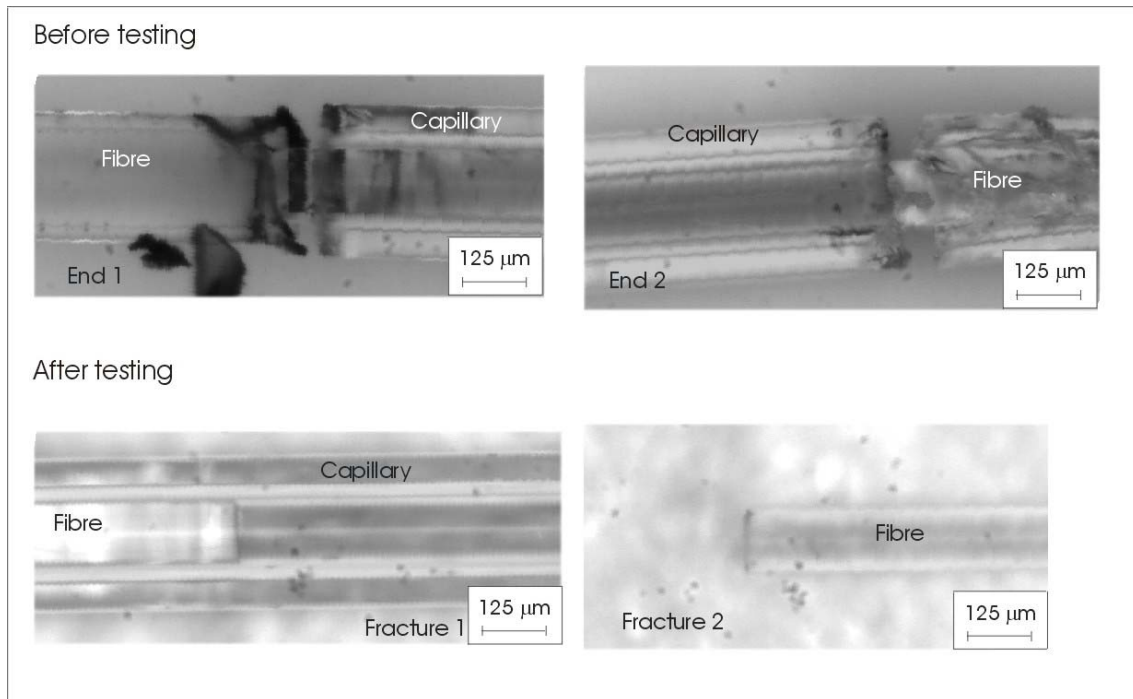


Figure 4-13 Images of an unreinforced sensor before and after tensile testing.

Figure 4-13 presents images of an unreinforced sensor that was subjected to tensile testing. It can be seen that the fibre fractured inside the capillary, at a position that corresponded to the fusion point location. This type of failure was noticed for all the unreinforced sensors examined. The fusion points were the locations of stress transfer from the fibre to the capillary and are therefore the likely failure locations. Lee *et al.* (2002) found similar results when mechanically evaluating EFPI sensors. In that case the fibre was joined to the capillary through the use of epoxy resin, but the failure locations for the sensors were still the fibre/capillary joints. There could also be affects from any distortions present from manufacturing, even if these were not visible during manufacture.

4.4.3 Reinforced EFPI sensors

In an attempt to improve the strength of the EFPI sensors, several resins were investigated as reinforcements for the fusion points. As described in Section 3.3.1, the ideal quantity of resin was just enough to seal the fibre into the capillary. This however was difficult to achieve in practise even though great care was taken, as can be seen by the images of reinforced sensors in Figure 4-14.

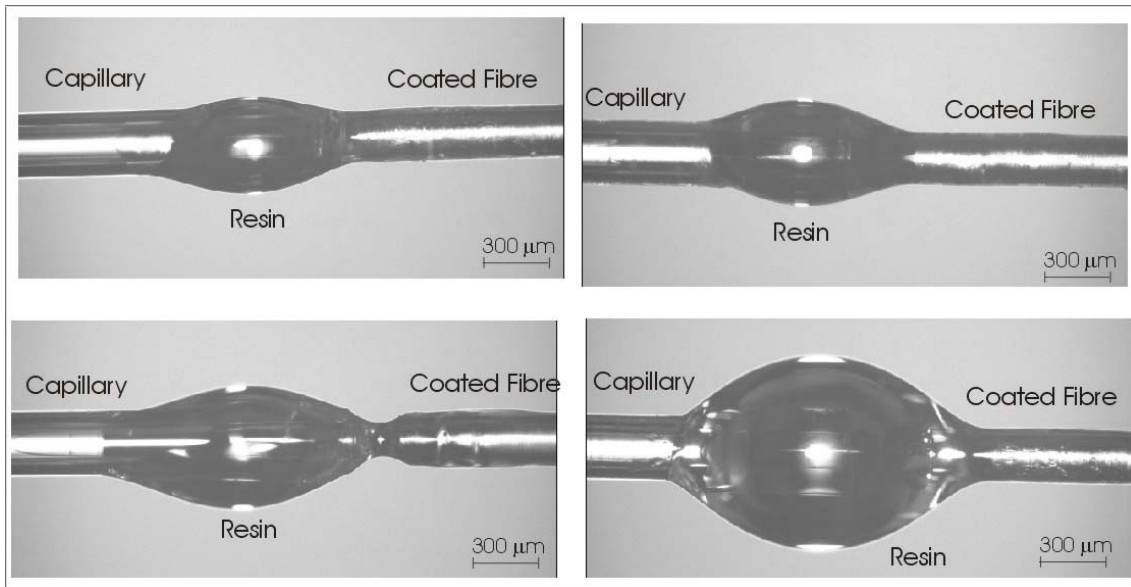


Figure 4-14 Variations in the size of resin reinforcement on the EFPI sensors.

It can also be noted from Figure 4-14 that the additional of the resin increases the dimensions of the sensors, which could lead to problems when embedded into fibre reinforced composite samples.

A minimum of 10 sensors were tested for each resin system. However, for the Araldite 2020 four of the results were excluded, as the adhesive appeared to not have cured fully prior to testing, probably due to insufficient mixing of the adhesive.

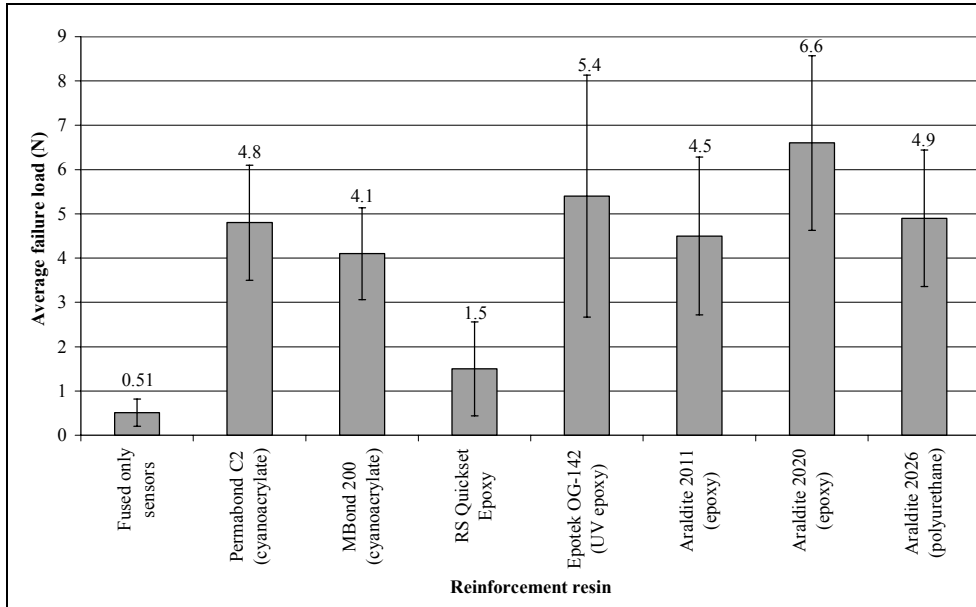


Figure 4-15 Graph shows the tensile load to failure of reinforced EFPI sensors.

All but the Quickset epoxy significantly improved the strength of the sensors; however there was a large deviation from sample to sample. This is likely to be due to the difficulties of applying similar quantities of resin in the same location for every sensor. A graph of the change in cavity length against applied load is presented in Figure 4-16, which shows that the different resins did not affect how the sensors responded to the applied load, only as to when the sensors failed.

From these results, it can be seen that the Araldite 2020 epoxy resin would be the most suitable for reinforcing the fibres.

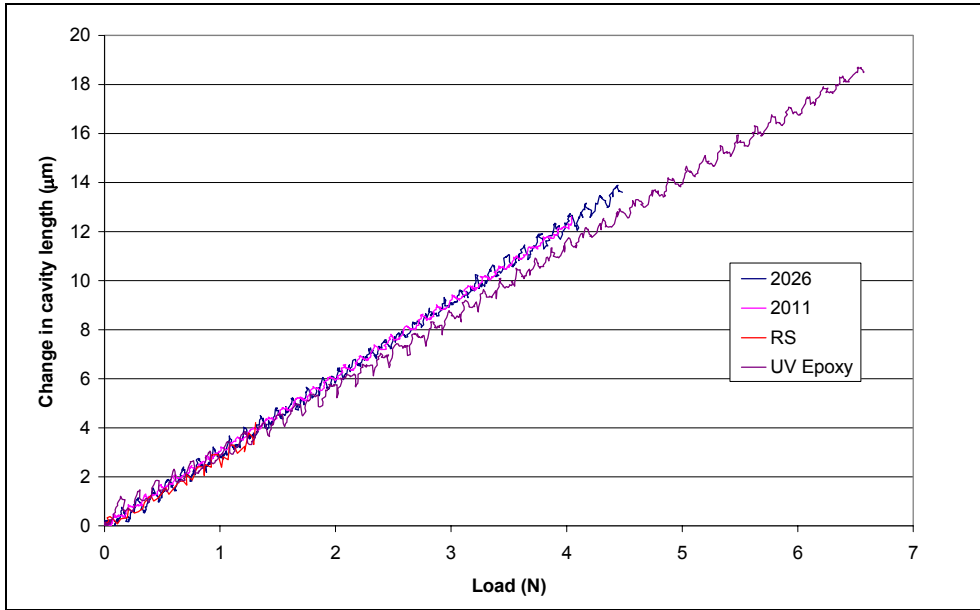


Figure 4-16 Graph showing the change in cavity length due to tensile loading for four sensors reinforced with different resins.

There were two main failure locations for the reinforced sensors, Type 1 failure is shown in Figure 4-17 where the complete fibre pulls out from the capillary with the main failure point at the resin.

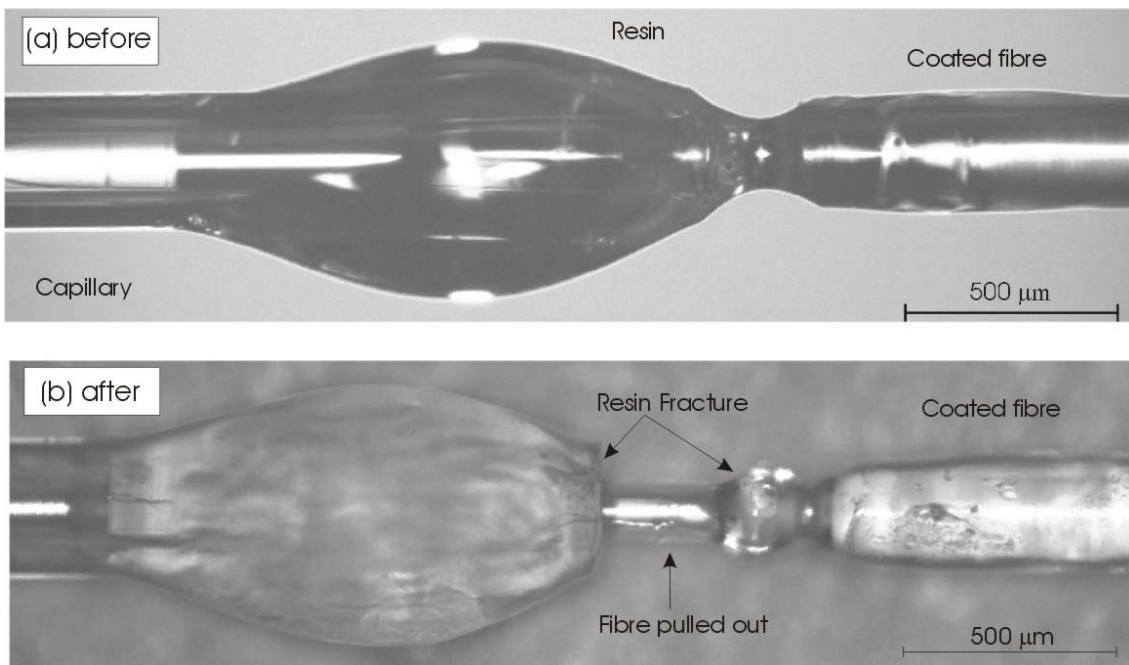


Figure 4-17 Micrograph of (a) before and (b) after testing a reinforced sensor, Type 1 failure.

Type 2 failure was where the fibre fails and then pulls out, an example of this is shown in Figure 4-18 with the fibre failing just within the capillary, possibly at the fusion point.

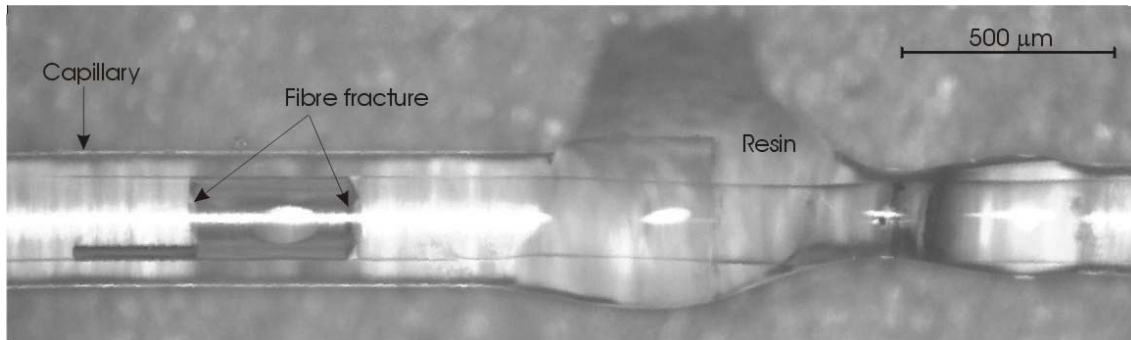


Figure 4-18 Failure of the fibre within the capillary during tensile testing, Type 2.

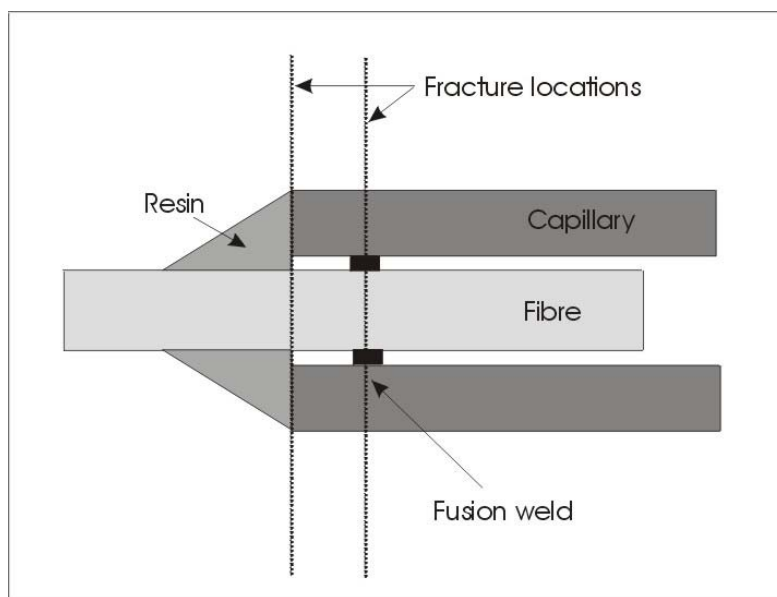


Figure 4-19 Schematic of the observed failure locations within resin reinforced sensors.

The two different types of failures are shown schematically in Figure 4-19.

Another issue when a resin was applied to a sensor was that locating the fusion point became more difficult as the resin covered the outside of the capillary obscuring the fusion points.

4.5 Conclusions

To enable confidence in the use of EFPI sensors at this stage each sensor had to be examined optically prior to use. There were two main reasons for this; the first is to ensure that no defects have been generated during manufacture, e.g. at the fusion points. The second reason is to determine the gauge length of the sensor, the optical measurements providing sufficient information for the set-up used in this project.

Unreinforced sensors are very fragile and must be handled with extreme care. The application of resins to the ends of the capillary can improve the strength of the sensors but care needs to be taken to ensure that any resin entering the capillary does not alter the gauge length. This care on the application of the resin also applies to any EFPI sensors that would be surface mounted.

One option for the reinforcement resin that could minimise the likelihood of affecting the gauge length would be to use a high viscosity UV curing resin. As it is high viscosity it would have limited travel into the capillary, and as UV curing resins can cure quickly it would have a reduced time to travel into the capillary. However, the final choice of resin for the reinforcement of the sensors would depend on the application. For example, in embedment applications into fibre reinforced composites, a resin that reduced the mismatch between the resin and matrix properties would be most suitable. Or in the case of a surface mounted sensor in an external environment, a resin that would withstand the changes in the weather would be required.

The main disadvantage of using a resin to reinforce the sensors is that it will increase the dimensions of the sensors, which could lead to extra deformation when the sensors are embedded into a composite. Also as found by Lee *et al.* (2001) the inclusion of a resin at the end of the sensors, that is not very carefully controlled, can generate large voids surrounding it leading to problems with the strain transfer to the sensors and the quality of the composite samples.

5 Interfacial Characterisation

The interface between the sensor and the sample is very important for all sensors. In the case of strain sensors to ensure that there is strain transfer between the sensor and sample there must be intimate contact between them. This chapter deals with the characterisation of this interface between the sensors and the sample. There were two main parts to this, the surface energy of the sensor and the interfacial shear strength (IFSS) between the sensors and the sample.

5.1 Surface Energy

Surface energy is the driving force behind an interface being formed. To examine the surface energy of the sensors, contact angle measurements based on the Wilhelmy technique were performed on the silica optical fibres. Figure 5-1 shows a typical result generated by Camtel Dynamic Contact Analyser (CDCA).

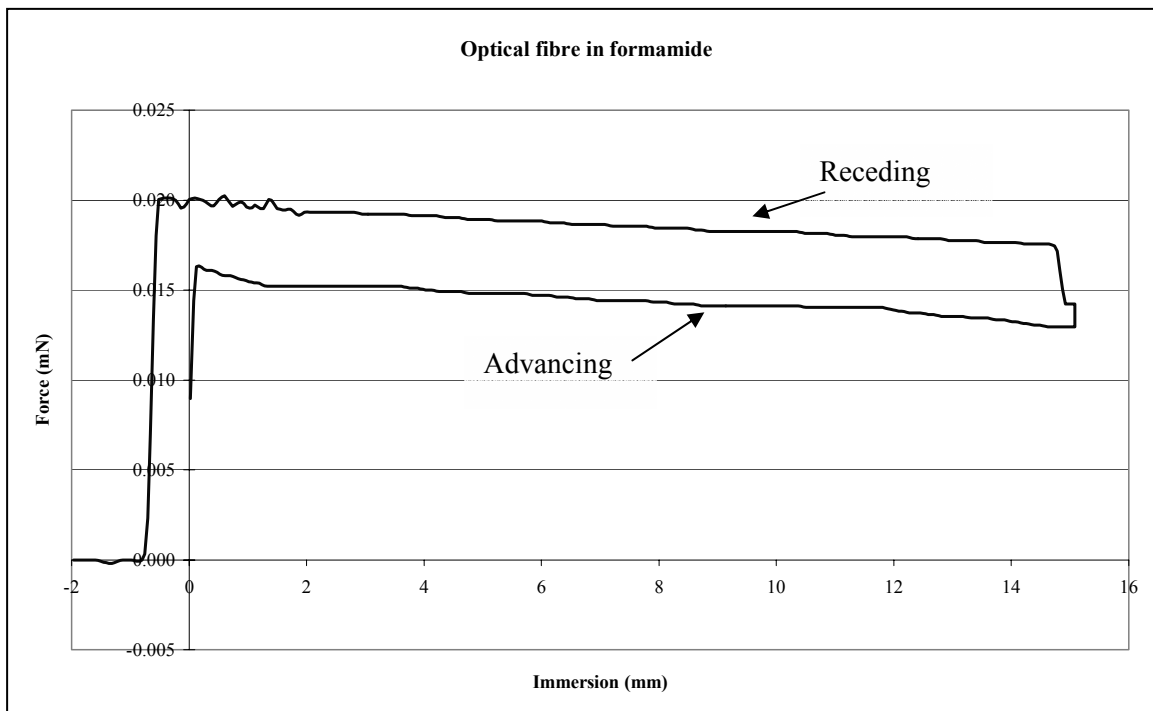


Figure 5-1 Graph showing the results generated by CDCA for an optical fibre immersed into formamide.

Advancing and receding refer to the liquid being either pushed or withdrawn over the sample respectively. These values are different usually due to the surface roughness or

chemical inconsistency in the solid surface (Kinloch, 1987). The difference can also be due to kinetic affects due to the movement of the liquid during testing (Myers, 1991). There was a negative immersion depth on the receding line because as the fibre was withdrawn from the liquid it had to break the surface tension of the liquid. From the graph in Figure 5-1, a linear regression was performed on the advancing and receding line to obtain the force at zero immersion. This value is then used to determine the contact angle, as described in Section 3.4.4.

5.1.1 Cleaning methods

The first stage was to determine a suitable preparation method for the silica samples. Initial work involved stripping the optical fibre of its acrylate coating, wiping with solvent and then cleaving the end. The data generated in these experiments showed a distinct variation along the length of the optical fibre. The method was then reversed so the samples were cleaved then solvent wiped, and this removed the variation. In Figure 5-2, this effect is shown in graphical format. These samples were tested against glycerol.

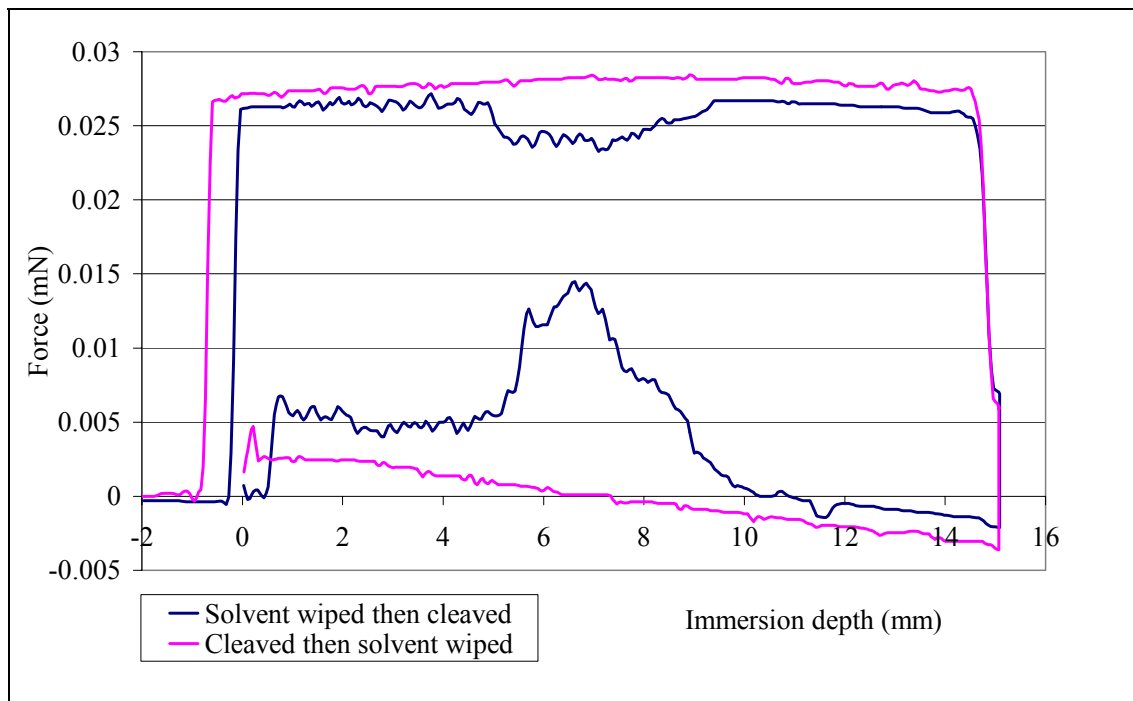


Figure 5-2 Variation in cleaning methods.

It can be seen that from Figure 5-2 that the sample with the final stage of cleaving a large inconsistency is present at approximately 6 mm from the endface of the fibre. When this distance was compared to the precision cleaver used to prepare the fibres, it was found that it matched with the rubber pads used to hold the fibre during cleaving. It was considered that these rubber pads were contaminating the fibres, the rubber pads were likely contaminated with dust particles from the environment and grease from the handling of the cleaver. Cleaning the rubber pads reduced this effect, as shown in Figure 5-3, but it was felt that to minimise the risk of contamination the samples should be cleaned after cleaving.

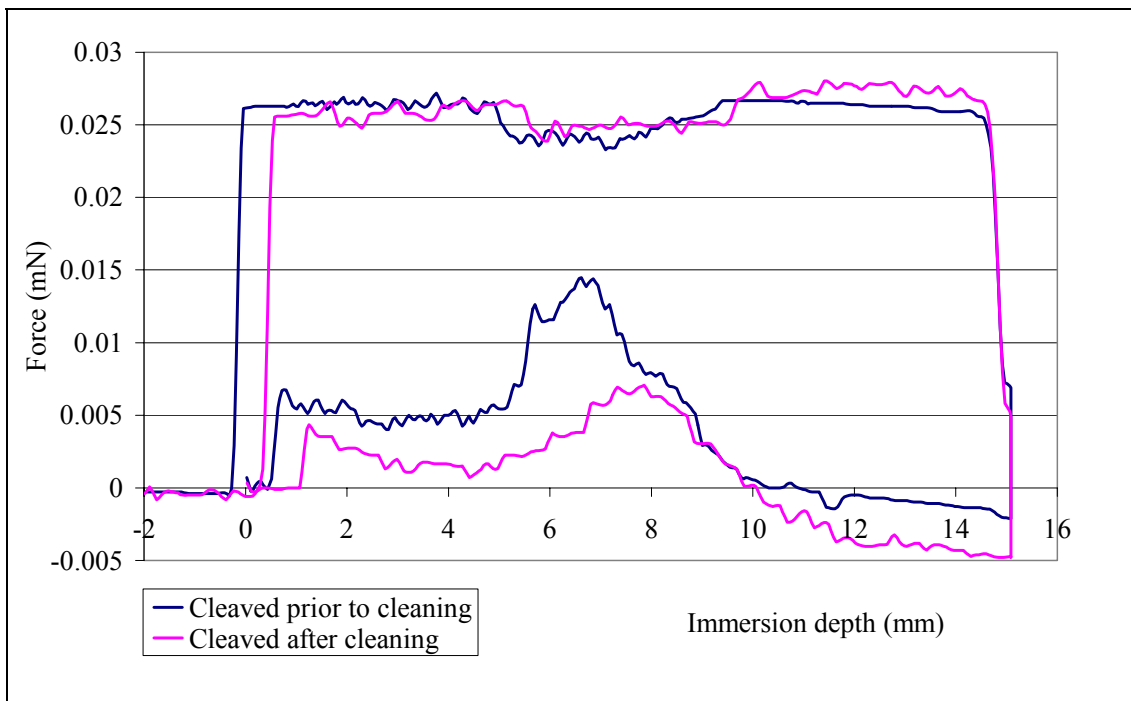


Figure 5-3 Graph showing the effect of cleaning the cleaver on the contact angle response of an optical fibre.

The results shown in Figure 5-2 and Figure 5-3 were still noisy as this testing was carried out in the early stages of the assessment of cleaning techniques.

The next stage was to optimise the preparation method, for which a reliable system was required. Figure 5-4 shows the summary of advancing contact angle results for the various preparation techniques investigated. On examining the results the average

contact angle values vary for the different methods but for consistency of results the Hellmanex™ cleaner appears to generate the lowest variations.

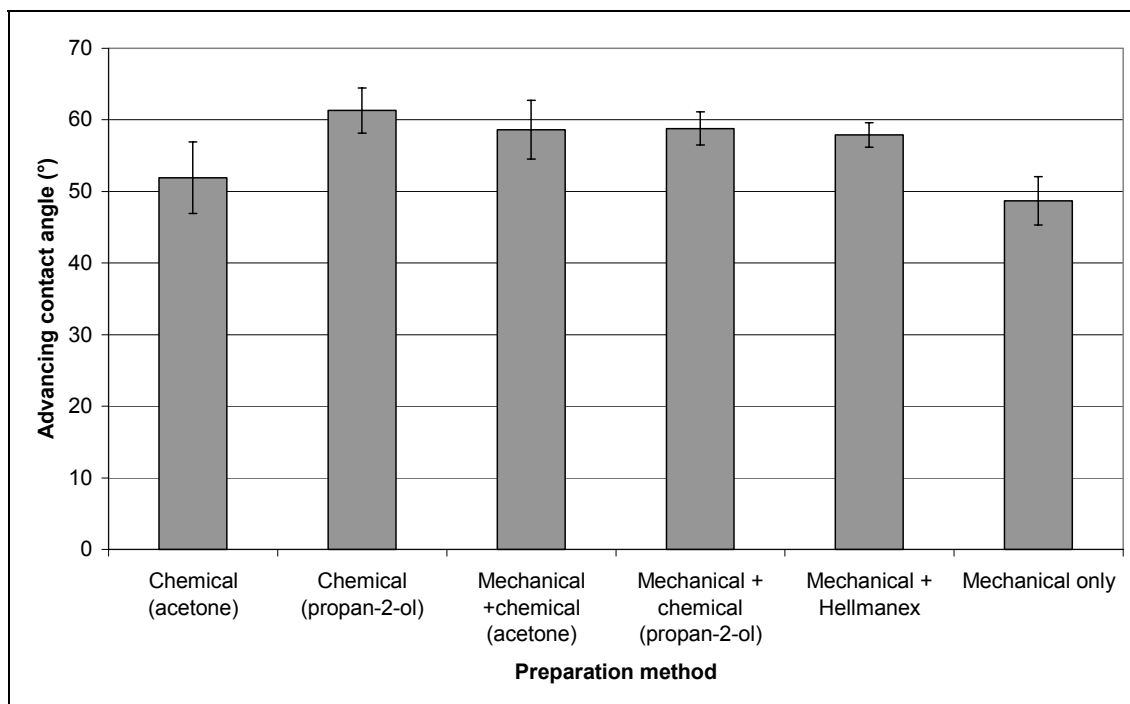


Figure 5-4 The effect of preparation method on the advancing contact angle of silica fibres.

The main difference between the Hellmanex™ method and the others was that the Hellmanex™ method did not require the silica surface to be wiped with a solvent and a lint-free cloth, which could have been leaving some contamination behind. Another possible reason for the improved consistency of the Hellmanex™ method is that it is designed for cleaning silica and quartz. As the Hellmanex™ preparation routine was the most consistent it was used for the remainder of the work in this project. It is also possible that the different treatments affected the surface chemistry of the silica. There were different types of treatment used were polar solvents (acetone and propan-2-ol), halogenated solvent (DCM) and an alkali solution (Hellmanex™). These different solvents could have affected the surface of the silica, but it would require further investigation which was outside the scope of this project.

5.1.2 Surface energy comparison between capillary and fibre

Although the capillary is the actual surface of the sensor that forms the interface within the matrix, it poses certain difficulties in the execution of the planned experiments.

Mainly these difficulties were associated with the IFSS measurements. It would have been very difficult to successfully pull a capillary from the samples as the capillary was found to fracture when placed within the grips of the testing machine. It was therefore planned to use optical fibres as a replacement for the capillary in the interfacial studies. The set of experiments reported in this section were obtained to examine the suitability of the optical fibre in replacing the capillary for the remainder of the work.

From the data obtained in the testing it was found that for several of the fibres and capillaries the receding angles were reported as zero. Therefore, the calculations for the surface energies were based on the advancing contact angles, as the calculations are not valid if the liquid completely wets the surface, i.e. zero contact angle. Figure 5-5 presents the average contact angle measured for the capillary and optical fibre against each of the test liquids, for each material/liquid combination at least 10 samples were tested.

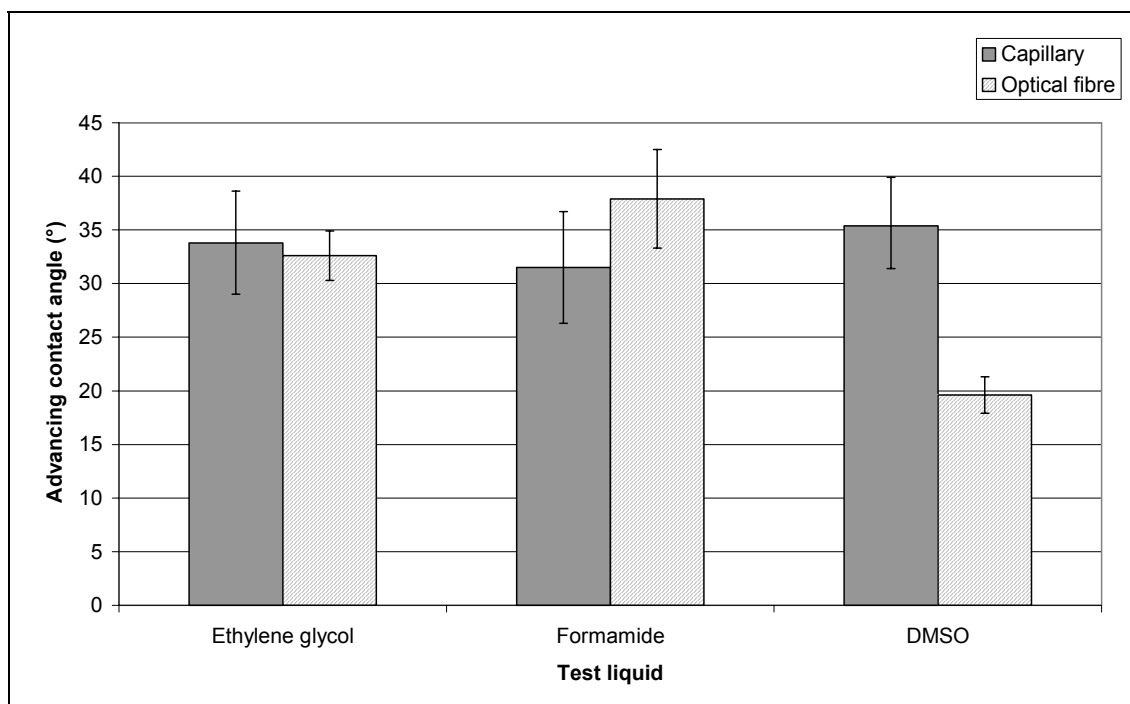


Figure 5-5 Results of contact angle measurements on capillary and optical fibre.

Overall, from Figure 5-5 it can be seen that the optical fibre behaves in a similar manner to the capillary. The exception to this was the results from testing against DMSO. With

hindsight, the testing of the capillary and optical fibre against DMSO should have been repeated. Also DMSO is a hygroscopic liquid and as the testing of the capillary and fibre samples were carried out on different days it is possible that the DMSO was not the same for all the testing. Ideally future work would use an alternative liquid although suitable liquids are difficult to find as many completely wet out the silica surface and can therefore not be used.

The obtained values of contact angles against the test liquids were then used to calculate the surface energy of the capillary and optical fibre through the Owens-Wendt approach. The Owens-Wendt plot for both the capillary and optical fibre are shown in Figure 5-6. In Figure 5-6, the data from the testing against the DMSO, formamide and ethylene glycol are at “x” values of 0.49, 0.69 and 0.81, respectively. It can be seen from this that the capillary and optical fibre samples behaved in a similar manner, with the ethylene glycol and formamide results overlapping and the DMSO showing more of a difference. The surface energies obtained for the optical fibre and capillary from Figure 5-6 are shown in Table 5-1.

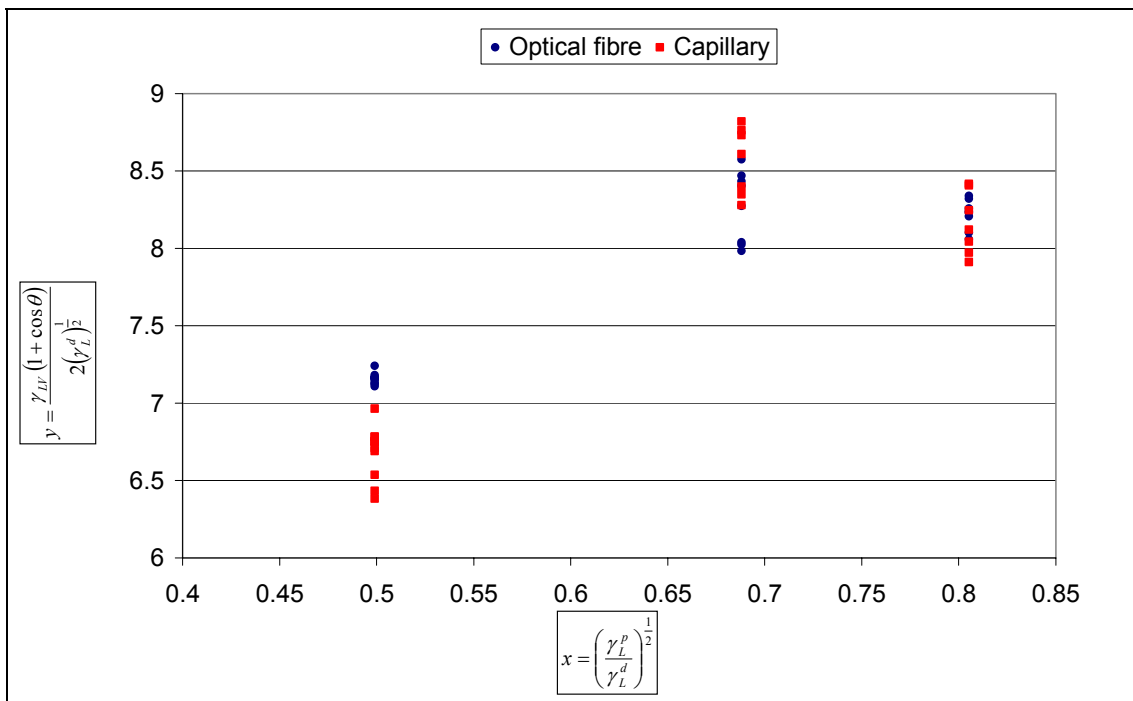


Figure 5-6 Owens-Wendt plot for capillary and optical fibre samples.

Material	Dispersive Energy (γ^d)	Polar Energy (γ^p)	Surface Energy ($\text{mN}\cdot\text{m}^{-1}$)
Capillary	16.3	31.5	47.9
Optical fibre	28.6	14.5	43.1

Table 5-1 Surface energy results for capillary and optical fibre.

From Table 5-1 the calculated surface energies of the capillary and optical fibres were similar, although the dispersive and polar components of the surface energy are different. This difference could partly be due to the scatter in the measurements of the contact angles, as presented in Figure 5-5 and Figure 5-6, but also it could be due to environmental factors. The scatter affects the straight line for the Owens-Wendt plot and even small changes in the position of the line of best fit can cause large changes in the calculated surface energies as the gradient and intercept are squared to obtain the surface energy components, which amplifies the error associated with the results. The environmental factor is the condition of the silica surface. Legrand (1998) and Jańczuk and Zdziennicka (1994) both stated that surface energy values of silica are dependent on the condition of that silica and in the case of the capillary and optical fibre there was an environmental consideration. Although the fibre and the capillary samples were prepared for testing using the HellmanexTM cleaning method a difference existed in their prior conditions. When manufactured the optical fibres were coated with a polymer to protect them from the environment, whereas the capillary did not have such a coating applied, this means that the capillary was exposed to the atmosphere from manufacture, whereas the optical fibre's exposure only began after the stripping away of the coating. This could lead to differences between the surfaces resulting in the disparity of the polar and dispersive surface energies components of the capillary and optical fibre.

It was decided to continue the work with the optical fibres used as the reference sample as the results were not vastly different, as shown in the Owens-Wendt plot (Figure 5-6). Also for the interfacial shear strength experiments the use of the optical fibre would enable the samples to be manufactured and tested with significant ease.

5.1.3 Silane treatments

This work was in two stages, the first involved the selection of a drying temperature for the silane treatment and the second was the application of two different silanes at different concentrations.

5.1.3.1 *Drying Temperature effects*

Part of the silane treatment process involves driving water from the surface to enable the formation of the siloxane network, as described in Section 2.3.3. In much of the published work involving the treatment of glass surfaces with silane couplings agents no information is given on the method of treatment. The works that do report the method used have significant differences in the drying regimes. For example, Berg and Jones (1998) dried the samples for 24 hours at 45°C, DiFrancia *et al.* (1996) allowed their samples to dry at room temperature for 24 hours, whereas Miller and Berg (2003) dried their samples for 2 hours at 125°C. Because of these reported differences it was felt that it was important to assess the drying schedule.

Therefore, after treating the optical fibres with the silane solution (5% APMS), they were dried at room temperature (RT), 60°C and 100°C. The contact angles between the fibre samples and formamide, ethylene glycol and DMSO were obtained, the results are shown in Figure 5-7.

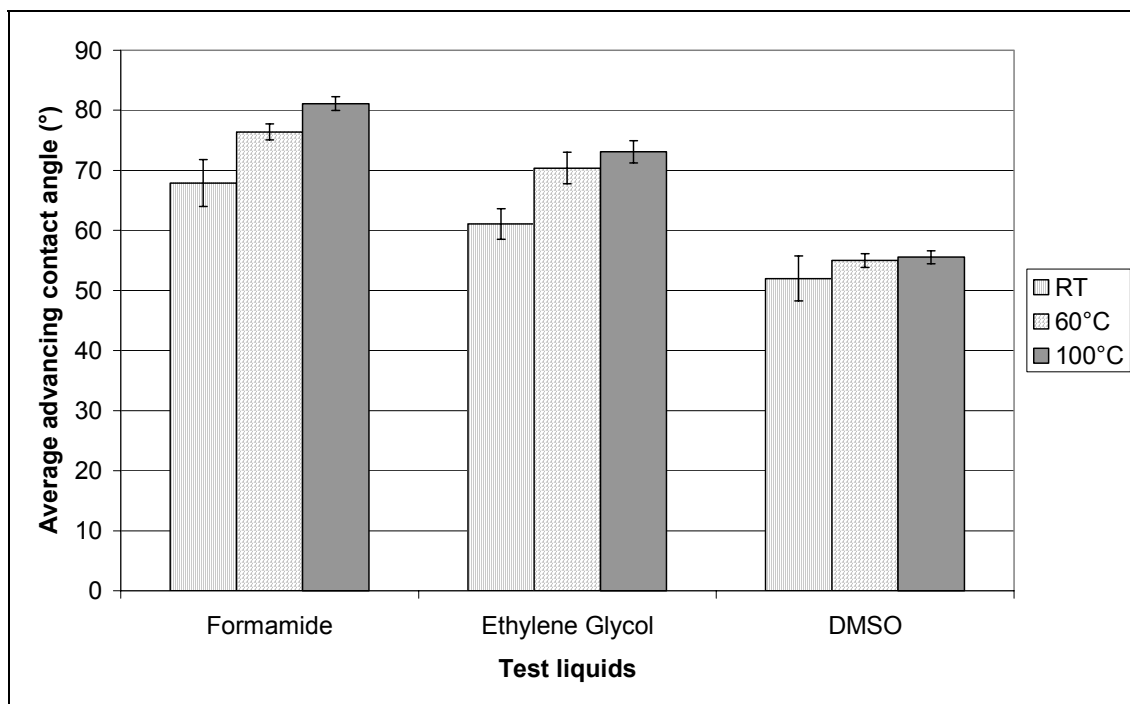


Figure 5-7 Contact angle results from silane treated fibres dried at three temperatures.

In Figure 5-7 there was a distinctive step up in contact angle from RT to 60°C, while between 60°C and 100°C there was less change. The higher drying temperatures also lead to a reduction in the standard deviation of the contact angles for all samples. The samples tested against DMSO show a smaller change, approximately 7% increase, compared to those of formamide and ethylene glycol, approximately 20% increase, but still showed the reduction in standard deviation.

Drying Temperature	Dispersive Energy (mN·m ⁻¹)	Polar Energy (mN·m ⁻¹)	Surface Energy (mN·m ⁻¹)
RT	23.76	4.69	28.46
60°C	30.82	0.17	30.99
100°C	33.59	0.06	33.65

Table 5-2 Effect of drying temperature on surface energies of silane treated fibres.

The calculated surface energies for the different drying temperatures are shown in Table 5-2. As the drying temperature was increased, the surface energy increased with the dispersive component also increasing, while there was a reduction in the polar component. It is possible that the reduction in the polar component was due to the reduction of the moisture content on the fibres, as water is a polar molecule.

As drying at 100°C showed a decrease the variation in the obtained contact angle results and possibly a reduction in the moisture present, it was decided to subject all further samples for this work to a that drying regime.

5.1.3.2 *Different silanes*

There were two silanes chosen, APMS and GPMS, the former has an amine end group and the later has an epoxy group, see Table 3-1. This means that both should be able to react with an epoxy-amine resin system. The reaction of silane coupling agents with glass and epoxy-amine systems has been demonstrated previously. For example, Ishida and Koenig (1979) demonstrated, through Fourier transform infrared spectroscopy (FTIR) that silane coupling agents connect to the glass surface through covalent bonding and the formation of SiOSi bonds. Wang and Jones (1991) used Time-of-Flight secondary ion spectrometry (ToF SIMS) to investigate the interactions between aminopropyltriethoxy silane (APS) and epoxy resins. On silane treated glass surface, peaks were found that correlated to the APS, while on silane treated glass surface then subjected to an epoxy resin, those peaks associated with the APS were absent and the presence of epoxy/APS reaction products were shown. This confirmed the reaction of an aminosilane with an epoxy resin.

The results for the contact angle measurements against the two types of silanes are presented in Figure 5-8, with the calculated surface energies for the APMS treated fibres shown in Table 5-3 and for the GPMS in Table 5-4.

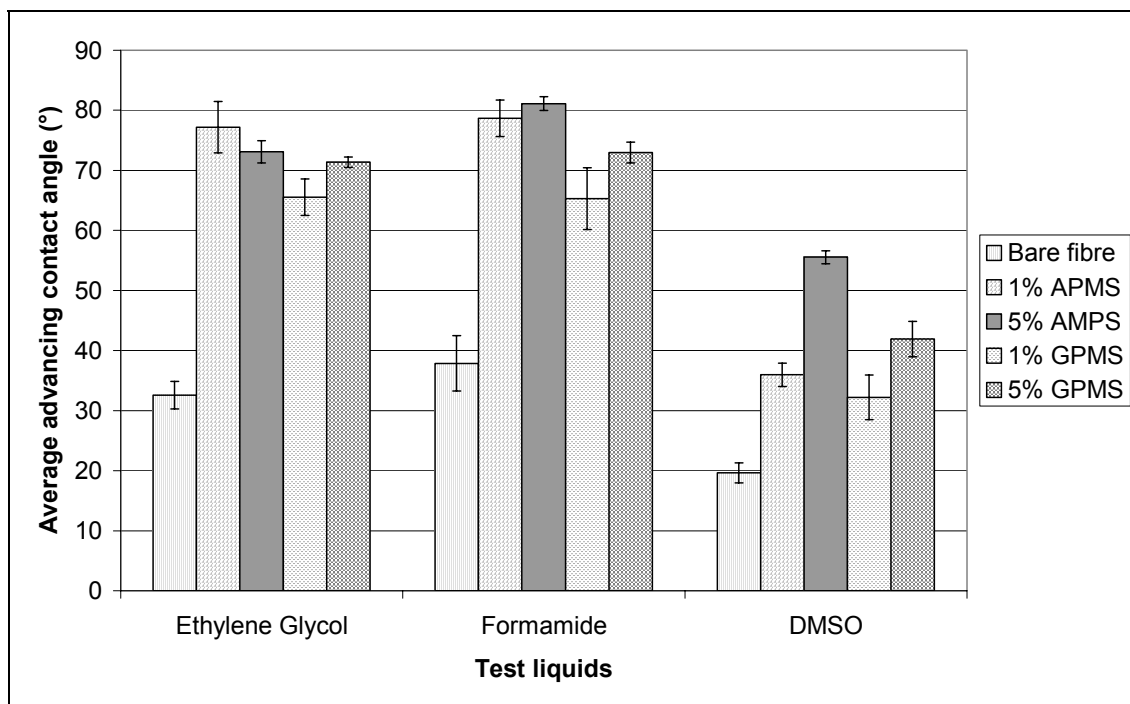


Figure 5-8 Graph showing the average advancing contact angles for the silane treated fibres.

	Dispersive Energy ($\text{mN}\cdot\text{m}^{-1}$)	Polar Energy ($\text{mN}\cdot\text{m}^{-1}$)	Surface Energy ($\text{mN}\cdot\text{m}^{-1}$)
Bare fibre	28.71	14.36	43.07
1% APMS	74.97	17.43	92.41
5% APMS	33.59	0.06	33.65

Table 5-3 Results of samples treated with APMS.

	Dispersive Energy ($\text{mN}\cdot\text{m}^{-1}$)	Polar Energy ($\text{mN}\cdot\text{m}^{-1}$)	Surface Energy ($\text{mN}\cdot\text{m}^{-1}$)
Bare fibre	28.71	14.36	43.07
1% GPMS	57.91	2.25	60.43
5% GPMS	53.39	3.30	56.70

Table 5-4 Results of samples treated with GPMS.

From Figure 5-8 it can be seen that all the silane treatments have a significant effect on the contact angle results, and overall the APMS samples show higher contact angle values than those samples treated with GPMS. Also the scatter of the 1% treated samples is greater than the corresponding 5% treatment; this could be caused by the 1% treatment being at an insufficient level to produce a consistent layer on the fibre surface. This would need further silane treatment levels to be examined before this could be confirmed.

From these surface energy results (Table 5-3 and Table 5-4) it can be seen that the polar component of the surface energy decreases with the application of a silane treatment, this is consistent with the literature reported values and expected as the organic silane molecule is non-polar and is replacing polar water molecules on the surface. However, in contrast to most of the reported literature, Mäder (1997) and Weinberg (1997), the total surface energy has increased. Bledzki *et al.* (1997) reported a slight increase in surface energy, $7 \text{ mN}\cdot\text{m}^{-1}$, but in this project the increase was almost $50 \text{ mN}\cdot\text{m}^{-1}$. Hull and Clyne (1996) suggested a possible reason for a similar behaviour observed for reinforcing fibres. In the case described the reinforcing glass fibre should have a surface energy in the range of $500 \text{ mN}\cdot\text{m}^{-1}$, but the presence of water on the surface can reduce this to around $20 \text{ mN}\cdot\text{m}^{-1}$. When a silane treatment is then applied to those fibres the surface energy increases to approximately $50 \text{ mN}\cdot\text{m}^{-1}$ as it replaces at least some of the water molecules. No reference is made to the dispersive and polar component of the surface energy for the case described. The only surface treatment that did not generate an increase in the surface energy was the 5% APMS treatment. From examination of Figure 5-8, it appears that the response to DMSO of the 5% APMS treated samples is inconsistent with the others, it had a substantially larger contact angle. As there were only three test liquids used, any irregularity would have a significant influence on any values calculated. To reduce the inaccuracy the best option would be to repeat the testing including at least another test liquid.

It has proved difficult to directly correlate the work done in this project with other published works due to the differences in glass types, silane treatments, preparation and test methods. The glass types vary from E-glass plates, E-glass fibres, fumed silica or optical fibres, with each type there are composition differences and surface variations making direct comparisons between any of these results difficult. There are many types of silane coupling agents available for examination, included in these are commercial sizes where the composition is not revealed, which makes direct comparisons complicated. Along with this are the various test preparations and methods used, for example, exposure times to the silane solutions, drying times, and contact angle techniques.

5.1.3.3 Work of adhesion between fibre and epoxy matrix

To examine if the alterations in the surface energy by the silane treatments would improve the interface between the silica and epoxy, it was decided to calculate the thermodynamic work of adhesion (W_A). This is a measure of the work required to separate a unit area of two phases in contact and is the sum of the surface free energies of the two phases minus the interfacial free energy, as shown in Equation 5-1 (Kinloch, 1987).

$$W_A = \gamma_{sv} + \gamma_{lv} - \gamma_{sl} \quad \text{Equation 5-1}$$

Then by applying the geometric mean approach for interfacial surface energies, as shown in Equation 2-6, the work of adhesion can be written the form of polar and dispersive components of surface energies, presented in Equation 5-2, where subscripts f and r represent fibre and resin respectively.

$$W_A = 2 \left[(\gamma_f^d \cdot \gamma_r^d)^{1/2} + (\gamma_f^p \cdot \gamma_r^p)^{1/2} \right] \quad \text{Equation 5-2}$$

Using this equation and the surface energy data obtained, work of adhesion values between the optical fibres and an epoxy resin were calculated for each of the fibre treatment used in this work, presented in Table 5-5. The epoxy resin values used were γ^d of $41.2 \text{ mN}\cdot\text{m}^{-1}$ and γ^p of $5 \text{ mN}\cdot\text{m}^{-1}$, from Comyn (1997) and Kinloch (1987). These data were used as there was no available surface energy data on the 913 matrix resin system.

Treatment	$\gamma^d \text{ (mN}\cdot\text{m}^{-1})$	$\gamma^p \text{ (mN}\cdot\text{m}^{-1})$	$W_A \text{ (mJ}\cdot\text{m}^{-2})$
None – Bare fibre	28.71	14.36	86
1% APMS	74.97	17.43	130
5% APMS	33.59	0.06	75
1% GPMS	57.91	2.52	105
5% GPMS	53.39	3.30	102

Table 5-5 Calculated work of adhesion values between epoxy resin and silane treated optical fibres.

From Table 5-5 it noticed that the silanes improve the work of adhesion compared to the bare fibre data, apart from the 5% APMS treatment level. The 5% APMS data was

likely to have been influenced by the inconsistency of the DMSO results, as described in Section 5.1.3.2. This work of adhesion data was used in comparison with the IFSS results.

5.2 Interfacial Shear Strength

The aim of this section was to quantify the strength of the bond between the sensors and the composite. From the review of the main methods currently used in IFSS testing, Section 2.3.2, it was felt that no one method was suitable for this project. It was hoped to develop a method that allowed the fibre reinforced composite to be used as in micro-indentation, but maintained the more practical approach of the single fibre pull-out method. Therefore, a new method was developed that involved the use of prepreg to manufacture the samples from which the fibres could then be pulled out from (Etches and Fernando, 2002). Certain aspects of the test method were improved during the project as the technique became more familiar.

5.2.1 Sample manufacture

The key difference between this development and the standard single fibre pull-out method was the use of fibre reinforced composite instead of neat resin to manufacture the samples. This has the advantage of being more representative of the actual situation when a fibre-reinforced composite has an embedded optical fibre. The effect of using a fibre-reinforced sample can be seen in Figure 5-9, there are areas where the reinforcing fibres are touching the optical fibre and others where there is a large area next to the optical fibre that is completely void of reinforcing fibres.

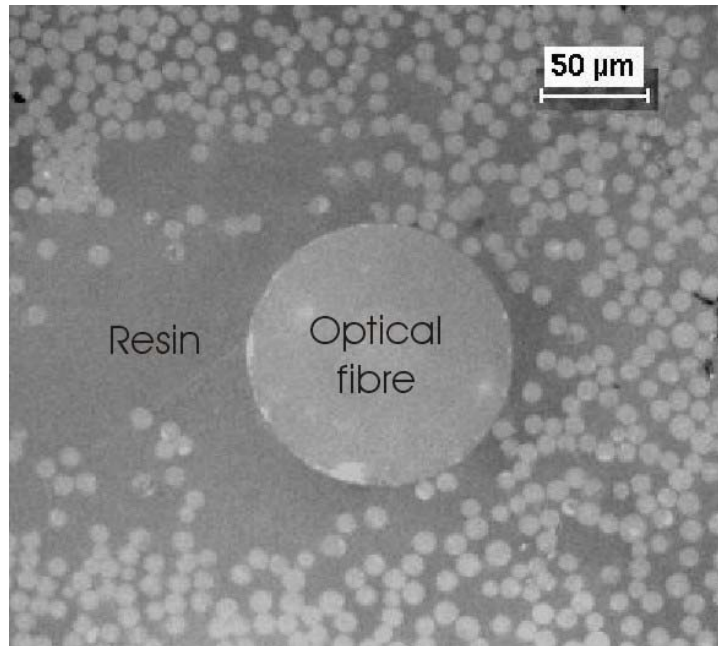


Figure 5-9 Optical microscope image showing a cross section of a pull-out sample.

Not only was there this variation within a sample, but also between samples, for example if Figure 5-9 and Figure 5-10 are compared it can be noticed that the pattern of reinforcing fibres surrounding the optical fibre is different. In Figure 5-10 the reinforcing fibres are more evenly spread around the optical fibre, but there are still areas where the reinforcing fibres are touching the optical fibres and other areas where they do not. The dark marks on both images are a result of the preparation of the samples for microscopic analysis.

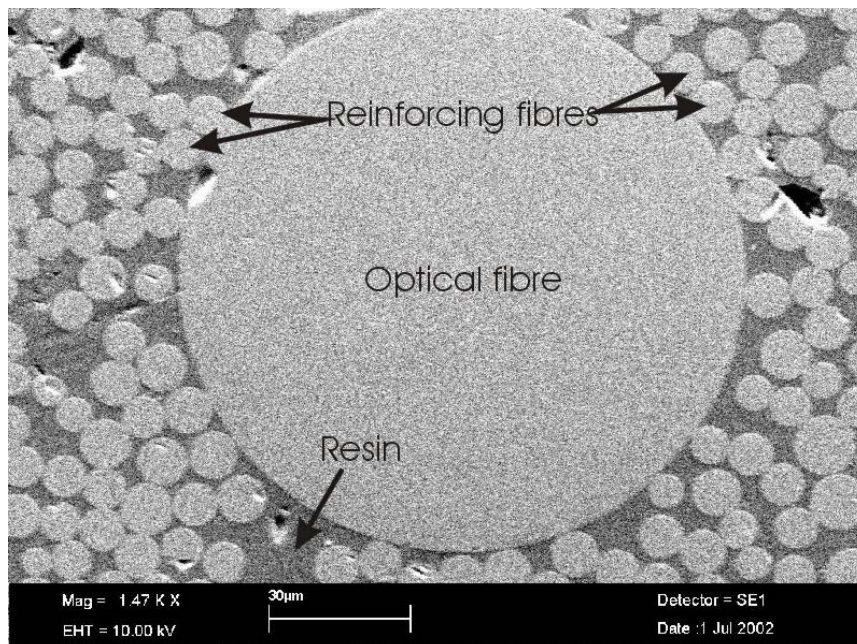


Figure 5-10 SEM image of a polished pull-out sample (transverse section).

These random patterns of reinforcing fibres could affect the results obtained from this method, as it could vary the stress build up around the fibre. Some work has been published on the modelling of the influence of reinforcing fibres on the pull-out method as applied to E-glass reinforcing fibres (Fu *et al.*, 2000, Kim *et al.*, 1994). However, the main assumption made for that modelling work was the use of a three phase model, where the fibre of interest was completely surrounded by matrix resin, which in turn was surrounded by the composite material, as shown in Figure 5-11.

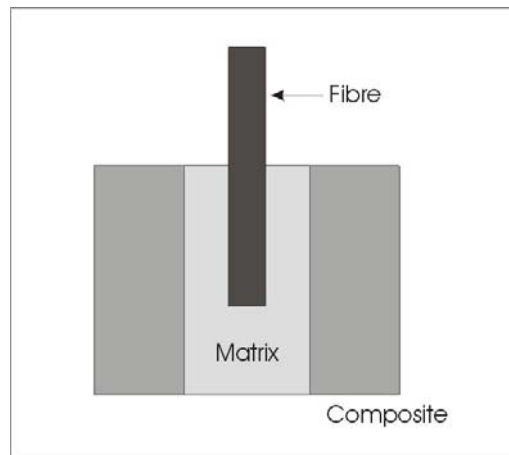


Figure 5-11 Schematic of the fibre pull-out model used by Fu *et al.* (2000) and Kim *et al.* (1994).

As can be seen from the micrographs, this is definitely not the case. The extreme of the fibre being completely surrounded by the resin might be possible but more likely is the random pattern of fibres with some fibres touching and other areas having no fibre contact. Even in the extreme case that was modelled, it was found that the neighbouring fibres play a significant part in the stresses around the fibre of interest. In the case of the inclusion of an optical fibre, the stress around it would already be substantially different to that a fibre reinforced composite sample, due the size difference at least. The reinforcing fibres that are in contact with the optical fibre could generate a non-adhered section, or a very weakly adhered section, which under loading could fail prematurely. In the other case of a resin rich region it would not have the same mechanical properties of the bulk composite and could also fail prematurely. However, the modelling of such a situation would be very difficult. Work would have to start at specific positions, such as a complete resin layer as in the model using for reinforcing fibres, then a resin and fibre mixture, finally moving onto a situation where the surrounding fibres are closely packed together.

During the manufacture of traditional fibre pull-out samples a meniscus forms at the fibre entry point into the resin. This meniscus causes inaccuracies in the measurement of embedment depths and affects the stress patterns at the fibre entry point (Herrera-Franco and Drzal, 1991). Some methods have been developed to prevent the formation of the meniscus, from notched dogbone samples (DiFrancia *et al.*, 1996) to a reverse casting method (Zholfaghar and Folkes, 1999). In this project, the use of composite prepreg and porous release fabric minimised the build up of a significant meniscus, as shown in Figure 5-12. It is believed that this works as any excess resin from the prepreg is absorbed by the release fabric during the cure processing.

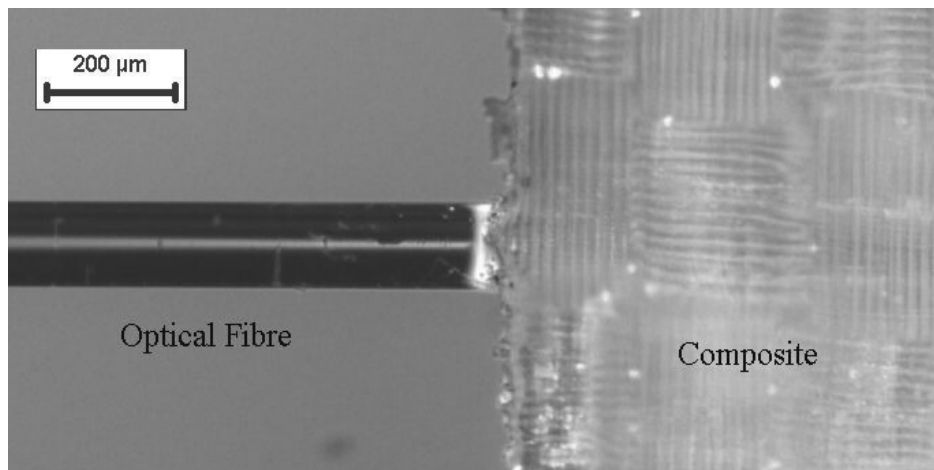


Figure 5-12 Image illustration the edge of the composite with protruding optical fibre.

5.2.2 Measurement of the embedment depth

Although it is widely believed that the measurement of the embedment depth is crucial to successful interpretation of the single fibre pull-out tests (Pitkethly *et al.*, 1993, Pisanova *et al.*, 2001), many of the published works neglect to inform the reader of the method or accuracy of measurement of the embedment depth. For example, Tsai and Kim (1991) report the embedment depths of all their samples at approximately 6 mm but give no explanation of how this figure was obtained, and DiFrancia *et al.* (1996) used notched dogbone samples for their single fibre pullout testing but again no indication was given on the method used to measure the embedment depth.

In other cases, the descriptions of the embedment depths have been reported, and these fall into two main categories, direct or inferred methods. The direct measurements usually take the form of measuring the fibre after extraction from the resin. According to Yue and Looi (2001), the embedded portion should be readily distinguished under optical microscopy, although from the current work carried out it was not always that simple to determine the embedded section of the fibre. Mäder *et al.* (1994) used an inferred method whereby the embedment depth was obtained from the force-displacement curve. This method could suffer significant errors in the opinion of this author, if the equipment in use had any slack or slippage as it relies on the displacement to infer the depths. Overall each of the methods has its advantages and limitations, with the choice of method most likely depending on the fibre/matrix combinations and equipment availability. Both methods require the user to judge where the defining points are for the depths, and with this there will always be a certain level of interpretation and error.

Initial Determination

In this current project it was decided to begin with the measurement of the embedment depth after the fibre had been withdrawn from the composite. Therefore, the first batch of samples was examined after failure using optical microscopy. From this image, an estimate of the embedment depth was made by judging the location of the fibre entry point. An example of this technique is shown in Figure 5-13.

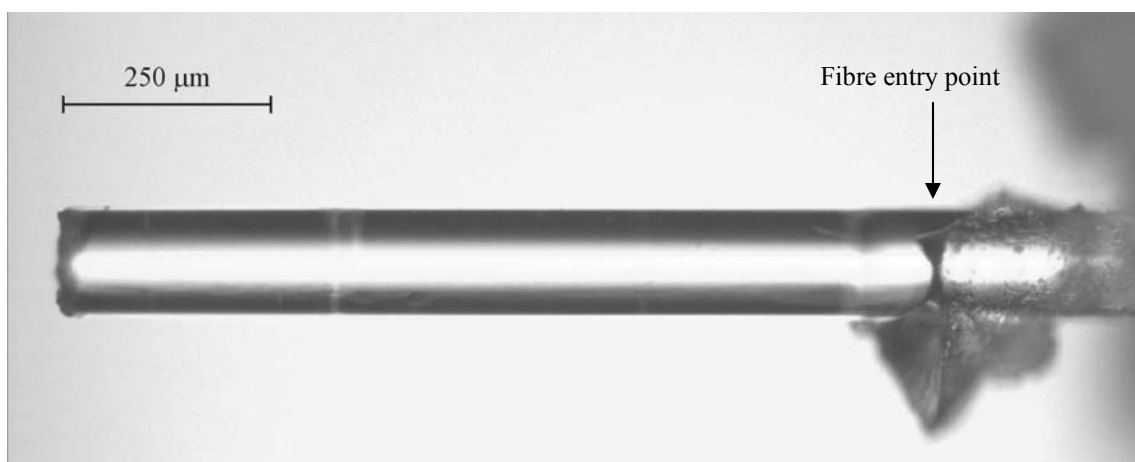


Figure 5-13 Example of embedment depth measurement after failure of the sample.

From Figure 5-13 it can be seen that the location of the entry point could be open to interpretation, and this could lead to variations in the range of 0.125 mm on the measured embedment depth.

In an attempt to reduce the possibility of errors caused by uncertainty or interpretation, it was decided to investigate a method which used the optical properties of the fibre.

Improvement 1

The optical fibre was used to guide white light through the fibre, thereby illuminating the end face of the fibre. The intention was to observe the light leaving the fibre which would then indicate the depth of embedment. This technique was found to only be applicable to the 2-ply glass fibre samples, as these were the only samples that were semi-transparent. An example of this method is shown in Figure 5-14. It can be seen that the light is visible from the surface.

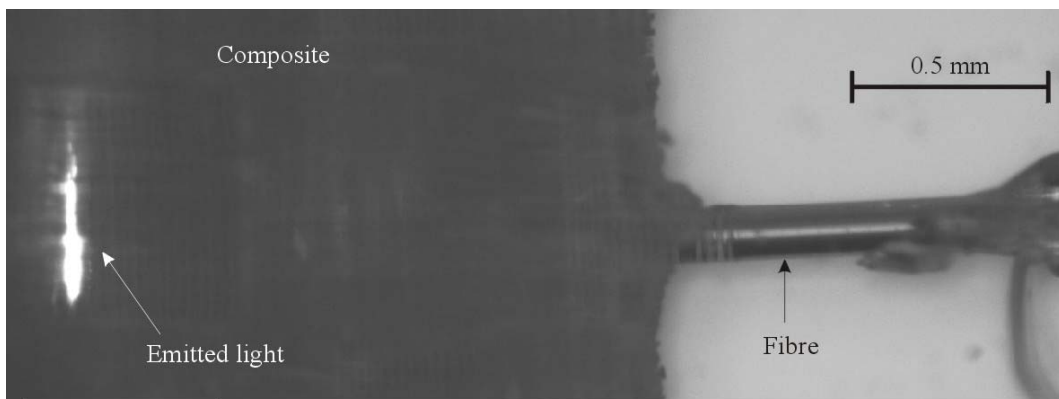


Figure 5-14 Demonstrating the use of light guiding properties of the optical fibre to determine the embedment depth.

To evaluate this method, several samples were prepared and examined under the microscope to measure the embedment depth prior to testing. After testing the samples were examined by optical microscopy to measure the embedment after failure. The results from this evaluation are presented in Table 5-6.

Sample Number	Embedment Depth (mm)	
	Optical technique	Post-Testing Method
1	1.58	1.49
2	1.50	0.84
3	0.89	0.69
4	1.57	1.4
5	0.41	0.64
6	0.36	0.72

Table 5-6 Comparison of embedment depths measured by light method and after testing.

It can be seen from the results that the light method does not accurately generate the embedment depth as measured after failure. The cause of this could be the release fabric used on the samples. The weave of the release fabric left an imprint on the composite surface that could have affected the apparent location of the fibre end. Another disadvantage of this technique was that it was limited to thin transparent samples, such as the 2-ply glass fibre composites.

Improvement II

The majority of the work was carried out using a method of examining the sample before and after testing using the optical microscope. Images were stored from before and after so that a comparison could be made. From the “before” image the distance of stripped fibre outside the composite was measured. The after image allowed the total length of the stripped fibre to be measured. On comparing these two images the length of stripped fibre that was embedded can be determined, this method is shown in Figure 5-15.

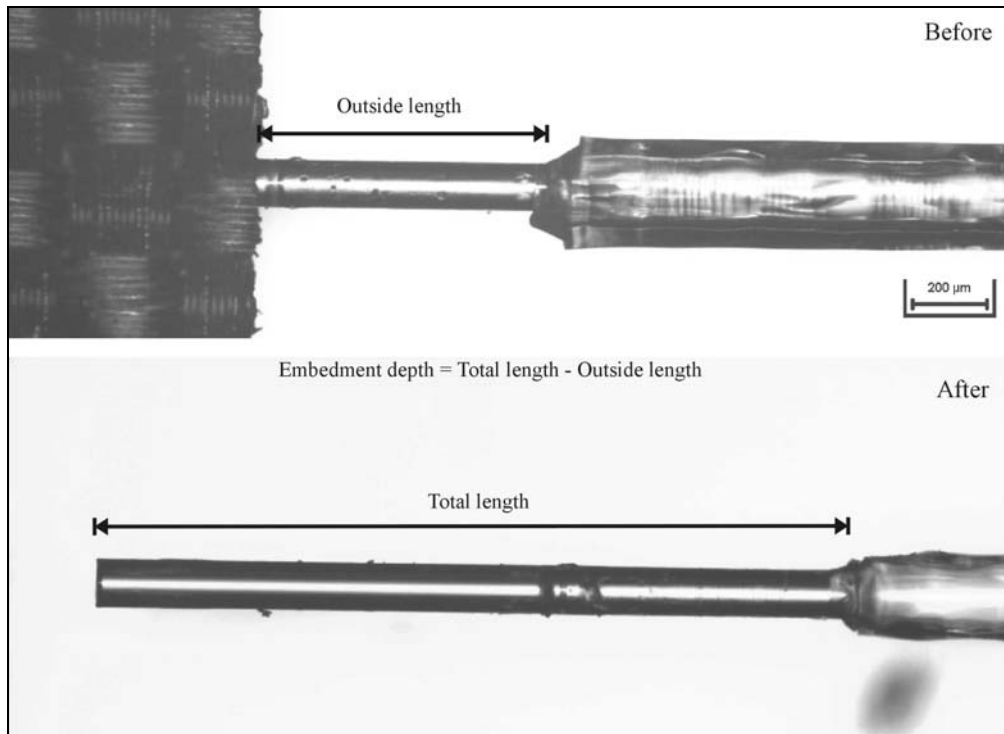


Figure 5-15 Images showing determination of embedment depth.

There were some errors, in the range of tens of microns, associated with this technique. As can be seen from Figure 5-15 the acrylate coating which is utilised as the starting point of both measurements can be damaged or deformed during testing. Therefore, there is still some interpretation to deal with to ensure that both measurements start at the same location.

Ideally what would be required is a method of controlling the depth to which the fibres were embedded. Although during this work an attempt was made to control the depth, through guides and measurements, due to the relatively small dimensions of the fibre and embedment depths required it proved too difficult to achieve manually. Some form of automated system or ability to perform the specimen manufacture under a microscope would improve the control of the embedment depth.

5.2.3 2-ply versus 16-ply glass fibre composite samples

Two thicknesses of composites were investigated initially, namely 2-ply and 16-ply samples. This was done to investigate if there was any influence on the resultant IFSS

measurements due to the thickness of the composite samples, as the optical fibre has a diameter of 125 μm which was the same thickness as a single ply of the composite prepregs.

The expected load/displacement plot for a single fibre pull-out has three stages (Hull and Clyne, 1996). The first is the elastic loading until debonding, then the propagation of the debonding front followed by the frictional sliding of the fibre out of the sample, as shown schematically in Figure 5-16.

After the first few experimental results from this work it was noticed that the load/displacement plots were not showing the frictional sliding section, as shown in Figure 5-17.

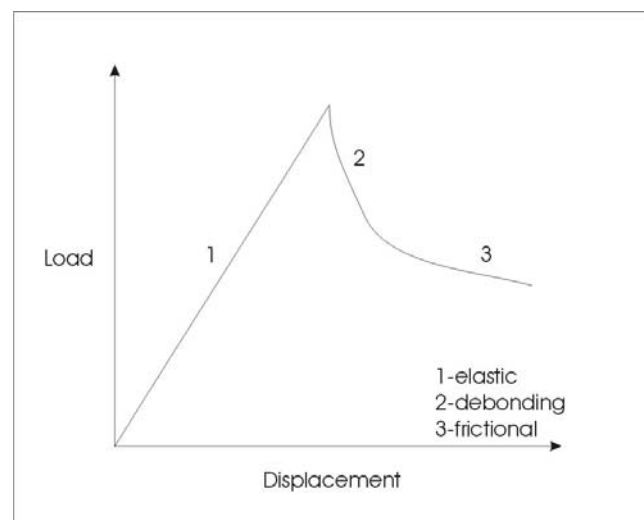


Figure 5-16 Schematic of a typical load/displacement for a pull-out sample.

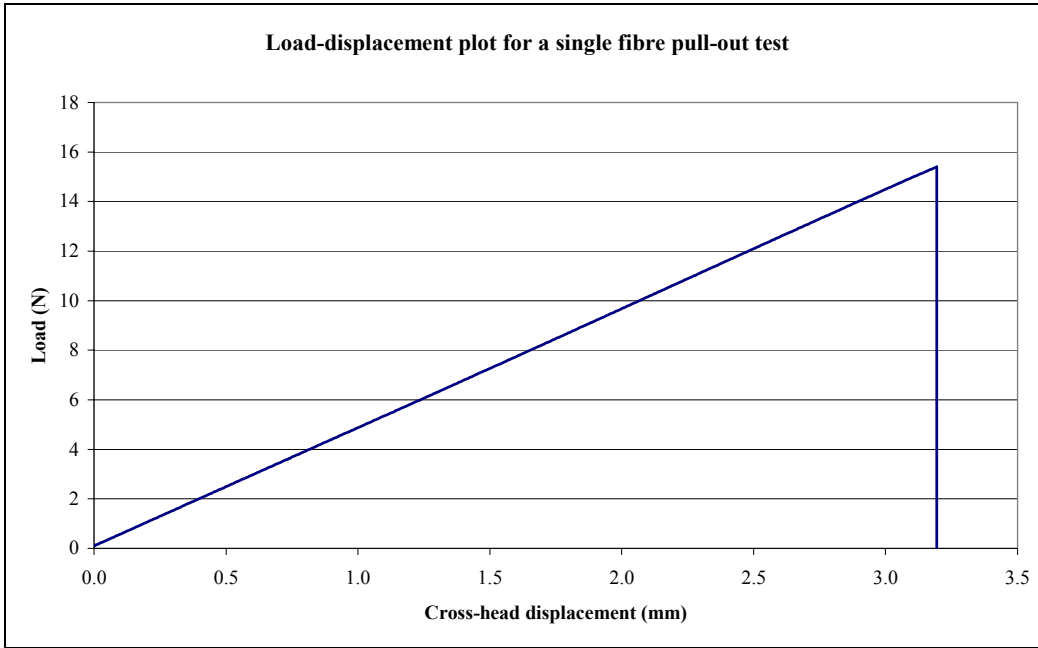


Figure 5-17 Load-displacement plot for a single fibre pullout sample.

It is possible that due to the relatively high loads required to initiate fracture of the interface that once debonding is complete the load completely overcomes any frictional resistance between the fibre and matrix.

From the graph shown in Figure 5-18, there appears to be little effect on the IFSS due to the different thickness of composite samples, although the 16-ply results have more scatter. Due to the more complex nature of the manufacture of the 16-ply samples compared to the 2-ply and the lack of significant effect on the IFSS results, the remainder of the work was carried out using 2-ply composite samples.

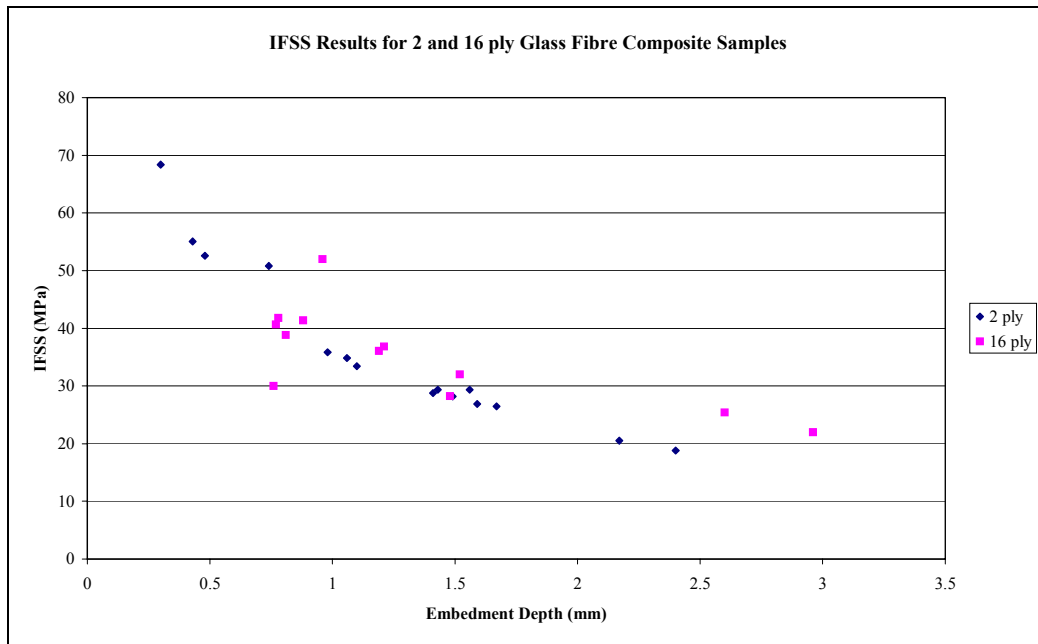


Figure 5-18 Graph showing IFSS results of 2-ply and 16-ply glass fibre composite samples.

These values obtained in the current study for the IFSS are similar to previously published results by other authors, as shown in Table 5-7. However, from this work it is apparent that the IFSS values are dependant of the embedment depth used and is therefore difficult to associate a single value to the results. Some of the published work overcomes this by manufacturing the samples with identical embedment depths and others attempt to perform an analysis to extrapolate back to an effective depth of zero. This means that the comparison of a single value for IFSS is difficult due to the different methods used to obtain that value.

Method	Materials	IFSS (MPa)	Reference
Single fibre pull-out	E-glass/epoxy	49.9	Mäder (1997)
Single fibre pull-out	E-glass/epoxy	43.5 ± 4.1	Yue and Looi (2001)
Single fibre pull-out	E-glass/epoxy	76.7	Pisanova <i>et al.</i> (2001)
Pushout	E-glass/epoxy	43 ± 15	Zhou <i>et al.</i> (2001)
Single fibre fragmentation	E-glass/epoxy	30 ± 7	Zhou <i>et al.</i> (2001)
Single fibre fragmentation	E-glass/epoxy	49 ± 8	Berg and Jones (1998)
Single fibre pull-out	Optical fibre/epoxy	8.1 ± 1.9	Zolfaghar and Folkes (1999)

Table 5-7 Published results on IFSS for glass/epoxy interfaces.

The main discrepancies were for the work done by Pisanova *et al.* (2001) and Zolfaghar and Folkes (1999). Pisanova *et al.* achieved much higher values of IFSS compared to the others, but did not quote any standard deviations. Zolfaghar and Folkes performed the testing using stripped optical fibres as in this current work, however their IFSS results are significantly lower. However, as the methods and the materials used were different from project to project it was difficult to directly compare the results, as shown by Pitkethly *et al.* (1993). In that round robin program although the same fibre/matrix combination was used there were significant differences in the results from the same methods performed in different locations as well as the different techniques used.

5.2.4 Glass fibre versus carbon fibre composite samples

As the composite involved in the durability aspects of the EFPI sensors was CFRP, it was felt that the IFSS should also be carried out using the same prepreg. As the resin for both prepreg is the same, Hexcel 913 epoxy, it was expected that there would be very little difference in the measured IFSS as the interface is the same in each case. The comparison between glass fibre and carbon fibre samples results is shown in Figure 5-19.

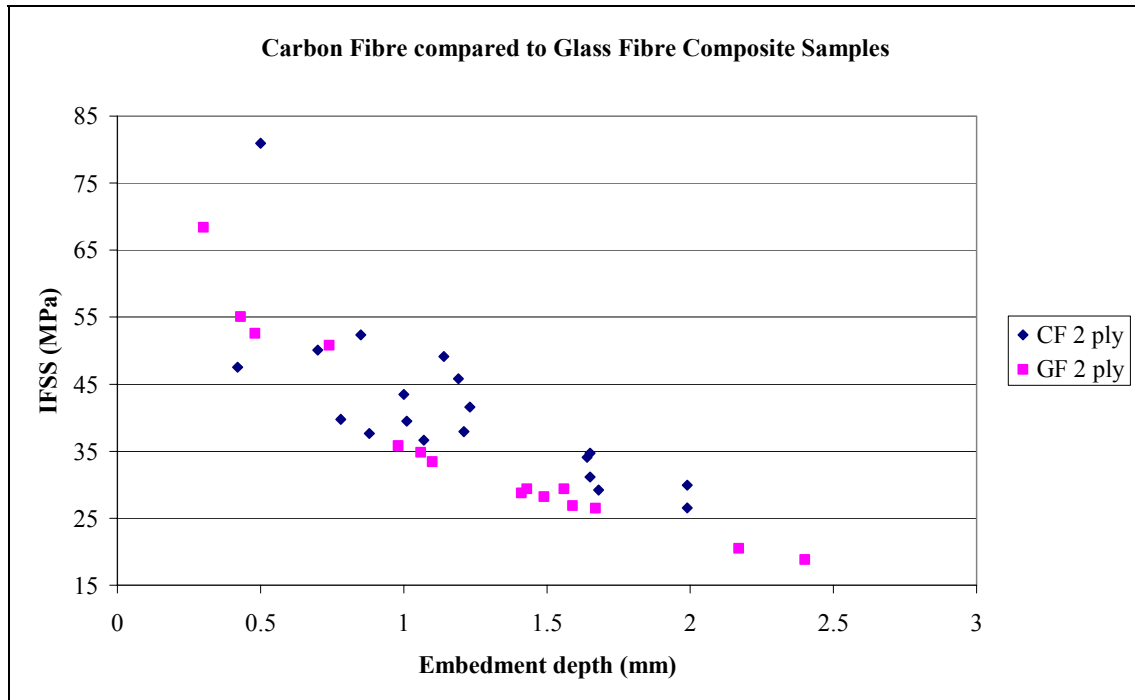


Figure 5-19 Comparison of GFRP to CFRP pull-out samples.

Overall the carbon fibre samples seem to generate slightly higher IFSS values than the glass fibre reinforced composite samples for similar embedment depths. However, due to the scatter present in the data it was felt that statistical analysis was required to determine whether the difference was significant, therefore a Student 't' test was carried out on the data (Rees, 1995).

5.2.4.1 Student 't' test

An assumption of the 't' test is that the population standard deviation for both sets of data is equal. Therefore an F test was carried out to ensure this assumption was correct for this set of data to a level of 5% significance. Both the 't' and F test require a parameter to be calculated from the data, which is then compared to that available in statistics tables (Neave, 1978). In the case of the F test it would be found that the population standard deviation was acceptable for use in the 't' test. However, the 't' test showed that at a significance level of 5% there was no significant difference in the IFSS results from the GFRP and CFRP samples.

The effect of different composite materials was further investigated through a limited finite element analysis (FEA) in collaboration with Dr A. Hameed (ESD, Cranfield University). A 2-dimensional linear analysis was carried out using ANSYS. A half symmetry model was chosen with a 0.5 mm embedment depth with either GFRP or CFRP properties used in the analysis. A schematic of the model used for the FEA is shown in Figure 5-20. The main difference between the two samples was the stiffness, with the carbon fibre samples having a much greater Young's modulus value. This is likely to affect the stress/strain field pattern around the pullout fibre.

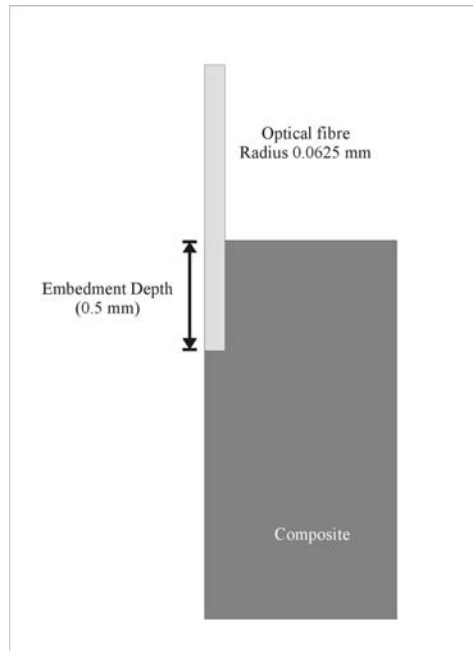


Figure 5-20 Schematic of the model for FEA.

From this FE analysis, data was obtained regarding the shear stress values along the length of the embedded section of the fibre for both the glass fibre and carbon fibre samples. These results are shown in Figure 5-21.

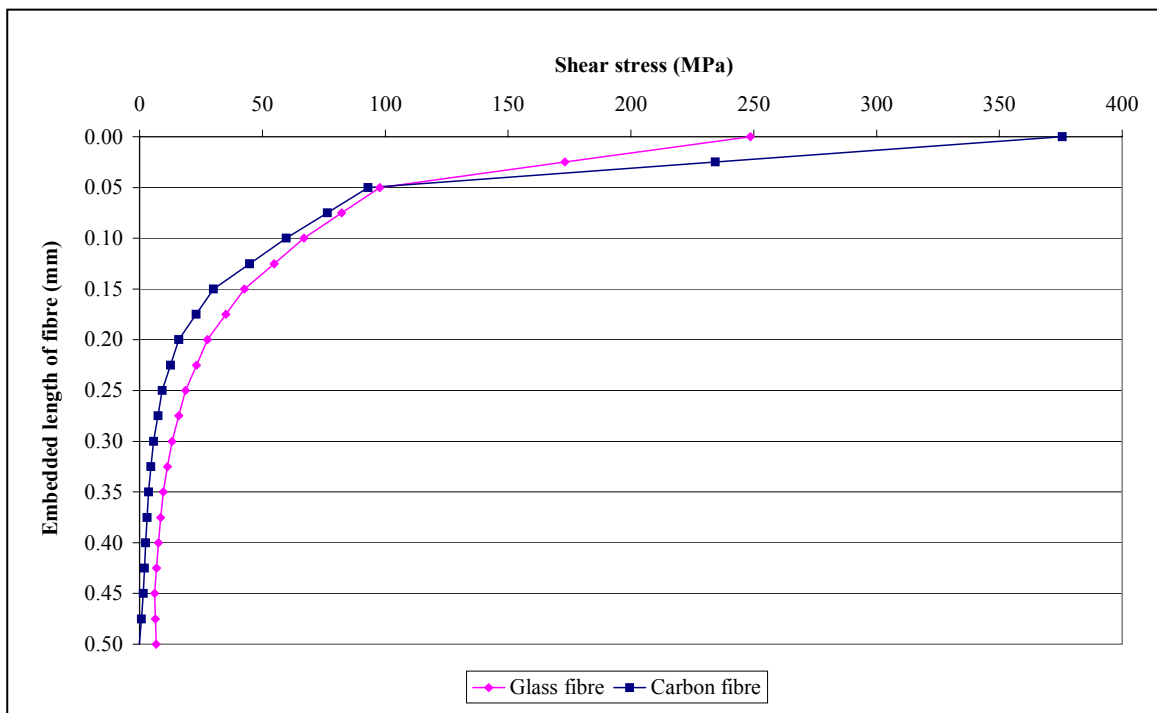


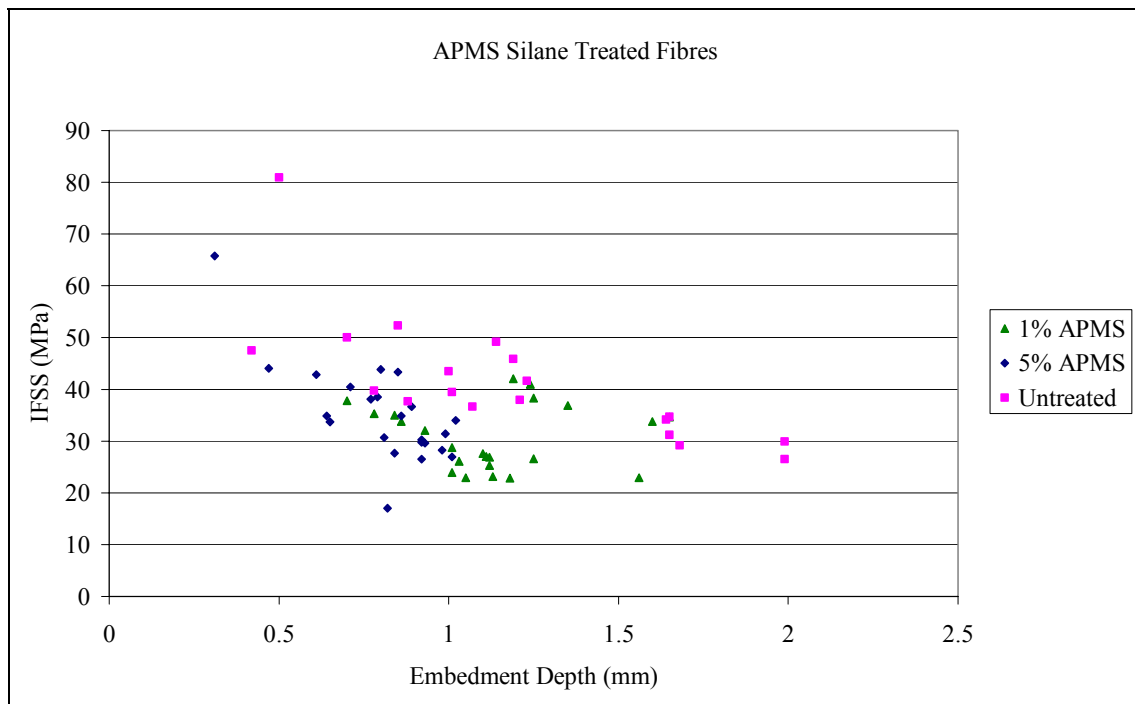
Figure 5-21 Results of the FEA analysis on the pull-out sample.

From Figure 5-21 it can be seen that for the same applied load, the glass fibre composite experiences a higher shear stress at the interface compared to that of the carbon fibre sample.

From Figure 5-19 and Figure 5-21 it can be seen that the type of reinforcing fibres present could have a slight affect on the IFSS from these single fibre pullout tests, even though the same resin matrix was used throughout the testing. At this stage further work would be required to elaborate on this effect, including more composite samples as well as experimental and modelling work on samples made from neat 913 resin. Improvements would be required to the experimental method to reduce the scatter to enable the differences, if any, to be more closely examined.

5.2.5 Silane treated fibres

This section deals with the results obtained from the pull-out testing carried out on the silane treated fibres. The first graph, Figure 5-22 shows the results from the APMS treated fibres.



The first noticeable factor is the large amount of scatter associated with the data. Although it appears by eye that there is a reduction of the IFSS for the silane treated samples, the student t test was again employed to examine the results. From this analysis it was found that there was a significant difference between the 1% APMS treated fibres and the bare fibres, when tested at a 5% significance level. However, the 5% APMS treated samples did not show this effect.

Figure 5-23 shows the second graph containing the results from the GPMS treated fibres. In this case there appears to be no change in the measured IFSS, although as for the APMS samples there is significant level of scatter within the results. However, the statistical analysis suggested that there was a significant difference between the bare fibre and 5% GPMS treated samples.

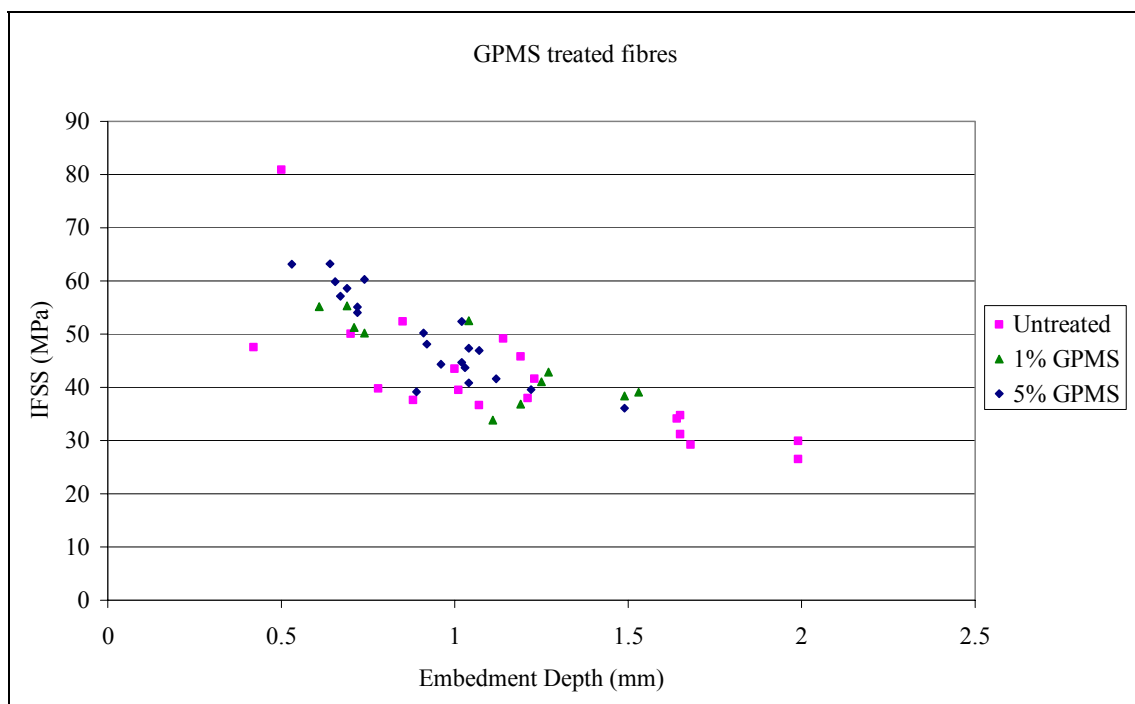


Figure 5-23 IFSS results for GPMS treated fibres.

From both Figure 5-22 and Figure 5-23, it can be seen that a large amount of scatter in the results has been recorded, which makes determining conclusions difficult regarding the effectiveness of the silane treatments on the IFSS, even through the use of statistic

analysis. In this respect any comparison with the work of adhesion values for the silane treated fibres obtained in Section 5.1.3.3 would not proved any more useful.

5.2.6 IFSS results summary

The main factor that has influence the discussions on the IFSS results obtained during this project was the large amount of scatter recorded in the data. There were several possible sources for the scatter, which are described below:

(i) *Pattern of reinforcing fibres*

It was seen from the cross-section micrographs of the pull-out samples that the pattern of the reinforcing fibres was not consistent within a sample or between samples. This could have lead to premature failures of samples or uneven stress patterns within samples, each a possible source of the scatter.

(ii) *Preparation of fibres*

Although great care was taken during the preparation of the samples, it is possible that it was not sufficient. Any of the thermoplastic coating left on the fibres could have prevented adhesion between the fibre and matrix or at least generated a weak interface. Also for the silane treated fibres, any variation in the treatment process could leave to scatter in the results. It is also not known for this case whether the silane treatment provided a consistent surface on the fibre.

(iii) *Surface contamination*

The time between the preparation of the fibres and the manufacture of the sample was kept to a minimum. However, it is possible that contaminants from the environment could have affected the surface of the fibres.

(iv) *Sample manufacture*

During the positioning of the fibres onto the prepreg samples it was possible that the optical fibres were not completely aligned with the reinforcing fibres. Any misalignment would alter the load required to pullout the fibre and possible the stress field within the sample.

(v) *Testing methods*

This involved two stages, the measurement of the embedment depth and the actual mechanical testing of the samples. It has already been shown that the

measurement of the embedment depth is open to interpretation. For the actual testing method, it was attempted to perform the experiments as repeatable as possible but errors can also occur for example sample misalignment in the test fixtures.

5.2.7 Possible improvements to the pull-out method

From the results presented in the previous sections it can be noted that the technique ideally needs some refinements to reduce the scatter recorded to enable conclusions to be drawn.

One path considered for improvement was the measurement of the embedment depth. The current method still relies on some interpretation on behalf of the person performing the testing. It was felt that if the interpretation aspect could be reduced it should remove some of the scatter. It was hoped to achieve this by the used of notched fibres.

To cleave an optical fibre a small notch is typically made and then the fibre is fractured. The idea was to notch the fibre and position the fibre in such a way that the distance from the notch to the edge of the composite was known. A schematic is shown in Figure 5-24.

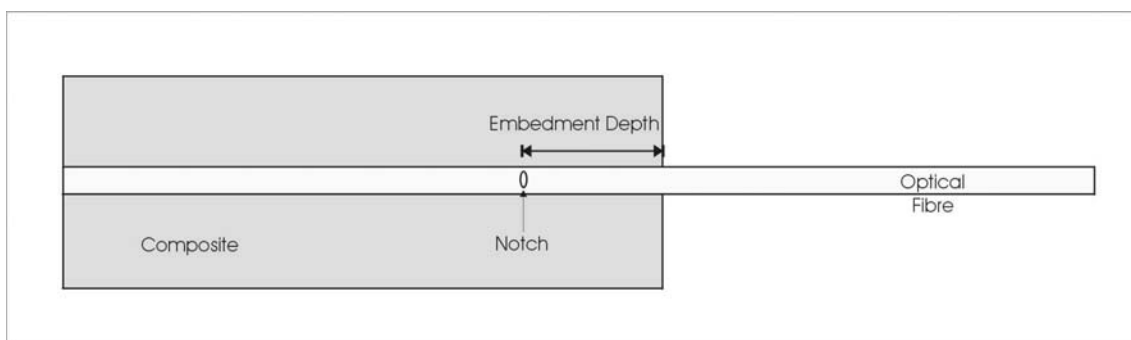


Figure 5-24 Schematic of proposed improvement to pull-out sample.

Then when the sample was tested during the initial part of the loading the notch should cause a fracture, thereby leaving a known embedment depth to be pulled out. This method also had the advantage of removing any adhesion effects over the endface of the

fibres. Another possible advantage was the use of the gap formed between the 2 endfaces acting as a Fabry-Perot cavity, enabling the displacement of the fibre to be monitored during testing.

This investigation began with the notching of stripped fibres followed by the tensile testing of them. An image of a notch generated by the precision cleaver is shown in Figure 5-25.

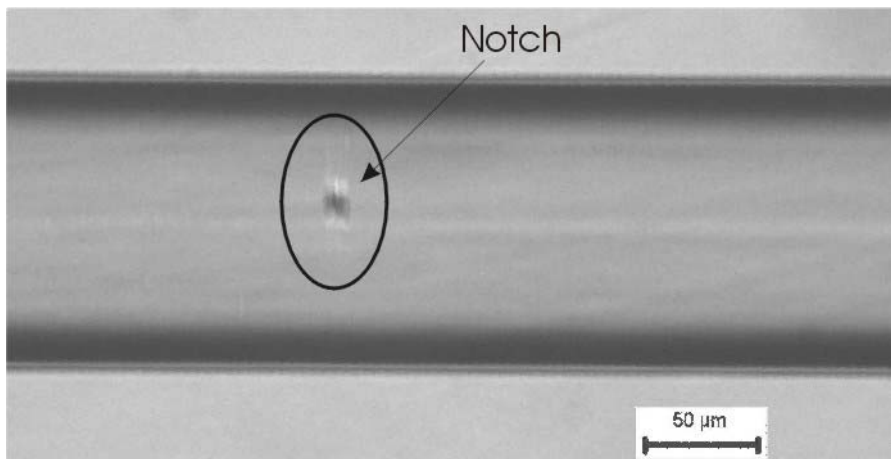


Figure 5-25 Micrograph showing a notch on an optical fibre.

The notches generated are quite small, approximately 10 μm wide by 20 μm long. In Table 5-8 the tensile results of stripped and notched fibres are presented, eight samples were tested for each case. As expected, the notching of the fibre significantly reduces the fracture loads.

Sample	Average Failure Load (N)	Std dev
Stripped	19.8	4.01
Notched	3.6	1.04

Table 5-8 Results of stripped and notched fibres.

Also the failure loads are lower than the loads typically required to pull a fibre from the composite samples. This means that a notched fibre should fracture before interfering with any pull-out measurements. Figure 5-26 presents a selection of the load/displacement plots for stripped and notched fibres.

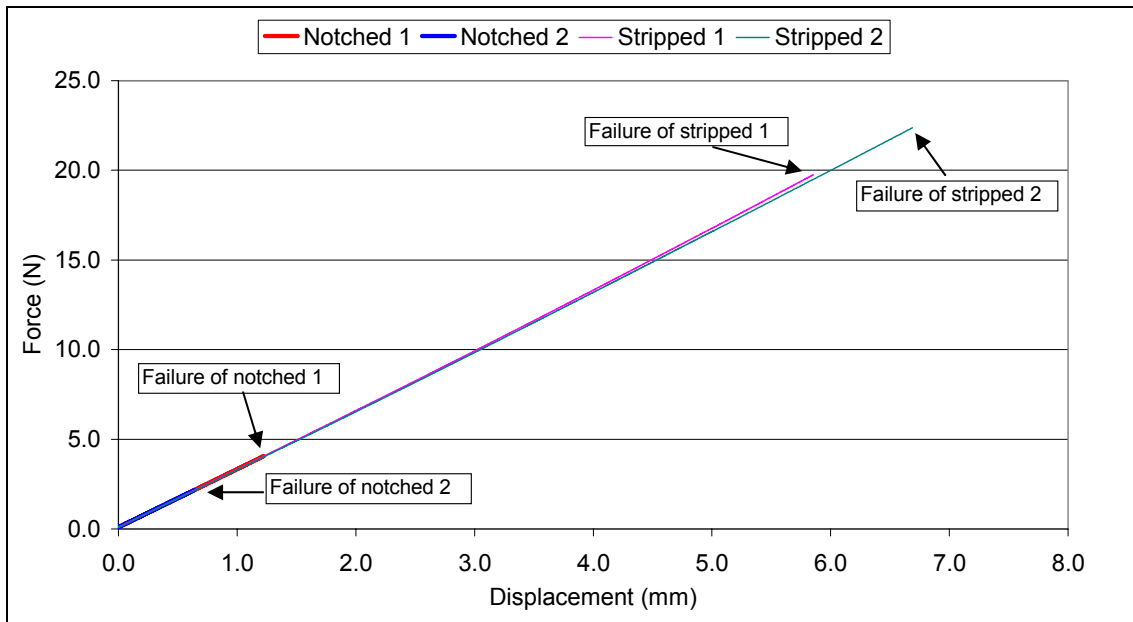


Figure 5-26 Load/displacement plot for stripped and notched optical fibres.

It can be seen from Figure 5-26 that the addition of a notch on to the fibres does not affect its initial elastic response to loading.

In Figure 5-27 are images of the endfaces of the notched fibres (A and B) compared to a standard cleaved endface (C). The standard cleave has a complete mirror as a surface, however the other fracture surfaces show partial mirrors with formation of hackles. The main difference in the sample preparation was the standard cleave was generated using a flexural failure, whereas A and B were formed from tensile loading. Under tensile loading hackles occur when the stress applied to initiate fracture is above a threshold limit (Miller, 1986). This threshold is approximately 208 MPa for silica fibres with a diameter of 125 μm , which equates to a tensile load of 2.6 N. This is lower than the recorded failure load, which means the stress to initiate fracture was higher than the threshold; this explains the formation of hackles on the endfaces of the tensile loaded fibres. The advantage of flexural bending is that there is a stress gradient across the fibre, preventing the stress level breaching the threshold value and thereby prevents the formation of hackles. Another factor that must be consider when cleaving fibres is that if the stress to initiate fracture is below another threshold a lip will form opposite the notch. Overall the flexural failure method allows a large margin in achievement of perfect mirror surfaces compared to the tensile loading method.

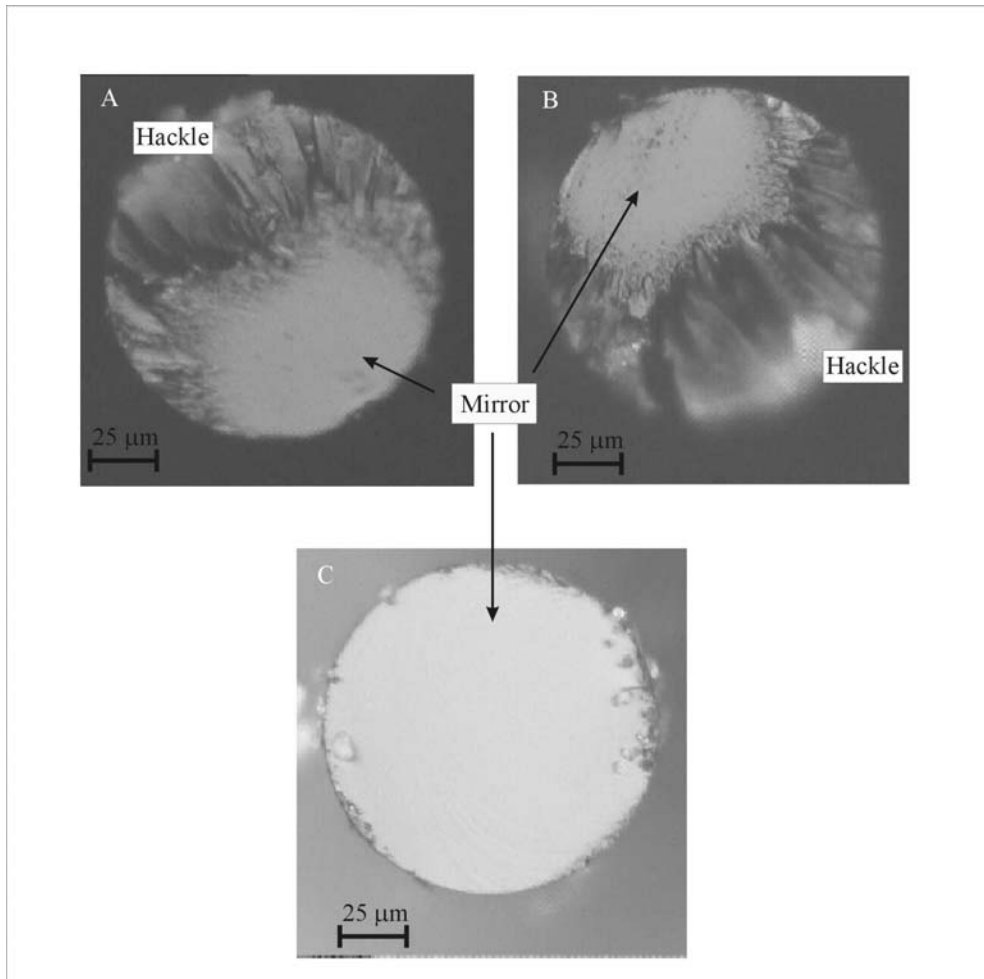


Figure 5-27 Images of endfaces of optical fibres. A and B are endfaces from notched fibres with C being a standard cleaved endface.

To lower the failure load either a larger notch would be required or a reduction in the diameter. An increase in the notch size would be difficult as the precision cleaver used creates very similar notches each time, and if a hand cleaver was used it would be difficult to obtain a repeatable notch size. Due to time restraints there was not the opportunity to investigate the use of smaller diameter optical fibres.

This has implications for interrogating the cavity formed using Fabry-Perot techniques, as without the mirrored surface there is a limited chance of obtaining good reflections and interference patterns to enable cavity lengths to be monitored.

An attempt was made to manufacture pull-out specimens using notched fibres. However, great difficulty was encountered during the placement of the fibres onto the

prepreg samples. As this was done under the microscope to enable the notch to be visible it caused problems in positioning the fibres parallel to the reinforcing fibres and with the notch the required distance from the composite edge. Due to these difficulties samples were not made using notched fibres. It was felt that to enable notched fibres to be used some form of translation stage and microscopy set-up would be required. Unfortunately due to time constraints this was not achieved during this project.

5.3 Conclusions

For the interfacial characterisation of the silica surface of the EPFI sensors, the first task was to assess the possible preparation methods for the samples. After examining several methods the one that presented least scatter was a commercial cleaning solution for quartz and glass, HellmanexTM, for which the manufacturer's instruction for use were followed.

Due to the requirements of the IFSS testing the use of optical fibre as the silica surface was preferential to using lengths of the silica capillary. To ensure that this was a suitable exchange a comparative contact angle study was carried out. Overall it was found that the two surfaces behaved in a similar manner and therefore for the remainder of the project optical fibre samples were used as the representative of the silica surface of the EFPI sensors.

The next stage was the application of silane treatments to the silica surface to promote the formation of a good interface between the silica and epoxy matrix of the composite. After an initial study into the appropriate drying temperature for the preparation of the silane surfaces, the surface energies of APMS and GPMS treated fibres were studied, along with the theoretical work of adhesion to an epoxy resin system. Generally the addition of a silane treatment increased the surface energy and work of adhesion of the system, the exception was the 5% APMS treated surfaces. This surface showed a decrease in surface energy and work of adhesion when compared to untreated surfaces. This variation was mainly attributed to the scatter within the results and the discrepancy with the contact angle results obtained when using DMSO as the test liquid.

For the IFSS measurements, a new method was developed based on the single fibre pull-out technique, which allowed the use of fibre reinforced prepreg and an optical fibre. After an initial examination of the technique and improvements to the measurement of the embedment depth, a study was carried out on the effect of using different prepreg materials on the IFSS results, namely glass fibre and carbon fibre prepreps. An FEA model predicted that for the same applied load the samples manufactured using the glass fibre prepreg should experience a higher interfacial shear stress compared to the carbon fibre composites. Unfortunately, this could not be confirmed experimentally as no significant difference could be determined between the carbon fibre and glass fibre results, due to the scatter within the results. The same problem was encountered when trying to assess the effect of silane treatments on the IFSS. Improvements need to be made to the control and measurement of the embedment depth to allow greater confidence in the results and to enable differentiation between different samples, such as glass and carbon fibres, or different silane treatments.

The combination of the large scatter in the IFSS measurements and the variations noted with the contact angle measurements meant that a comparison between the two sets of results was unproductive at this stage.

6 Sensor and Composite Durability

This chapter discusses the results obtained during the investigation of the durability of EFPI sensors embedded within CFRP samples. As described in Chapter 2 there has been significant work carried out on EFPI sensors subjected to T/T loading regimes, however, limited work has been published on loading regimes that contained a compressive region. Therefore it was decided to concentrate on the effect of the T/C fatigue loading on the embedded sensors, and also include tensile and compressive static limits of the sensors and the influence of the inclusion on the mechanical properties of the CFRP.

6.1 *Quality of Composite Samples*

All composite panels made were quality checked using the C-scan technique. Any panel that showed significant defects were not used for this project, after some initial problems with the quality of the prepreg only one panel was rejected due to the presence of significant voids after manufacture. Figure 6-1 shows a C-scan image of a good panel and Figure 6-2 that of a panel with significant defects.

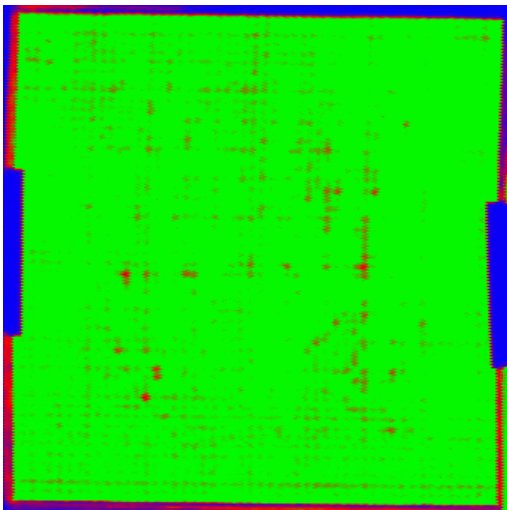


Figure 6-1 C-scan of good quality plate.

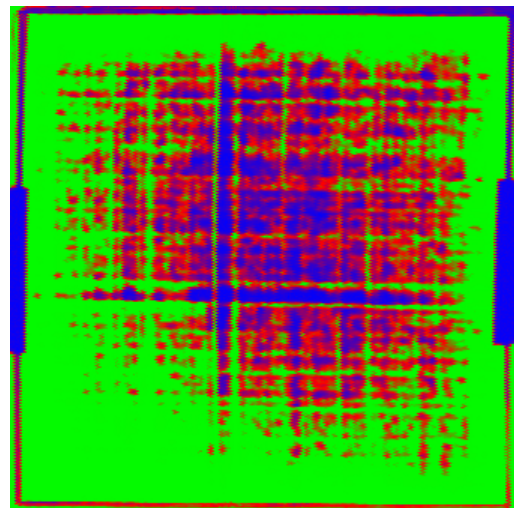


Figure 6-2 C-scan of a plate with significant defects.

In Figure 6-1 and Figure 6-2, the blue colour shows areas of high attenuation, with green showing low attenuation. The attenuation of the signal is caused by voids (trapped air) within the samples. Some attenuation can also be caused by surface variations and tiny air bubbles on the surface.

To confirm the results obtained from the C-scan tests were that of defects within the composite panels, sections of the panels were taken and mounted to enable examination by microscopy. In Figures 6-3(a,b) and 6-4(a,b) below are examples of the microscope images obtained from the polished sections of CFRP. Figures 6-3(a) and 6-3(b) show a sample that had a good C-scan result and from these microscope images there appeared to be no significant voids present. In Figures 6-4(a) and 6-4(b) voids within the composite structure can be seen and the respective C-scan for this image also showed significant signal attenuation.

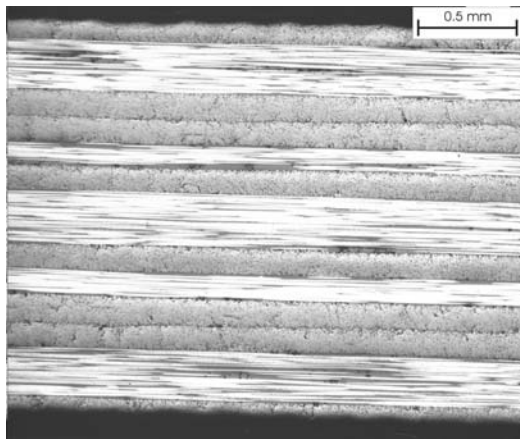


Figure 6-3(a) Micrograph of a good quality plate.

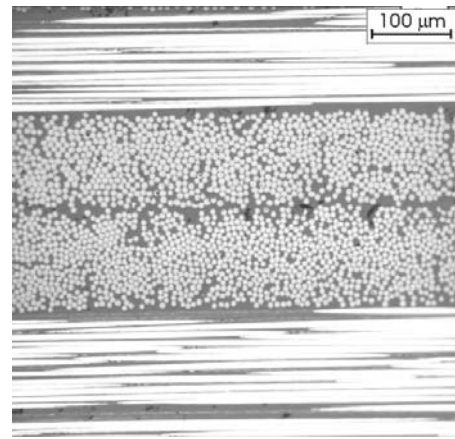


Figure 6-3(b) Higher magnification micrograph of good quality composite.

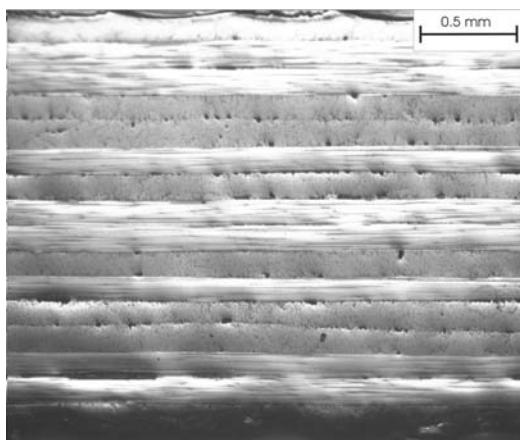


Figure 6-4(a) Micrograph showing voids within the composite.

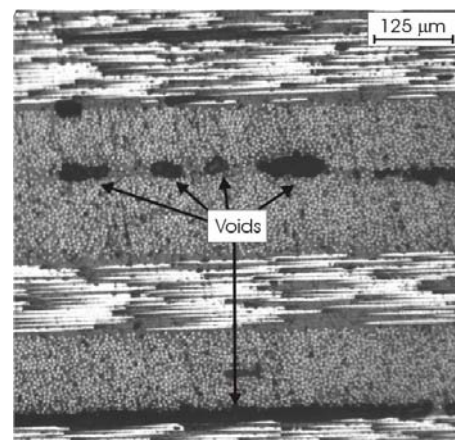


Figure 6-4(b) Higher magnification micrograph of a poor quality composite.

Panels with EFPI sensors were also C-scanned prior to use, however in this case some attenuation was expected around the location of the sensors, as it was more difficult to lay-up these samples, especially where the PTFE tubing was used to protect the lead-in/out fibres.

The main difficulty in the lay-up of samples with EFPI sensors is that once the sensors are placed onto the composite prepreg, the plies cannot be pressed around the sensors, as this would be likely fracture the sensors. Due to the lack of consolidation of the prepreg around the sensors during lay-up some air could be trapped around the sensors that could lead to the attenuation. Figure 6-5 and Figure 6-6 show C-scan images of plates manufactured with embedded sensors. The attenuation shown is not as large as that shown in Figure 6-2, which correlated to significant voids in the composite. The application of the vacuum and pressure will still consolidate the prepreg but if there was a significant amount air trapped the consolidation would not be complete.

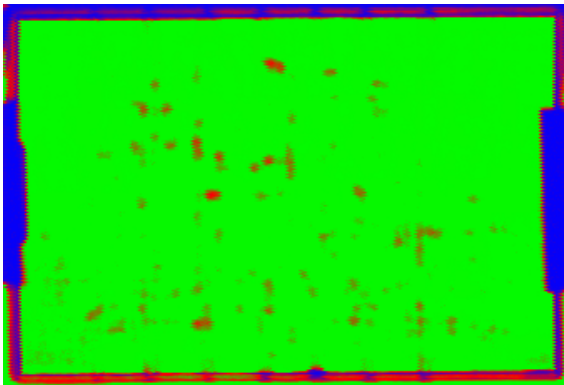


Figure 6-5 C-scan of plate J with embedded EFPI sensors.

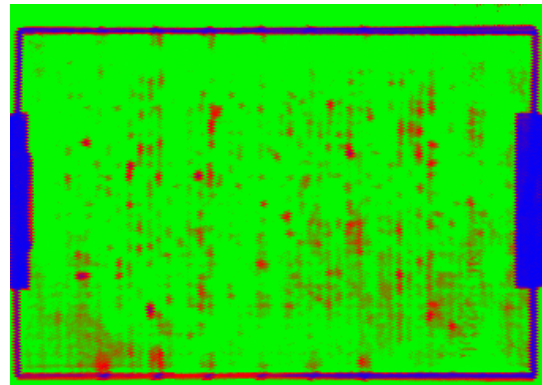
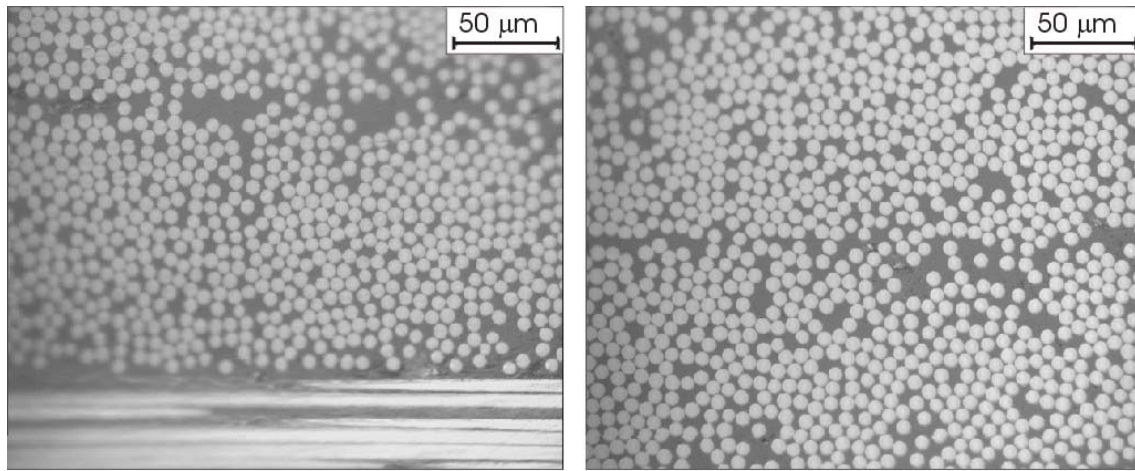


Figure 6-6 C-scan of plate N with embedded EFPI sensors.

Some of the attenuation could be due to the presence of the optical fibre or capillary as silica has a different attenuation response compared to that of CFRP. However, most of the attenuation is likely to be due to small voids that have been generated due to the slight differences in lay-up process due to the inclusion of the sensors. In the cases for the plain panels, each ply could be consolidated as it was positioned during lay-up. However for the panel with EFPI sensors, this procedure could not be followed once the sensors were in place as this could have fractured the sensors.

6.1.1 Fibre volume fraction of CFRP samples

A selection of samples was examined under the optical microscope to enable the determination of the fibre volume fraction (V_f). The prepreg was quoted by the manufacturer to have a resin content of 34%, leaving a fibre volume fraction of 66%. Therefore it was expected that the V_f of the composite samples would be in the range of 66%. Two examples of the images acquired from the optical microscope are shown in Figure 6-7.



(a) Cross section perpendicular to 0° plies (b) Cross section perpendicular to 90° plies

Figure 6-7 Examples of the images used for the determination of fibre volume fraction.

A total of 12 images were taken, 6 from the 0° direction and 6 from the 90° direction. From these the fibre volume fraction was calculated to be 62.7% with a standard deviation of 3.32. It can also be seen from Figure 6-3 and Figure 6-7 that the level of voids in the samples that passed the quality testing was very low and therefore difficult to assess quantitatively.

6.2 *Quasi-static Tensile Testing*

This section reports on the tensile experiments carried out on the reference and samples with embedded EFPI sensors. The aim was to observe the tensile limit of the embedded EFPI sensors and if the embedded sensors had any effect on the mechanical properties of the composite.

6.2.1 Tensile properties of reference CFRP samples

Table 6-1 shows the results of the reference carbon fibre composite samples with Figure 6-8 showing the stress/strain traces for these samples.

Sample	Failure Strain (ϵ)	Failure Stress (MPa)	Young's Modulus (GPa)
A1	0.0180	1155	63.7
A2	0.0170	1150	66.6
A3	0.0175	1182	67.9
B1	0.0169	1132	66.7
B2	0.0168	1131	66.1
B3	0.0158	1061	66.1
Average	0.0170	1136	66.2
St dev	0.0007	41	1.38

Table 6-1 Tensile results for reference CFRP samples.

The Young's modulus values were calculated using linear regression from the stress-strain graphs for each of the samples.

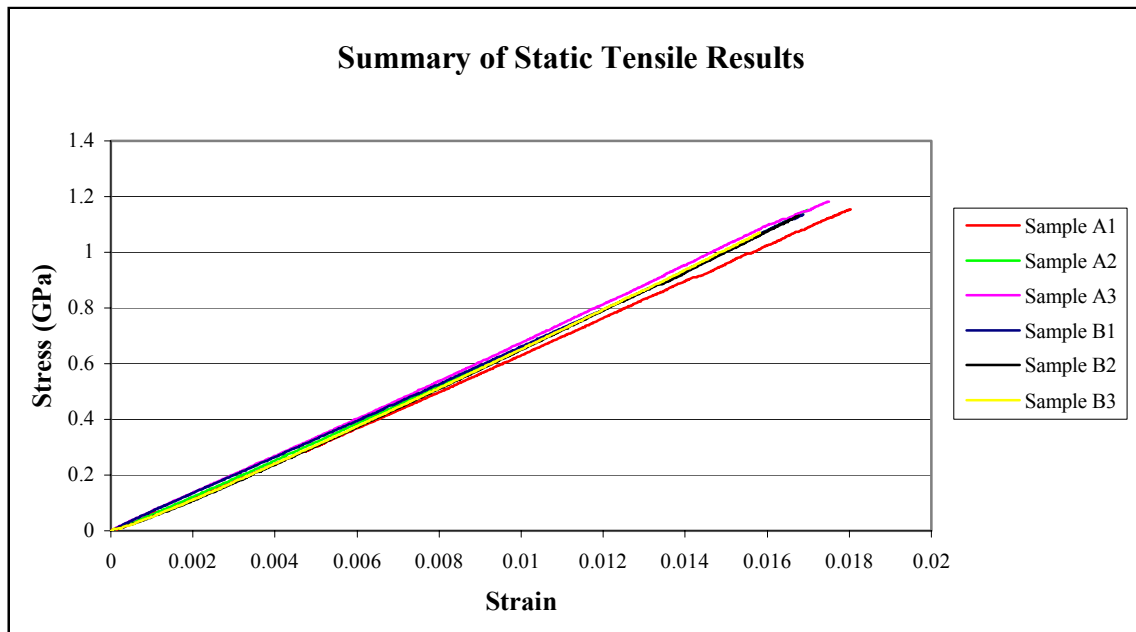


Figure 6-8 Typical stress-strain charts for tensile reference CFRP samples.

To check the quality of the composite and the test program, manufacturers' data for unidirectional composite samples was used to obtain an estimate of the Young's modulus and tensile strength for this cross-ply lay up. The Rule-of-Mixtures (Hull and Clyne, 1996) was used for the basis of the calculation. The data used are shown in

Table 6-2 with the comparison between calculated and obtained data shown in Table 6-3.

Property	Value
Tensile strength parallel to fibres	2000 MPa
Tensile strength perpendicular to fibres	80 MPa
Young's modulus parallel to fibres	130 GPa
Young's modulus perpendicular to fibres	9 GPa

Table 6-2 Manufacturer's data for a unidirectional carbon fibre composite.

	Tensile Strength, MPa (Std dev)	Young's modulus, GPa (Std dev)
Experimental Values	1136 (41)	66.2 (1.38)
Calculated Values	1040	69.5

Table 6-3 Comparison of experimental and calculated values for tensile strength and modulus, standard deviations shown in parentheses.

It was seen from Table 6-3 that the calculated values are very close to those experimentally obtained within this project; thereby confirming the quality of the composite and that the test methods were suitable.

6.2.2 Tensile properties of CFRP samples with embedded EFPI sensors

All these samples were first subjected to a 5 kN ramp loading at $10 \text{ kN}\cdot\text{minute}^{-1}$ to check on the response of the EFPI sensors. Figure 6-9 shows an example of an EFPI responding during three ramp loadings to 5kN. The strain data in the plot was obtained from a surface mounted ERSG.

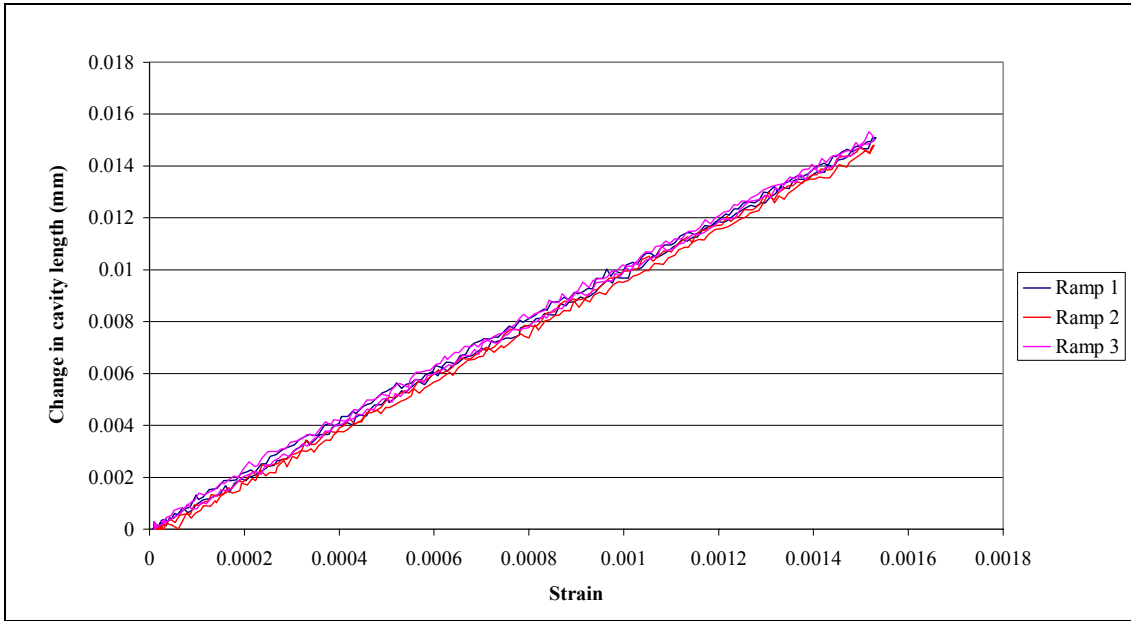


Figure 6-9 Plot of strain against change in cavity length for an embedded EFPI sensors.

From Figure 6-9 the effective gauge length of the EFPI sensor can be obtained from Equation 6-1:

$$\varepsilon = \frac{\Delta d}{GL}$$

$$\Delta d = GL \cdot \varepsilon$$

$$y = mx$$

Equation 6-1

In practise, linear regression was applied to the strain/change in cavity plot and the gradient of the line of best fit was taken as the gauge length. For sample J6 the gauge length determined from each ramp is presented in Table 6-4 alongside the R^2 value.

Ramp	Gauge Length (mm)	R^2
1	9.83	0.9987
2	9.87	0.9989
3	9.86	0.9986
Average	9.85	-

Table 6-4 Calculated Gauge lengths for sample J6.

It can be seen from Figure 6-9 and Table 6-4 that the response of the EFPI sensor was repeatable under these conditions.

The calculated gauge length for each sample is shown in Table 6-5 along with the gauge length determined by microscopy prior to embedment.

Sample Number	Designed Gauge Length (mm)	Measured Gauge Length (mm)
J1	14.2	7.1
J2	14.1	14.5
J3*	14.1	N/A
J4	14.0	8.8
J5	13.9	10.8
J6	13.7	9.9

Table 6-5 Gauge lengths of embedded sensors.

**-Lead-in fibre was damaged during installation into test machine.*

From Table 6-5 it can be noticed that the calculated gauge lengths are typically smaller than those measured prior to embedment. In an attempt to explain this effect a sample was sectioned and polished to reveal the embedded sensor. Figure 6-10 is one of the images taken during the observation. In this figure it is suggested that the thin orange line is matrix resin that has entered the capillary.

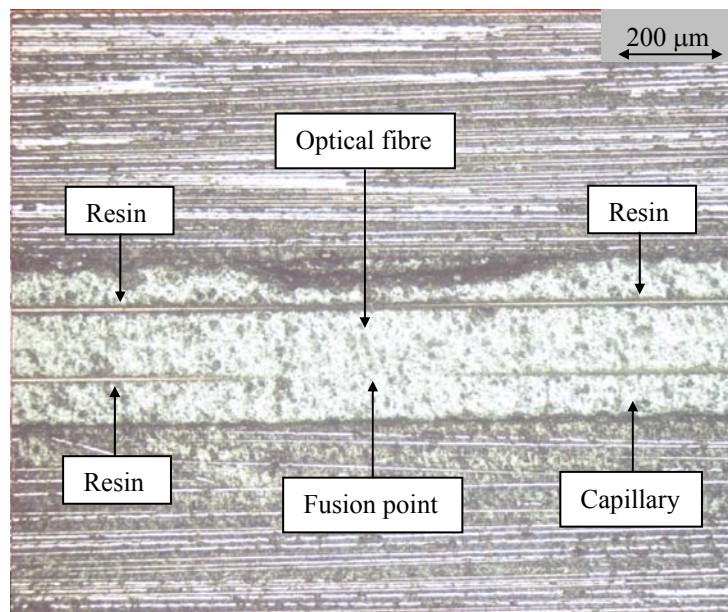


Figure 6-10 Image showing the fusion point surrounded by resin.

Figure 6-10 shows the location of the fusion point generated by the electric arc, however, it appears to have been overtaken by the resin flow. On the lower side of the

image the join between the capillary and fibre can be seen, which appears to have prevented resin flow along that side. But on the upper side the resin has flowed past the fusion point, this would then alter the actual gauge length of the sensor.

The only method currently available to prevent this would be to seal the capillary ends with a resin. But it was felt that at this stage of the project this would introduce a further complication of an extra disturbance in the prepreg structure due to the resin bead. Therefore, the sensors were left as manufactured with each sample being subjected to a ramp loading to determine the gauge length prior to testing.

The tensile testing to failure was then carried out on the samples and the results for the composite response are presented in Table 6-6.

	Sample	Failure Strain (ϵ)	Failure Stress (MPa)
	J1	0.0132	988
	J2	0.0146	1026
	J3	0.0140	1006
	J4	0.0148	1057
	J5	0.0159	1137
	J6	0.0158	1124
CFRP with embedded EFPI sensors	Average	0.0147	1056
	St dev	0.0010	62
Reference CFRP samples	Average	0.0170	1136
	St dev	0.0007	40

**Table 6-6 Tensile results for CFRP samples with embedded EFPI sensors.
The reference data has been included to aid comparison.**

If these results are compared to the reference samples, it can be seen that the reference samples have a slightly higher average stress (1136 MPa) and strains to failure (0.0170). This reduction is likely to be due to the inclusion of the EFPI sensors. From a visual examination of both sets of failed samples, reference and with embedded sensors, there were no noticeable differences.

So the inclusion of the EFPI sensors only had a slight effect on the tensile mechanical properties of the composite, a reduction of 7% for strength and 13.5% for strain. This

was as expected as the sensors were placed between two 0° plies in the 0° direction and according to the published works this positioning should minimise any influence.

Sample	Gauge length (mm)	Total cavity length change of EFPI (µm)	Composite stress at failure of EFPI (MPa)	Composite strain at failure of EFPI (ESRG)
J1	7.1	36.3	361	0.0049
J2	14.5	61.6	300	0.0044
J4	8.8	34.4	253	0.0038
J5	10.8	70.5	441	0.0063
J6	9.9	61.2	389	0.0056

Table 6-7 Failure stress and strain for the embedded EFPI sensors.

Table 6-7 shows the responses of the embedded EFPI sensors to the application of tensile load. The sensors all failed at levels below that of the failure of the composite. The composite samples with embedded sensors failed at an average strain of 0.0147 (see Table 6-6); however, the sensor response was lost at an average strain level of 0.005 (0.5%). There appears to be no correlation between gauge length and the strain to failure of the sensors. The failure of the sensors was the complete loss of signal, likely to be caused by a fibre fracture at some point within the composite. The likely failure locations are similar to those discussed in Section 4.4.3, with the additional possibility of a fracture in the lead in/out optical fibres.

6.3 Quasi-static Compressive Testing

This section reports on the results obtained when the reference composite samples and the composite samples with embedded sensors were subjected to compressive loads. All samples were tested with the anti-buckling guide in place.

6.3.1 Compressive properties of reference CFRP samples

Figure 6-11 shows a typical stress/strain plot for the reference samples tested. The stress/strain plot is not completely linear, possibly due to the guide allowing a small amount of buckling to occur. Therefore, the elastic modulus values calculated were based on the data up to a strain level of 0.4%.

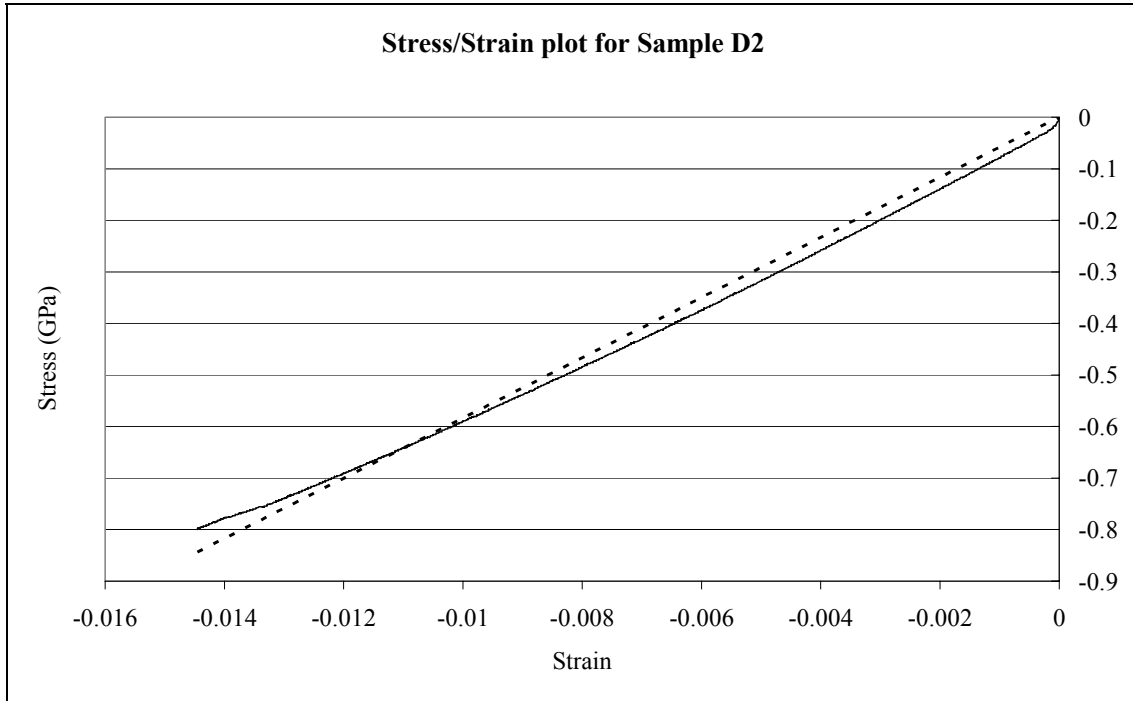


Figure 6-11 Typical stress-strain graph from a compression test.

Various attempts were made to minimise the buckling associated with the testing. For the anti-buckling guide different thickness spacers for the end-tabs and sample were tried as well as the level of torque applied to the bolts that held the guide together. However, the anti-buckling guide had to allow the sample to move in response to the applied load, this meant the bolts could not be too tight and the spacers had to be thicker than the samples. Through this process it was found that even a small difference in thickness between the spacers and the sample was sufficient to allow some buckling to occur and without the manufacture of specific spacers for each sample this buckling could not be avoided. Table 6-8 shows the summary of the compressive results of the reference samples.

Sample	Failure Strain (ε)	Failure Stress (MPa)	Secant Modulus at 0.4% strain (GPa)
C1	-0.0120	-694	59.6
C2	-0.0142	-790	58.9
C3	-0.0157	-850	62.4
D1	-0.0134	-734	59.4
D2	-0.0144	-789	60.4
D3	-0.0158	-834	62.0
Average	-0.0143	-782	60.5
St dev	0.00142	59	1.44

Table 6-8 Compressive results for reference CFRP samples.

It can be seen from Table 6-1 and Table 6-8 that the compressive strength and modulus values are significantly lower than the tensile results. This is due to the difference in failure mechanisms; the tensile strength of the composite predominately relies on the tensile strength of the reinforcing fibres, whereas the compressive properties are controlled by the buckling of the fibres (Hull and Clyne, 1996). Also the compressive samples have to be prevented from buckling through the use of guides. However, it is possible that the samples still experienced buckling during testing and this could also lead to a reduction in the strength and modulus results as compared to the tensile samples.

6.3.2 Compressive properties of CFRP samples with embedded EFPI sensors

As with the tensile samples, these samples were subjected to a ramp loading of -5kN prior to testing to failure to allow the gauge length of the sensors to be determined. These results are shown in Table 6-9 below.

Sample Number	Designed Gauge Length (mm)	Measured Gauge Length (mm)
N3	13.9	3.2
N4	14.3	3.8
N5	14.1	5.9
J7	14.3	8.0
M6	14.3	11.7

Table 6-9 Experimental gauge lengths values for compression testing

Again, as with the tensile samples the measured gauge lengths were lower than those measured prior to embedment, as it can be seen from Table 6-5 and Table 6-6, this effect appears to be random. This was also attributed to the ingress of the 913 resin matrix in to the capillary, as discussed previously in Section 6.2.2.

	Sample	Failure Strain (ϵ)	Failure Stress (MPa)
	N3	-0.01274	-692
	N4	-0.01162	-742
	N5	-0.00997	-652
	J7	-0.00887	-590
	M6	-0.00914	-577
CFRP with embedded EFPI sensors	Average	-0.0105	-651
	St dev	0.0017	69
Reference CFRP samples	Average	-0.0143	-782
	St dev	0.00142	58.9

Table 6-10 Compressive properties of CFRP samples with embedded EFPI sensors. Reference data has been included to aid comparison.

Table 6-10 shows the composite's response to the compression loading to failure. If these are compared to the reference compression samples, the reference samples have average higher stress and strain to failure. It is possible that the inclusion of the EFPI sensors affects the resistant of the fibres to buckling, thereby lowering the compressive strength of the samples by 16% and the compressive failure strain by 26%. There was no noticeable difference between the reference samples and those with embedded sensors when a visual comparison was made on the failed specimens. Table 6-11 shows how the EFPI sensors responded to the compressive failure of the composite samples.

Sample	Gauge length (mm)	Total cavity length change of EFPI (μm)	Composite stress at failure of EFPI (MPa)	Composite strain at failure of EFPI (ERSG)
N3	3.2	75.3	-692	-0.0127
N4	3.8	74.8	-742	-0.0119
N5	5.9	52.5	-652	-0.0099
J7	8.0	91.5	-590	-0.0088
M6	11.7	137	-577	-0.0091

Table 6-11 Response of EFPI sensors to compression loading.

Unlike the tensile samples, all the sensors survived until failure of the composites at an average strain level of -0.011 . Under tension loading it was felt that the fibre was fracturing causing the loss of the sensor signals, however, under compressive loading if any fractures did occur they would be compressed reducing the risk of signal loss from the sensor. Also as the sensor and optical fibres were compressed then it would tend to fail by buckling, but the composite would resist that movement.

6.4 Influence of Loading Rate

The response of certain fibre reinforced materials can be rate sensitive, as shown by Rotem (1993) and described by Hull and Clyne (1996). Barron *et al.* (2001) examined CFRP samples under different test frequencies and significant affects of the test frequency were also observed in the angled ply samples, not the unidirectional or cross-ply. The static and dynamic parts of the current project were carried out at significantly different loading rates ($0.17 \text{ kN}\cdot\text{s}^{-1}$ and $250 \text{ kN}\cdot\text{s}^{-1}$ respectively). It was felt, therefore, that any loading-rate dependency of the mechanical properties of either the composite or sensors should be investigated.

6.4.1 Rate sensitivity of CFRP samples

Figure 6-12 shows the stress/strain plot of a CFRP reference sample tested at each of the chosen loading rates up to a stress level of 342 MPa, with the insert showing an expanded scale between the stress range of 100 and 130 MPa. From Figure 6-12 it can be noticed that there appeared to be no significant difference in the response of the composite due to increasing testing rates. On the expanded scale view it can be seen that there are slight differences between the different rates, but unlikely to be more than experimental differences.

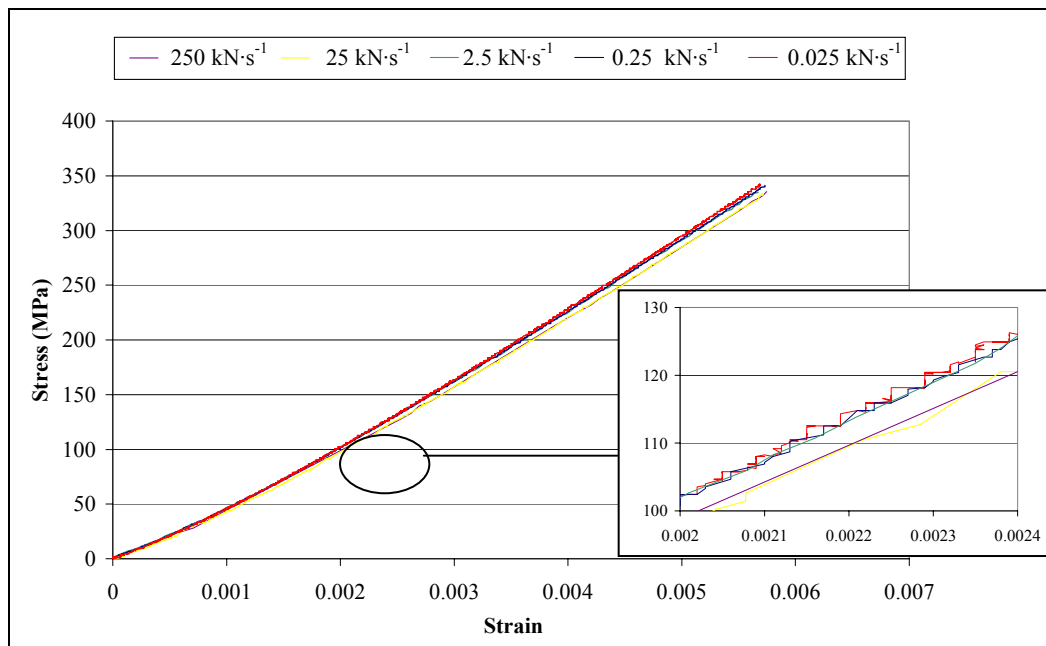


Figure 6-12 Stress/strain plot for a sample tested at different loading rates. The insert shows an expanded scale.

Table 6-12 shows the Young's modulus values determined for each of the samples tested at each of the loading rates. There is a small change for Sample 3 at the higher loading rates, but overall the modulus value appears consistent.

Loading Rate (kN·s ⁻¹)	Average Young's Modulus (GPa)		
	Sample 1	Sample 2	Sample 3
0.025	63.1	62.3	63.7
0.25	63.1	62.5	63.5
2.5	63.4	62.6	63.7
25	63.3	62.6	64.6
250	63.4	63.0	65.0

Table 6-12 Young's modulus calculation for the reference loading rate samples

At higher loading rates the data acquisition program was designed to run as fast as possible. Even so it could not acquire the data at an even spacing as shown in Figure 6-13. The data acquired at 250 kN·s⁻¹ has gaps due to the time required by the program to record the data, it can be seen that at 25 kN·s⁻¹ the data was more evenly spaced. These gaps in the data could lead to some slight error with the data acquired at the fastest loading rate although from examination of the results it did not appear to have any significant effect. It is also possible that the method of data acquisition could have affected the results, due to it examining each of the three data channels in sequence, not simultaneously. Therefore, at the higher test speeds this delay between the data from each channel means that the values do not absolutely correlate.

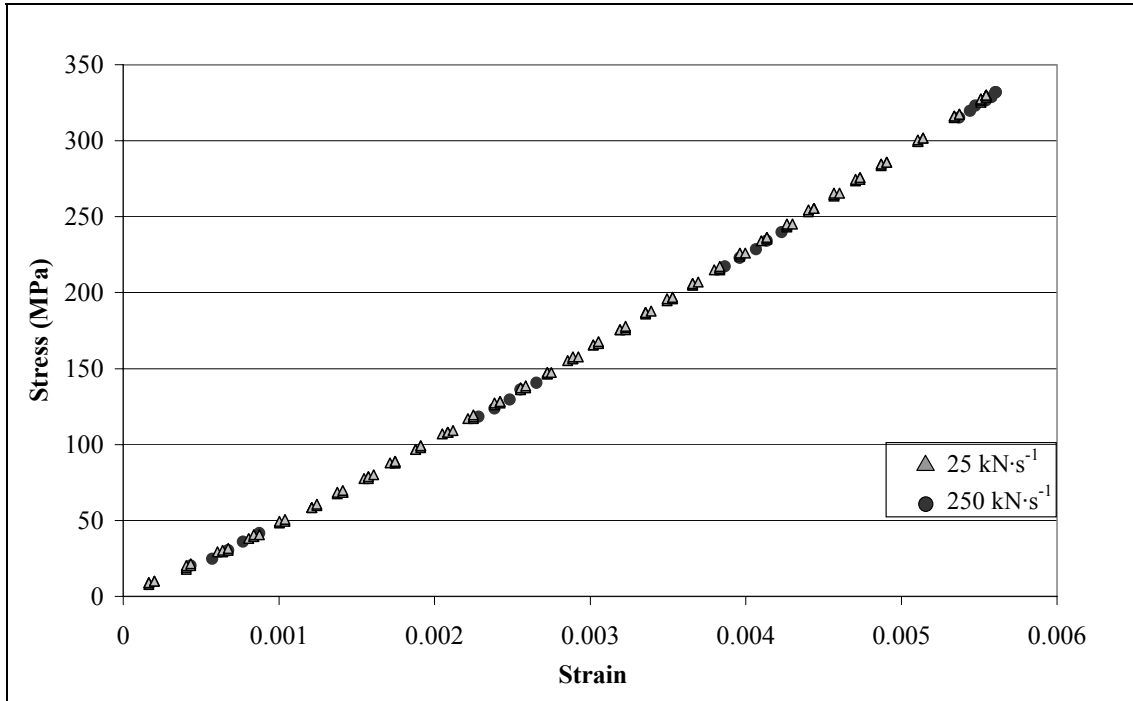


Figure 6-13 Graph showing the data acquired at 25 kN·s⁻¹ and 250 kN·s⁻¹.

6.4.2 Rate sensitivity of CFRP samples with embedded EFPI sensors

The same loading rate experiments were carried out on composite samples with embedded EFPI sensors. The reason for this was two-fold, the first was to examine the sensor's response to loading rate and the second to see if the inclusion of EFPI sensors altered the loading-rate response of the composite. Table 6-13 shows how the composite samples with the embedded sensors responded to the different loading rates. As with the reference samples, there appears to be no significant influence on the calculated Young's modulus due to the loading-rate changes.

Loading Rate (kN·s ⁻¹)	Average Young's Modulus (GPa)	
	Sample 1	Sample 2
0.025	66.0	69.8
0.25	65.5	69.5
2.5	65.1	-*
25	64.3	69.5
250	66.0	69.1

Table 6-13 Young's modulus value for composites with embedded sensors

*-due to a mistake in the data acquisition no load information was recorded

These results are inline with work done by Lafarie-Frenot (2002) on the strain rate behaviour of CFRP laminates. Cross-ply laminates were subject to tensile loading at three rates, 0.01, 1 and 10 mm·min⁻¹. Carbon fibre composites only begin to show significant strain rate dependency when the testing enters impact testing (Hsiao and Daniel, 1998, Melin and Asp, 1999).

As described in Section 3.4.8 the response of the sensors at the higher loading rates was unobtainable due to hardware limitations. The sensors could only be investigated at 0.025, 0.25 and 2.5 kN·s⁻¹, this was still three orders of magnitude difference in loading rate. Also due to the hardware limitations only a few data points were obtainable at the loading rate of 2.5 kN·s⁻¹.

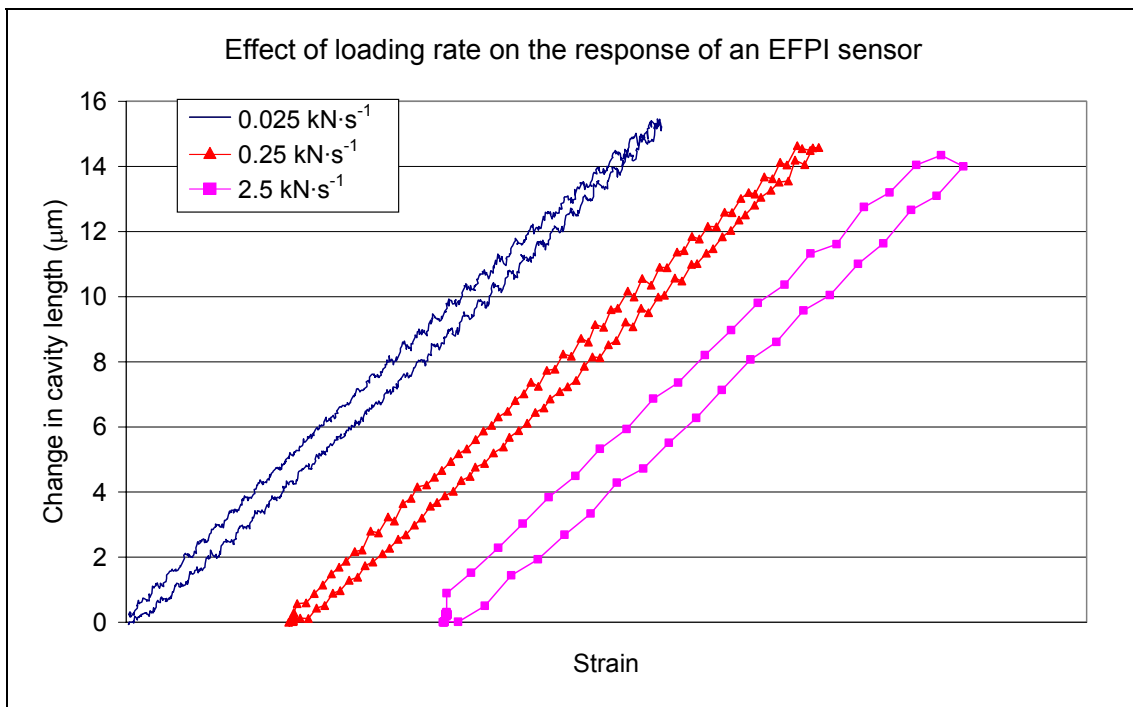
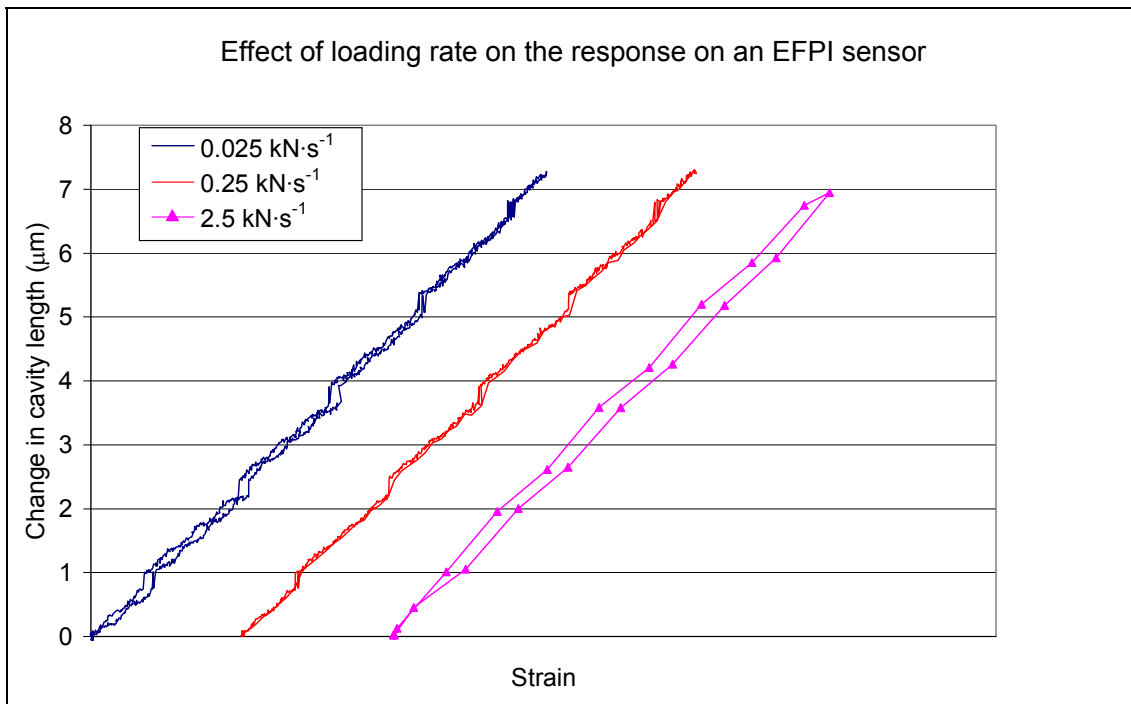


Figure 6-14 Response of the EFPI sensor from sample 1 to the changes in loading rate. The strain axis has been offset to aid comparison of the data.

Figure 6-14 shows the sensor's response from sample 1 to the different loading rates, noting that to aid the comparison of the data the strain axis has been offset. From Figure 6-14 it can be noted that there was some hysteresis in the response of the sensor to the application of the load, also the hysteresis appeared to get worse as the loading rate was increased. It was also observed that the amount of data obtained reduced dramatically as the test speed was increased. It was therefore difficult to tell whether

the hysteresis observed was a function of the data acquisition system or a rate sensitive response of the EFPI sensor.

Figure 6-15 shows the sensor's response from sample 2 to the changing loading rate, again the strain axis has been offset. In this case the hysteresis was not so apparent but as the loading rate increased to $2.5 \text{ kN}\cdot\text{s}^{-1}$ the data obtained was different.



**Figure 6-15 EFPI sensor from sample 2 responses to changing loading rate
The strain axis has been offset to aid comparison of the data.**

From these samples there appears to be some affect on the sensors due to the loading rate. Whether this is due to the hardware limitations that prevent higher speed acquisition or an actual property of the sensors is unclear at this stage. To enable this to be investigated further would require an improvement to the sensor interrogation system to eliminate this as a possibility for causing the change in data with loading rate. To improve the system sufficiently would require a major redesign of the system, which was outside the scope and time frame of this project.

There currently appears to be no published work on the strain rate dependency of EFPI sensors. However, there has been work published on the strain rate dependency of

optical fibres. Glaesmann *et al.* (1998) published work relating to the high speed testing of the tensile strength of optical fibres. A wide range of speeds were used from 7×10^{-6} GPa·s⁻¹ to 1530 GPa·s⁻¹ to test the strength of acrylate coated silica fibres, which varied from 0.4 GPa to 0.9 GPa, respectively. It was also shown that at the higher rates there is a non-linear relationship between the test speed and strength. Therefore it is possible that the EFPI sensors could be affected by different test speeds, this is an issue which needs further investigation.

6.5 Dynamic Evaluation of Composite Samples

This section reports on the effect of T/C fatigue loading on the composite samples with and without embedded sensors. As the research currently stands the fatigue testing on EFPI sensors has been mainly limited to T/T regimes, as previously described in Section 2.2.3. Badcock and Fernando (1995) examined CFRP composite samples under T/C loading; finding that embedment of the EFPI sensor had no detrimental affect on the composite fatigue resistance. However, in that work the sensors were designed such that the cleaved faces of the optical fibres were butted together, which prevented the sensor being interrogated during the T/C fatigue loading. As the majority of the published work on embedded sensors had been concentrated on T/T fatigue, and as T/C regimes are known to be more detrimental to the CFRP samples (Curtis, 1997), it was decided to investigate the effect of T/C loading regimes on the embedded EFPI sensors.

6.5.1 Stress ratio of -1

The fatigue work in the current study began with a stress ratio (R) of -1, which meant the magnitude of the applied stress in the tensile and compressive phases of the fatigue cycles was the same.

6.5.1.1 Reference Samples at R=-1

Shown below in Figure 6-16 is the S-N plot for the reference CFRP samples. The number of cycles to failure (N) is plot against the maximum stress level (S) applied to the sample. This stress level is reported in percentage terms of the average ultimate compressive strength (UCS). In Figure 6-16 the arrow symbolises a sample that did not fail prior to the end of testing at a million cycles.

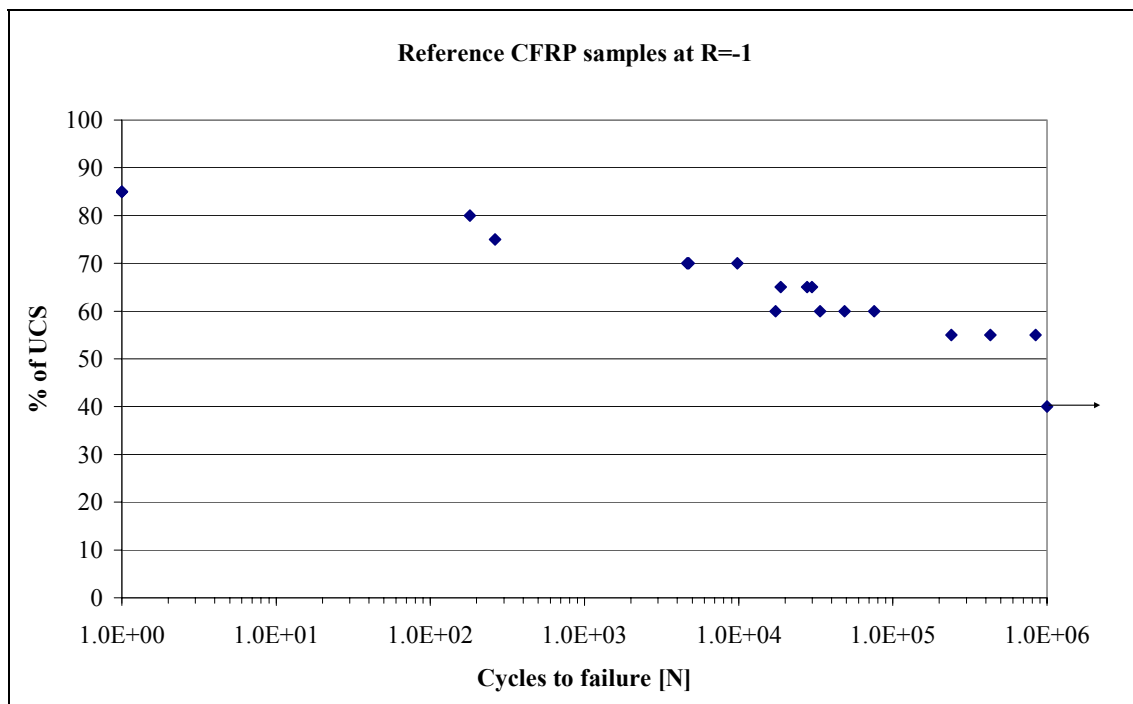


Figure 6-16 S-N plot for the reference carbon fibre composite samples.

As expected, the number of cycles to failure increases as the maximum applied stress decreases. The failed specimens also change appearance as the stress level changes. At the higher stress level the specimens show very little damage, aside from the actual failure location. As the stress level decreases so does the apparent damage, for the samples tested at stress levels between 60% and 70% UCS specimens begin to show edge damage, with delaminations in the 0° plies. At the 55% UCS stress the outer 0° plies showed significant damage after failure. This is consistent with the affects of damage build up during fatigue loading.

6.5.1.2 Sensors at $R=-1$

The next stage was to investigate the composite samples with embedded EFPI sensors. However, these samples could not be tested at the high stress levels as from the static tensile results, see section 6.2.2, it can be seen that the embedded EFPI sensors fail when the composite sample is subjected to tensile stress around 350 MPa. This corresponds to 45% of UCS, therefore only tensile stress levels below that can be used to investigate the fatigue performance of the current range of EFPI sensors. The initial stage of fatigue testing used was $R=-1$ with a maximum stress level of 40% UCS (313 MPa). For the compressive phase, no limit was required on the maximum stress as the sensors survived until composite failure under the static compressive loading conditions, see section 6.3.2. At a fatigue loading of $R=-1$ with the stress set to 40% of UCS the reference samples survived a million cycles (see section 6.5.1.1). Hence, it would be hoped that the CFRP samples with embedded sensors should also survive to a million cycles.

The sensors could not be interrogated during the fatigue cycling due to hardware limitations. The loading rate for the fatigue samples was $250 \text{ kN}\cdot\text{s}^{-1}$ and as shown in section 6.4.2, the data acquisition system for the sensors could only just acquire usable data at $25 \text{ kN}\cdot\text{s}^{-1}$. Therefore the cycling was stopped at intervals to allow the monitoring of the response of the sensors to a load. Ramp loadings between 5 kN and -5 kN were carried out before the start of the fatigue regime and at the required intervals.

Sample N1

At $R=-1$ at 40% UCS

At each of the ramp intervals, the response of the EFPI sensor to the loading was recorded as well as the strain response of the CFRP sample. In Figure 6-17 the change in cavity length and strain levels for sample N1 for each ramp loading at the maximum and minimum loads are presented, $+5 \text{ kN}/-5 \text{ kN}$, respectively.

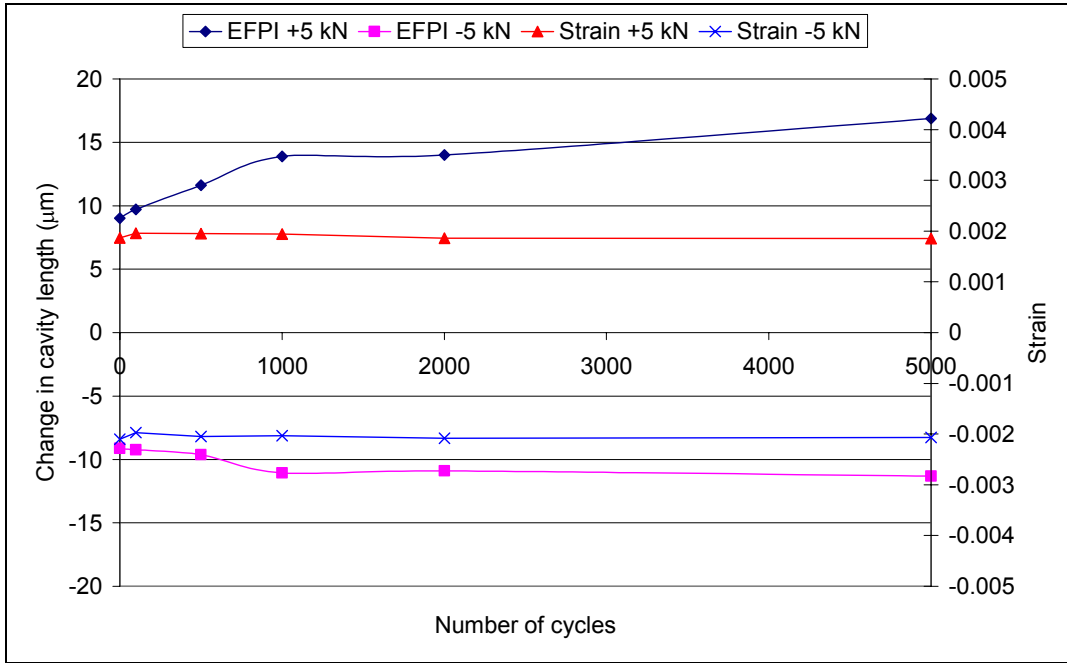


Figure 6-17 A plot showing the variation in cavity length for ramp loadings of sample N1.

It can be seen from this graph that although the strain within the composite was not affected by the fatigue cycling, the response of the EFPI was altered. As the cycling progressed the response of the EFPI continued to degrade, particularly in the tensile ramp loading. A further example of this degradation of the sensor response is shown in Figure 6-18.

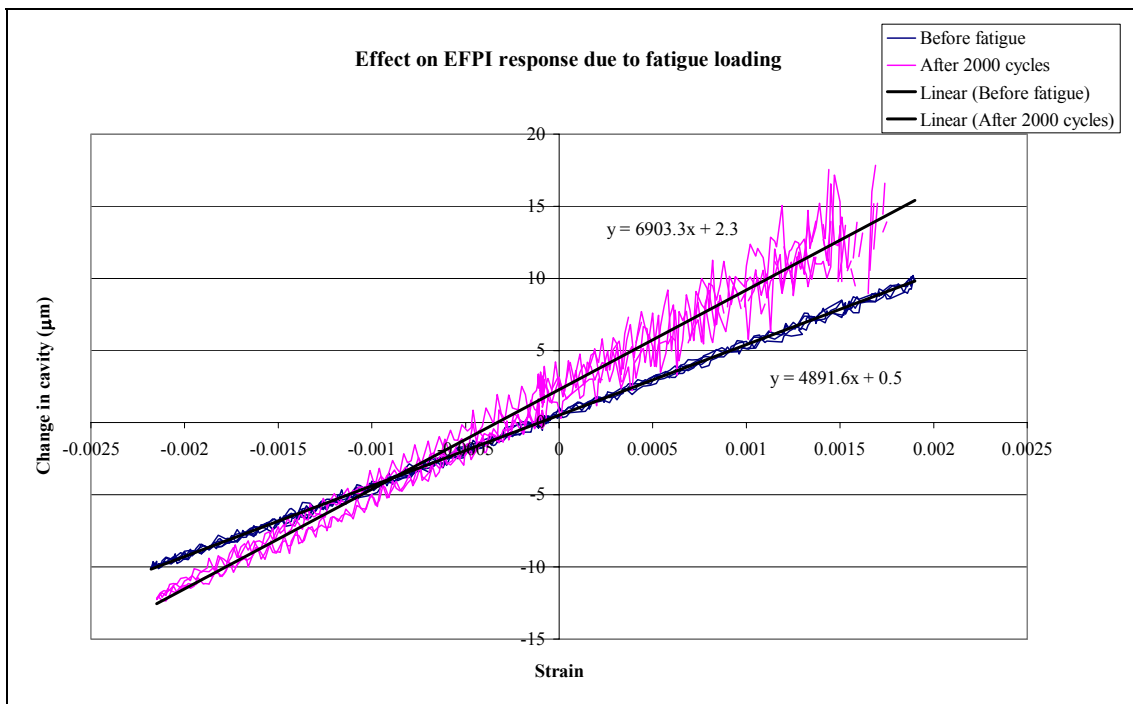


Figure 6-18 EFPI response differences after 2000 cycles of fatigue loading.

Figure 6-18 shows the response of the embedded EFPI sensors during the ramp carried out prior to testing and that carried out after the samples had been subjected to 2000 cycles of fatigue loading. The most obvious difference was the noise present in the sensors response after 2000 cycles. The noise was more significant in the tension portion of the graph, as is the change in the sensor performance. Also the gradient of the line of best fit has significantly changed, which is the gauge length, in this case the gauge length has apparently increased from 4.9 mm to 6.9 mm due to the fatigue cycling. To further examine this, the spectral response of the sensors was also recorded during the ramp loading. The spectra obtained from the sensor after 5000 cycles is shown in Figure 6-19 along side the spectrum obtained after 100 cycles.

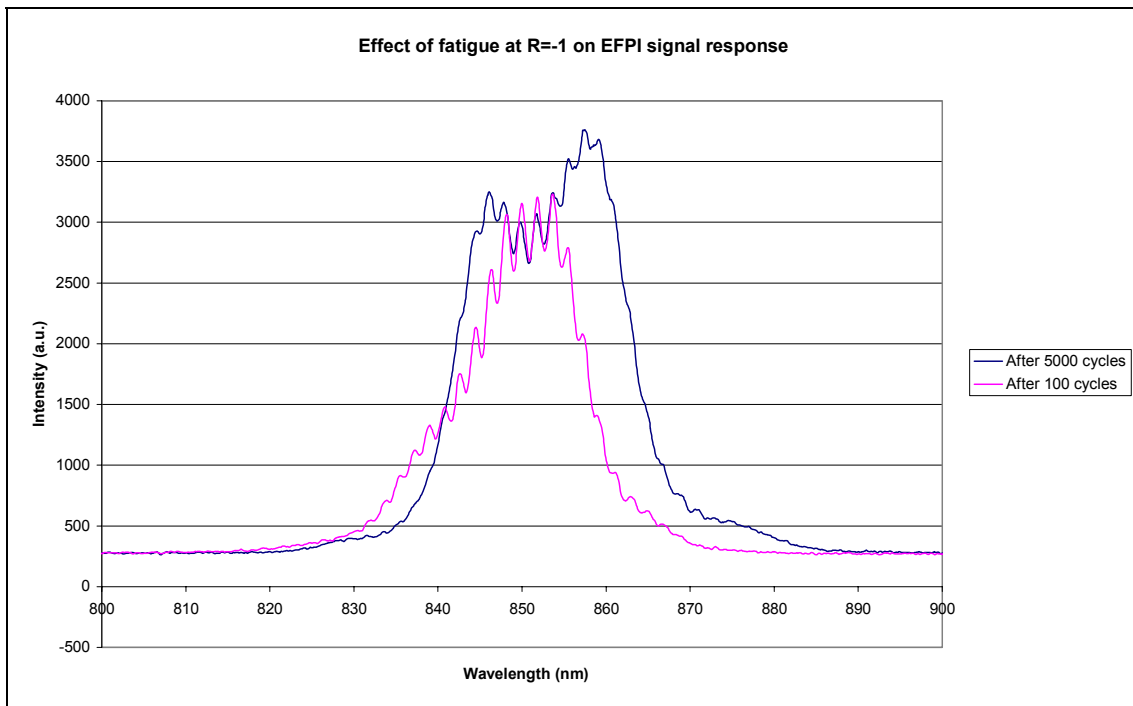


Figure 6-19 Spectrum responses from the sensor after 100 and 5000 cycles.

Figure 6-19 shows how the fatigue of the sensor has altered the spectrum. After 5000 cycles it is not possible to determine reliably the cavity length, the sinusoidal interference pattern is insufficiently clear. This is probably because the spectrum is actually the interference patterns of several different cavities that could have been formed by fractures along the length of the lead in/out fibre and the sensor. Although the FFT analysis can separate multiple cavity responses, it only works when the cavity

lengths are distinctly different and of approximately equally intensity. In the case of fractures it is unknown how many cavities could have been formed or the approximate sizes, also fractures surfaces would not necessarily give good spectra, as they would be unlikely to form good-mirrored surfaces. This also explains why the compression performance of the sensor in these ramp loadings was better than the tensile. As the fatigue continues, fractures within the optical fibre system increase. When the samples are tensile ramp loaded the fractures can turn into cavities and affect the spectra. However, under a compressive load these cavities would be pushed together thereby reducing the effect on the spectra obtained. At 5000 cycles the degradation of the spectra prevented continued examination of this embedded sensor.

Sample N6

At R=-1 at 40% UCS

Figure 6-20 shows the results for the ramp loadings of sample N6 at the various stages of the fatigue regime. This sample showed similar alterations to the cavity length change due to fatigue loading as sample N1, however, the changes in this sample were less severe than those seen for sample N1.

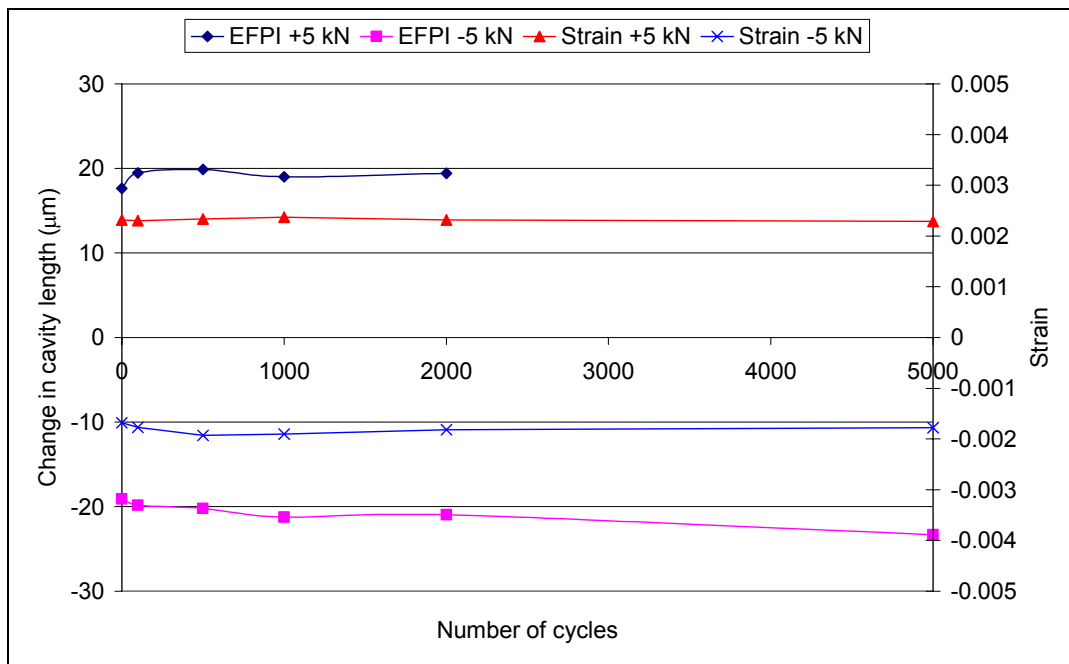


Figure 6-20 A plot showing the variation in cavity length for ramp loadings of sample N6.

The test was stopped after 5000 cycles, as the sensors response had been seriously affected by the fatigue loading. In this case the problem was more related to the loss of sensor response during tensile loading as can be seen in Figure 6-21. A likely cause for this is the creation of a fracture within the fibres, as for sample N1.

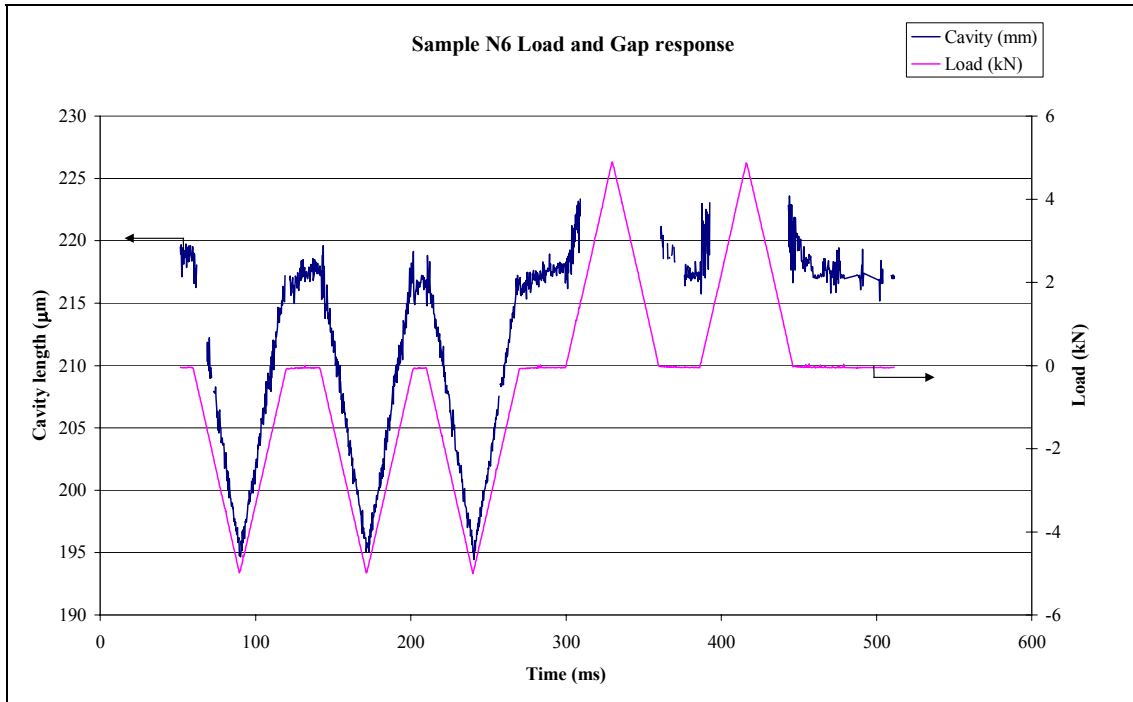


Figure 6-21 EFPI response from sample N6 after 5000 cycles.

Sample L3

At R=-1 at 40% UCS

The main difference between this sample and the two previous samples is that this sensor maintained a useable response up to a million cycles.

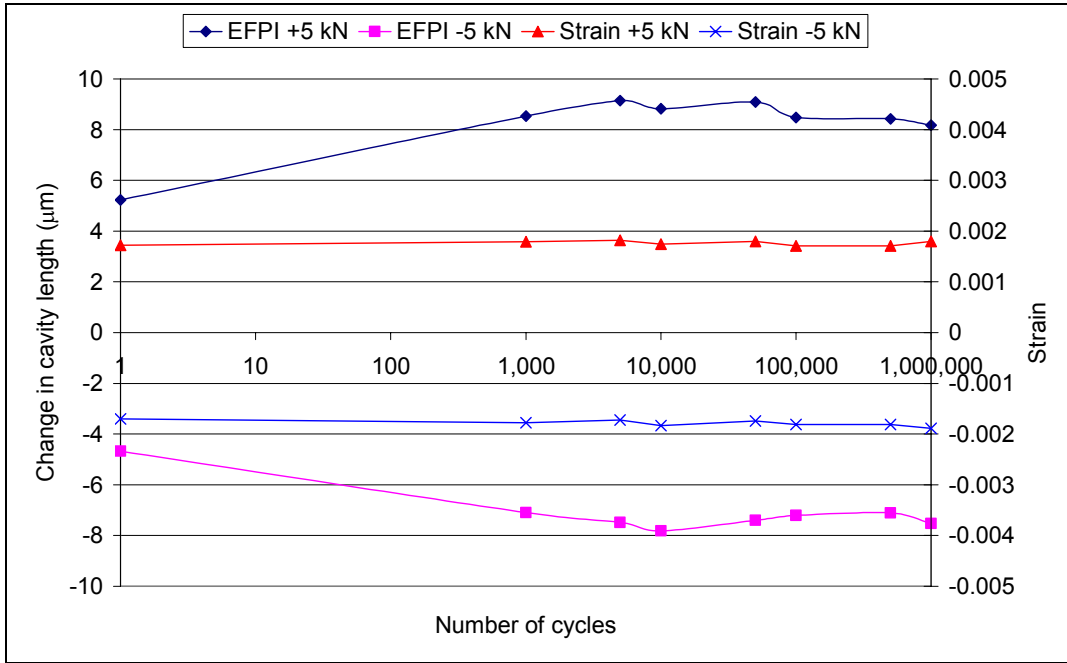


Figure 6-22 A plot showing the variation in cavity length for ramp loadings of sample L3.

Figure 6-22 again shows that the response of an EFPI sensor changes during the application of a fatigue loading regime.

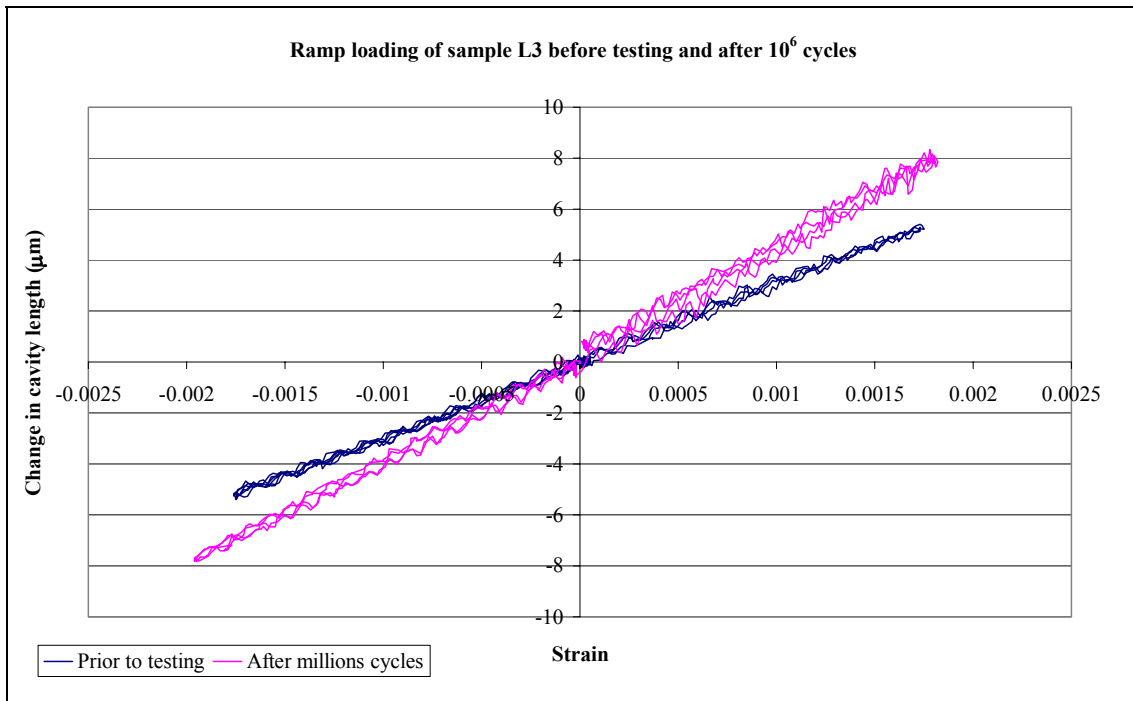


Figure 6-23 Response of L3 before testing and after 10^6 cycles

Figure 6-23 shows how the cavity length changed with applied strain before testing and after a million cycles. It can be seen that the slope of the line has changed, however this sample does show that an EFPI sensor can survive a million cycles under T/C loading ($R=-1$) at a stress level of 313 MPa, even though at this stage the reliability of that sensor is not satisfactory.

6.5.1.3 Summary of testing at $R=-1$ at 40% UCS.

Most of the problems appeared in the tensile sections of the ramp loading, however for compression loading the sensors were still responding well. This is likely to be related to the static limits of the sensors. At a stress level of 313 MPa (40% UCS) the sensors are being subjected to strain very near to the average failure strain found in the static tensile testing. This level of stress does not cause this problem in the compressive region of the testing, as under static compressive testing the sensors failed at the same point as the composite. Also as one sample survives to a million cycles this shows that the sensors can survive T/C fatigue but there is a significant reliability issue.

The increasing cavity length changes as the fatigue cycling continued was probably due to the resin that has flowed into the capillary. This resin is only a thin layer joining the capillary to the optical fibre, which has not necessarily penetrated a uniform distance along the capillary. As the sensor was subjected to strain, the resin could start to degrade and alter the gauge length of the sensors, thereby altering the cavity length changes monitored.

To allow further investigation of the sensors performance under T/C fatigue, it was decided to reduce the tensile component of the fatigue while increasing the compressive component. A tensile stress level was chosen equivalent to 20% of the UCS (156 MPa). The work then involved increasing the compressive stress level, while maintaining the tensile stress, leading to work being carried out at stress ratios of -2.5 and -3 . This resulted in applied compressive stresses of -389 MPa (50% UCS) and -469 MPa (60% UCS) respectively.

6.5.1.4 Embedded EFPI sensor tested at R=-1 at 20% UCS

A sample, M5, was tested at this stress level with a stress ratio of R=-1 to ensure that this level of tensile stress did not significantly impair the performance of the sensors. Figure 6-24 shows the data obtained for sample M5 during the ramp loadings.

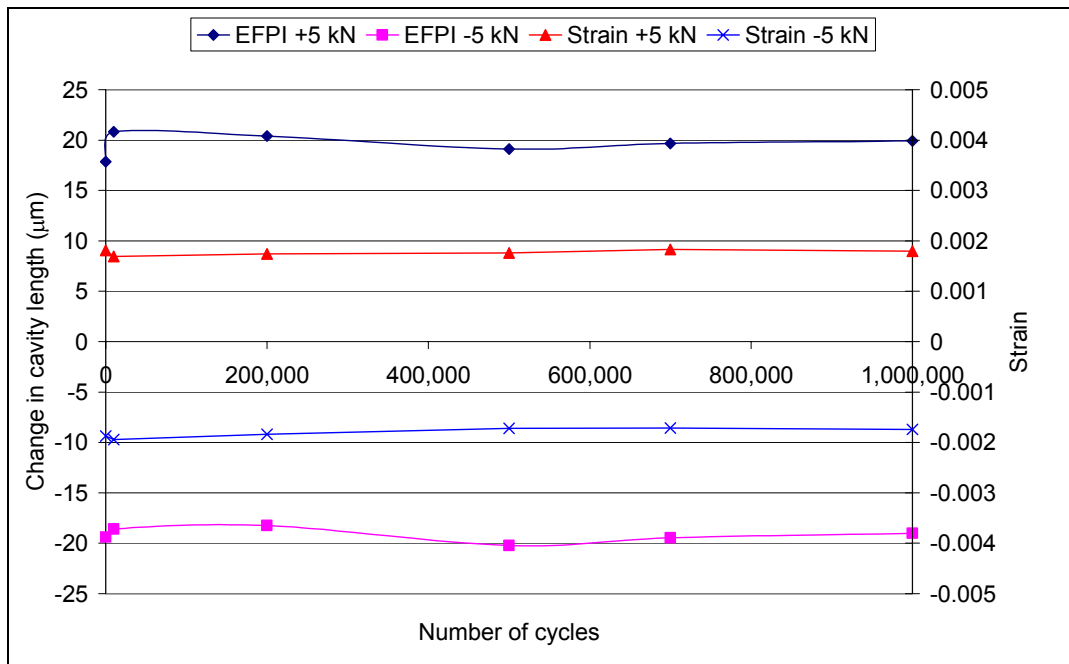


Figure 6-24 A plot showing the variation in cavity length for ramp loadings of sample M5.

From Figure 6-24 and Figure 6-25 it can be seen that there is little effect on the sensor's response due to the fatigue loading, even after a million cycles. There were slight variations in the cavity length response to the loading and a difference in the variation of the sensor's response in the tensile region. But these effects are significantly smaller than those seen for samples tested at 40% UCS. From these results it was felt that the tensile stress level of 20% UCS was suitable to use in the remainder of the testing.

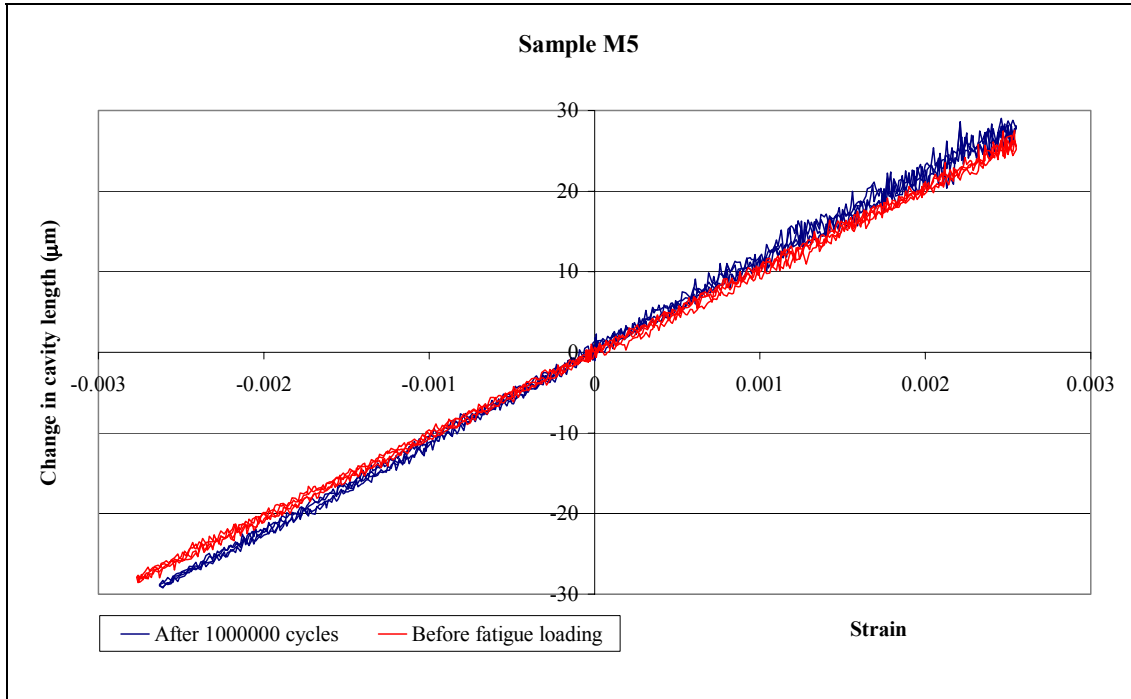


Figure 6-25 Cavity length response of sample M5 fatigued at 20% UCS.

6.5.2 Varying fatigue stress ratios

This section reports on the results of the fatigue testing carried out at a stress ratios of -2.5 and -3. This work was done to enable the investigation of the EFPI performance under increasing compression stress levels.

6.5.2.1 Sample tested at $R=-2.5$

Reference

This involved a tensile stress of 156 MPa (20% UCS) and a compressive stress of -389 MPa (50% UCS). Three reference samples were tested, two of these survived to a million cycles with the third failing after 610,270 cycles. Figure 6-26 shows the maximum and minimum strain experienced by the sample during the fatigue loading.

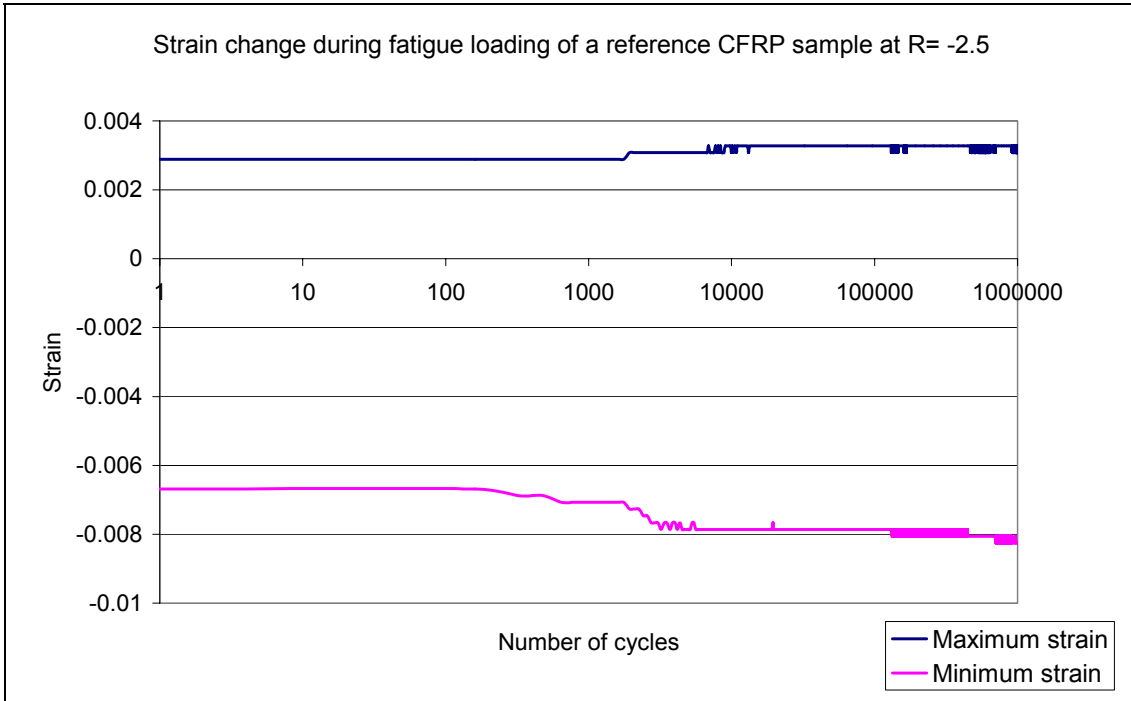


Figure 6-26 Reference CCRP sample subjected to a million cycles at R= -2.5.

It can be seen from Figure 6-26 that after an initial strain change the sample does not undergo large strain changes. As the fatigue was done under load controlled conditions, this means that the stiffness of the sample was not altering significantly during this testing at R= -2.5.

Sensors
Sample L5

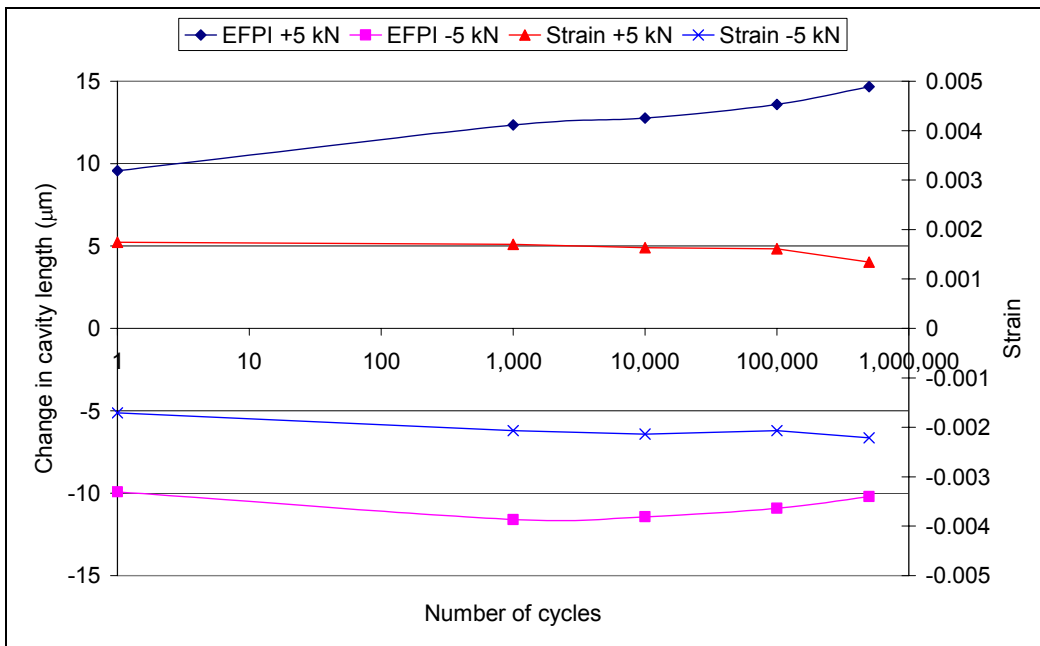


Figure 6-27 A plot showing the variation in cavity length for ramp loadings of sample L5.

Figure 6-27 shows the response of sample L5 to the various ramp loadings during fatigue regime. The composite sample failed after 629,903 cycles, with the sensor still able to generate a spectrum after the sample had failed. From this data it can be seen that the EFPI sensors can survive fatigue loading at this level, but there is still the issue of reliability. The change in cavity length continues to degrade during the fatigue cycling. Figure 6-28 shows the sensor was still responding after failure of the composite sample.

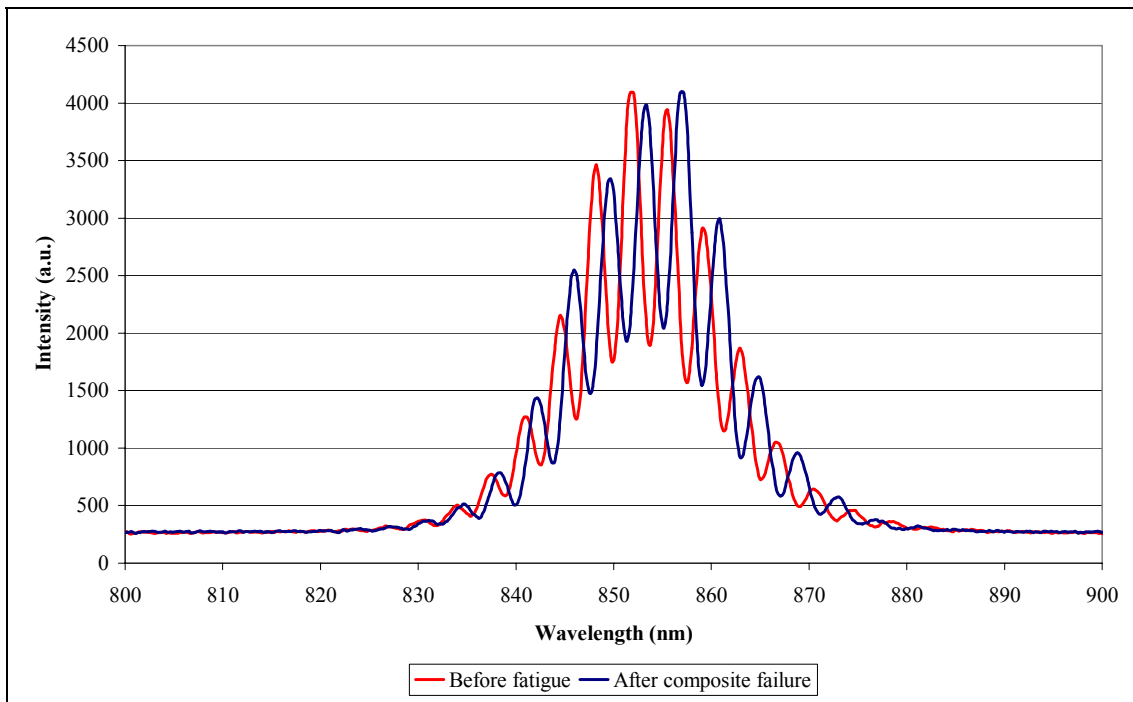


Figure 6-28 Spectral response of embedded EFPI before testing and after composite failure.

From Figure 6-28 it can be seen that in this case the fatigue loading regime has not significantly altered the spectral response of the sensor, although the cavity length at zero load had reduced from 98.8 μm to 94.4 μm due to the cycling. From this and the alteration in the cavities length during fatigue it seems that the sensors has not suffered any cracking or serious fractures, therefore it appears that the cause for the change in behaviour of the sensor must related to the resin that was generating the gauge length. As this resin suffered fatigue damage the gauge length was allowed to increase causing larger cavity length changes for a specified applied strain.

Sample L2

In this sample, the response of the sensor was lost between the ramp loading at 100,000 and 500,000 cycles. As it was not possible to monitor the sensor during the fatigue cycling, it was unknown as to when the sensor actually failed. The loss of the sensor response was due to the spectrum generated having insufficient visibility of the peaks to allow cavity length determination either by peak counting or FFT analysis. The raw spectrum generated after 500,000 cycles is shown in Figure 6-29 alongside the initial spectral response. It can be seen that the peaks of the spectrum are no longer clearly defined after the fatigue loading. Possible reasons for this loss of signal could include the optical fibres within the capillary moving thereby causing the endfaces to no longer be parallel. Also, if resin had entered the sensors and degraded during the fatigue regime it is possible that resin debris has accumulated between the endfaces preventing the light from passing cleanly through the cavity.

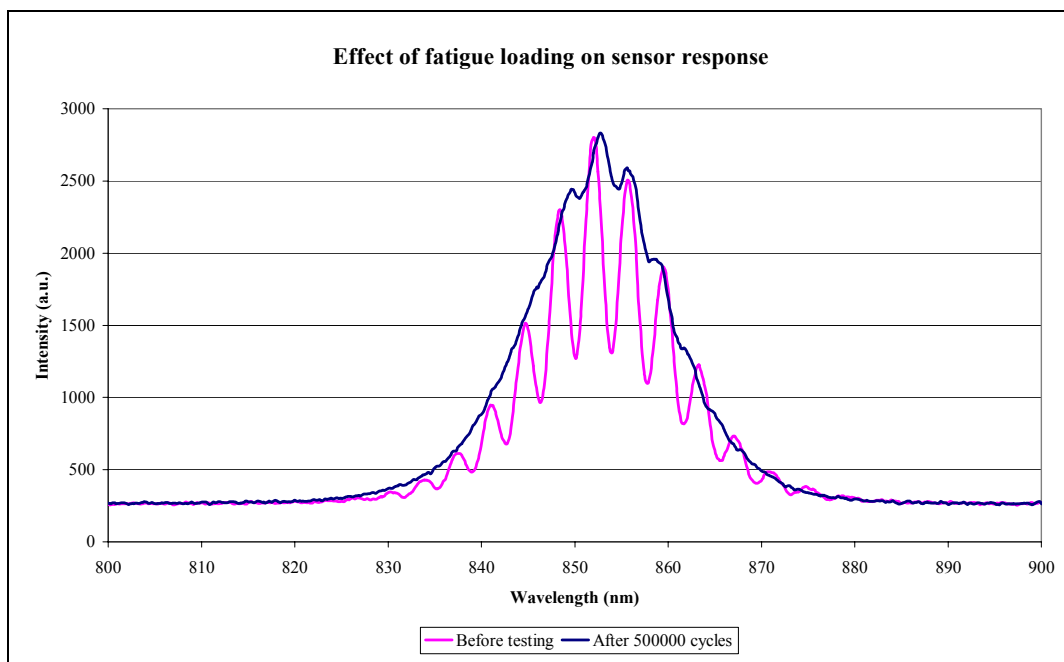


Figure 6-29 Spectral responses from Sample L2 from start and after 500,000 cycles

As with the previous embedded sensors results reported, the response of the sensor in sample L2 was affected by the exposure to T/C fatigue loading. This is shown in Figure 6-30 in terms of the cavity length change associated with loading to 5 kN and -5 kN. The effect is similar to the other sensors, with the cavity length change increasing after

fatigue loading for a specific applied stress, without the strain as measured by the extensometer significantly changing.

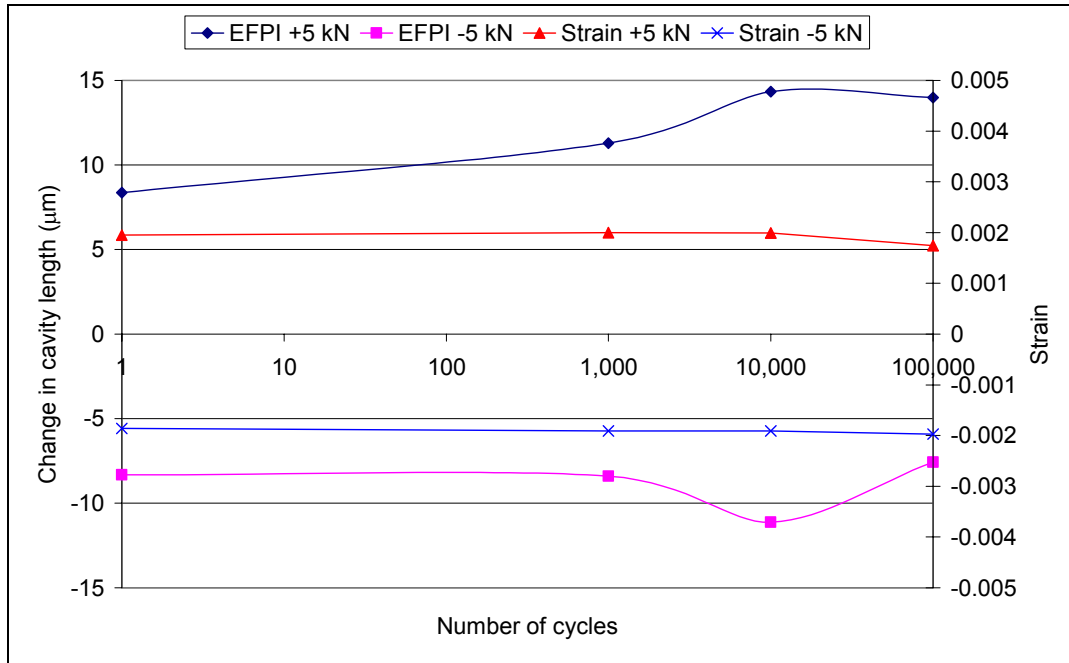


Figure 6-30 A plot showing the variation in cavity length for ramp loadings of sample L2.

Summary of fatigue testing at R=-2.5

There appears to be no significant effect on the composite survival at the fatigue level due to the inclusion of EFPI sensors. Out of the reference samples two survived up to a million cycles with the third failing at 610,000 cycles, whereas for samples with embedded sensors failed at 630,000 and 599,600 cycles, respectively. Similar to the results obtained at R=-1 the sensors do not provide reliable data during the fatigue regime. However, the sensors do appear to survive, on average, longer at R=-2.5 than R=-1, possible due to the reduction in the tensile stress applied. At R=-1 at 40% UCS two of the three sensors only provided data up to 5000 cycles, whereas both sensors tested at R=-2.5 survived part 100,000 cycles. But survival is not enough the data provided must be useful, therefore this area still needs further work.

6.5.2.2 R=-3

As the testing at R=-2.5 showed that the sensors at least survived longer than at R=-1 it was decided to extend the compressive range of the fatigue regime to further investigate the effect of compressive loading on the embedded EFPI sensors. Therefore testing was performed with a maximum stress of 156 MPa (20% UCS) and a minimum stress of -469 MPa (60% UCS). The results of the composite performance are shown in Figure 6-31.

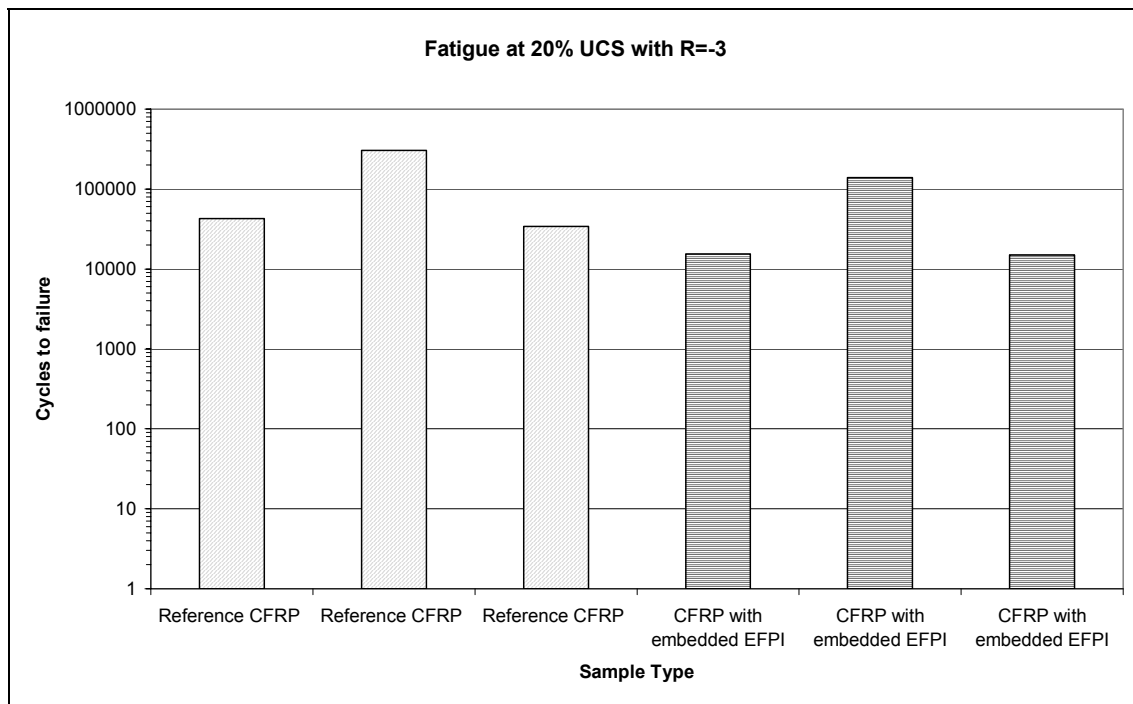


Figure 6-31 Number of cycles to failure for CFRP reference samples and those with embedded EFPI sensors at R=-3

From this it can be seen that the samples with embedded sensors, on average, have less resistance to this fatigue regime, but with the scatter in these results still quite large it is not possible to definitely determine the effect of the inclusion of EFPI sensors. At this stress ratio of -3 the fatigue life of the reference composite samples was reduced in comparison to those at R=-2.5, when two of the reference samples survived up to a million cycles.

Sensors

The performance of the sensors under this load were similar to those experienced for the other test conditions. The results for the embedded sensors tested at R=-3 are shown in Table 6-14. The ‘*’ signifies there was insufficient data to determined those results.

	Sample	Load condition	Number of fatigue cycles		
			1	1000	10,000
Change in cavity length associated with application of specified load	M3	At 5 kN	13.29	*	*
		At -5 kN	-13.25	-14.79	-13.94
	M4	At 5 kN	9.21	12.96	*
		At -5 kN	-9.08	-10.35	*
	M8	At 5 kN	5.4	10.43	8.43
		At -5 kN	-5.31	-6.78	-9.71

Table 6-14 The variation in change of cavity length for a specified load for the embedded sensors subjected to fatigue at R=-3.

At this stress ratio of -3, the behaviour of the EFPI sensor varies greatly as can be seen in Table 6-14. In sample M4 the sensor fails prior to 10,000 cycles, whereas for M3 the composite fails at 138,715 cycles with the sensor responding until at least 10,000 cycles in compression but not in tensile. Finally for M8, the composite fails at 14,899 cycles and the sensor still works but has undergone significant variations in its response to loading. Overall, the sensors do not seem to perform well at this stress level, there is just far too much variation between sensors to enable any useful analysis to be completed.

6.5.3 Modification of gauge length values using UV glued sensors

From the previous section it has been shown that the sensors are adversely affected by the T/C fatigue loading regimes performed. One of the reasons for this may be the ingress of the matrix resin during the processing of the composite panels, as discussed in section 6.2.2.

In an attempt to prevent the composite resin from entering the capillary during autoclave processing it was decided to block the ends. To achieve this, a resin was chosen that was highly viscous to minimise entry into the capillary and that cured

quickly so that the time for any resin to enter the capillary was minimised. The resin chosen was a UV-curable resin Epotek OG-142 with a relatively high viscosity of 9.25 Pa·s (Promatech Ltd).

Gauge Length Determination

In order to check that the UV resin had not flowed into the capillary and that it had prevented matrix resin entering the capillary all samples were ramp loaded to determine the gauge lengths. These results are shown in Table 6-15.

Sample	Optical determined gauge length (mm)	Experimental determined gauge length (mm)
P2	14.0	11.1
P3	13.8	14.1
P4	14.0	13.6
P5	14.2	13.4
P6	14.2	12.6
P8	14.2	13.1

Table 6-15 Gauge lengths from UV-resin reinforced sensors.

From these results it can be seen that the determined gauge length are more inline with those from optical measurements, with the slight variation likely to be due to experimental errors, or a slight ingress of resin.

To check the sensors would survive the initial loading, the samples were subjected to the compressive stress appropriate to the fatigue regime required.

6.5.3.1 Quasi-static testing of embedded resin reinforced EFPI sensors

The initial testing was carried out to a stress of -456 MPa, which is the compressive stress reached during the use of the fatigue stress ratio of R=-3. The sensors did not survive to this stress level and in Table 6-16 the stress levels of the composites at which the EFPI sensors failed are presented.

Sample	Failure stress of sensors (MPa)	Failure strain of sensors
P8	-290.8	-0.459%
P4	-365.3	-0.608%
P5	-354.8	-0.560%

Table 6-16 Results of static compressive testing on embedded resin reinforced EFPI sensors.

As these samples failed at a stress level below that required for testing at $R=-3$, the fatigue testing was carried out at a stress ratio of -1 with a stress level of 20% UCS (156.4 MPa).

However, these samples were still subjected to the fatigue loading, as it allowed a comparison of the effect of the embedded sensors, with and without reinforcement on the resistance of the CFRP to the fatigue. The results shown in Table 6-17 are the number of cycles to failure for the CFRP samples at $R=-3$.

	Reference Samples	Standard EFPI samples	Resin reinforced EFPI samples
Cycles to failure	42,715	15,477	9,029
	304,295	138,715	47,356
	34,347	14,899	39,497

Table 6-17 Comparison of fatigue results at $R=-3$ for CFRP samples.

Table 6-17 shows that overall there does appear to be some degradation of fatigue performance of the composite due to the inclusion of the EFPI sensors at this fatigue level. The extra resin reinforcement could be increasing this degradation. But the scatter is such that further work would need to be done to corroborate this.

6.5.3.2 *Fatigue Testing of embedded resin reinforced sensors at $R=-1$.*

For this fatigue level the maximum stress was 156 MPa (20% UCS) in tension and compression. At this level, two of the resin reinforced EFPI samples were investigated for their response to fatigue. The results obtained in this section can be compared to those acquired in section 6.5.1.4, which dealt with an unreinforced embedded sensor (sample M5) being subjected to fatigue loading at $R=-1$ with a stress level of 20% UCS.

In Table 6-18 the cavity lengths of the reinforced sensors in sample P6 and P2, and the unreinforced sensor in M5 at zero loads are presented. It can be noticed that while the unreinforced sensor maintains the cavity length to within a couple of microns during the entire fatigue testing, the reinforced sensors (P6 and P2) shows significant changes as the fatigue cycling progresses.

Total number of cycles	Cavity length (μm) of sample P6 <i>reinforced</i>	Cavity length (μm) of sample P2 <i>reinforced</i>	Cavity length (μm) of sample M5 <i>unreinforced</i>
0	100.6	195.7	197.4
10,000	80.0	130.3	196.7
200,000	92.3	110.8	197.5
500,000	44.0	sensor failure	198.4
800,000	81.4	-	197.5
1,000,000	32.5	-	197.4

Table 6-18 Results of reinforced sensor sample P6 compared to unreinforced sensor sample M5.

The reduction in cavity length during the fatigue testing of the reinforced sensors must be caused by some form of slippage of the optical fibres within the capillary; the endfaces are getting closer together. In the unreinforced sensors the trend was for the cavity length to remain reasonably stationary while the amount of change increased for a specific strain level. That increase was probably due to the thin resin film inside the capillary degrading under fatigue, thereby increasing the gauge length. However, in the case of the reinforced sensors it seems most likely that the UV epoxy resin is allowing the optical fibre to move in relation to the capillary. This could be due to the resin being not fully cured or having an insufficient shear strength. This work gives an indication of what properties of a reinforcing resin for the sensors will be important. The resin must minimise ingress into the capillary, cure quickly, be compatible with the matrix resin and have sufficient strength to hold the fibre to the capillary.

6.5.4 Heat generation during fatigue

Heat generation within composite samples subjected to fatigue loading can cause premature failure of the composite as discussed in section 2.2.3.1. It is for this reason that the fatigue testing of composites is carried out at relatively low frequencies.

To check that the frequency chosen for this fatigue regime did not cause significant heating effect, the temperature of two samples was monitored using a thermal imaging camera during a fatigue loading of $R=-1$ at 40% UCS running at 4.5 Hz. One of the samples had an embedded EFPI included.

6.5.4.1 Reference CRFP sample

Image 1, $t=0$ min, (start)

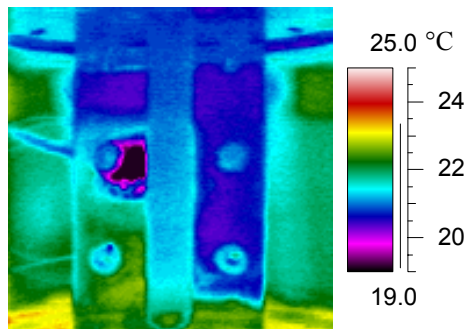


Image 3, $t= 145$ mins (40,000 cycles)

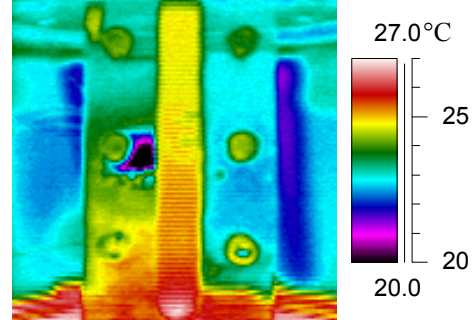
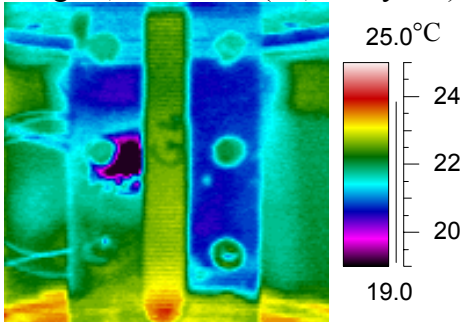


Image 2, $t=25$ mins (10,000 cycles)



At end, $t=340$ mins (100,000 cycles)

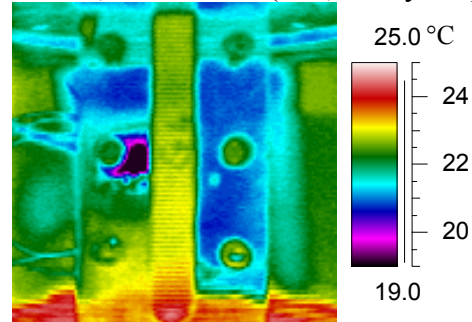


Image 1 shows the thermal response of the sample prior to testing; the hydraulic oil in the Instron frame causes the slight elevation in temperature at the bottom of the picture. The oil typically runs at a temperature of 50°C and some of this heat is radiated to the sample location. The other images show an increase in the temperature of the sample as the number of cycles increases.

This temperature rise is concentrated at the bottom of the sample. This lower end of the sample is the moving end in relation to the anti-buckling guide. It is therefore likely

that this temperature increase is related to frictional heating between the sample and guide. The total surface temperature increase over 100,000 cycles is approximately 6°C and this should not cause any degradation of the properties of the composite matrix. However, this method is unable to assess the internal temperature of the sample, which could be increased due to the fatigue and possibly cause premature failure. During all the fatigue testing the loading rate was kept constant at $250 \text{ kN}\cdot\text{s}^{-1}$, and according to Curtis (1989) the use of a constant loading rate reduces any effect of hysteresis heating on the fatigue response of the fibre reinforced composites. Also all the testing has been at frequencies below 10 Hz, which is the level suggested by published works to minimise any heating of the samples (Curtis, 1989, Rotem, 1993 and Barron *et al.*, 2001).

6.5.4.2 Sample with embedded sensor

Image 1, t=0 min (start)

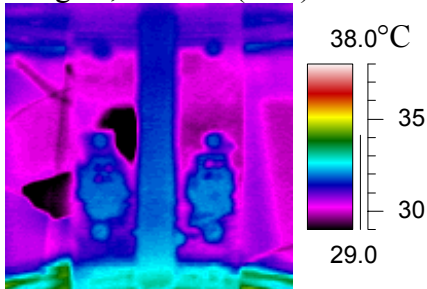


Image 3, t=150 mins (40,000 cycles)

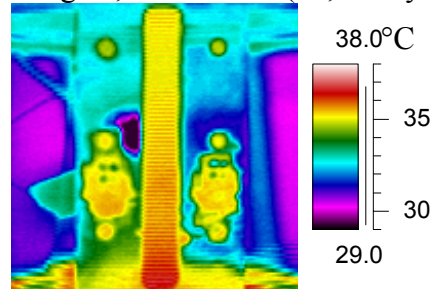
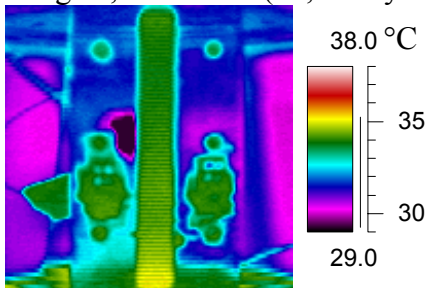
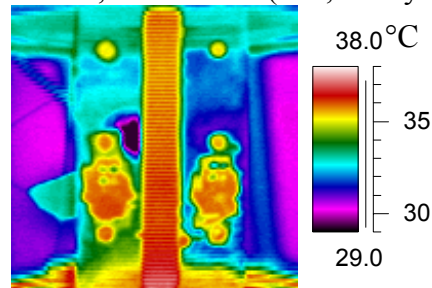


Image 2, t=30 mins (10,000 cycles)



At end, t=300 mins (100,000 cycles)



These images are from the sample with the embedded EFPI sensors. This testing was carried out to ensure that the sensors did not act as a heat generation point. The scale on

these images is different to those shown for the reference sample as the ambient conditions had changed. The overall increase in temperature is approximately the same after 100,000 cycles. It is worth noting that the sensors could still be causing extra heat generation at a resolution below which the equipment used was capable of detecting. From this work it appears that the frequency level of 4.5 Hz chosen for this testing did not cause significant heat build up, at least none that is apparent from this thermal imagery method.

6.6 Summary

The CFRP samples used in this work were of a suitable quality as determined by C-scan and microscopy methods.

From the quasi-static tensile and compressive results the properties of the CFRP matched the manufacturer's data. When EFPI sensors were embedded into the samples, a slight reduction was noticed in the average failure strength in tension and compression, 80 MPa and 130 MPa respectively. This could have been within experimental or batch variations as there was some scatter within the results. Under tensile loadings the EFPI sensors failed at an average strain of 0.005. When examined under compressive conditions the sensors survived until composite failure, which caused fracture of the sensors.

The choice of loading rate appeared to have no significant effect on the CFRP between the rates of $0.025 \text{ kN}\cdot\text{s}^{-1}$ and $250 \text{ kN}\cdot\text{s}^{-1}$ for either the reference CFRP samples or those with embedded EFPI sensors. The sensors themselves, however, did appear to have a hysteresis associated with the loading rates of $0.025 \text{ kN}\cdot\text{s}^{-1}$, $0.25 \text{ kN}\cdot\text{s}^{-1}$ and $2.5 \text{ kN}\cdot\text{s}^{-1}$. It is unclear at this stage whether this effect is inherent to the EFPI sensors or a function of the data acquisition system.

Under dynamic conditions it was again the tensile phase of the testing that causes the sensor most problems. EFPI sensors can survive T/C fatigue cycling but the strains to which the samples will be exposed to must be restricted to a relatively small range,

particularly for the tension phase. The limit for tension loading is approximately 0.003 strain, which relates to a stress of 156 MPa (20% UCS) in the CFRP samples. In compression the limit is around 0.005, which relates to a stress of 313 MPa or 40% UCS.

Two main types of EFPI sensors were examined, both arising from slightly different manufacturing methods. The first set of sensors allowed the matrix resin to enter the capillary during processing of the composite and formed the gauge length. The other set used an UV-curing resin to seal the capillary ends allowing the fusion points to determine the gauge length. During fatigue testing two different behaviours were noticed. For the matrix resin sensors, the cavity length remained consistent for the duration of the testing, but the change in the cavity length in response to applied strain increased. For the UV epoxy sensors the most noticeable effect was that the cavity length reduced dramatically during the fatigue regime, in one case the cavity length reduced by 70 μm . There are likely to be two different failure modes, the first for matrix resin sensors, it that the matrix resin is present within the sensor as a thin layer between the capillary and optical fibre. During fatigue cycling this thin layer degrades thereby increasing the gauge length of the sensor. For the UV epoxy sensors it was felt that the epoxy was in some way allowing the optical fibres to move within the capillary, thereby allowing the distance between the endfaces to alter non-linearly with the applied strain.

At this stage of the work it is unclear what effect the sensor/composite interface is having on the responses recorded from the sensors. Before that can be successfully investigated the sensors themselves must be reliable. This will only be achieved through an improved manufacturing method. Ideally this method should ensure that the join between the fibre and capillary is no longer a point but is completely circumferential. This would also remove the issue of resin flow into the capillary altering the gauge length, as the resin would not be able to flow past the fusion region.

7 Conclusions and Recommendations for Further Work

This chapter summarises the finding from the work carried out in this research project. It also includes some suggestions for further work in each of the areas covered during this project.

7.1 EFPI Evaluation

The project began with an assessment of the EFPI sensors that were manufactured in-house. An initial study into the available methods to interrogate the EFPI sensors was carried out, after which it was decided to use an FFT analysis method for the majority of the work. This was because the FFT analysis method chosen was found to be the more reliable out of those methods available, as it was based on the frequency of the interference pattern and not directly on the wavelength of the spectra.

The EFPI sensors used in this project were constructed through the use of a fusion weld to join the optical fibres to the capillary. With this technique, it was observed that care was required during the sensor manufacture to ensure that the settings of the electric arc allowed a suitable weld to be generated. This needed to avoid distortion of the sensors and to ensure the fibres fused to the capillary. Also, as part of the manufacturing process the gauge length of the sensors had to be determined. After performing comparison testing it was found that visual measurement through optical microscopy was suitable for characterising the gauge lengths.

The EFPI sensors as manufactured were very fragile with fracture loads in the region of 0.5 N. Therefore, an investigation into the possibility of reinforcing the sensors to improve their handleability was carried out. The presence of a reinforcing resin did improve the tensile strength of the sensors by approximately 10 times. However, due to the difficulties in applying similar quantities of resin to all the sensors and the possibility of inducing voids into the composite samples due to the relative size of the resin reinforcement, the project proceeded to use unreinforced sensors.

7.2 *Interfacial Aspects*

As part of this work, it was intended to assess the interface between the EFPI sensors and the fibre reinforced composite that the sensors were embedded within. From an examination of the literature, it was felt that surface energy and interfacial shear strength measurements had proved informative in the examination of the glass fibre/resin interfaces within composites, and that these techniques could be useful in the case of optical fibre sensors.

7.2.1 Surface energy

For the surface energy measurements, the Wilhelmy plate technique was chosen to obtain the contact angle measurements between the silica and test liquids. This data are required for the Owens-Wendt approach to the determination of the surface energy of a solid. The initial stage of this work focussed on establishing a reliable sample preparation method for the contact angle measurements. After examining several possible cleaning routines, it was decided to use a quartz/silica cleaning solution, Hellmanex™, as this produced the most consistent results. A comparative contact angle study was carried out between the capillary and stripped optical fibres. From those results and due to sample practicalities for the IFSS samples, it was decided to use the optical fibres in the remainder of the interfacial work. At the end of the section of work, the silica surface had been tested against the chosen liquids and the surface energy had been determined which correlated to published data for glass and silica surface.

The next stage was the application of silane treatments to the silica optical fibre surface to promote the formation of a good interface between the silica and epoxy matrix of the composite. Generally, the addition of a silane treatment increased the surface energy and work of adhesion of the system. The silane treatment of the optical fibre was found to decrease the polar components of the surface energy, probably due to the replacement of polar water molecules with non-polar molecules from the silane on the silica surface. In the case of the GPMS treatment, the reduction was from $14.4 \text{ mN}\cdot\text{m}^{-1}$ to $2.3 \text{ mN}\cdot\text{m}^{-1}$.

Also, there is likely to be an optimal level of silane treatment as the 5% levels of both the APMS and GPMS show a decrease on work of adhesion compared to the 1% levels.

7.2.2 Interfacial shear strengths

A new variation on the single fibre pull-out test was developed during the course of this project. The technique allowed the interface between an optical fibre and fibre reinforced composite to be investigated.

From the samples manufactured, it was observed that the reinforcing fibres do not form an even pattern around the optical fibres, and can, in fact, have large resin only areas. This type of variation could lead to significant difference in the results from these samples as the stress patterns around the pullout fibre could be vastly different in the case of resin rich region to a region with a high fibre fraction. This also shows a further disadvantage of the other methods of IFSS determination, which rely on resin only results. However, this is likely to represent the reinforcing fibre pattern when an optical fibre sensor is embedded with a fibre reinforced composite. The method for measuring the embedment depth for these samples was improved during the project, leading to a comparison of before and after images to measure the embedment depths.

Two thicknesses of samples were initially investigated, 2- and 16-ply laminates. From the obtained IFSS results there appeared to be no significant influence of the sample thickness on the results. Therefore, the remainder of the work was carried out on 2-ply samples due to an easier sample manufacture process.

Overall the IFSS values obtained in this work were within the ranges reported in the literature for E-glass/epoxy testing, which is the closest comparison available for optical fibre/epoxy composite samples. However, much of the published data is quoted as a single value and from the results obtained in this work the IFSS is very dependant on the embedment depth and therefore, particularly in this case, reporting a single value is not suitable.

A comparison was made on samples made from GFRP and CFRP. From the initial modelling work it was suggested that the choice of reinforcing fibres in the samples had an effect on the IFSS values, even though both types of composites had the same matrix resin. However, there were insufficient differences between the experimental results of the GFRP and CFRP samples to back up this model. However, it is possible that the choice of reinforcing fibre could have an effect on the measured IFSS, as the type of reinforcing fibre significantly changes the stiffness of the composite and therefore, the stress pattern that would form during a pull-out test. The IFSS study then moved on to the effect of silane treatment on the optical fibre. Two silanes were used, an amine and an epoxy terminated as per the surface energy investigations. Again it was difficult to differentiate the IFSS results of the different silane treatments.

This technique showed the single fibre pull-out can be achieved by using an optical fibre and composite prepreg to manufacture the sample. The benefits of this method included no meniscus formation and better representation in the case of an optical fibre sensor embedded in fibre reinforced composite sample. To enable further investigation of the choice of composite and the affect of a silane treatment, it was felt that an improvement to the control of the embedment depth would be beneficial. If the embedment depth could be reliably set to a specific value, it would make the results for different samples easier to compare.

One method of control was attempted which involved the use of notched optical fibres. As the notch lowers the failure load of the optical fibres to below the load required for pullout, the concept was to embed a notched optical fibre throughout the sample. Under loading the fibre would fracture at the notch leaving the required length to be involved in the pull-out. The obstacle found for this method was the positioning of the optical fibre so that the notch was at a specific position. With further investigation into the method of positioning the optical fibre it should be possible to use this method.

7.3 Durability Aspects

This section deals with the testing carried out on embedded EFPI sensors, starting with static responses, followed by the dynamic responses due to the fatigue regimes implemented.

7.3.1 Quasi-static results

Under tensile loading the embedded EFPI sensors failed at an average strain of 0.0050, whereas under compression the sensors only failed when the composite samples failed, at an average strain level of -0.0105. This is similar to the EFPI responses reported in the literature. The composite samples did not appear to suffer any degradation due to the inclusion of an EFPI sensor under tensile testing. Under compressive testing a slight loss in ultimate strength was noticed for the samples with embedded samples. The effect of the embedded EFPI sensors was expected to be minimal as the sensors were aligned to the test direction and placed between two plies of the composite with parallel reinforcing fibres.

7.3.2 Strain rate results

The CFRP samples showed no significant effect of the changing loading rates from $0.025 \text{ kN}\cdot\text{s}^{-1}$ to $250 \text{ kN}\cdot\text{s}^{-1}$. However, the EFPI sensors showed a tendency for increased hysteresis during loading as the loading rate increases from $0.025 \text{ kN}\cdot\text{s}^{-1}$ to $2.5 \text{ kN}\cdot\text{s}^{-1}$, it was not possible to test the sensors at the higher rates of $25 \text{ kN}\cdot\text{s}^{-1}$ and $250 \text{ kN}\cdot\text{s}^{-1}$. It was unclear though, whether this change was due to a hardware irregularity or an actual sensors response.

7.3.3 Dynamic results

The embedded sensors were subjected to a range of T/C fatigue loading conditions during this project. Overall, it was found that tensile strain levels needed to be kept below 0.3% to ensure the sensors could survive to a million cycles, above this level the sensors response was typically lost within a few thousand cycles. For the compressive

region of the cycling the maximum strain to allow survival to a million cycles was higher than that in tension at 0.5% strain. This difference in behaviour is likely to be related to the static failures levels of the sensors, being 0.4% in tension and 1% in compression.

For the samples tested the sensor could survive the loading, but did not necessarily behave in a reliable manner during the whole cycling of the sample. The responses of the sensors tended to degrade as the number of cycles increased. For most of the samples examined this was felt to be caused by the degradation of the fusion points leading to a varying gauge length during testing, thereby causing the sensor response to change for a specific strain level. Therefore, improvements are required to the method of formation for the fusion point before a detailed investigation into the effect of the interface on the sensor response can be carried out.

7.4 Recommend Further Work

This section describes some of the possibilities for extending the work investigated in this project, based on the obtained results and observations.

7.4.1 EFPI sensors

The manufacture of the sensors needs to be improved in the area of the capillary join with the optical fibres. Ideally, the join needs to be completely circumferential, as this would improve the strength of the sensors, would prevent any resin flow into the capillary and eliminate the need for an extra reinforcing resin. The current technique of using an electric arc could be modified to achieve this through rotating the sensor and performing the join multiple times, or alternatively by increasing the number of electrodes available.

7.4.2 Interface

7.4.2.1 Characterisation of fibres

To increase confidence on the surface energy results further information is required for the Owens-Wendt calculations. To obtain this data would require the silica surface to be tested against more liquids. However, the choice is fairly limited due to the nature of the silica surface, which means most standard test liquids completely wet out the silica and do not form measurable contact angles. For the silane treatments, as well as more liquids being used in the testing, the types and levels of silanes used should be further investigated. The aim being to achieve an optimum silane treatment for the case of embedded EFPI sensors.

7.4.2.2 Interfacial Shear Strengths

The method developed in this work allows the use of composites in the manufacture of the samples. This leads to the samples being more representative of the actual embedded sensors. As this method was developed during this project there is still room for improvement with the main areas being the control and measurement of the embedment depth and the understanding of the reinforcing fibres interaction with the optical fibre during testing.

By improving the control and measurement of the embedment depth, sets of samples could have the same depth leading to simpler comparisons between different factors, such as composite choice or silane treatments. The concept of using the notched fibres as described in Section 5.2.7 appears to be a promising avenue. Alternatives could include other placement methods under the microscope or some form of jig which could improve the repeatability of the embedment depths.

To investigate the interaction between the reinforcing and optical fibres in the sample would be two-fold. The first stage would be to carry out a visual inspection of samples under the microscopy to allow an assessment of the different patterns that form around an embedded optical fibre. As part of this investigation the effect of processing

conditions and lay-up sequences on the patterns formed could be assessed. The second part would involve modelling the effects of the various patterns on the stress distribution within a sample.

7.4.3 Durability

To enable a more complete picture of the durability of the EFPI sensors they need to have an improved fusion point and defined gauge length. Once that has been achieved the fatigue regimes attempted in this project should be repeated as it is likely, in the author's opinion, that the sensors should be able survive and provide useful data at these levels. At this stage the assessment into the durability of the interface under fatigue conditions can be investigated, followed by the investigation of the effects of a silane treatment on the response of the embedded sensors.

8 References

- Ageorges, C, Friedrich, K, Schüller, T and Lauke, B. (1999) "Single fibre Broutman test: fibre-matrix interface transverse debonding", **Composites Part A**, Vol. 30, p.1423-1434.
- Ansari, F and Libo, Y. (1998) "Mechanics of bond and interface shear transfer in optical fiber sensors", **Journal of Engineering Mechanics**, Vol. 124, No. 4, p.385-394.
- Askeland, DR (1994), **The Science and Engineering of Materials**, 3rd edition, PWS Publishing Company.
- Badcock, RA and Fernando, GF. (1995) "An intensity based optical fibre sensor for fatigue damage detection in advanced fibre-reinforced composite materials" **Smart Materials and Structures** Vol. 4, p. 223-230.
- Barron, V, Buggy, M and McKenna, NH. (2001) "Frequency effects on the fatigue behaviour on carbon fibre reinforced polymer laminates", **Journal of Materials Science**, Vol. 36, p.1755-1761.
- Barton, EN, Ogin, SL, Thorne, AM and Reed, GT. (2002) "Optimisation of the coating of a fibre optical sensor embedded in a cross-ply GFRP laminate", **Composites: Part A**, Vol. 33, p.27-34.
- Benchechou, B and Ferguson, NS. (1998) "The effect of embedded optical fibres on the fatigue behaviour of composite plates", **Composite Structures**, Vol. 41, p.113-120.
- Benzarti, K, Cangemi, L and Dal Maso, F. (2001) "Transverse properties of unidirectional glass/epoxy composites influence of fibre surface treatments", **Composites Part A**, Vol. 32, p.197-206.
- Berg, A and Johansen, M. (1995), "Arc fusion splices with improved strength (4.8 GPa) approaching the strength of the fibre", **Electronics Letters**, Vol. 31, No. 4, p.308-309.
- Berg, J and Jones, FR. (1998) "The role of sizing resins, coupling agents and their blends on the formation of the interphase in glass fibre composites", **Composites: Part A**, Vol. 29A, p.1261-1272.
- Bhatia, V, Murphy, KA, Claus, RO, Jones, ME, Grace, JL, Tran, TA and Greene, JA. (1996) "Optical fibre based absolute extrinsic Fabry-Perot interferometric sensing system" **Measurements Science and Technology**, Vol. 7, p.58-61.
- Bledzki, AK, Lieser, J, Wacker, G and Frenzel H. (1997), "Characterisation of the surface of treated glass fibres with different methods of investigation", **Composite Interfaces**, Vol. 5, No. 1, p.41-53.
- Carman, GP, Murphy, K, Schmidt, CA and Elmore, J. (1993) "Extrinsic Fabry-Perot interferometric sensors survivability during mechanical fatigue loading", **SEM 50th Anniversary Spring Conference on Experimental Mechanics**, Dearborn, MI, USA 7-9 June, p.1079-1087
- Carman, GP and Sendekyj GP. (1995) "Review of the mechanics of embedded optical sensors", **Journal of Composites Technology and Research**, Vol. 17, No. 3, p.183-193.
- Case, SW and Carman, GP. (1994) "Compression strength of composites containing embedded sensors or actuators" **Journal of Intelligent Materials Systems and Structures**, Vol.5, p. 4-11.

- Claus, RO, Bhatia, V, Gunther, MF, Murphy, KA, Tran, TA and Greene, JA. (1994) "Absolute strain measurements in polymer matrix composites" **39th International SAMPE Symposium**.
- Comyn, J (1997) **Adhesion Science**, Royal Society of Chemistry.
- Curtis, PT. (1987) "A review of the fatigue of composite materials", **Royal Aircraft Establishment**, Technical Report 87031.
- Curtis, PT (1988) "CRAG Test Methods for the Measurement of the Engineering Properties of Fibre Reinforced Plastics", **Defence Evaluation and Research Agency**, Technical Report 88012.
- Curtis, PT. (1989) "The fatigue behaviour of fibrous composite materials" **Journal of Strain Analysis**, Vol. 24, No.4, p.235-244.
- Daniel, HS, Moore, DR and Tekippe, VJ. (1994) "A glass solder for packaging fiber optic components", **12th Annual Conference on European Fibre Optics Communications and Networks**, June 22-24, Heidelberg, Germany.
- Degamber, B and Fernando, GF. (2003) "Fiber optic sensors for noncontact process monitoring in a microwave environment", **Journal of Applied Polymer Science**, Vol. 89, p.3868-3873.
- DiFrancia, C, Ward, TC and Claus, RO. (1996) "The single fibre pullout test. 1:Review and interpretation", **Composites Part A**, Vol. 27A, p.597-612.
- Doyle, C and Fernando, GF (1997), "A novel fibre-optic vibration sensor", **Journal of Materials Science Letters**, Vol. 16, p.1101-1105.
- Eske, LD and Galipeau, DW. (1999) "Characterization of SiO₂ surface treatments using AFM, contact angles and a novel dewpoint technique", **Colloids and Surfaces A: Physicochemical and Engineering Aspects**, Vol. 154, p.33-51.
- Etches, JA and Fernando, GF. (2002) "A method to measure the interfacial shear stress for optical fibres embedded in fibre reinforced composites", **Advanced Composites Letters**, Vol. 11, No. 5, p.199-206.
- Fernando, GF, Liu, T, Crosby, P, Doyle, C, Martin, A, Brooks, D, Ralph, B and Badcock, R. (1997) "A multi-purpose optical fibre sensor design for fibre reinforced composite materials" **Measurements Science and Technology**, Vol. 8, p.1065-1079.
- Fox, N, Shead, P and Steadman, S. (1992) "The influence of fiber optic sensors on the performance of advanced composite components", **1st European Conference on Smart Structures and Materials**, Glasgow, p.267-275.
- Fu, S-Y, Yue, C-Y, Hu, X and Mai, Y-W (2000) "Analyses of the micromechanics of stress transfer in single- and multi-fiber pull-out tests", **Composites Science and Technology**, Vol. 60, p.569-579.
- Gamstedt, EK and Sjögren, BA. "Micromechanisms in tension-compression fatigue of composite laminates containing transverse plies", **Composites Science and Technology**, Vol. 59, p.167-178.
- Gathercole, N, Reiter, H, Adam, T and Harris, B. "Life prediction for fatigue of T800/5245 carbon-fibre composites: I. Constant amplitude loading", **International Journal of Fatigue**, Vol. 16, No. 8, p.523-532.
- Glaeseman, GS, Clark, DA, Hanson, TA and Wissuchek, DJ (1998) "High speed strength of optical fiber", **Reliability of Photonics Materials and Structures**, Materials Research Symposium Proceedings, Vol. 531, p.249-260.

- Grattan, KTV and Meggitt, BT (1999) **Optical Fibre Sensor Technology, Vol.3 Applications and Systems**, Kluwer Academic Publishers.
- Harding, PH and Berg, JC. (1997) “The characterization of interfacial strength using single particle composites”, **Journal of Adhesion Science and Technology**, Vol. 11, No. 8, p.1063-1076.
- Hartwig, G, Hübner, R, Knaak, S and Pannkoke, C. “Fatigue behaviour of composites”, **Cryogenic**, Vol. 38, p.75-78.
- Hecht, E. (1998) **Optics**, 3rd edition, Addison Wesley Longman Inc.
- Herrera-Franco, PF and Drzal, LT (1992) “Comparison of methods for the measurement of fibre/matrix adhesion in composites”, **Composites**, Vol. 23, No. 1, p.2-27.
- Hsiao, HM and Daniel, IM. (1998) “Strain rate behaviour of composite materials”, **Composites: Part B**, Vol. 29B, p.521-533.
- Hull, D and Clyne, TW. (1996) **An Introduction to Composite Materials**, 2nd Edition, Cambridge University Press.
- Ishida, H and Koenig, JL (1979) “An investigation of the coupling agent/matrix interface of fiberglass reinforced plastics by Fourier transform infrared spectroscopy”, **Journal of Polymer Science**, Vol. 17, p.615-626.
- ISO/PRF 13003 Fibre reinforced plastics-Determination of fatigue properties under cyclic loading conditions (Draft – Enquiry stage)
- Jaycock, MJ and Parfitt, GF. (1981) **Chemistry of Interfaces**, Ellis Horwood Limited.
- Kalamkarov, AL, Fitzgerald, SB, Macdonald, DO and Georgiades, AV. (1998) “Smart pultruded composite reinforcements incorporating fiber-optic sensors”, **SPIE 3400** p.94-105.
- Kalamkarov, AL, MacDonald, DO, Fitzgerald, SB and Georgiades, AV. (2000) “Reliability assessment of pultruded FRP reinforcements with embedded fiber optic sensors” **Composite Structures**, Vol. 50, p.69-78.
- Kalinka, G, Leistner, A and Hampe, A. (1997) “Characterisation of the fibre/matrix interface in reinforced polymers by the push-in technique”, **Composites Science and Technology**, Vol. 57, p.845-851.
- Kang, H-K, Ryu, C-Y, Hong, C-S and Kim, C-G (2001), “Simultaneous measurement of strain and temperature of structures using fiber optic sensors”, **Journal of Intelligent Material Systems and Structures**, Vol. 12, p.277-281.
- Kao, TW and Taylor, HF (1996) “High-sensitivity fiber-optic Fabry-Perot pressure sensor”, **Optic Letters**, Vol. 21, No. 8, p.615-617.
- Khoe, GD and Lydtin, H. (1986), “European optical fibers and passive components: status and trends”, **IEEE Journal on Selected Areas in Communications**, Vol. 4, No. 4, p.457-471.
- Kim, J-K, Zhou, L, Gryan, SJ and Mai, Y-W (1994), “Effects of fibre volume fraction on the stress transfer in fibre pull-out tests”, **Composites**, Vol. 25, No. 7, p.470-475.
- Kinloch, AJ. (1987) **Adhesion and Adhesives**, Chapman and Hall.
- Lafarie-Frenot, MC. (2002), “Influence of strain rate and temperature on transverse ply cracking of CFRP laminates”, **10th European Conference on Composite Materials**, June 3-7, Brugge, Belgium.

- Lamela, MJ, Fernández-Canteli, A, Reiter, H and Harris, B. “Comparative statistical analysis of the fatigue composites under different modes of loading”, **Journal of Materials Science**, Vol. 32, p.6495-6503.
- Lee, B (2003) “Review of the present status of optical fiber sensors” **Optical Fiber Technology**, Vol. 9, p.57-79.
- Lee, CE and Taylor, HF. (1987) “Interferometric optical fibre sensors using internal mirrors”, **Electronics Letters**, Vol. 24, No. 4, p. 193-194.
- Lee, DC, Lee, JJ and Yun, SJ. (1995) “The mechanical characteristics of smart composite structures with embedded optical fiber sensors” **Composite Structures**, Vol. 32, p.39-50.
- Lee, DC, Lee, J, Kwon, IB and Seo, DC. (2001) “Monitoring of fatigue damage of composite structures by using embedded intensity based optical fiber sensors”, **Smart Materials and Structures**, Vol. 10, p. 285-292.
- Lee, DG, Mitrovic, M, Friedman, A, Carman, GP and Richards, L. (2002) “Characterization of Fiber Optic Sensors for Structural Health Monitoring” **Journal of Composite Materials**, Vol. 36, No. 11, p.1349-1365.
- Lee, W, Lee J, Henderson, C, Taylor HF, James, R, Lee, CE, Swenson, V, Atkins RA and Gemeiner, WG. (1999) “Railroad bridge instrumentation with fiber-optic sensors”, **Applied Optics**, Vol. 38, No. 7, p.1110-1114.
- Legrand, AP. (1998) **The Surface Properties Of Silica**, John Wiley & Sons Ltd.
- Leka, LG and Bayo, E. (1989) “A close look at the embedment of optical fibers into composite structures”, **Journal of Composites Technology and Research**, Vol. 11, No. 3, p.106-112.
- Levin, K and Nilsson, S. (1996) “Examination of reliability of fibre optic sensors embedded in carbon/epoxy composites” **Third ICIM/ECSSM Lyon**, p.222-229.
- Liu, T, Fernando GF, Rao, YJ, Jackson, DA, Zhang L and Bennion I. (1997) “Simultaneous strain and temperature measurements in composites using multiplexed fibre Bragg grating sensor and an extrinsic Fabry-Perot sensor”, **SPIE 3042**, p.203-212.
- Liu, T, Wu, M, Rao, Y, Jackson, DA and Fernando, GF (1998) “A multiplexed optical fibre-based extrinsic Fabry=Perot sensor system for *in-situ* strain monitoring in composites”, **Smart Materials and Structures**, Vol. 7, p.550-556.
- Mäder, E, Grundke, K, Jacobasch, H-J and Wachinger, G (1994) “Surface, interphase and composite properties relations in fibre-reinforced polymers”, **Composites**, Vol. 25, No. 7, p.739-744.
- Mäder, E. (1997) “Study of fibre surface treatments for control of interphase properties in composites”, **Composite Science and Technology**, Vol. 57, p.1077-1088.
- Mai, K, Mäder, E and Mühle, M. (1998) “Interphase characterization in composites with new non-destructive methods”, **Composites Part A**, Vol. 29A, p.1111-1119.
- Melin, LG and Asp, LE. (1999) “Effects of strain rate on transverse tension properties of a carbon/expoy composite: studied by moiré photography”, **Composites: Part A**, Vol. 30, p.305-316.
- Méndez, A, Morse, TF and Reinhart, LJ. (1993) “Experimental results on embedded optical fiber sensors in concrete”, **SPIE Smart Sensing, Processing and Instrumentation**, Vol. 1918, p.420-427.

- Miller, AC and Berg, JC. (2003) "Effect of silane coupling agent adsorbate structure on adhesion performance with a polymeric matrix", **Composites: Part A**, Vol. 34, p.327-332.
- Miller, C (1986) **Optical fiber splices and connectors**, Marcel Dekker Inc
- Mitrovic, M and Carman, GP. (1994) "Monitoring the fatigue behaviour of composite materials with fiber optic sensors", **39th International SAMPE Symposium**.
- Murphy, KA, Gunther, MF, Vengsarkar AM and Claus, RO. (1992) "Fabry-Perot fiber-optic sensors in full-scale fatigue testing on an F-15 aircraft", **Applied Optics**, Vol. 31, No. 4, p.431-433.
- Myers, D, (1991) **Surfaces, Interfaces, and Colloids: Principles and Applications**, VCH Publishers Inc.
- Naviroj, S, Culler, SR, Koenig, JL and Ishida, H. (1984) "Structure and adsorption characteristic of silane coupling agents on silica and E-glass fiber; Dependence on pH", **Journal of Colloid and Interface Science**, Vol. 97, No. 2, p.308-317.
- Neave, HR (1978) **Statistics Table**, Routledge Ltd.
- Nyman, T. (1996) "Composite fatigue design methodology: a simplified approach", **Composite Structures**, Vol. 35, p.183-194.
- Pape, PG. (1996) "Silane coupling agents: Enhancements of physical properties of plastics", **Engineering Plastics**, Vol. 9, No. 2, p.109-115.
- Park, J-M, Kim, D-S and Han, S-B. (2000) "Properties of interfacial adhesion for vibration controllability of composite materials as smart structures", **Composites Science and Technology**, Vol. 60, p.1953-1963.
- Park, SJ, Kim, JS, Rhee, KY and Min, BG. (2001), "Filler-elastomer interactions: surface and mechanical interfacial properties of chemical treated silica/rubber composites", **Materials Physics and Mechanics**, Vol. 4, p.81-84.
- Peters, K, Pattis, P and Botsis, J, (2002) "Novel technique to measure axial strain distribution along the fiber during pullout test", **Journal of Materials Science Letters**, Vol. 21, p.887-891.
- Pisanova, E, Zhandarov, S, Mäder, E, Ahmad, I and Young, RJ. (2001), "Three techniques of interfacial bond strength estimation from direct observation of crack initiation and propagation in polymer-fibre systems", **Composites: Part A**, Vol. 32, p.435-443.
- Pitkethly, MJ, Favre, JP, Gaur, U, Jakubowski, J, Mudrich, SF, Caldwell, DL, Drzal, LT, Narding, M, Wagner, HD, DiLandro, L, Hampe, A, Armistead, JP, Desaegeer, M and Verpoest, I. (1993) "A round-robin programme on interfacial test methods", **Composite Science and Technology**, Vol. 48, p.205-214.
- Plueddemann, EP (1991) **Silane Coupling Agents**, 2nd edition, Plenum Press, New York.
- Quirion, M and Ballivy, G. (2000) "Concrete strain monitoring with Fabry-Pérot fiber-optic sensor" **Journal of Materials in Civil Engineering**, Vol. 12, No. 3, p.254-261.
- Rees, DG (1995) **Essential Statistics**, 3rd Edition, Chapman & Hall.
- Roberts, SSJ and Davidson, R. (1991) "Mechanical properties of composite materials containing embedded fibre optic sensors" **SPIE Fiber Optic Smart Structures and Skins IV**, Vol. 1588, p.326-340.

- Roberts, SSJ and Davidson, R. (1992) "Short term fatigue behaviour of composite materials containing embedded fiber optic sensors and actuators", **1st European Conference on Smart Structures and Materials**, Glasgow, p.255-262.
- Rotem A. (1989) "Stiffness change of a graphite epoxy laminate under reverse fatigue loading", **Journal of Composites Technology and Research**, Vol. 11, No. 2, p.59-64.
- Rotem A. (1993) "Load frequency effect on the fatigue strength of isotropic laminates", **Composites Science and Technology**, Vol. 46, p.129-138.
- Rotem, A and Nelson, HG. (1989) "Failure of a laminated composite under tension-compression fatigue loading", **Composites Science and technology**, Vol. 36, p.45-62.
- Shyprikevich, P, Fogg, BR, Murphy, KA and Claus, RO. (1993) "Performance of Extrinsic Fabry-Perot Fiber Strain Sensors in the Presence of Cyclic Loads", **SPIE Smart Sensing, Processing and Instrumentation**, Vol. 1918, p.388-399.
- Singh, M, Tuck, CJ and Fernando, GF. (1999), "Multiplexed optical fibre Fabry-Perot sensors for strain metrology" **Smart Materials and Structures**, Vol. 8, p.549-553.
- Skontorp, A. (2000) "Structural integrity of quasi-isotropic composite laminates with embedded optical fibers", **Journal of Reinforced Plastics and Composites**, Vol. 19, No. 13, p.1056-1077.
- Soutis, C, Fleck, NA and Smith PA. "Compression fatigue behaviour of notched carbon fibre-epoxy laminates", **International Journal of Fatigue**, Vol. 13, No. 4, p.303-312.
- Srinivasan, AV and McFarland, DM. (2001) **Smart Structures: Analysis and Design**, Cambridge University Press.
- Surgeon, M and Wevers, M. (1999) "Static and dynamic testing of a quasi-isotropic composite with embedded optical fibres", **Composites Part A**, Vol. 30, p.317-324.
- Surgeon, M and Wevers, M. (2001) "The influence of embedded optical fibres on the fatigue damage progress in quasi-isotropic CFRP laminates", **Journal of Composite Materials**, Vol. 35 No. 11, p.931-940.
- Suzuki, N and Ishida, H (1996) "A review on the structure and characterization techniques of silane/matrix interphases", **Macromolecular Symposium**, Vol. 108, p.19-53.
- Tripathi, D and Jones, FR. (1998) "Review: Single fibre fragmentation test for assessing adhesion in fibre reinforced composites", **Journal of Materials Science**, Vol. 33, p.1-16.
- Tsai, K-H and Kim, K-S (1991) "A study of stick slip behavior in interface friction using optical fiber pull out experiment", **Speckle techniques, birefringence methods and applications to solid mechanics**. SPIE Vol. 1554A, p.529-541.
- Urruti, EH and Wahl, JF. (1990) "Coatings affect fiber performance in smart-skin sensing", **Laser Focus World**, January, p. 165-170.
- de Vries, M, Arya, V, Meller, S, Masri, SF and Claus, RO (1997) "Implementation of EFPI-based optical-fiber sensor instrumentation for the NDE of concrete structures", **Cement and Concrete Composites**, Vol. 19, p.69-79.
- Waite, SR, Tatam, RP and Jackson, A. (1988) "Use of optical fibre for damage and strain detection in composite materials", **Composites**, Vol. 19 No. 6, p.435-442.
- Wang, D and Jones FR, (1991) "The interaction of epoxy resins with a silanized E-glass surface", **Interfacial Phenomena in Composite Materials**, Leuven, Belgium, edited by Verpoest and Jones.

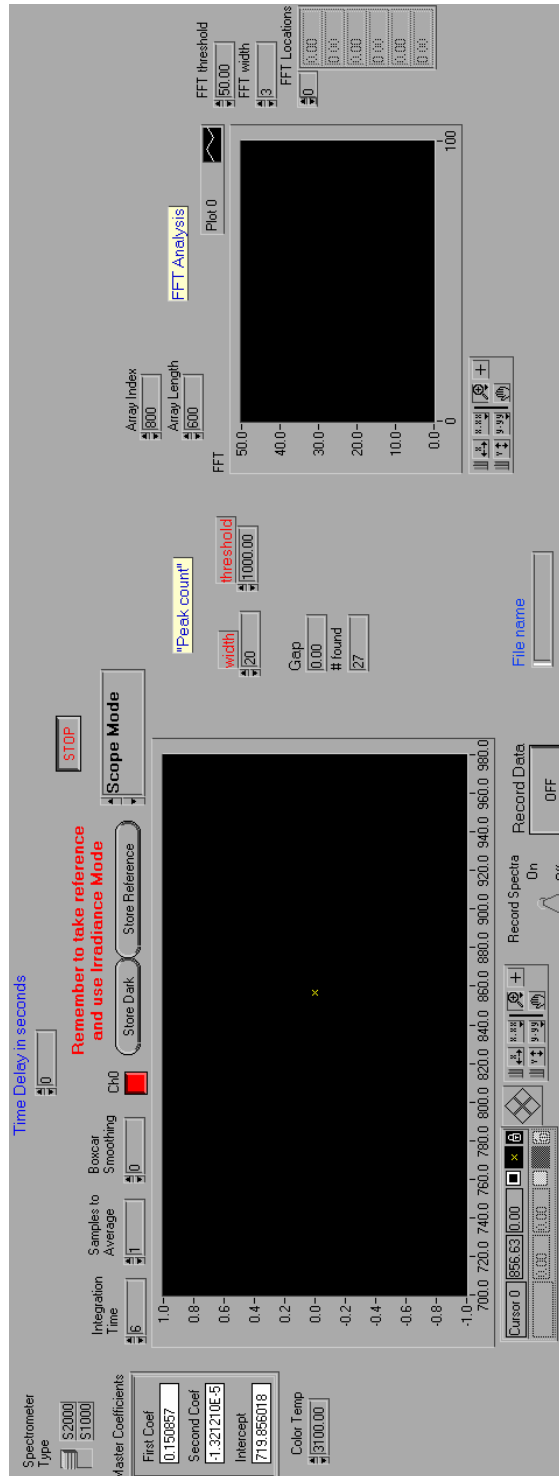
- Weinberg, M. (1987) "Surface energy measurements of graphite and glass filaments", **Toughened Composites**, ASTM STP 937, p.166-178.
- Wolff, V, Perwuelz, A, El Achari, A and Caze, C. (1999) "Determination of surface heterogeneity by contact angle measurement on glass fibres coated with different sizings", **Journal of Materials Science**, Vol. 34, p.3821-3829.
- Wu, HF, Gu, W, Lu, G-Q and Kampe, SL. (1997a) "Non-destructive characterization of fibre-matrix adhesion in composites by vibration damping", **Journal of Materials Science**, Vol. 32, p.1795-1798.
- Wu, HF, Dwight, DW and Huff, NT. (1997b) "Effects of silane coupling agents on the interphase and performance of glass-fiber-reinforced polymer composites", **Composite Science and Technology**, Vol. 57, p.975-983.
- Yuan, L and Zhou, L. (1998) "Sensitivity coefficient evaluation of an embedded fiber-optic strain sensor", **Sensors and Actuators A**, Vol. 69, p.5-11.
- Yue, CY and Looi, HC (2001) "Factors which influence the reliability of the assessment of interfacial bonding in fibrous composites using the pull-out test" **International Journal of Adhesion & Adhesives**, Vol. 21, p.309-323.
- Zhou, G and Sim. LM. (2002) "Damage detection and assessment in fibre-reinforced composite structures with embedded fibre optic sensors – review" **Smart Materials and Structures**, Vol. 11, p. 925-939.
- Zhou, XF, Wagner, HD and Nutt, SR. (2001), "Interfacial properties of polymer composites measured by push-out and fragmentation tests", **Composites: Part A**, Vol. 32, p.1543-1551.
- Zolfaghar, K and Folkes, MJ. (1999) "The effect of surface coatings on optical fibers on the interfacial shear strength in epoxy resins", **Journal of Materials Science Letters**, Vol. 18 (1999) p.2014-2020.

Appendix 1 – Labview data acquisition programs

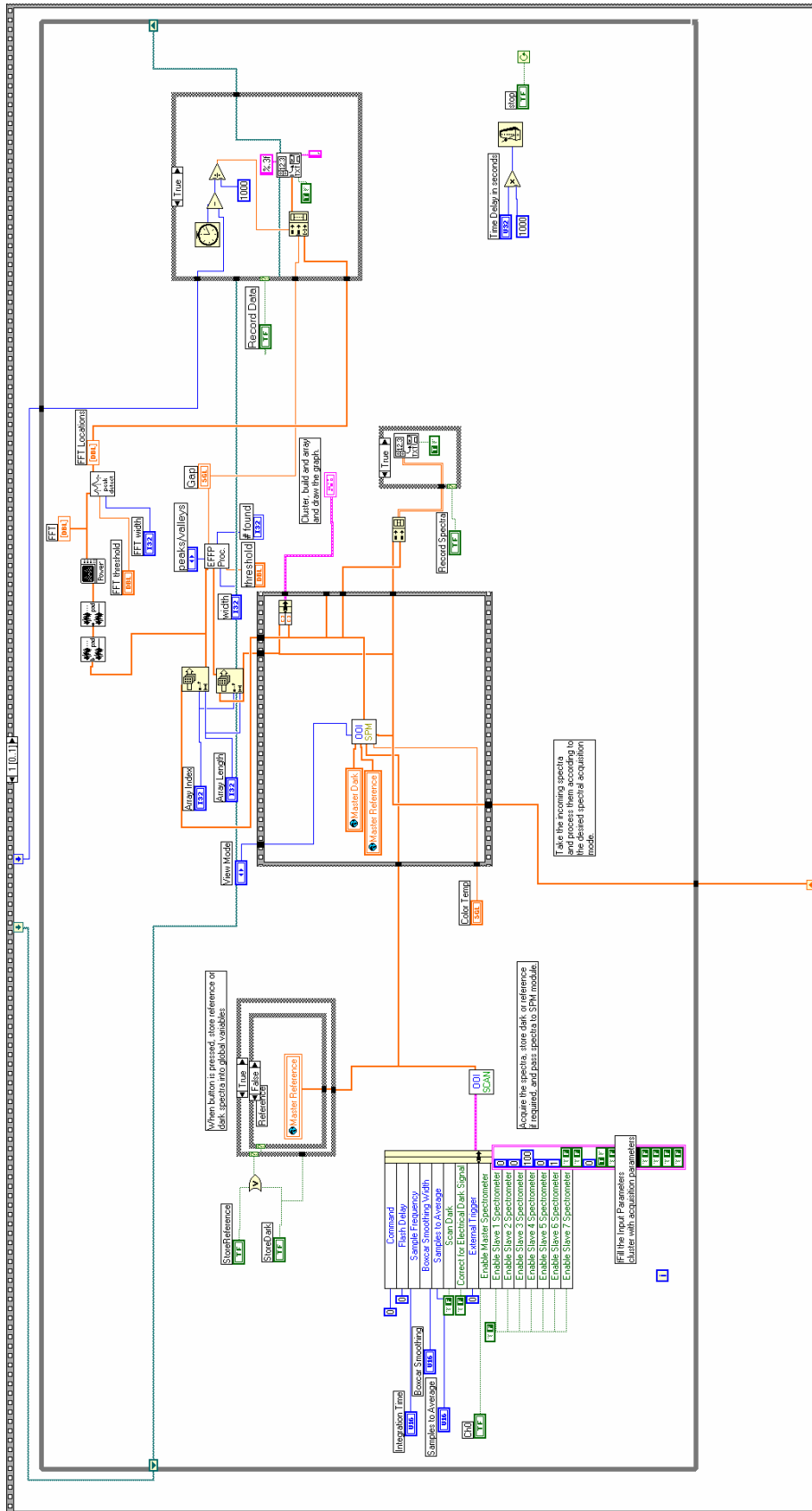
DAQ Method 1 – Interrogation of EFPI sensors using a CCD spectrometer

With base blocks from Ocean Optics and help from Dr R. Badcock.

Front Panel (DAQ 1)



Main section of Block Diagram (DAQ 1)



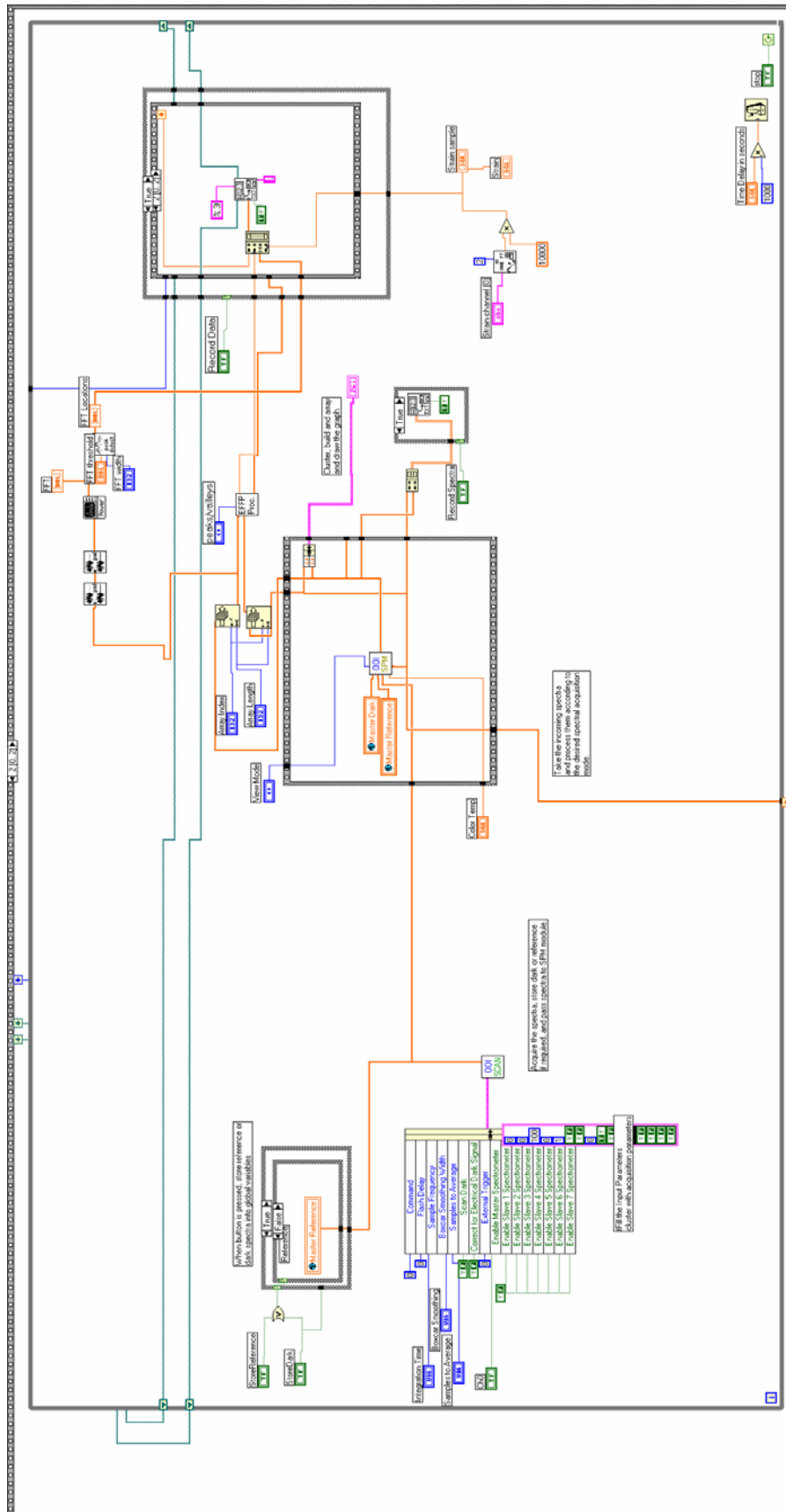
DAQ Method 2 – Interrogation of EFPI sensors and Strain gauge response

Front Panel (DAQ 2)

The software interface is divided into several functional areas:

- Top Left:** A 'File name' input field.
- Top Center:** A 'Scope Mode' panel with a 'STOP' button and a 'Remember to take reference and use Irradiance Mode' warning. It includes controls for 'Integration Time' (6), 'Samples to Average' (1), 'Boxcar Smoothing' (0), and 'Ch0' (checked). Buttons for 'Store Dark' and 'Store Reference' are also present.
- Top Right:** A 'Time Delay in seconds' control set to 0.00.
- Middle Left:** A 'Plot 0' graph showing FFT data. The y-axis is labeled 'FFT' and ranges from 0.0 to 345.6. The x-axis ranges from 0 to 233. Parameters include 'Array Index' (1019), 'Array Length' (350), 'FFT threshold' (150.00), 'FFT width' (3), and 'FFT Locations' (a table of 10 values, all 0.00).
- Middle Right:** A 'Strain channel (0)' control set to 5, and a 'Strain sample' control set to 0.000. Below is a 'Strain' plot with a y-axis from 0.0 to 500.0 and an x-axis from 0 to 1023.
- Bottom Left:** A 'Spectrometer Type' dropdown (set to S2000) and a 'Master Coefficients' panel with 'First Coef' (0.150857), 'Second Coef' (-1.321210E-5), and 'Intercept' (719.856018). A 'Color Temp' control is set to 3100.00.
- Bottom Center:** A large plot showing a signal over time. The y-axis ranges from -1400.0 to 600.0, and the x-axis ranges from 810.4 to 883.2. A yellow 'x' cursor is positioned at approximately 856.63 on the x-axis and -119.20 on the y-axis. A 'Record Delta' control is set to OFF.
- Bottom Right:** A 'Record Spectra' control with 'On' and 'Off' options, and a 'Record Delta' control set to OFF.

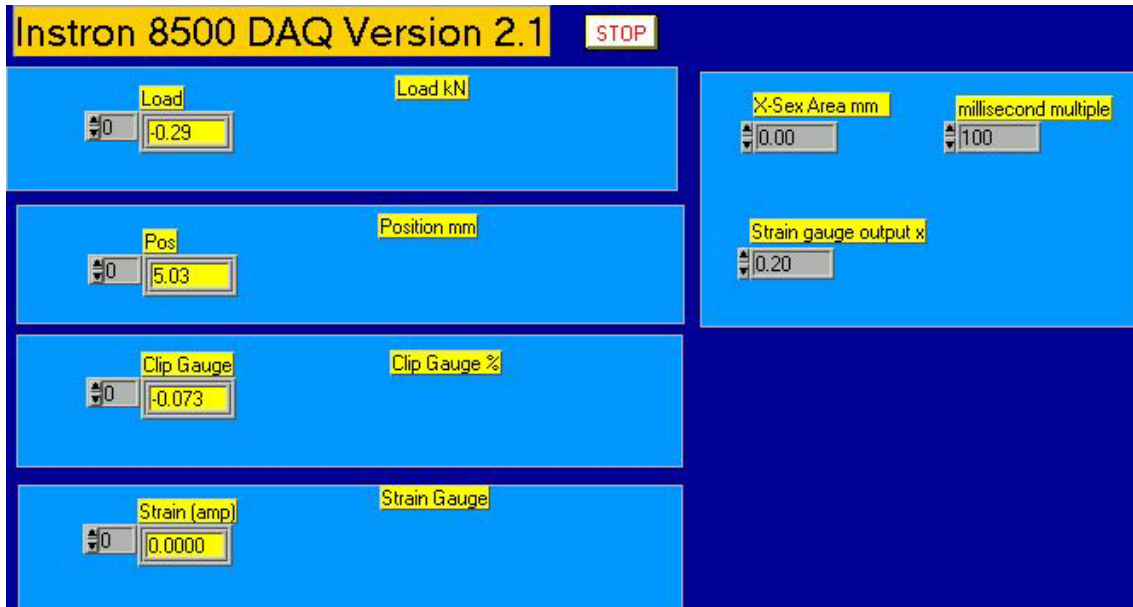
Main section of Block Diagram



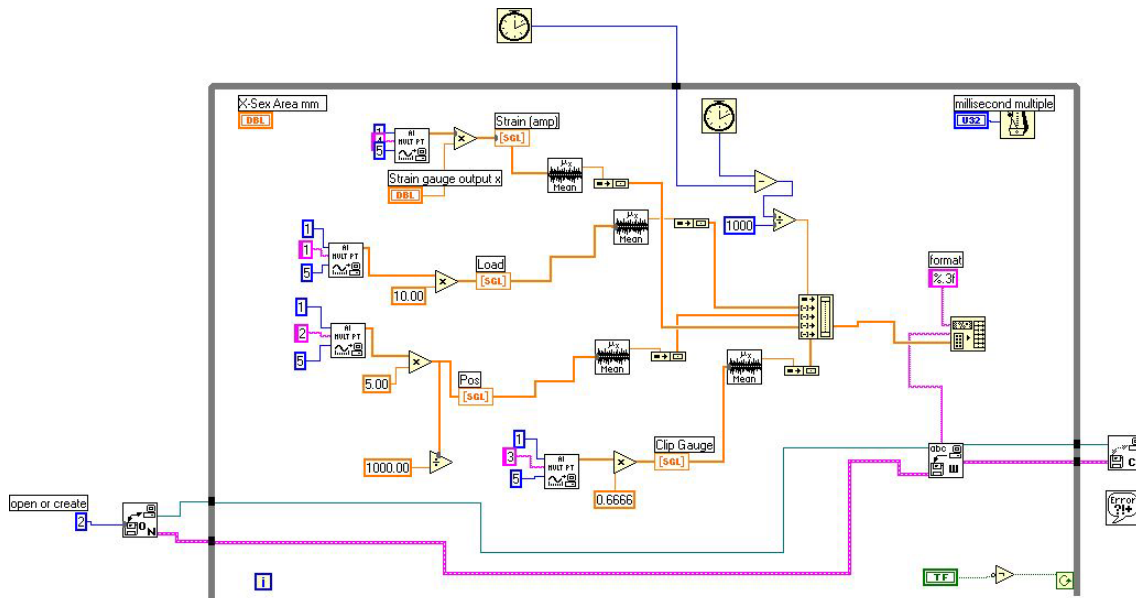
DAQ Method 3 – Strain gauge response and Instron 8501 load data

Based on a program written by Mr D. Brooks

Front Panel (DAQ 3)

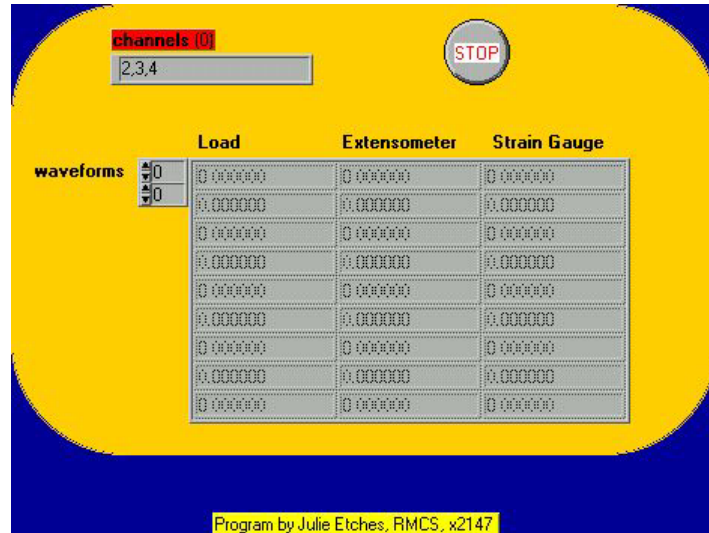


Block Diagram (DAQ 3)

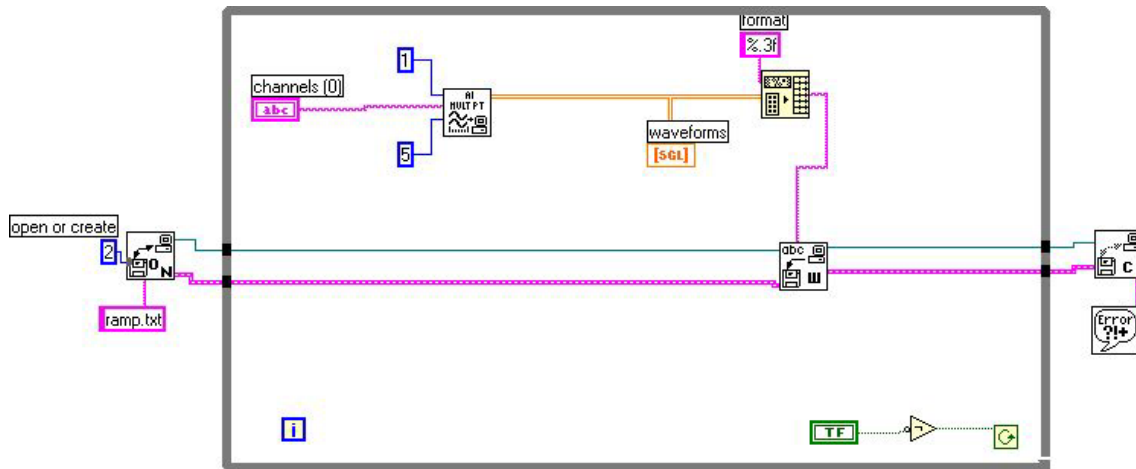


DAQ Method 4 – Higher speed data acquisition for loading rate experiments

Front Panel (DAQ 4)



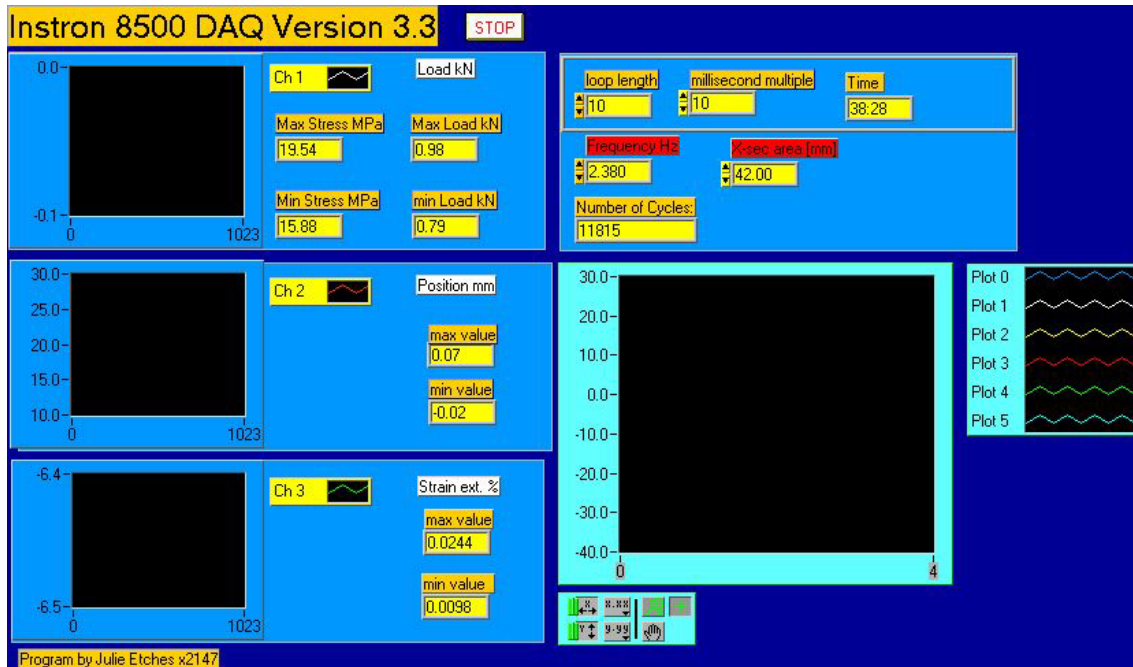
Block Diagram (DAQ 4)



DAQ Method 5 – Fatigue data recording

Based on a program written by Mr D. Brooks

Front Panel (DAQ 5)



Main section of Block Diagram (DAQ 5)

